Reza Taghipour

Efficient Prediction of Dynamic Response for Flexible and Multi-Body Marine Structures

Thesis for the degree of philosophiae doctor

Trondheim, October 2008

Norwegian University of
Science and Technology
Faculty of Engineering Science and Technology
Department of Marine Technology

NTNU
Norwegian University of
Science and Technology

NTNU
Norwegian University of Science and Technology

Thesis for the degree of philosophiae doctor

Faculty of Engineering Science and Technology
Department of Marine Technology

ISBN 978-82-471-1219-9 (printed ver.)
ISBN 978-82-471-1220-5 (electronic ver.)
ISSN 1503-8181

Theses at NTNU, 2008:262

Printed by Tapir Uttrykk

To Dr. Davoud Naderi

Abstract

Waves contribute to major loads on marine structures. Therefore, it is important to quantify wave-induced load effects to ensure a reasonable, safe and robust design of floating systems. One can accomplish this task by using the simplified analysis procedures of classification societies, running experiments, or applying direct calculation procedures.

Direct calculation of wave loads is currently the only reliable procedure for evaluating ocean structures of novel design. This is due to the very limited or absence of service experience accumulated by the classification societies on these structures due to novelty of the concept, material, and unusual dimensions.

The main objective in this thesis is to develop methods for the direct calculation of wave-induced load effect analysis for novel stationary floating structures. These load effects consist of motions, displacements, stresses, and internal structural forces. The focus is on flexible and multi-body systems which can be used in food production, transportation, infrastructure and extraction of wave power. Each example structure analyzed in this thesis is still at the research level, and is not commercially available.

One of the challenges regarding direct load analysis of floating systems is to provide links between available general–purpose hydrodynamic and structural software. Motivated by this, the thesis presents frequency-domain calculation of hydroelastic response for the MegaFloat airport prototype by linking WAMIT and ABAQUS. A generalized modes approach is used. The accuracy of the calculations are ensured by validation using experimental measurements. It is clearly shown by the results that hydroelasticity becomes dominant as the length of the waves increases.

Moreover, a systematic structural analysis procedure is developed between WAMIT and ABAQUS. Using this methodology, the wave-induced structural forces of different components in a 22 body wave energy converter are studied. The hydrodynamic loads and motions are calculated in an efficient manner by using a generalized modes

approach. The results show strong influence of wave-attenuation on axial forces and bending moments in column- and guide-deck connections. Also wave-attenuation affects the power absorbed by the buoys. It is found that the main power absorption is independent of the mean wave direction in a short crested sea. However, the mean wave direction influences the layout of the power absorbed by the device. The power absorption significantly affects the motions of each component specially around the natural frequencies. Significant motions and structural loads are observed for the wave energy converter without off-take which could be connected to inherent hydrodynamic interactions.

Another challenge exists in response simulations of marine structures in time domain. The time-domain models based on Cummins's equation are widely used to investigate the linear transient or nonlinear responses. A common feature of all these models is the convolution integral which has to be calculated separately at each simulation step. The convolutions may become computationally demanding if the simulation time, number of simulation steps, and system degrees of freedom increase. There are different ways to approximate the convolutions. In this thesis the focus is mainly on the state-space representations. The state-space models are attractive not only because they support more efficient simulations but also because they are well-suited for implementing in control and automation packages and stability analyses of systems.

There are different ways to obtain state-space models based on convolution integral kernels. This fact raises the question of which method is better and easier to implement and if one provides more stable calculations. Moreover, how sensitive are the simulation results to the identifications and how much can be gained in efficiency by using state-space representations. These questions will be addressed in this thesis.

To date, the state-space models have been used to investigate the motions for single rigid bodies. The thesis complements the previous works by extending the applications to time-domain flexible and multi-body simulations. Comparison between simulation results and experiments for transient response of a very elastic barge, show reasonably accurate calculations. The results suggest a significant gain in the CPU–time for simulations with state-space models.

With respect to simulation of nonlinear response for floating structures and application of control, the thesis includes analysis of a two-body heaving wave energy converter with off-take and phase

control. The time-domain model is based on a Cummins equation formulation. The convolutions are replaced by state-space models to obtain greater efficiency. The influence of nonlinear drag force on the device output is investigated in the calculations by using a simplified formulation proportional to quadratic velocity. The results show the absorbed power by the device is reduced when the viscous effects increase. For most of the wave conditions, the considered two-body heaving wave energy converter has produced less output in comparison to a single body wave energy converter. Moreover, the phase control can lead to a much better performance for the wave energy device.

Acknowledgements

The four–year course of my PhD study at CeSOS was a mixture of hard work and a memorable living in the company of some amazing people. I may say life has been good to me not just because that I reached the goal I came across the seas for, but also because of all the things I learned and the great friends I met.

Thanks go in the first place to Prof. Torgeir Moan for providing me with the opportunity of working at CeSOS and allowing me to be his PhD student. Apart from many scientific lessons, he taught me to be critical, focused and patient. I will always appreciate him as an inspiring professional in my career.

I would also like to thank my collaborators: Dr. Shixiao Fu; Dr. Tristan Perez; PhD students Jørgen Hals and Arswendy; and Master student Mélanie Devergez, for their assistance and team work during the projects. It is only because of them that I could have gone this far. I am particularly very thankful to Tristan for his superb scientific support and guidance.

Furthermore, I express gratitude to every professor and staff at the Department of Marine Technology for their kind help and friendship. I am also grateful to my fellow PhD students, postdocs and visiting researchers at CeSOS and the Department for their social company and scientific discussions.

And to my guitar for helping me through some dark lonely winter nights when there was absolutely no one around.

Finally, I would like to thank my parents and brothers for their motivation and emotional support; after all, there is no meaning to life without the kindness and love from the beloved ones.

Thank you all!

Reza Taghipour
Centre for Ships and Ocean Structures–CeSOS
Trondheim, August 22, 2008

Contents

Nomenclature

General Rules

Bold symbols denote vectors or matrices.

Dots over symbols represent differentiation with respect to time.

Greek Symbols

$\ddot{\eta}_1$	Acceleration of the column
$\dot{\eta}_1$	Velocity of the column
η_1	Horizontal motion of the column
ω	Wave frequency
ρ	Density of water
Δt	Time step
τ	Time variable

Roman Symbols

$\mathbf{A}$	Added mass matrix
$\mathbf{A}'$	State-space parameter in continuous time
$\mathbf{A}'_d$	State-space parameter in discrete time
$\mathbf{A}^\infty$	Infinite frequency added mass
a_1	Wave-induced water particle acceleration at the center of the strip
$\mathbf{B}$	Potential damping matrix
$\mathbf{B}'$	State-space parameter in continuous time
$\mathbf{B}'_d$	State-space parameter in discrete time
$\mathbf{B}^\infty$	Infinite frequency hydrodynamic damping
$\mathbf{C}$	Restoring coefficient matrix
$\mathbf{C}'$	State-space parameter in continuous time

$\mathbf{C}'_d$	State-space parameter in discrete time
C_d	Drag coefficient
C_m	Mass coefficient
$\mathbf{D}$	Structural damping matrix
$\mathbf{D}'$	State-space parameter in continuous time
$\mathbf{D}'_d$	State-space parameter in discrete time
D	Cylinder diameter
dz	Height of a strip in an arbitrary position along the cylinder
$\mathbf{f}'^{\mathrm{R}}(t)$	The component of the radiation force from only the retardation function
$\mathbf{F}^{exc}$	Wave exciting forces
$\mathbf{h}(t)$	System impulse response function in continuous time
$\mathbf{h}_d(t)$	System impulse response function in discrete time
j	Complex variable
$\mathbf{K}$	Structural stiffness matrix
k	current time index variable
l	Auxiliary time index variable
$\mathbf{M}$	Mass matrix
N	Number of flexible modes
t	Time variable
$\mathbf{u}$	System input
u_1	Wave-induced water particle velocity at the center of the strip
$\mathbf{X}$	Response vector
$\mathbf{y}$	System output
$\mathbf{z}$	State vector

List of Publications

This thesis is presented in the form of a collection of six papers and some additional related work. Three of the papers are published in journals and the rest are published in conference proceedings. The complete papers are presented in Appendix C.

1. Taghipour, R., Fu, S. and Moan, T., 2006, Validated Two and Three Dimensional Linear Hydroelastic Analysis Using Standard Software, *Proceedings of 16th Int. Offshore and Polar Engineering Conference*, San Francisco, California, USA.

2. Taghipour, R. and Moan, T., 2008, Efficient Frequency-Domain Analysis of Dynamic Response for the Multi-Body Wave Energy Converter in Multi-Directional Waves, *Proceedings of 18th Int. Offshore and Polar Engineering Conference*, Vancouver, BC, Canada.

3. Taghipour, R., Perez, T., and Moan, T., 2008, Hybrid Frequency-Time Domain Models for Dynamic Response Analysis Of Marine Structures, *Ocean Engineering*, Vol. 35, pp: 685-705.

4. Taghipour, R., Perez, T., and Moan, T., 2007, Time-Domain Hydroelastic Analysis of A Flexible Marine Structure Using State-Space Models, *International Journal of Offshore Mechanics and Arctic Engineering*, In press.

5. Hals, J., Taghipour, R., and Moan, T., 2007, Dynamics of a Force Compensated Two-Body Wave Energy Converter in Heave with Hydraulic Power Take-Off Subject to Phase Control, *Proceedings of the 7th European Wave and Tidal Energy Conference*, Porto, Portugal.

6. Taghipour, R., Arswendy, A. Devergez, M., and Moan, T., 2008, Structural Analysis of a Multi-Body Wave Energy Converter in the Frequency Domain by Interfacing WAMIT And ABAQUS, *International Journal of Offshore Mechanics and Arctic Engineering*, Accepted for publication.

Declaration of Authorship

The papers are co-authored. The work has been done in the following manner:

Paper 1 S. Fu did the modal analysis by ABAQUS. He also provided his own numerical results for comparison purposes. I am responsible for the rest of the work, i.e. interface programming, modeling the structure in WAMIT, benchmark studies, and writing the paper.

Paper 2 I am responsible for the entire work in the paper.

Paper 3 The paper was formed based on a mutual collaboration between me and T. Perez. He helped me closely to understand the theory behind the identification methods. I did the literature survey, set up the examples and case studies and carried out the comparisons. I generated the hydrodynamic data for the container ship and did the numerical modeling and programming in the paper. I wrote the paper together with T. Perez.

Paper 4 I am responsible for the entire paper. The identification work in this paper is based on the knowledge transferred to me by T.Perez as part of the process in Paper 3.

Paper 5 I am responsible for the hydrodynamic modeling of the wave energy converter and generating the wave environment in SIMULINK. I also did the MATLAB/SIMULINK programming for the hybrid frequency-time domain model with convolution replacement. The nonlinear drag force on the platform pontoons was included in the dynamic model (in SIMULINK) by me. I also linked the hydraulic power take-off model by J. Hals to the dynamic model in SIMULINK and contributed to writing the paper. J. Hals is responsible for the rest.

Paper 6 M. Devergez set up the FE model in ABAQUS. I performed the hydrodynamic and motion analysis based on my work in Paper 2. I am also responsible for the theoretical work, programming, and running the interface between WAMIT and

ABAQUS. A. Arswendy explained the ABAQUS commands required for the interfacing. He also worked on the mechanisms in the FE model and ran the calculations in ABAQUS and contributed to writing the section entitled "The Structural Model". I am also responsible for writing the paper and interpreting the results.

In all the above papers, Professor Moan has contributed to the initiating ideas, support, recommendations and constructive criticism to increase the scientific quality of the publications.

1. Introduction

1.1. General Background

Man has always tried to invent and develop facilities to exploit the Earth's oceans. The oceans contribute to food and energy as well as mineral resources. They provide means for transportation and other infra-structure. The oceans also play an strategic role and will play an increasing role for recreation (Moan, 2003). Various industries are running actively to take advantage of the opportunities offered by the oceans. The most frequent use of ocean structures is within the oil and gas industry, in which hydrocarbons are extracted from sub-sea reservoirs. They are also being used in other industrial activities such as in production of fish in aquaculture, renewable energy and transportation industry.

Figure 1.1.: MegaFloat, the largest floating runway prototype in the world, Tokyo, Japan is an example of a VLFS.

The world's increasing population demands larger scale food production, infrastructure, transportation system, and energy extraction, especially from renewable resources. This demand has partly led to larger and more complicated structures. An example is the MegaFloat (Fig. 1.1), a floating airport prototype constructed in Tokyo Bay (Suzuki, 2005). This class of structures is known as very large floating structures (VLFS) because of its enormous displacement and unprecedented size. The dimensions of the prototype

MegaFloat structure are 1000 × 60 (120) × 3 meters. Due to its large length to height ratio, the MegaFloat will behave as a very flexible structure. This implies that the airport structure will be easily deformed by the exerted loads (see Fig. 1.2) and it will have mutual interactions with sea waves, referred to as hydroelasticity (see the descriptions in Bishop and Price (1979), MOB Project Team (2000) and Faltinsen (2005)). Hydroelasticity may lead to significant increases in the load effects experienced by large vessels (see e.g. Taghipour et al. (2006)/ Paper 1). This issue will be discussed further in Section 2.4.2. Within the VLFS subclass, floating bridges have already been built (e.g. Watanabe (2003)). Yet, industrial products like airports are only at the model or prototype stages.

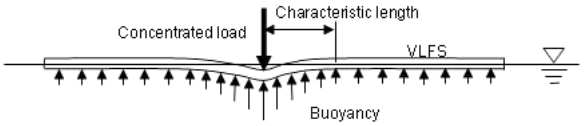

Figure 1.2.: Flexible behavior of the MegaFloat (ISSC, 2006d).

Other examples of future marine structures are wave energy converters (see Fig. 1.3). Experience tells us that a successful wave energy device should be constructed in the form of an array of floating components (Cruz, 2008). These components are often considerably smaller in size than the components of a floating terminal or airport. However, assessment of their dynamic response is still a complicated task because they normally involve complex kinematics, (nonlinear) hydrodynamic interactions and intricate mechanisms like control or power take off units (e.g. Leirbukt (2006), Henderson (2006)). To date, most of the wave energy devices are still at a research level and have not been realized as industrial products.

The unconventional size of the future marine structures together with their complex form and mechanisms represent significant challenges for the engineering design and analysis. Operation of these intricate and/or gigantic structures in harsh ocean environments and large water depths during a 20-100 years life time involves extraordinary design loads, large risks and huge investments (see e.g. ISSC (2006d)). Therefore, physical realization of such mega projects is highly dependent on persuasion of investors and public opinion, which is possible only when one can address the critical issues like loads, responses and risks.

Figure 1.3.: An array of wave energy converters. Picture Courtesy of SEEWEC project (www.seewec.org).

In the design of floating ocean structures, wave loads are often the most important loads. The calculation of wave loads and their effect is a complex task. For common ocean structures such as ships and offshore platforms, there exist design codes or rules issued by various regulatory bodies, including classification societies. However, for novel marine structures, there are limited or no design guidance (ISSC, 2006b). Moreover, existing approaches can not be directly implemented because of the difference in concept, geometry or materials or possibly due to forces from the automatic control. Thus one needs to address the design by explicit limit state criteria and direct calculation of the load effects and resistance.

Design codes contain design criteria, formulated as limit states, such as for ultimate fatigue and progressive failure which are expressed in terms of load effects (motions, stresses etc.) Moreover, they give specifications of strength and how load effects should be estimated.

For new concepts, experimental investigations are crucial for evaluating the load effects (response) e.g. due to wave action. However, experiments are not perfect and are impossible to generalize without theory. Moreover, they are very expensive and time consuming. It is therefore also important to have numerical methods to evaluate the load effects such as motions, structural displacements, forces or stresses in different design sea-states for the relevant design criteria (limit state). The available numerical methods for e.g. ships and offshore structures need to be tailor-made, interfaced or even extended to allow for application to novel concepts.

Another issue is automation and control. For instance, automatic control may be needed to maximize the output of a wave energy device (Cruz, 2008), or to maintain performance of e.g. semisubmersible platforms in a mobile offshore base (MOB Project Team, 2000; Girard et al., 2003). However, application of control algorithms to dynamic response of marine structures may come to reality only when the dynamic model can predict the response accurately and efficiently. More important, the dynamic model must be integrable with the control strategy so that it becomes implementable in the control simulation package. For instance, simulation packages like SIMULINK prefer dynamic models which are in the form of state-space models rather than the ones with convolution integrals. These facts emphasize the need for efficient and consistent models for prediction of dynamic response for marine structures.

As indicated above, an important aspect of the design is to determine the wave-induced load effects. This would involve description of the waves, hydrodynamic loads and motions as well as their structural effects, correspondingly.

In principle, it is possible to model the random ocean waves by superimposing a series of single, discrete waves of different phase and frequency. The normal approach is a probabilistic one. The waves are assumed to be Gaussian. The wave spectrum is taken to be in the form of available models e.g. JONSWAP spectrum (Ochi, 1998). If the load effects of the marine structure to regular waves can be represented by the linear theory, then a spectral approach can be conveniently applied to describe the load effects in irregular waves (Faltinsen, 1990; Newland, 1993). In that case, the wave-induced load effects will also follow a Gaussian distribution. If the dynamics of the system involve nonlinearities, then statistical properties of the load effects must be calculated by analyzing their time series. Also, the distribution of load effects must be obtained by other formulations (Ochi, 1998).

As stated above, an intermediate step in determining the load effects is to calculate the wave loads on the floating structures. The starting point of the hydrodynamic analysis is a boundary value problem (BVP): a partial differential equation (PDE) uniquely solved by satisfying a set of boundary conditions. Within the range of problems considered herein, the assumption of incompressibility of water is made. The governing principles are the continuity and conservation of momentum in the fluid flow. Description of the momentum conservation for fluid flow classifies the hydrodynamic problems into

viscous and inviscid flow equations.

The state-of-the-art in viscid flow hydrodynamic methods in marine applications include RANS[1] (Weymouth et al. (2005)), SPH[2] (Monaghan (2005)) and CIP[3] (Yabe et al. (2001)): Although they seem natural and are potentially accurate in capturing nonlinear and/or violent fluid structure interaction effects, they are quite cumbersome to implement and are computationally demanding. Moreover, these methods provide specific information about the detail of the fluid flow around the floating structure which may not be practically important for understanding the global load effects. In this thesis, the focus is on the numerical methods which assume inviscid irrotational flows and use Boundary Element Methods (BEM). A comprehensive review of the state-of-the-art concerning developments in analysis of fluid-structure interactions and numerical techniques can be found in Ferziger and Peric (2002), ITTC (2005), Faltinsen and Timokha (to be published) and Pákozdi (2008).

Load effects due to waves may be calculated by BEM in the frequency or time domain. In this regard, frequency-domain models are very attractive to deal with linear steady-state responses (Beck et al., 1996; Bertram, 2000; ITTC, 2005; ISSC, 2006a). They are by far more efficient than time-domain approaches. Frequency dependent added mass and damping are easily accommodated. Besides, in analysis of response to irregular waves, they are more accurate since the statistical uncertainty implied by time domain sampling is avoided. However, for very large floating bodies or problems consisting of many floating structures, even the frequency domain methods can become very time-consuming and therefore alternative reformulation of the mathematical problems may be needed. This is one of the topics contained in this thesis (Taghipour and Moan, 2008).

When it comes to evaluating the linear transient response e.g. in landing of an airplane on the floating airport, or response which involves nonlinear effects e.g. due to wave slamming, linear frequency-domain approaches are inapplicable. While it is in principle possible to deal with such problems in the frequency-domain based on a Volterra series expansion of the solution (Bendat, 1998), capturing the transient effects requires expanding to an impractically large order. This reasoning implies that the formulation becomes cum-

[1] Reynolds Averaged Navier-Stokes
[2] Smoothed Particle Hydrodynamics
[3] Constrained Interpolation Profile

bersome to implement and/or computationally demanding. A more natural way of modeling nonlinear problems would be in the time domain. Several different approaches exist to accomplish this task. Some of them are based on transient Green function method and account only for the dominant nonlinearities in the dynamic simulations contributed by hydrostatics and Froude-Krylov terms (see e.g. Sen (2002)). A higher level approximation would include nonlinear radiation and diffraction forces by accounting for instantaneous body boundary conditions, which is referred to in the literature as the 'exact body' approach (see e.g. Lin and Yue (1996)). Again, the problem size and simulation efforts are increased to a large extent when time-domain procedures are applied. For an extensive review of nonlinear hydrodynamic methods based on potential theory approach, see ITTC (2005).

One alternative strategy for solving nonlinear problems is to obtain a linear time-domain model based on the frequency-domain solution and add the nonlinearities as additional features. This model is referred to as the hybrid frequency-time domain model in this thesis. Such models have been developed and used successfully, e.g. in evaluation of nonlinear response of ships such as whipping (e.g. in Wu and Moan (1996)) or in prediction of linear transient response of very large floating structures (VLFS) (see e.g. Kashiwagi (2000)). In Paper 5, a simulation of a wave power device is performed in time domain by using a hybrid frequency-time domain model using data from potential theory calculation. By applying this model, the effect of nonlinear viscous drag force on the output of the wave energy converter is also investigated in a simplified manner.

An important issue in all the above time-domain models is the associated convolution integrals. The convolution terms appear due to the frequency-dependency of radiation forces, implying that the change in the momentum of the fluid at a certain time affects the future response of the vessel. This is also known as 'fluid memory effects', and is discussed further in Section 2.6 and Paper 3 (Taghipour et al., 2008). The importance of considering the frequency dependency of added mass and potential damping in forming the time-domain equations of motion of marine structures was clearly accentuated in the papers by Tick (1959) and Cummins (1962).

Cummins immediately suggested what is known today as Cummins's equation (see Eq. (2.7)). Later, Ogilvie (1964) complemented the work of Cummins (1962) by relating the retardation functions and the added mass and potential damping. So far, the information

has been enough to set up hybrid frequency-time domain models in the form of integro-differential equations.

Convolutions need to be time-marched at every single step of the simulation. This implies that convolutions may become computationally demanding as the simulation time, number of DOFs and refinement of the simulation increases. Moreover, in design and analysis of automatic control, other mathematical representations of the systems like state-space models are preferred. Also, analysis of stability for systems is more easily performed for models with state-space models than the ones possessing convolutions.

There are techniques available which approximate the convolution integrals. Among them, approximations by using state-space models are of great interest. Finding a state-space model approximation for the convolution term involves the use of system identification. System identification is a general term to describe physical (dynamic) systems in the form of mathematical models based on available data e.g. from experiment (Ljung, 1999). There is a vast literature on system identification techniques (see references in Taghipour et al. (2008)). Some of these techniques infer state-space models from samples of the impulse response functions in time domain (see e.g. Yu and Falnes (1998)). Others obtain the state-space models from the transfer functions of the impulse response functions (see e.g. McCabe et al. (2005)). One may raise the question that 'Which method will do best?', or 'How sensitive are the simulation results to the accuracy of the identifications?'. Also, 'Would state-space models be more efficient compared to simulations integrating the convolutions?'. Such issues are among the topics raised in the thesis (see Paper 3). Developing hybrid frequency-time domain models accelerated by state-space models with application to simulation of flexible and multi-body marine structures is carried out in this work as well (see Taghipour et al. (2007), Paper 4 and Hals et al. (2007), Paper 5).

The aim of this thesis is the evaluation of load effects induced by waves. Besides motions, this for instance includes structural response in terms of displacements, internal forces and stresses. Linear theory of structural mechanics is well established and well covered by general-purpose software based on Finite Element Method (FEM), e.g. ABAQUS. The built-in hydrodynamic modules in these software (e.g. AQUA in ABAQUS) provide one alternative for marine structural analysis applications. There are also approaches that link the hydrodynamic software to the structural analysis packages

(SESAM). In this respect, most of the available studies are in the frequency domain (e.g. Malenica et al. (2006, 2008)) and a few work has focused on time-domain analyses of floating systems (Raj and Edwards (2001) and Iijima et al. (2008)). The range of applications are mainly within ships, VLFS and offshore structures. According to ISSC (2006b), the current status of state-of-the-art in interconnectivity and model exchange between 3D hydrodynamic and structural software is not satisfactory.

There are very few studies on the structural response of multiple floating bodies, especially within offshore renewable energy applications. Structural analysis of multiple floating structures is of interest because significant load effects may occur due to hydrodynamic interactions (Maniar and Newman, 1996; Evans and Porter, 1997). In this context, structural analysis of a multi-body floating system by interfacing WAMIT and ABAQUS with application to wave energy converters is included in this thesis (see Taghipour et al. (2008), Paper 6).

1.2. Objective and Scope

Fig. 1.4 shows the objective and scope of the thesis. The objective is to establish robust and efficient simulation methods to determine the wave-induced load effects of novel marine structures. Load effects include motions and structural displacements, internal forces and stresses. Determination of wave-induced load effects involves description of the waves, hydrodynamic load assessment, and motion and structural analysis, as reflected in the papers (Structural analysis is carried out in Paper 4 only). For some analyses like hydroelastic simulations, the calculations are interconnected. This has been shown in Fig. 1.4 by double arrows. The scope of the thesis can be described by the following three major features:

1. Example problems addressed

   - Body types

     The structures studied in this thesis are either single rigid bodies (Paper 3), single flexible bodies (Papers 1 and 4) or multiple rigid bodies (Papers 2, 5 and 6).

   - Ocean Environment

     The studies consider calm sea environment (Paper 3) or

waves (Papers 1 and 2) or both (Papers 4, 5 and 6). No effect from wind and current is included in the present studies. The waves are either regular sinusoidal waves or irregular waves.

2. Methodologies

   - Hydrodynamic load assessment

     The numerical method adapted for hydrodynamic load assessment in the entire work is founded exclusively on frequency-domain BEM theory as implemented in WAMIT. The software is based on potential theory (inviscid incompressible and irrotational flow) and uses a Green function to satisfy the free surface boundary conditions. The pressure is obtained using the linearized Euler-Bernoulli's equation. In paper 5, viscous drag force is also considered by using a simple model.

   - Motion analysis

     Approaches for motion analysis have been established both in time and frequency domain. The frequency-domain simulations only deal with linear steady-state motions (Papers 1 and 2). The methodology in Paper 6 utilizes the motion analysis in Paper 2. The time-domain models address linear transient dynamics (Papers 3 and 4) or nonlinear steady-state motions (Paper 5).

   - Structural analysis

     The structural analysis in this thesis is exclusively performed in the frequency domain (Paper 6). This implies that only linear steady-state structural responses are considered. The method is based on a quasi-static approach by using the FE analysis implemented in ABAQUS.

3. Load effects

   - Motions

     Papers 1 to 5 deal explicitly with structure motions.

   - Structural response

     The goal of Paper 6 is to address structural responses. It utilizes the motions obtained in the earlier work in Paper 2.

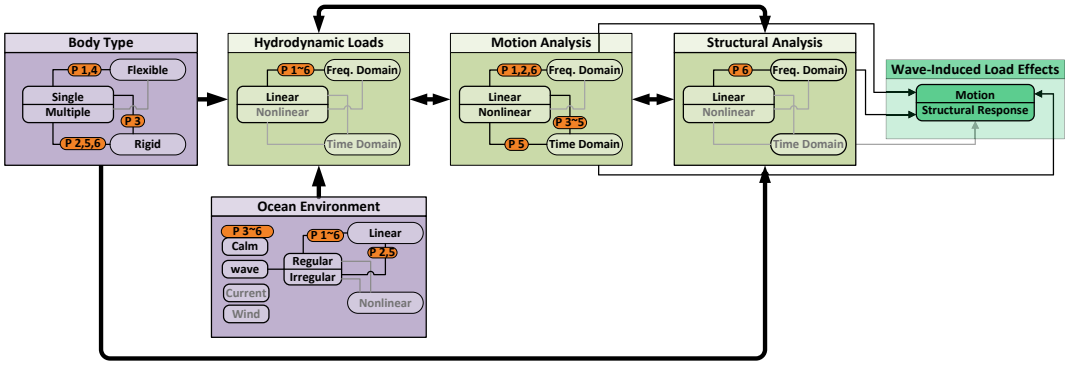

Figure 1.4.: The objective and scope of the thesis and interconnection between the different papers. The black solid text and lines are the studied subjects and the paths taken. The grey lines are the alternative paths which were not chosen in this work. Grey text shows the alternative topic or methodology which has not been studied. P stands for Paper.

One of the subjects dealt with in this thesis is the motion analysis of VLFSs by considering hydroelasticity. A method is developed in the frequency domain by interfacing ABAQUS and WAMIT to estimate the linear steady-state wave-induced response of flexible marine structures. The approach has been applied in the analysis of the MegaFloat airport prototype, as described in Paper 1.

Another theme in this thesis is motion analysis of multi-body marine structures by using generalized modes. In Paper 2, a model is developed in the frequency domain to predict the wave-induced motions and overall performance of a multi-body wave energy converter with and without power take-off.

Evaluation of structural responses of multi-body marine structures is another important theme in this thesis. A frequency-domain method is developed for linear steady-state wave-induced structural response analysis of the multi-body wave energy converter with power take-off. This study is based on the work reported in Paper 2 as well as the combined use of WAMIT and ABAQUS software systems, which is reported in Paper 6.

Another topic addressed in this thesis is the building of time-domain motion analysis models based on the frequency-domain hydrodynamic data of marine structures, referred to as hybrid frequency-time domain models. The focus is on avoiding the convolution integrations by replacing them by approximately equivalent representations in terms of state-space models. Different aspects such as the

estimated model order, accuracy of fit, use of available(input) data, ease of use and generation of stable results are discussed in Paper 3. The accuracy and efficiency of the simulations that circumvent the convolution integrations are as well discussed in this paper. Application of the state-space models to time-domain hydroelastic models of flexible marine structures, as reported in Paper 4, is an extension to the results in Paper 3.

In automatic control procedures, time-domain models of marine structures are mostly preferred. Yet, the time-consuming convolution integrals are not convenient for such applications and are usually be avoided. In Paper 5, a time-domain model is developed for a two-body wave energy converter with heave motion. The convolutions are approximated by the state-space models. A simple drag force model is also included in the study to investigate .

1.3. Thesis Outline

Chapter 2 deals with theoretical features that are relevant for the research done in this thesis. A short description about ocean wave modeling is made in Section 2.2. It is followed by a review of the state-of-the-art in hydrodynamic methods relevant to this research. Moreover, the chapter looks into frequency-domain equations of motion for flexible and multi-body marine structures and their corresponding challenges. In this context, the ideas and objectives behind Paper 1 and Paper 2 are presented.

The goal of Section 2.5 is to review some literature regarding structural response analysis of marine structures. The focus will be on the approaches that are applicable to structural response assessment of multiple floating structures. An example problem for a multi-body wave energy converter is described in Chapter 2.5 for which the structural response analysis methodology and results are reported in Paper 6.

In Section 2.6, the transformation from frequency to time domain to describe the equations of motion and appearance of convolution integrals is described. The contributions in Paper 3 is then presented. It will be shown how state-space models approximate the convolution integrals. The gain in efficiency by using such models is reviewed briefly. The application of the theory to flexible and multi-body marine structures is addressed in Papers 4 and 5, respectively.

Chapter 2 is concluded with an overview of the example structures studied within the thesis.

Chapter 3 introduces the case studies considered in the papers. It describes the objectives and the methodologies of each paper and explains briefly the results and conclusions made by the methods.

Finally, concluding remarks as well as suggestions for future research work in relevance to the topics are given in Chapter 4.

Appendix A provides a short introduction to WAMIT. An introduction to ABAQUS is given in Appendix B. The published papers are appended in Appendix C. Appendix D describes the analysis of the FO^3 platform in the vertical plane by means of a generalized modes approach. In Appendix E, the interface method and software described in Paper 6 is validated to some extent by comparison with simple analytical solutions of wave induced structural response for a clamped circular column.

2. Selected Theory and Literature

2.1. General

The goal of this chapter is to summarize the theoretical issues which are relevant for the research made in this thesis. More in-depth information can be found in the papers which constitute this thesis as well as other cited references.

2.2. Ocean Environment Modeling

Marine structures are affected by various types of loads. In this context, waves make up the dominant loads on floating structures. The ocean waves are disperse and random. This is predominantly due to the action of wind being the wave generating mechanism. For deep water waves, which are also considered in this thesis, the instantaneous wave elevation can be described accurately by a Gaussian distribution (Ochi, 1998). One can in general use linear theory to describe the ocean surface by superposition of a series of monochrome sinusoidal (airy) waves. For derivations of the linear wave theory see Newman (1977) or Dean and Dalrymple (1991). One may use a sea spectrum model such as JONSWAP or Pierson Moskowitz. The designated spectrum corresponds to a specific marine operational site. It is calculated by knowing the significant wave height of the waves and the peak period and choice of a specific wave spectrum model. Recommended models are available from ITTC and ISSC. This usually describes a long-crested (unidirectional) sea spectrum, but corrections can be made to obtain short-created sea waves by using spreading functions.

If one could obtain the load effects for a monochrome wave in a linear sense[1], then one can combine such information with the wave

[1] As we will see in the next section, there are accurate methods which can

data by using the spectral approach (see e.g. Faltinsen (1990) or Newland (1993)). The result is the spectral description of the wave-induced load effects for the designated operational site. Once the spectra are known, it is possible to comment on the statistics of the load effects like extremes and the number of occurrences of maxima within a certain period of time by choosing a probability density function (Newland, 1993). For linearized dynamic systems, the load effects to Gaussian waves will be Gaussian as well. If the system output could be assumed to be a narrow-band process, then the probability density of its maxima will follow the Rayleigh distribution. For dynamic systems with nonlinearities, other distributions may apply.

2.3. Hydrodynamic Loads and Motion Analysis

Calculation of wave-induced loads on ships and ocean structures is normally carried out by semi-empirical methods, computational fluid dynamics (CFD) methods, or experimental fluid dynamics (EFD) methods. All methods need to be validated against model tests or full scale measurements. However, experiments are time-consuming and subject to uncertainty.

Perhaps one of the simplest, and yet the most extensively used, semi-empirical methods in computing the hydrodynamic loads on slender marine structures is Morison's equation (see e.g. Sarpkaya and Isaacson (1981) or Faltinsen (1990)). Morison's equation ignores the diffraction effects in the fluid-structure interactions and considers the viscous drag and inertia forces in a semi-empirical manner. The formula is originally intended for problems with flow transverse to a cylinder. If one considers a floating vertical cylindrical column moving as a result of waves, one may explain the horizontal wave-induced hydrodynamic force on the cylinder using a slightly modified form of the Morison's equation (see e.g. Faltinsen (1990)):

$$F = \oint \rho C_m \pi \frac{D^2}{4} a_1 dz - \oint \rho (C_m - 1) \frac{\pi D^2}{4} \ddot{\eta}_1 dz + \oint \frac{\rho}{2} C_d D |u - \dot{\eta}_1| (u - \dot{\eta}_1) dz, \tag{2.1}$$

where the symbols are explained in the list of symbols.

calculate the load effects accurately in a linear sense in situations where the load effects are linear or weakly nonlinear.

In Eq. (2.1), the first term of the force represents the inertia term and corresponds to the Froude-Krylov force. The second term represents the radiation force. The last term represents the viscous drag force. The formula is valid for platforms with column cross sections that have a small diameter compared to the wave length i.e. $\frac{D}{\lambda} < \frac{1}{5}$. The Morison's formula is useful for design of offshore structures if the drag and inertia coefficients are selected cautiously, based on the flow characterizing parameters e.g. Keulegan-Carpenter number. A discussion of these parameters can be found in Sarpkaya and Isaacson (1981). The coefficients in Morison's equation have to be determined by experiments as done in for instance Airey et al. (1989). In some studies, as e.g. Sauder and Moan (2007), an equation of the type (2.1) has been used to determine the forces on marine structures.

Morison's formula provides a quick and convenient way for estimating wave and current loads on slender marine structures. Examples are risers, mooring lines and jack-up structures. However, it cannot give any information regarding the details of the flow pressure around the body and evolution of free-surface due to wave/body interactions. Moreover, the applicability of the formula also becomes questionable for large volume structures and wave conditions in which diffraction effects become important. Platforms with large cross-sections relative to the wave-length, like tension leg platforms (TLPs), require consideration of diffraction effects. Therefore, computer codes are generally applied.

Within the scope of this thesis, we focus on hydrodynamic codes that are based on potential theory and Boundary Element Method (BEM) to solve the flow problems in 3D, known as the panel methods. The conventional panel methods discretize the body surfaces by a number of quadrilateral panels (Hess, 1990). They are referred to as the low-order panel methods. The more recent panel methods discretize the geometry by a series of B-splines (Maniar, 1995). They are referred to as higher-order or B-Spline panel methods. A well described text regarding explanation of the panel methods is Lee and Newman (2004).

There exist panel codes based on Green function or Rankine singularities (e.g. ISSC (2006a)). The available codes in the first group are the ones being routinely used in the industry due to their robustness and accuracy. They calculate the loads in the frequency or time domain. Since the free-surface boundary condition is satisfied automatically in these methods using the Green function formulation,

one needs to discretize only the underwater surfaces.

Several levels of approximation are available for the Green function panel codes to account for nonlinear effects (e.g. ITTC (2005)). One approach is the so-called "body-exact" (body-nonlinear) formulation which evaluates the nonlinear radiation, diffraction forces, restoring and Froude-Krylov (e.g. Lin and Yue (1996)). Fully nonlinear methods based on potential theory are still at a developing stage. In general, analyses by using nonlinear 3D codes are time consuming and to address the needs at design stages, one may apply modifications to results by linear codes in a simplified manner. A simpler approach consists of accounting for the predominant nonlinearities by exactly evaluating Froude-Krylov and restoring forces while keeping the radiation and diffraction terms linear (e.g. Sen (2002)). In Paper 5, modifications are made to linear potential theory results by adding viscous drag associated with pontoons of a semi-submersible platform in a simplified manner.

When it comes to violent flow and highly nonlinear problems, potential theory codes do not produce reasonable results. As mentioned before, there are modern CFD methods like SPH (Monaghan, 2005) and CIP (Yabe et al. (2001)) that can deal with such problems in a much more sophisticated manner. For an extensive review of numerical techniques in hydrodynamics, refer to Ferziger and Peric (2002), ITTC (2005), Faltinsen and Timokha (to be published) and Pákozdi (2008).

For a given problem, the choice of the hydrodynamic solver, and thus the extent of the approximations and the numerical scheme, determines the necessary size of the computer, the time for computation, and most importantly, the quality of the solution relative to physical reality. In view of such considerations, when calculating the global response of mega-structures or other multi-body systems at early design stages, it may be impractical to obtain information about the details of the flow at very local regions of the fluid domain. For such problems, capturing the details of the flow with CFD is almost impossible with today's computing capacities. Even by neglecting such details and applying potential theory codes, the problem may still be time consuming. An example is the calculation of wave-induced loads for multi-body marine structures where problem or geometrical symmetry cannot be used by standard approach. In such cases, particular reformulation of the mathematical problem may be required to estimate the wave loads in an efficient manner (see Paper. 2).

In conclusion, BEM is currently the state-of-the-art approach in hydrodynamic load assessment of flexible and multi-body marine structures. The hydrodynamic load analysis in this study has been based on WAMIT software. WAMIT has been developed based on potential theory and a Green function formulation and uses BEM to discretize the mathematical equations. A brief introduction to this software is given in Appendix A.

2.4. Frequency-Domain Motion Analysis

2.4.1. Rigid Structures

As long as linear hydrodynamic models are applied, equations of motion of a rigid floating system (6 DOF) with zero forward speed in sea waves are described in the frequency domain by the vector equation:

$$-\omega^2[\mathbf{M}+\mathbf{A}(\omega)]\mathbf{X}(j\omega)+j\omega\mathbf{B}(\omega)\mathbf{X}(j\omega)+\mathbf{C}\mathbf{X}(j\omega) = \mathbf{F}^{\text{exc}}(j\omega), \quad (2.2)$$

where the symbols are explained in the list of symbols. Eq. (2.2) is a system of simultaneous linear algebraic equations. The unknowns are the six DOF responses embedded in the $\mathbf{X}$ vector. The solution of these equations is obtained easily and efficiently due to simple structure of the mathematical formulation.

The wave exciting forces are integrated pressure forces obtained from the solution of diffraction potential over the mean wetted surface of the body.

The integrated pressure forces obtained from the solution of the radiation potentials define the radiation forces:

$$\mathbf{F}^r = -[-\omega^2\mathbf{A}(\omega)\mathbf{X} + j\omega\mathbf{B}(\omega)\mathbf{X}]. \quad (2.3)$$

The components of the radiation force in phase with acceleration and velocity of the body are known as the added mass ($\omega^2\mathbf{A}(\omega)\mathbf{X}$) and the hydrodynamic damping forces (-$j\omega\mathbf{B}(\omega)\mathbf{X}$), respectively.

The restoring forces in Eq. 2.2 (the $\mathbf{CX}$ term) are the final form of the Taylor expansion of gravity and buoyancy contributions up to the first order. All the above vector quantities (force or response) are defined with respect to the body's equilibrium frame.

2.4.2. Flexible Structures

One of the challenges in dynamic response analysis of novel marine structures is the study of flexible floating bodies. In this context, VLFSs are classified as a special type of marine structures. VLFSs are grouped into pontoon-type and semisubmersible-type structures, respectively (ISSC, 2006d). Examples of the first and second groups are the MegaFloat[2] (Suzuki, 2005) and the Mobile Offshore Base (MOB Project Team, 2000), respectively. A review of literature regarding the studies on the MegaFloat can be found in Watanabe et al. (2004) and Suzuki (2005). Palo (2005) gives a thorough description of the analysis efforts relevant to MOB.

An important and yet challenging aspect regarding analysis of flexible floating bodies is the hydroelasticity implied as the influence of floating body flexibility on the hydrodynamic pressure and thus the load effects (MOB Project Team, 2000; Faltinsen, 2005). Research on VLFS and hydroelasticity are quite recent subjects. Recently, Riggs et al. (2008) has compared some frequency domain hydroelastic codes based on the ISSC VLFS benchmark (ISSC, 2006d). Their comparison considered both stress and displacement studies. A similar comparative study was published by Jiao et al. (2006), but it was restricted to a shallow draft plate, and considered only displacements. Chen et al. (2006) also reviewed several hydroelasticity theories applied to global response analysis of marine structures.

Some of the methods use a mode expansion approach (e.g. Bishop and Price (1979); Newman (1994); Kashiwagi (2000)), also known as generalized modes approach (see e.g. WAMIT). In the mode expansion approach, the response of the structure is decomposed into a temporal and a spatial function. The spatial function is a selection of the so-called mode shapes. Hydrodynamic loads corresponding to the radiation are evaluated for unit modal response and are then integrated into the equations of motion where the wave-exciting forces are included. The solution gives the response of the structure. The number of required modes to represent the response depends highly on the problem and can become quite large for VLFS response solutions. However, not all the modes contribute to the actual response. Another approach is the so-called direct method (Yago and Endo, 1996b; Yasuzawa et al., 1997; Kim et al., 2005), where the hydro-

[2]There are MegaFloat concepts that are partly or fully implemented by semisubmersible columns.

dynamic BVP (pressure distribution) and the elastic response are solved simultaneously. Therefore, the direct method avoids the incorporation of any modes into the solution of response. But the method is computationally expensive and requires interfacing between the hydrodynamic and structural numerical techniques like BEM and FEM. There are also more certified hydrodynamic methods in the frequency domain than in the time domain. As a result, the generalized modes approach have often been used in the previous studies. The generalized modes approach is also used within the contents of this thesis.

In case of a deformable body with a mode expansion approach, one can rewrite the equations of motion in Eq. (2.2) in a generalized form as done e.g. by Newman (1994):

$$\Big[-\omega^2[\mathbf{M}+\mathbf{A}(\omega)]+j\omega[\mathbf{B}(\omega)+\mathbf{D}]+[\mathbf{C}+\mathbf{K}]\Big]\mathbf{X}(j\omega) = \mathbf{F}^{\mathrm{exc}}(j\omega). \quad (2.4)$$

Now, the matrices and vectors have a dimension of $(6+N)\times(6+N)$ and $(6+N)\times 1$, respectively. N is the number of flexible modes defined in addition to the six rigid body modes. $\mathbf{K}$ and $\mathbf{D}$ are the generalized structural stiffness and the generalized structural damping matrices, respectively. All the other coefficients are also generalized.

2.4.3. Multi-body Structures

Another important aspect is the response of floating interconnected or multi-body ocean structures, such as wave energy converters. A good review of the state-of-the-art concerning wave energy devices can be found in ISSC (2006c) and Cruz (2008).

To best of the author's knowledge, only a few methods and computer programs are available for handling 3D radiation/diffraction analysis of multi-body marine structures, including their mutual interactions. A typical approach is to evaluate the hydrodynamic loads corresponding to each floating body oscillating in each of the 6 DOF first and then postprocess the radiation and diffraction forces together with other loads like the power take-off force (PTO) externally and then reduce the DOF to the original DOF of the oscillating device by applying the kinematic constraints.

Following this approach and utilizing a software similar to WAMIT (e.g. Rogne (2007)), no symmetry can be exploited for either the radiation or for the diffraction problem. Therefore, such an evaluation of hydrodynamic loads and motions requires substantial simulations when the number of bodies increases. In addition, exporting the field particle information such as pressure and wave elevation, becomes quite cumbersome since the information passes through the postprocessing stage for each DOF and each body.

Fortunately, for linear hydrodynamic load assessment of multiple floating bodies one can alternatively use the generalized modes approach to transform the problems to a single body with several DOF. Such an approach is well known in studying the response of flexible bodies in waves as mentioned earlier in Section 2.4.2. All the geometries in the problem are then merged and considered as one. This "single body" will have "pseudo-flexibility" in the sense that different parts of the body (sub-bodies) are allowed to have different DOF depending on the problem. In this way, assuming n to be the number of floating bodies, the $6 \times$ n mandatory DOF for the initial multi-body problem reduces to one single body with the original m DOF where $m << 6 \times n$. Solution by taking account of geometrical or problem symmetry is also a possibility.

2.5. Structural Analysis

As mentioned above, various general-purpose computer tools based on Finite Element Method provide the state of the art. Some programs calculate the wave-induced load effects using built-in hydrodynamic modules (e.g. AQWA module in ANSYS, AQUA module in ABAQUS). Some studies accomplish the structural analysis by interfacing the general-purpose structural and hydrodynamic software. In this context, one of the available software systems is SESAM which integrates all the hydrodynamic, motion and structural response analyses in one package. The marine structural response analysis in the frequency domain is well-established. The applications are mostly for ships, offshore platforms and VLFS. Malenica et al. (2006) and Malenica et al. (2008) reported several frequency domain structural analyses for a single flexible body with and without forward speed by linking the hydrodynamic program HYDROSTAR to ABAQUS. Iijima et al. (2008) reports a nonlinear time-domain structural analysis by interfacing a 3D BEM hydrodynamic program and ABAQUS or NASTRAN. In calculation of the

hydrodynamic loads in Iijima et al. (2008), hydrostatic and Froude-Krylov forces are considered nonlinear. Fujikubo (2005); Fujikubo and Yao (2001) carried out a global and detailed structural response analysis of the MegaFloat using the hydroelastic approach developed by Kashiwagi (1996), Ohmatsu (1997), Seto et al. (2003), and Yago and Endo (1996b).

Few studies have been concerned with the structural response assessment of multi-body marine structures, especially multi-body wave energy converters. Raj and Edwards (1999) reported a time domain structural analysis methodology of an MOB by using linear frequency domain hydrodynamic method of HIPAN (Lee and Newman, 1998) and nonlinear time domain structural analysis in ABAQUS. In their analysis, radiation forces are calculated as modal quantities and are distributed over the wetted surface as pressures. An interfacing procedure named HIP2FEA (Letcher, 1998) developed by AeroHydro Inc was used to extract the diffraction pressure information from HIPAN results. An ABAQUS user written subroutine (UEL) was used to interface the pressures in ABAQUS. Unfortunately, no numerical results seem to have been published from this study.

Structural analysis by coupling standard software may be advantageous, since the interfaced software are often general-purpose and is therefore applicable to a variety of structural configurations and components. Moreover these software are often validated and well documented. How accurate the strength assessment of the marine structure will be is heavily dependent on how accurate representation and application of the hydrodynamic loads is to the structural software. To date, the mutual compatibility between the structural and hydrodynamic software is not at a satisfactory level (ISSC, 2006b).

Paper 6 deals with an alternative approach to the structural analysis of multi-body floating structures in the frequency domain by interfacing WAMIT and ABAQUS. The methodology complements the study of the wave energy converter performed in Paper 2, as described in Section 3.3. An introduction to Paper 6 is given in Section 3.6. A brief description of ABAQUS is given in Appendix B.

2.6. Hybrid Frequency-Time Domain Models

The equations of motion in Eq. (2.2) do not incorporate nonlinearities[3]. The most convenient way to include nonlinear features is to replace Eq. (2.2) by proper time-domain models. The nonlinear equations of motion may be solved directly in the time domain. However a more efficient approach may be to first solve the linear problem in the frequency domain and utilize these results when solving the full problem. Such a model is referred to here as a hybrid frequency-time domain model and has been initially introduced by Cummins (1962). To date, it has been utilized successfully in different motion analysis applications (see e.g. Wu and Moan (1996); Kashiwagi (2004)). Nonlinear loads are normally added to these models as additional features. In order to have a better understanding of the hybrid-frequency time domain models and its properties, a derivation of the equations are presented here.

One may start by adding $-\omega^2[\mathbf{A}^\infty - \mathbf{A}^\infty]X(j\omega)$ and $j\omega[\mathbf{B}^\infty - \mathbf{B}^\infty]X(j\omega)$ to the L.H.S. of Eq. (2.2). A reformulation of the equations may then be as follows:

$$-\omega^2[\mathbf{M}+\mathbf{A}^\infty]\mathbf{X}(j\omega)+j\omega\mathbf{B}^\infty\mathbf{X}(j\omega)+\mathbf{C}\mathbf{X}(j\omega)+j\omega\mathbf{K}(j\omega)\mathbf{X}(j\omega)=\mathbf{F}^{\text{exc}}(j\omega), \tag{2.5}$$

where

$$\mathbf{K}(j\omega)=[\mathbf{B}(\omega)-\mathbf{B}^\infty]+j\omega[\mathbf{A}(\omega)-\mathbf{A}^\infty]. \tag{2.6}$$

Taking the inverse Fourier transform of Eq. (2.5) gives the following vector integro-differential equation

$$[\mathbf{M}+\mathbf{A}^\infty]\ddot{\mathbf{x}}(t)+\mathbf{B}^\infty\dot{\mathbf{x}}(t)+\int_{-\infty}^{\infty}\mathbf{k}(t-\tau)\,\dot{\mathbf{x}}(\tau)\,d\tau+\mathbf{C}\mathbf{x}(t)=\mathbf{f}^{\text{exc}}(t). \tag{2.7}$$

The above equation is known as Cummins's Equation (Cummins, 1962). One can see how the frequency dependency of added mass and damping has resulted in the appearance of a convolution integral. The $\mathbf{k}(t)$ function in the above equation is known as the retardation or memory function.

[3] It is possible to linearize the formulation of a nonlinear phenomenon, but the accuracy of the solution may in some cases be severely damaged.

Taking the inverse Fourier of Eq. (2.6) results in

$$\begin{aligned}\mathbf{k}(t) &= \frac{1}{2\pi}\int_{-\infty}^{\infty}\mathbf{K}(j\omega)e^{j\omega t}d\omega = \\ &\frac{1}{2\pi}\int_{-\infty}^{\infty}\Big[[\mathbf{B}(\omega)-\mathbf{B}^{\infty}]\cos(\omega t)+j[\mathbf{B}(\omega)-\mathbf{B}^{\infty}]\sin(\omega t) \\ &+ j\omega[\mathbf{A}(\omega)-\mathbf{A}^{\infty}]\cos(\omega t)-\omega[\mathbf{A}(\omega)-\mathbf{A}^{\infty}]\sin(\omega t)\Big]d\omega,\end{aligned} \tag{2.8}$$

where $\mathbf{k}(t)$ is a real function of time and thus the imaginary terms in the above equations must be ignored. Moreover, $\mathbf{A}(\omega)$ and $\mathbf{B}(\omega)$ are even functions of frequency which reduces the above equation to

$$\mathbf{k}(t) = \frac{1}{\pi}\int_{0}^{\infty}\Big[[\mathbf{B}(\omega)-\mathbf{B}^{\infty}]\cos(\omega t)-\omega[\mathbf{A}(\omega)-\mathbf{A}^{\infty}]\sin(\omega t)\Big]d\omega. \tag{2.9}$$

The first term in the R.H.S. of Eq. (2.9) is an even function of time while the second term is an odd function. In other words:

$$\mathbf{k}(t) = \mathbf{k}_e(t) + \mathbf{k}_o(t). \tag{2.10}$$

One must note that radiation force is a causal[4] system. There is no force before the structure is oscillated and vice versa. In mathematical terms:

$$\mathbf{k}(t) = 0; \quad \text{if} \quad t < 0. \tag{2.11}$$

Thus for $\mathbf{k}(t)$ to represent a causal system in Eq. (2.10), there must be

$$\mathbf{k}_e(t) = \begin{cases}\mathbf{k}_o(t), & \text{if} \quad t \geq 0, \\ -\mathbf{k}_o(t), & \text{if} \quad t < 0,\end{cases} \tag{2.12}$$

Therefore Eq. (2.9) reduces to

$$\mathbf{k}(t) = \frac{2}{\pi}\int_{0}^{\infty}[\mathbf{B}(\omega)-\mathbf{B}^{\infty}]\cos(\omega t)\ d\omega \tag{2.13}$$

$$= -\frac{2}{\pi}\int_{0}^{\infty}\omega[\mathbf{A}(\omega)-\mathbf{A}^{\infty}]\sin(\omega t)\ d\omega. \tag{2.14}$$

Eqs. (2.13) and (2.14) are two important relations which relate added mass to potential damping and to the retardation function

[4] A causal or non-anticipatory system implies a system for which there is no output for input occurring in the future.

(Ogilvie, 1964). For sake of numerical convergence, the relation based on the hydrodynamic damping is preferred to the one with added mass.

For floating structures with zero forward speed, the hydrodynamic damping vanishes as the frequency of oscillation approaches infinity. In practice, the retardation kernel $\mathbf{k}(t)$ tends to vanish for times passing a certain value, say t_{mem}. Knowing this information and by using causality one can change Eq. (2.7) to

$$[\mathbf{M} + \mathbf{A}^{\infty}]\ddot{\mathbf{x}}(t) + \int_0^{t_{mem}} \mathbf{k}(t-\tau)\,\dot{\mathbf{x}}(\tau)\,d\tau + \mathbf{C}\mathbf{x}(t) = \mathbf{f}^{\mathrm{exc}}(t). \quad (2.15)$$

Nonlinearities like instantaneous hydrostatic or Froude-Krylov force etc. may then be added to the R.H.S. of this equation. In Paper 5 viscous drag is added to the equations using a simple formulation. Equation (2.15) also provides a suitable means of calculation for linear transient response of marine structures due to e.g. moving loads etc which has been addressed in Paper 3 and Paper 4.

If we take

$$\mathbf{f}'^{\mathrm{R}}(t) = -\int_0^{t_{mem}} \mathbf{k}(t-\tau)\,\dot{\mathbf{x}}(\tau)\,d\tau, \quad (2.16)$$

then Eq. (2.15) can be rewritten as:

$$[\mathbf{M} + \mathbf{A}^{\infty}]\ddot{\mathbf{x}}(t) + \mathbf{C}\mathbf{x}(t) = \mathbf{f}'^{\mathrm{R}}(t) + \mathbf{f}^{\mathrm{exc}}(t) = \mathbf{f}(t) \quad (2.17)$$

In a time-domain simulation code, given the values of the function $\mathbf{f}(t)$, the differential equation in Eq. (2.17) must be calulcated by an integration method such as Runge-Kutta or Newmark-β (e.g. Langen and Sigbjörnsson (1979)). This in fact implies that regardless of the chosen numerical scheme, the convolution integral must be evaluated numerically at each simulation step by e.g. the trapezoidal method.

This is a drawback because integrating the convolution may become computationally demanding depending on the simulation length, simulation step and the DOF of the system. Kashiwagi (2000) stated:

> The present method is still too time-consuming for practical use. A large part of the computation is taken up

> in evaluating the convolution integral for the memory effects.

Similar statements have been made in other texts such as ITTC (2005); ISSC (2006d). These reasons have stimulated significant efforts towards replacing the convolution terms by other approximately equivalent models which yield more efficient solutions. A thorough review and description of these efforts can be found in Paper 3. Some of these approaches replace the convolution integrals by instead using a state-space model which is also a focus in Paper 3. State-space models are of practical interest since they not only provide efficient means of numerical calculations of the convolutions, but also since they are well suited for the computer models used in automatic control (Fossen, 2002; Perez, 2002). Moreover, analysis of stability for dynamic systems is conveniently performed using state-space formulation. In Section 2.7, a description of the state-space equations with an introduction to Paper 3 is presented.

2.7. State-Space Models

Every linear time-invariant system with a finite number of inputs $\mathbf{u}(t)$ and outputs $\mathbf{y}(t)$ can be described by means of a convolution integral in continuous time as

$$\mathbf{y}(t) = \int_0^t \mathbf{h}(t-\tau)\,\mathbf{u}(\tau)d\tau. \tag{2.18}$$

In relevance to the discussion made in Section 2.6, the entries of $\mathbf{y}(t)$ and $\mathbf{u}(t)$ in Eq. (2.18) represent $\mathbf{f}'^{\mathrm{R}}(t)$ and $\dot{\mathbf{x}}(t)$ in Eq. (2.16).

The discretized form of Eq. (2.18) is

$$\mathbf{y}[k] = \sum_{l=1}^{m} \mathbf{h}_d[k-l]\,\mathbf{u}[l], \qquad k = 0, 1, ... \tag{2.19}$$

The system in Eq. (2.18) can also be described by a set of equations of the following form (e.g. Chen (1999)):

$$\begin{aligned} \dot{\mathbf{z}}(t) &= \mathbf{A}'\,\mathbf{z}(t) + \mathbf{B}'\,\mathbf{u}(t) \\ \mathbf{y}(t) &= \mathbf{C}'\,\mathbf{z}(t) + \mathbf{D}'\mathbf{u}(t). \end{aligned} \tag{2.20}$$

In the above equation, $\mathbf{z}$ is the state variable which gives an internal description of the system.

Solution of Eq. (2.20) in continuous time is

$$\mathbf{z}(t) = e^{\mathbf{A}'t}\mathbf{z}(\mathbf{0}) + \int_0^t e^{\mathbf{A}'(t-\tau)}\mathbf{B}'\mathbf{u}(\tau)d\tau \tag{2.21}$$

$$\mathbf{y}(t) = \mathbf{C}'e^{\mathbf{A}'t}\mathbf{z}(\mathbf{0}) + \mathbf{C}'\int_0^t e^{\mathbf{A}'(t-\tau)}\mathbf{B}'\mathbf{u}(\tau)d\tau + \mathbf{D}'\,\mathbf{u}(t) \tag{2.22}$$

One needs to discretize the set of equations in Eq.(2.20) in time, if a digital computer is used. Based on:

$$\dot{\mathbf{z}}(t) = \lim_{\Delta t \to 0} \frac{\mathbf{z}(t+\Delta t) - \mathbf{z}(t)}{\Delta t}, \tag{2.23}$$

and by assuming a piecewise constant input ($\mathbf{u}(t)$):

$$\mathbf{u}(t) = \mathbf{u}(k\Delta t) \equiv \mathbf{u}[k], \qquad k\Delta t \le t < (k+1)\Delta t, \qquad k = 0, 1, ... \tag{2.24}$$

and computing Eq. (2.21) at $t = k\Delta t$, one may arrive at

$$\mathbf{z}[k] \equiv \mathbf{z}(k\Delta t) = e^{\mathbf{A}'kt}\mathbf{z}(0) + \int_0^{k\Delta t} e^{\mathbf{A}'(k\Delta t-\tau)}\mathbf{B}'\mathbf{u}(\tau)d\tau. \tag{2.25}$$

A similar computation of Eq. (2.21) at $t = (k+1)\Delta t$ and reformulation of the results with respect to $\mathbf{z}[k]$ in Eq. (2.25) yields in

$$\mathbf{z}[k+1] \equiv \mathbf{z}((k+1)\Delta t) = e^{\mathbf{A}'\Delta t}\mathbf{z}[k] + \Big(\int_0^{\Delta t} e^{\mathbf{A}'\tau}d\tau\Big)\mathbf{B}'\mathbf{u}[k]. \tag{2.26}$$

Thus, the alternative form of state-space equations in Eq. (2.20) in discrete time will be (Chen, 1999)

$$\begin{aligned} \mathbf{z}[k+1] &= \mathbf{A}'_d\,\mathbf{z}[k] + \mathbf{B}'_d\,\mathbf{u}[k] \\ \mathbf{y}[k] &= \mathbf{C}'_d\,\mathbf{z}[k] + \mathbf{D}'_d\,\mathbf{u}[k], \qquad k = 0, 1, \dots \end{aligned} \tag{2.27}$$

with

$$\mathbf{A}'_d = e^{\mathbf{A}'\Delta T}, \quad \mathbf{B}'_d = \Big(\int_0^{\Delta t} e^{\mathbf{A}'\tau} d\tau \Big) \mathbf{B}', \quad \mathbf{C}'_d = \mathbf{C}', \quad \mathbf{D}_d = \mathbf{D}'. \tag{2.28}$$

where k denotes the current time index. $\mathbf{z}$ is called the state vector and gives an internal description of the system. For a system with p input, q outputs and n state variables, $\mathbf{A}'(\mathbf{A}'_d)$, $\mathbf{B}'(\mathbf{B}'_d)$, $\mathbf{C}'(\mathbf{C}'_d)$ and $\mathbf{D}'(\mathbf{D}'_d)$ are respectively $n \times n$, $n \times p$, $q \times n$ and $q \times p$ constant matrices know as state-space parameters.

In calculating the memory effects in time-domain response simulation of a marine structure, i.e. solving Eq. (2.17) using a numerical time integration method e.g. Newmark-β (e.g. Langen and Sigbjörnsson (1979)), an equation similar to Eq. (2.19) must be calculated at every time step by e.g. the trapezoidal integration method. It must be noted that the calculation of the convolution integral must be performed at each time step regardless of the chosen numerical scheme used for Eq. (2.17).

For a system with scalar input and output, integration of the convolution integral in Eq. (2.19) requires storing m data points at each time step. By using the state-space representation of Eq. (2.27), one needs to save n data points equal to the length of the state. Usually n is less than m, which implies a significant save in the memory.

Moreover, for the scalar-input scalar-output system at each time step k, the total number of multiplications and addition operations needed for Eq. (2.19) are equally m times. The number of multiplication and addition operations in Eq. (2.27) are equally $(n+1)^2$ times. m is usually larger than $(n+1)^2$ and therefore, one may conclude that the state-space model calculations require less CPU time than the convolution integrations. An important note here is the extra CPU consumption from reading the data in the memory during these operations.

For the above reasons, state-space models have become convenient methods for replacing the convolution integrals. There have been numerous efforts in the literature dedicated to such a replacement. These alternatives have been reviewed in Paper 3. The paper discusses how to obtain the replacement models via system identification techniques based on the hydrodynamic data from standard software like WAMIT. Identification methods were categorized depending on the input data used to pose the identification problem.

A comparison was made of the retardation functions that were identified using the following parameter estimation methods:

- Impulse response curve fitting,
- Realization theory,
- Regression in the frequency domain.

The theoretical basis of each method has been reviewed. Identifications by these three methods can be compared in a simple example in terms of estimated model order, accuracy of fit, use of available(input) data, ease of use and generation of stable results. Then, the realization theory and frequency domain regression methods have been compared as applied to a modern container vessel. MATLAB and its built-in functions are used as a platform for coding the identification method and SIMULINK is used to implement the time-domain simulations. Two scenarios have been studied: the dynamic response of the ship due to regular wave induced excitations, and the transient response of the ship after it was released from a displaced condition.

Although some discrepancies have been observed between the results of the realization theory and the frequency domain regression at the identification stage, it is found from the dynamic simulations that both methods are equally accurate in simulating the vessel's response. It is also observed that the fit does not need to be highly accurate to obtain acceptable accuracy. With respect to computational time, it is shown that models based on state-space formulations require less computational effort than models which involve solving for the convolutions. In addition, state-space representation may offer significant savings in memory usage.

2.8. Example Structures

The following structures have been considered in this thesis:

1. The Mega-Float prototype

   The Mega-Float prototype-Phase I has been considered (ISSC, 2006d) in Paper 1. This structure is a pontoon-type VLFS as shown in Fig 2.1. The dimensions of this box-shaped structure are 300 m length, 60 m width and 2 meters height. The VLFS has a draft equal to 0.5 meters. During the tests, the model

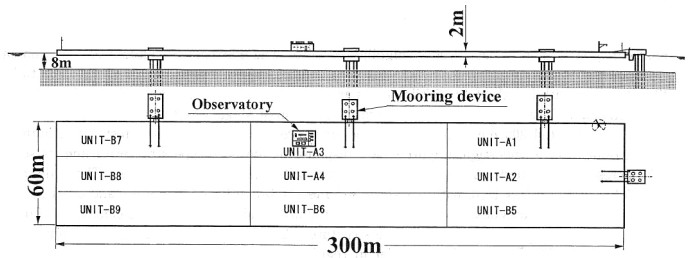

Figure 2.1.: The Mega-Float prototype as studied in Paper 1 (Yago and Endo, 1996a,b).

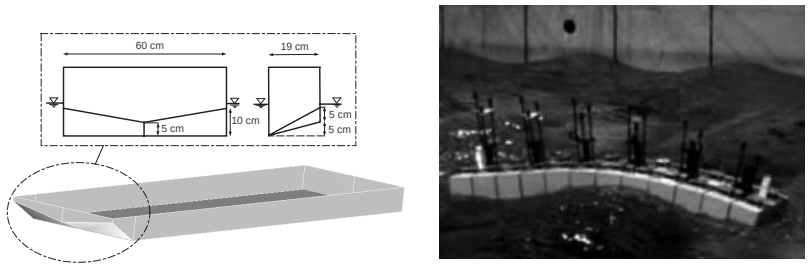

Figure 2.2.: The flexible barge studied in Paper 4 for which test results are available from Malenica et al. (2003). The left figure shows the underwater geometry and the foremost pontoon dimensions. The right figure shows a snapshot of the model during the tests.

is disallowed to move horizontally while it is free to oscillate vertically (Yago and Endo (1996a)).

2. Flexible barge

   This structure is a model of a back-bone type vessel formed by connecting 12 floating sections (Malenica et al., 2003). The sections are 19 cm long, 60 cm wide and 25 cm high. They are connected to each other using steel plates. There is a 15 mm gap between the floats to avoid any contacts between them. The draft of the model is 12 cm. In one of the cases, denoted in the reference as Configuration 2, the foremost floating section is not completely prismatic –as it is the same for the other sections– but is slightly modified (See Fig. 2.2). For this model, the thickness of the joint plates is 6 mm. Further information can be found in the original reference. Some measurements were obtained by releasing the barge from a displaced position. These results are also contained in this thesis (See also Paper 4).

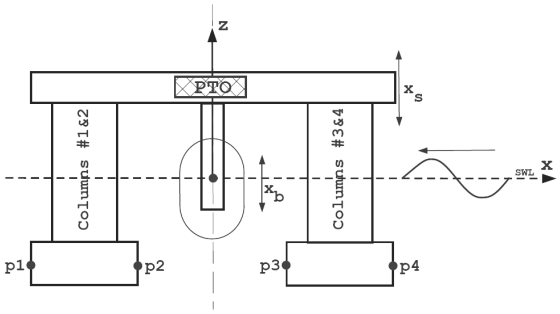

Figure 2.3.: The two-body heaving wave energy converter studied in Paper 5. The power is extracted by the power take-off machinery installed on the deck of the semisubmersible platform from the relative motion between the heaving buoy and the platform.

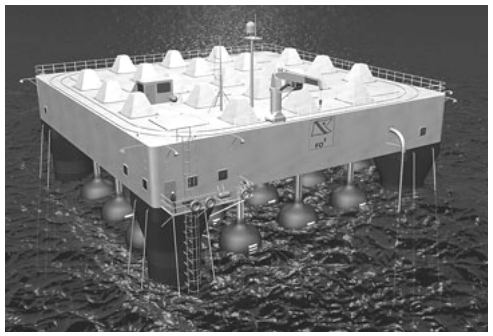

Figure 2.4.: The FO^3 platform, the wave energy converter concept used as the case study in Paper 2 and Paper 6. The concept is novel and thus there are only a very few studies available related to its performance and corresponding load effects in sea waves.

3. A two-body WEC in heave motion

   This wave energy converter consists of two rigid floating bodies: a buoy and a semi-submersible platform, which are restricted to heave only (see Paper 5). Fig. 2.3 shows the schematic view of the concept. The power is extracted from the relative motion between the two bodies using a hydraulic power take-off mechanism. With the objective to increase the performance of the device, a latching control algorithm was also included in the studies. The platform pontoons have a specific design so as to increase the viscous drag force on the supporting structure (Sauder and Moan, 2007).

4. The FO^3 WEC

The studies in Papers 2 and 6 focus on the wave-induced behavior of the so-called FO^3 wave energy converter (see Fig 2.4). The WEC consists of a semisubmersible platform and 21 buoys (see e.g. Leirbukt (2006)). Each buoy in this layout can slide along a corresponding guide which is connected to the deck of the semisubmersible platform. The motion of the buoy is transmitted to hydraulic machinery on the platform deck. In this way, the wave energy is transformed into electricity from the relative motion of each buoy and platform.

3. Case Studies

3.1. General

An important aspect of the thesis work has been to develop a methodology to determine the wave-induced load effects in flexible and multiple-body dynamic systems and implement it in computer codes. These methods have been applied in the following case studies to illustrate the applicability of the methodology and to illustrate certain features of the physical behavior:

1. Hydroelastic analysis of VLFS in the frequency domain
2. Motion analysis of multi-body WEC in the frequency domain
3. Flexible-body simulations in the time domain
4. Two-body WEC simulations in the time domain
5. Structural analysis of multi-body WEC in the frequency domain

In the following sections, a brief description of each case study and its results will be given.

3.2. Hydroelastic Analysis of VLFS in the Frequency Domain

The generalized modes approach is applied in Paper 1 to analyze the linear steady-state motions of arbitrarily-shaped single or multiple flexible bodies. It is a frequency-domain approach based on interfacing the information between FEM and BEM. Both two and three dimensional mode shapes can be used in the analysis. The 3D mode shapes have been generated by using ABAQUS. Two different interface codes have been written to introduce the 2D or 3D mode shape data to WAMIT by interacting with the software during run-time.

The method has been validated by comparing the numerical results with available numerical studies by Fu et al. (2006) and experimental results by Yago and Endo (1996b) for a 300 meters long model of the MegaFloat airport (1^{st} phase experiments, see Suzuki (2005)). Comparisons made for the frequency response functions of displacements at different points along the structure strongly suggest that the approach is accurate (see Fig. 3.1). Moreover, the method can use double plane symmetry which enables a more efficient response analysis.

The results also clearly show a significant contribution to wave-induced (pressure and thus displacement) responses from the elastic modes, which accentuates the importance of the hydroelasticity. This can be seen from the rigid and flexible body displacements in Fig 3.1. The contributions from flexible modes become higher for longer waves.

The analysis showed that the displacements are larger at the two ends of the structure than the responses in the middle of the structure. This is in agreement with the test results. Another finding of this study is that the structural displacements in the up-stream wave were larger than the ones in the down-stream wave which is explained by larger diffraction (wave-structure interaction) effects in the up-stream region. Such effects vanish as the wave length increases.

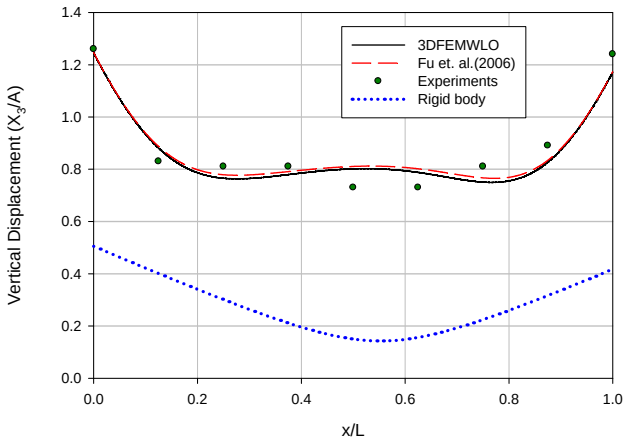

Figure 3.1.: Typical result from Paper 1: comparison of the predicted displacements with available experimental measurements by Yago and Endo (1996b) and another study by Fu et al. (2007). Hydroelastic behavior of the structure is evident from the comparison between results obtained for the rigid and flexible body.

The study in Paper 1 increased the level of confidence in WAMIT and showed the feasibility of using (adapting) the software in hydroelastic calculations. A similar tailor-made approach has been developed in Paper 2 based on the idea, knowledge and experience gained in this work that interprets the multi-body modes of motion to WAMIT by using a generalized modes approach.

3.3. Motion Analysis of Multi-Body WEC in the Frequency Domain

Using a generalized modes approach, linear wave-induced steady-state motions of different components in the so-called FO^3 platform WEC has been studied in the frequency domain (see Appendix. D and Paper 2). The WEC consists of a semisubmersible platform and 21 buoys (see e.g. Leirbukt (2006)). Each of the buoys slides along a corresponding guide which is connected to the deck of the semisubmersible platform. Based on this consideration, the motions of the components in the WEC may be decomposed into the following 27 modes (Paper 2):

- System surge (platform and buoys),
- System sway (platform and buoys),
- (Independent) heave of the platform,
- Roll of platform and buoys considering the buoys to slide along the guides,
- Pitch of platform and buoys considering the buoys to slide along the guides,
- System yaw (platform and buoys),
- (Independent) heave of each of the 21 buoys.

Dynamic analysis of such a concept is challenging even in the frequency domain due to its kinematic complexity and hydrodynamics caused by the interactions between the wave and the structure. No previous studies were found for this FO^3 concept that could provide information regarding wave-induced load effects on the components of the WEC and the device performance in a realistic ocean environment. The main objective of Paper 2 is to develop a method that could address the following questions:

- What is the performance of the WEC in low to moderate waves?
- Will all the buoys in the current layout contribute to power absorption?
- What is the effect of wave directionality on the absorbed power?
- What kind of motions will be experienced by the WEC components in waves?
- Are there any considerable effects from power take-off mechanisms on the response of each component?
- How strong are the interaction effects between the bodies and the waves?
- Provide a basis for structural response assessment of the WEC, as reported in Paper 6.

Observation of the results with regard to problem symmetry along the wave direction and trend of the wave attenuation verified the method to some extent. Typical results are shown in Fig. 3.2. Buoys 2 and 3 are located upstream and between the platform columns parallel to the wave propagation direction, respectively. The results were compared with available results obtained by Rogne (2007) who considers the motions in the vertical plane due to a following-seas wave. For comparison of the results of other components see Paper 2). The validation procedure in this analysis was limited to this case only, because no relevant experimental results were available.

The results of the power absorption for different power absorption coefficients, b_u, at different sea states suggest the optimal value of b_u to be between 100 to 150 $\frac{kNs}{m}$.

The results show a significant reduction in the power-absorption by the buoys located at the down-stream wave compared to the buoys in the up-stream wave. Similar results have been observed for other wave directions. This suggests that the wave is attenuated along the WEC and most of the wave energy is already absorbed by the buoys in the up-stream wave condition (see Paper 2). The buoys in the fore most down-stream wave, produce almost no power compared to the ones in the up-stream waves. This result may suggest a reduction in the number of buoys.

Observing the reported plots of the power absorption for different mean wave directions in short-crested irregular seas, it was found

that the total power absorption was independent of the mean wave direction. However, the mean wave direction affects the pattern of the power absorbed by the individual buoys.

Large motions were observed for the buoys at certain wave frequencies when power-take off mechanism is neglected. This could be related to near-trapping of the waves occurring in the gaps between the columns and the buoys. Further research needs to be carried out to address this issue in more detail.

Fig. 3.2 shows that the power take-off has reduced the motions of different components of the WEC (especially around the natural frequencies). Similar results have been found for motion response in the oblique waves (see Paper 2).

The method could be used conveniently to export the hydrodynamic information e.g. pressure and wave elevation for post processing purposes. An interfacing procedure has been developed in Paper 6 to introduce the pressure information by the method to the structural software.

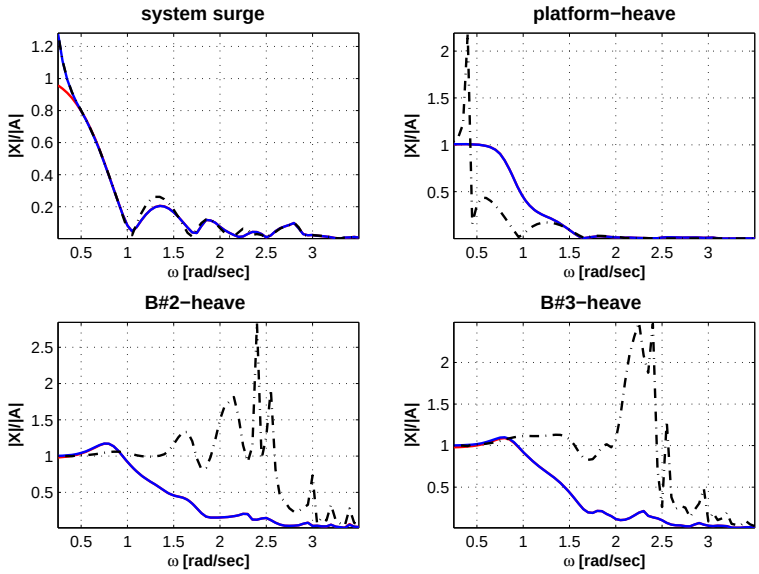

Figure 3.2.: Typical results from Paper 2: WEC motion response in following-seas waves with/without consideration of power take-off. Note that the results from the current method have been plotted on top of the results by Rogne (2007), i.e. they yield identical results. The dash-dotted lines indicate the results in the absence of any power-absorption mechanism while the solid lines represents the response in a power take-off mode.

3.4. Flexible-Body Simulations in the Time Domain

As mentioned in Section 3, one of the most suitable applications of state-space models could be in the simulation of flexible marine structures. In these simulations, there are typically many DOF associated with the elastic modes of the structure. In addition, the simulation steps need to be small enough so as to capture the dynamics associated with the higher order modes (Kashiwagi, 2004). In this context, the equations of motion described in Paper 3 have been extended to account for the flexibility of marine structures (see Paper 4). Paper 4 also gives further substantiation regarding the accuracy and efficiency of the simulations using state-space models as initially addressed in Paper 3.

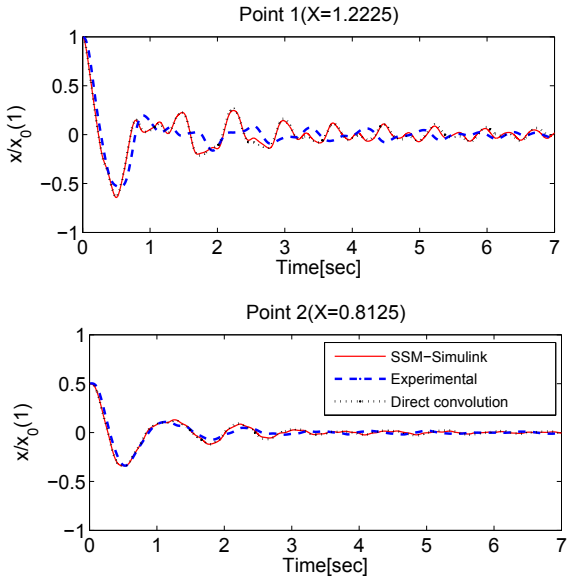

Figure 3.3.: Typical results from Paper 4: Transient response of the barge released from an initial displaced condition. Position x= 1.2225 corresponds to the bow. Dashed lines represent the results of the measured response reported by Malenica et al. (2003); and solid lines represent the results for dynamic response simulations using state space models. The dotted lines are the simulation results by directly integrating the convolutions.

Application of the method was exemplified by considering a (very) flexible barge (Malenica et al., 2003). Dynamic response of the vessel due to regular waves as well as its transient response after release

from an initial displacement was simulated.

Typical results are shown in Fig. 3.3. Some discrepancies between the numerical and experimental results of the transient response of the initially displaced barge were experienced. Further details about the analysis may be found in Paper 3. The source of discrepancies could be related to the inhomogeneous distribution of structural and hydrodynamic properties of the experimental model. Another source of the discrepancy between numerical simulations and the experimental results could be the fluid flow in the gaps between the floating sections which exert nonlinear viscous forces which are not represented by the numerical model.

Mode shape sensitivity analysis (reported in the paper) showed that five modes were enough to represent the hydroelastic behavior of the barge. Heave mode was found to be the most contributing mode to the steady-state wave-induced response of the barge. For dynamic response of the barge due to its release from an initial displacement, pitch was found to be the most contributing mode to the response. Both heave and the first flexible bending mode were found to be equally important in this case.

Moreover, it was found that the state-space models can accurately replace the convolution integrals. For the same level of accuracy, simulations based on the state-space model representations were found to be much more efficient than those integrating the convolutions, as described in Paper. 3.

3.5. Two-Body WEC Simulations in the Time Domain

In Paper 5, a two-body WEC with hydraulic power take-off subject to phase control is studied. The wave energy converter consists of two rigid floating bodies: a buoy and a semi-submersible platform, which are restricted to heave only. The power is extracted from their relative motions.

The dimensions of the platform pontoons were tuned such that the wave exciting force on the platform will be about the same in magnitude as the buoy but in the opposite phase within a design wave range of 5 to 12 seconds.

A hybrid frequency-time domain model has been set up. Fluid mem-

ory effects have been considered using a state-space representation instead of the convolution integrals. The hydrodynamic interactions of the two bodies have also been accounted for in the modeling.

One of the objectives of the paper was to address the effect of drag on the performance of the WEC. This was accomplished by utilizing a drag force formulation proportional to $|u - \dot{\eta}_1|(u - \dot{\eta}_1)$ similar to Eq. (2.1) in Section 2.3. The drag coefficient was chosen based on the work by Sauder and Moan (2007). The water particle velocity in the drag force formulation for each column is found by averaging the simulated particle velocities of two specific points belonging to the pontoon of the given column. The convolution integrals corresponding to calculations of the particle velocities stemming from the radiation potential were also replaced by using state-space models.

A power take-off mechanism was accommodated in the model. A latching control algorithm was also included in the simulations, but these are not among the contributions of the author. Yet, the details can be found in the paper. No experimental measurements were available for validation of the results.

Using this model, it was concluded that the viscous drag force in the pontoons of the semisubmersible platform reduces the absorbed power by the device.

A large influence on the absorbed power was found from the force compensation. By decreasing the pontoon size and thus decreasing the wave exciting force on the platform within the design ranges, more output power was observed for the WEC.

An indication was made regarding the output of the system when the platform was fixed or free to oscillate. For most of the considered wave conditions, fixing the platform improved the absorbed power results. However, at one of the wave conditions (denoted in the paper as I2), more power could be absorbed for a free platform.

Although it was possible to consider nonlinearities e.g. buoyancy corresponding to instantaneous position of the bodies, it was decided by the first author of the paper not to include them and instead limit the parametric study to the ones already addressed in the paper.

3.6. Structural Response Analysis of Multi-Body WEC in the Frequency Domain

In Paper 6, the linear steady-state structural response of the FO^3 concept (the multi-body WEC described in Section 3.3) with power take-off, is analyzed in the frequency domain. The hydrodynamic and structural problems are solved by means of WAMIT and ABAQUS.

The motion analysis is carried out based on the work reported in Paper 2. The hydrodynamic effects of the guides, which were neglected in Paper 2, are considered in this study. A general procedure is established to interface the relevant information between the two software systems. Such information includes the radiation, diffraction and restoring force pressures and inertia loads, etc. The structural response is obtained by a quasi-static approach. The power take-off mechanism is replaced by four beams. The sliding of the buoys along the guides has been considered, as well.

The objective is to investigate the still water and wave induced internal loads in the column-deck and guide-deck connections in the form of transfer functions. To demonstrate the approach, calculations are performed for following- and oblique-sea wave conditions. The RAOs obtained in this way are well suited for the statistical analysis of loads under certain design sea-states.

One important issue of this analysis was to ensure that the information is transferred correctly by the interfacing procedure between the motion analysis module (WAMIT) and the structural analysis module (ABAQUS). To do this, a comparison was made between the power take-off force results for each of the 21 buoys from the motion analysis stage and the sum of the axial forces in the corresponding structural elements (four beams) representing the power-take off mechanism for the buoy in the structural analysis module. In addition, total force balance in the WEC structural model has been monitored and the unbalance (error) was ensured to be small relative to the dynamic forces.

Some validation of the interfacing procedure was made by comparing the numerical results with analytical solutions for a cantilever circular cylinder, which is reported in Appendix E. Some verification has been made by checking the results for symmetry along the wave direction and the trend of wave attenuation. No experimental results were available for validation of this concept.

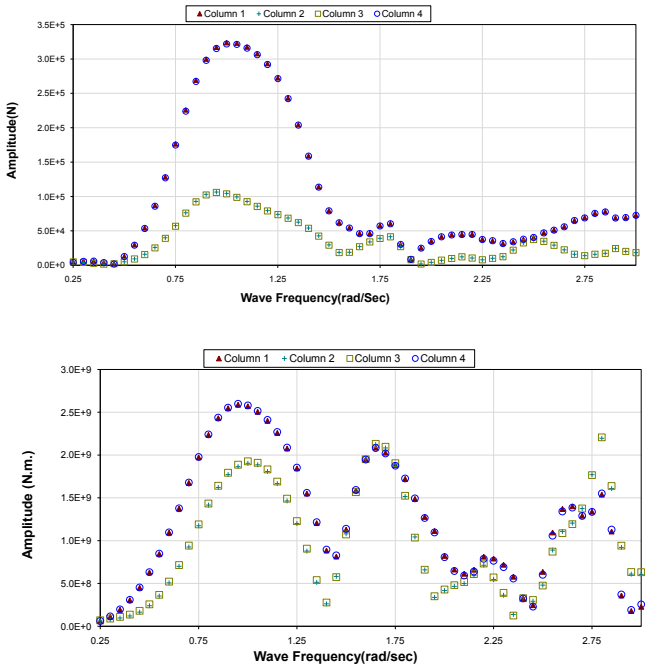

Figure 3.4.: Typical results from Paper 6: The frequency response functions of the axial forces in the column-deck connections (Top) and the frequency response functions of the bending moment in the column deck connections (Bottom). The results are given for a unit wave amplitude. Columns 1 and 4 are located in the up-stream wave, while columns 2 and 3 are located in the down-stream wave.

Typical results are shown in Fig. 3.4. The results of the axial force and bending moments in the figure (together with the ones in the paper) clearly suggest that the wave is attenuated along the structure due to the action of the buoys and existence of power absorption mechanism. Wave attenuation has been observed previously from the results of the power absorption of each of the 21 buoys in Paper. 2. The results also show that the loads on the structure decrease as the incident waves become longer and the structure rides the waves. The maximum loads on the columns occur at wave lengths equal to two time the distance of the two columns.

Another interesting result comes from the wave-induced load effects in short waves. The axial forces tend to decrease for decreasing wave lengths as the wave-induced pressure decreases at the bottom of the columns and pontoons. However, for wave lengths of about the distance between a buoy and a column (about 8 meters), one observes

significant increase in the column bending moments. This may suggest that there is wave-trapping occurring between the columns of the semisubmersible and the adjacent buoys.

The wave-induced axial forces become comparable to the ones from static load case (i.e. when structure is at rest in still water) when the wave height increases to more than about 4 meters.

4. Conclusions and Recommendations about Further Research

4.1. Conclusions

4.1.1. General

The focus of this thesis is the development and application of methods to determine wave-induced load effects of stationary flexible and multi-body floating systems. The numerical studies are based on the linear 3D radiation/diffraction code WAMIT, and 3D FE analysis software ABAQUS. Both software are among the state-of-the-art in marine structure applications. In some of the studies, information was shared between the two programs by means of an interfacing procedure. The case studies in this thesis comprise the Mega-Float prototype, a flexible barge and two different multi-body wave energy converter concepts. Since these concepts are very recent, there are no or limited information about them in the literature. In the following, the conclusions are given based on the developed methodologies and lessons on the physics of the case studies.

4.1.2. Methodologies

An alternative method was developed and validated to predict the frequency domain linear wave-induced steady-state displacements of VLFS. Since the method is based on the generalized modes approach in WAMIT, it thus provides further validation of the hydrodynamic software, as well. Comparisons suggest that the differences are minor between the current approach and the other available method. Both methods predicted the VLFS displacements accurately.

Following a similar approach (generalized modes), a method was developed to study the frequency-domain linear wave-induced steady-

state motions of multi-body wave energy converters. The method gives the statistics of device motions and theoretical absorbed power for different sea states and directions. While maintaining the same accuracy with standard means of solution, the current method is more efficient and enables easier handling of data export like field or body surface pressure. Extension of the method enabled predicting linear wave-induced steady-state structural response of multi-body WECs in the frequency domain. The methodology allows for three dimensional hydro-structural analysis and accounts for directionality of the waves. It also considers hydrodynamic interactions between the floating bodies and the waves. An equivalent approach that could address structural response analysis of multi-body wave energy converters considering their hydrodynamic interactions was not available in the literature.

Some of the work in this thesis focused on developing time-domain models of marine structures based on their frequency-domain data for the linear behavior. The convolution integral that appears in the time-domain formulation implies significant computational efforts for long simulations with large degrees of freedom or short time steps. Part of the work in this thesis (Paper 3) reviewed, classified and investigated different methods to approximate the radiation force models. It concluded that a significant reduction in computation and memory is achieved by using state-space models to approximate convolution integrals of radiation forces. It was shown that the state-space models maintain practically the same accuracy as of the convolution integrals. The identification methods by which state-space models are usually obtained were compared with respect to the estimated model order, accuracy of fit, use of available (input) data, ease of use and generation of stable results. It was shown that the investigated methods were equally accurate. Moreover, it was suggested that there is no need for a highly accurate identification fit i.e. it is sufficient to use relatively low order identifications. Such lessons were not already known within the literature.

Based on the above achievement, an efficient time-domain approach was developed to simulate the transient response for a flexible structure. The method accounts for fluid memory effects using computationally efficient state-space models. Validation of results with experimental measurements further substantiated the accuracy and efficiency of simulations that incorporate state-space models to approximate the radiation forces. In this way, the paper accentuated the application of state-space models in simulation of hydroelastic response for structures like VLFS. The application of state-space

models to simulation of response for flexible marine structures is an original contribution for this thesis.

The application of state-space models was extended to simulation of response and performance for a two-heaving-body wave energy converter with power take-off and control. The contributed dynamic model provided a suitable basis for motion analysis. It considered the fluid memory effects using a state-space formulation. It also addressed nonlinear viscous drag to some extent using a simple formulation. The motion simulator was linked to models of power take-off and latching control.

4.1.3. Findings and Lessons on the Physics

Comparison between the hydroelastic response of the Mega-Float and rigid body response results suggests that hydroelasticity becomes significant as wave length increases. The displacements vary along the length of the structure. However they are larger towards the two ends of the vessel. In addition, the results conclude that there are diffraction effects occurring at the upstream wave which result in larger displacements in that region. This effect vanishes as the waves become longer.

The study of the flexible barge clearly substantiated the accuracy and efficiency of the state-space models for time-domain response simulation of marine structures. By a mode sensitivity study, the method suggested the number of required modes and showed the contribution of each individual mode to the wave-induced displacements.

The analysis of the two-body-heaving WEC provided information regarding the statistics of the absorbed power. Comparison of the two-body oscillations to a one-body oscillation revealed that the two-body concept can be beneficial in terms of power output if the geometry and the parameters are chosen correctly. Moreover, the effect of increasing the drag force on the platform seem to have a decreasing effect on the absorbed power. It was understood that latching control can significantly increase the performance of the WEC. Moreover, flow losses in the hydraulic system can become substantial and must be investigated in the design process. It should be mentioned that the investigations of latching and power take-off in this work were not directly among the contributions of the author, but these findings were based on the motion analysis model of the

author.

The analysis of the FO^3 WEC with and without off-take shows a significant motion reduction for the components of the device as a consequence of power absorption, especially around the resonance frequencies. The results clearly show that the wave attenuates along its progressing direction. It was also found that the power absorbed by the device was independent of the mean wave direction. However, wave direction changes the pattern of motions and absorbed power (and in turn the experienced internal forces) by each individual component. Monitoring the power absorbed by each individual buoy suggests reduction in the number of buoys. The structural response analysis of the FO^3 WEC shows reduction in the internal forces in the components along the wave direction. This is again due to the action of the point absorbers which leads to attenuation of the wave passing along the WEC. The results also suggest wave-trapping between the columns and buoys as well as between pairs of buoys which results in significant increase in the wave-induced internal forces. The observation seems to be identified as a novel feature.

4.2. Original Contributions

The original contributions of this thesis comprise developed methodologies and findings based on these tools, which is reviewed in the following:

4.2.1. Methodologies

The thesis

1. Established a method for linear frequency-domain wave-induced 3D motion analysis of VLFS with arbitrary (complex) geometry,

2. Review and classification of the methods for replacing convolution integrals and investigation of identification techniques to obtain state-space model approximations for radiation force convolutions with respect to the estimated model order, accuracy of fit, use of available (input) data, ease of use and generation of stable results.

3. Efficient time-domain simulation of dynamic response for flexible and multi-body marine structures by considering memory effects and convolution replacement by means of state-space models.

4. Established an interface between WAMIT and ABAQUS for structural response analysis of marine structures with emphasis on multi-body systems.

5. Developed a time-domain simulation tool for a two body-heaving wave energy converter considering fluid memory forces using state-space models, accounting for off-take and latching control and addressing the effect of viscous drag on the pontoons of the supporting structure.

6. Linear wave-induced 3D motion and structural response analysis for the FO^3 wave energy converter considering power take-off and hydrodynamic interactions. The developed method can be applied to direct design of the novel WEC concept.

4.2.2. Findings and Lessons on the Physics

The thesis

1. Demonstrated a significant reduction in computation and memory achieved by using state-space models to approximate convolution integrals of the radiation forces.

2. Demonstrated that state-space models maintain practically the same accuracy as the convolution integrals.

3. Understanding the degree of identification needed to achieve a desired accuracy for simulations using state-space models.

4. Demonstrated the sensitivity of the wave-induced response to the individual modes of motion for the flexible barge and suggested the number of modes required for the hydroelastic analysis of the structure.

5. Provided information regarding the absorbed power and performance of the FO^3 wave energy converter and its dependence on the power absorption coefficient.

6. Investigated the influence of wave directionality on the power absorption of the FO^3 wave energy converter.

7. Demonstrated the effect of power absorption on the motions of different components in the FO^3 wave energy converter.

8. Provided information about wave attenuation along the wave progression direction for the FO^3 wave energy device and its influence on the absorbed power and structural loads.

9. Provided information about the axial force and bending moment in the column- and guide-deck connections of the FO^3 platform and observing the diffraction/interaction effects on the loads.

10. Nonlinear wave-induced response simulation of a two-body heaving wave energy converter in time domain considering hydrodynamic interactions, fluid memory effects, power take-off, and latching control and accounting for viscous drag due to novel pontoon design.

11. Showed the effect of increasing the viscous drag on the performance of the two-body heaving wave energy converter.

12. Demonstrated the influence of force compensation on the power output i.e. geometrical aspects of the design.

13. Comparison of power off-take performance in a fixed and free platform in the two-body heaving wave energy device.

4.3. Recommendations for Future Work

In any research study, there will always be room for further improvements. In the following, the author would like to mention some of the key ideas which may be pursued as a continuation of the research presented in this thesis.

The work in Paper 4 can be complemented by applying state-space models to time-domain study of a full-size VLFS. Although the previous works in Papers 3 and 4 clearly showed that there can be significant reduction of CPU time and memory for simulations by using state-space models, it may be interesting to see the benefits of such an approach in the simulation of a full-size VLFS.

Another interesting issue could be to extend the state-space model identifications to handle second-order force model approximations in terms of quadratic transfer functions for marine structures. A major concern in this context is that such calculations involve double

convolutions which would increase the simulation time significantly. However, there are no techniques available to date that could enable a state-space model approximation of the convolutions corresponding to the quadratic transfer functions.

As a continuation of the work in Paper 5, one can include the nonlinear hydrodynamic forces using nonlinear Froude-Krylov and/or buoyancy loads for example. The model in Paper 2 can be transformed into time domain by the available techniques and can also consider nonlinear hydrodynamic forces. A more complete analysis could be carried out by including the effect of e.g. the mooring lines.

The structural methodology presented in this thesis was applied in the frequency domain. However, the interfacing approach also applies to simulation of time-domain structural responses. A topic of interest could be inclusion of nonlinear interactions in the structure e.g. due to the connectors etc. All these studies are feasible by running the entire analysis using a time-domain ABAQUS simulation.

The interfacing procedure in this thesis has been applied to transfer the information from the hydrodynamic and motion analysis of rigid floating bodies. The interface code can be extended to transfer the pressure and body forces due to the elastic modes, as well. In this way, structural response analysis of flexible floating bodies with hydroelasticity can be carried out.

As mentioned earlier, the methods reported in Papers 2, 5 and 6 have been verified to some extent by using other available methods, testing for special conditions, or comparison with simple analytical solutions. Validation of such models may be accomplished by comparison with possible experimental results. This corresponds to motion (and perhaps absorbed power) measurements for Paper 2 and Paper 5 and load measurements for Paper 6.

References

ABAQUS. Simulia. www.simulia.com.

Airey, R., G. Hartnup, and R. Kenison (1989). Identification of Morison coefficients from test results of a model production riser. In *The International Offshore Mechanics and Arctic Engineering Symposium*.

ANSYS. http://www.ansys.com/products/multiphysics.asp.

Beck, R. F., A. M. Reed, and E. Rood (1996). Application of modern numerical methods in marine hydrodynamics. In *Transactions of the Society of Naval Architects and Marine Engineers*.

Bendat, J. S. (1998). *Nonlinear Systems Techniques and Applications*. John Wiley & Sons Inc.

Bertram, V. (2000). *Practial Ship Hydrodynamics*. Elsevier Butterworth-Heinemann.

Bishop, R. E. D. and W. Price (1979). *Hydroelasticity o Ships*. Cambridge University Press.

Brebbia, C. and J. Dominguez (1989). *Boundary Element: An Introductory Course*. Computational Mechanics Publications, Southampton, Boston.

Chen, C. (1999). *Linear System Theory and Design*. Oxford University Press.

Chen, X.-J., Y.-S. Wu, W.-S. Cui, and J. J. Jensen (2006). Review of hydroelasticity theories for global response of marine structures. *Ocean Engineering 33*, 439–457.

Cruz, J. (2008). *Ocean Wave Energy*. Springer Verlag.

Cummins, W. (1962). The impulse response function and ship motions. *Schiffstechnik 9*, 101–109.

Dean, R. G. and R. A. Dalrymple (1991). *Water Wave Mechanics for Engineers and Scientists*. World Scientific.

Evans, D. V. and R. Porter (1997). Near-trapping of waves by circular arrays of vertical cylinders. *Applied Ocean Research 19*, 83–99.

Faltinsen, O. M. (1990). *Sea Loads on Ships and Offshore Structures*. Cambridge University Press.

Faltinsen, O. M. (2005). *Hydrodynamic of High-speed Marine Vehicles*. Cambridge University Press.

Faltinsen, O. M. and A. Timokha (to be published). Sloshing.

Ferziger, J. H. and M. Peric (2002). *Computational Methods for Fluid Dynamics*. Springer-Verlag.

Fossen, T. (2002). *Marine Control Systems: Guidance, Navigation and Control of Ships, Rigs and Underwater Vehicles*. Marine Cybernetics, Trondheim.

Fu, S., T. Moan, X. Chen, and W. Cui (2006). Hydroelastic analysis of flexible floating interconnected structures. In *4th Int. Conference on Hydroelasticity in Marine Technology, , Shanghai, China.*

Fu, S., T. Moan, X. Chen, and W. Cui (2007). Hydroelastic analysis of flexible floating interconnected structures. *Ocean Engineering 34*, 1516–1531.

Fujikubo, M. (2005). Structural analysis for the design of vlfs. *Marine Structures 18*, 201–226.

Fujikubo, M. and T. Yao (2001). Structural modeling for global response analysis of vlfs. *Marine Structures 14*, 295–310.

Girard, A. R., D. M. Empey, W. C. Webster, and J. K. Hedrick (2003). An experimental testbed for mobile offshore base control concepts. *Journal of Marine Science and Technology 7*, 109–118.

Hals, J., R. Taghipour, and T. Moan (2007). Dynamics of a force-compensated two-body wave energy converter in heave with hydraulic power take-off subject to phase control. In *Proceedings of The 7th European Wave and Tidal Energy Conference, Porto, Portugal.*

Henderson, R. (2006). Design, simulation, and testing of a novel hydraulic power take-off system for the pelamis wave energy converter. *Renewable Energy 31*, 271–283.

Hess, J. (1990). Panel methods in computational fluid dynamics. *Annual Review of Fluid Mechanics 22*, 225–274.

Hess, J. and A. Smith (1964). Calculation of nonlifting potential flow about arbitrary three-dimensional bodies. *Journal of ship research 8*, 22–44.

HYDROSTAR. Bureau Veritas.

Iijima, K., T. Yao, and T. Moan (2008). Structural response of a ship in severe seas considering global hydroelastic vibrations. *Marine Structures*. In Press.

ISSC (2006a). Report of Specialist Task Committee I.2, Loads.. In P. Frieze and R. Shenoi (Eds.), *Proceedings of the 16th International Ship and Offshore Structures Congress, Elsevier, Southampton, UK*, pp. 85–173.

ISSC (2006b). Report of Specialist Task Committee II.1, Quasi-static Response. In P. Frieze and R. Shenoi (Eds.), *Proceedings of the 16th International Ship and Offshore Structures Congress, Elsevier, Southampton, UK*, pp. 173–257.

ISSC (2006c). Report of Specialist Task Committee V.4, Ocean Wind and Wave Energy Utilization. In P. Frieze and R. Shenoi (Eds.), *Proceedings of the 16th International Ship and Offshore Structures Congress, Elsevier, Southampton, UK*, pp. 165–211.

ISSC (2006d). Report of Specialist Task Committee VI.2, Very Large Floating Structures. In P. Frieze and R. Shenoi (Eds.), *Proceedings of the 16th International Ship and Offshore Structures Congress, Elsevier, Southampton, UK*, pp. 391–442.

ITTC (2005). The Seakeeping Commitee: Final Reports and Recommendations to the 24th ITTC.

Jiao, L.-L., S.-X. Fu, and W.-C. Cui (2006). Comparison of approaches for the hydroelastic response analysis of very large floating structures. *Journal of Ship Mechanics 10*, 71–91.

Kashiwagi, M. (1996). A b-spline galerkin method for computing hydroelastic behavior of a very large floating structure. In *International workshop on very large floating structures, VLFS96, Hayama, Japan,*, pp. 149–56.

Kashiwagi, M. (2000). A time-domain mode-expansion method for calculating transient elastic responses of a pontoon-type vlfs. *Marine Science and Technology 5*, 89–100.

Kashiwagi, M. (2004). Transient response of a VLFS during landing and take-off of an airplane. *Journal of Marine Science and Technology 9*, 14–23.

Kim, B. W., J. H. Kyoung, S. Y. Hong, and S. K. Cho (2005). Investigation of the effect of stiffness distribution and structure shape on hydroelastic responses of very large floating structures. pp. 210–217.

Langen, I. and R. Sigbjörnsson (1979). *Dynamic analysis of Marine structures(In Norwegian)*. TAPIR.

Lee, C.-H. and J. Newman (1998). *HIPAN 2.0.2 User's Manual*. Massachussets Institute of Technology.

Lee, C.-H. and J. Newman (2004). *Numerical models in fluid-structure interaction*, Chapter Computation of wave effects using the panel method. WIT press. preprint.

Leirbukt, A, A. (2006). A wave of renewable energy. *ABB review*, 29–31.

Letcher, J. S. (1998, April). *HIP2FEA, XYZ2NUV User Documentation*. AeroHydro Inc.

Lin, W. and D. Yue (1996). Numerical simulations for large amplitude ship motions in the time domain. In *18th Symposium on Naval Hydrodynamics,USA*.

Ljung, L. (1999). *System Identification, Theory for the user*. Prentice Hall.

Malenica, S., B. Molin, F. Remy, and I. Senjanović (2003). Hydroelastic response of a barge to impulsive and nonimpulsive wave loads. In *3rd Int. Conference on Hydroelasticity in Marine Technology, Oxford UK*.

Malenica, S., E. Stumpf, and F.-X. S. X.-B. Chen (2008). Consistent hydro-structure interface for evaluation of global structural responses in linear seakeeping. In *27th International Conference in Offshore Mechanics and Arctic Engineering, Estoril, Portugal*.

Malenica, S., E. Stumpf, V. Delafosse, X. B. Chen, and I. Senjanović (2006). Some aspects of hydro-structrue interfacing in seakeeping. In *16th International Offshore and Polar Engineering Conference, San Francisco, CA, USA*.

Maniar, H. D. (1995). *A three-dimensional higher order panel method based on B-splines*. Ph. D. thesis, Department of Ocean Engineering, MTi.

Maniar, H. D. and J. Newman (1996). Wave diffraction by a long array of cylinders. *Journal of Fluid Mechanics 339*, 309–330.

MATLAB. Mathworks. www.mathworks.com.

McCabe, A., A. Bradshaw, and M. Widden (2005). A time-domain model of a floating body using transforms. In *Proceedings of the 6th european wave and tidal energy conference*. University of strathclyde, Glasgow.

Moan, T. (2003). Marine structures for the future. In *The Inaugural Keppel Lecture held at the National University of Singapore*.

MOB Project Team (2000). Mobile offshore base (MOB) science and technology program final report. Technical Report TR-2125-OCN, Naval Facilities Engineering Service Center Port Hueneme, California 93043-4370.

Monaghan, J., J. (2005). Smoothed particle hydrodynamics. *Reports on Progress in Physics 68*, 1703–1759.

NASTRAN. MSC Software. www.mscsoftware.com.

Newland, D. E. (1993). *An Introduction to Random Vibrations, Spectral and Wavelet Analysis*. Prentice Hall.

Newman, J. (1977). *Marine Hydrodynamics*. MIT Press.

Newman, J. (1994). Wave effects on deformable bodies. *Applied Ocean Research 16*, 47–59.

Ochi, M. K. (1998). *Ocean Waves*. Cambridge University Press.

Ogilvie, T. (1964). Recent progress towards the understanding and prediction of ship motions. In *5th Symposium on Naval Hydrodynamics*, Bergen, Norway, pp. 3–79.

Ohmatsu, S. (1997). Numerical calculation of hydroelastic responses of pontoon type vlfs. *J Soc Naval Arch Jpn 182*, 329–340. (in Japanese).

Pákozdi, C. (2008). *A Smoothed Particle Hydrodynamics Study of Two Dimensional Nonlinear Sloshing in Rectangular Tanks*. Ph. D. thesis, Norwegian University of Science and Technology.

Palo, P. (2005). Mobile offshore base: Hydrodynamic advancements and remaining challenges. *Marine Structures 18*, 133–147.

Perez, T. (2002). *Ship Motion Control: Course Keeping and Roll Reduction using Rudder and Fins*. Springer, London.

Raj, D. and M. J. Edwards (1999). Nonlinear time-domain structrual finite element analysis of a mobile offshore base using distributed hydrodynamic loads. In *The Third International Workshop On Very Large Floating Structures, Honolulu, Hawaii, USA*.

Raj, D. and M. J. Edwards (2001). Coupling linear hydrodynamics to non-linear structural analysis of large floating structures. In *The International Conference on Offshore Mechanics and Arctic Engineering*.

Riggs, H., H. Suzuki, R. Ertekin, J. W. Kim, and K. Iijima (2008). Comparison of hydroelastic computer codes based on the ISSC VLFS benchmark. *Ocean Engineering 35*, 589–597.

Rogne, Y. (2007). Dynamic analysis of a wave energy converter-a frequency domain approach. Master's thesis, Norwegian University of Science and Technology.

Sarpkaya, T. and M. Isaacson (1981). *Mechanics of Wave Forces on Offshore Structures*. Van Nostrand Reinhold Company: New York.

Sauder, T. and T. Moan (2007). Experimental investigation of the hydrodynamic characteristics of a novel column design for semi-submersible platforms. In *The Seventeenth International Offshore and Polar Engineering Conference*.

Sen, D. (2002). Time-domain computation of large amplitude 3d ship motions with forward speed. *Ocean Engineering 29*, 973–1002.

SESAM. Det Norske Veritas. www.dnv.com.

Seto, H., H. Ochi, M. Ohta, and S. Kawakado (2003). Hydroelastic response analysis of real very large floating structures in regular waves in open/sheltered sea. In *Fourth International Workshop On Very Large Floating Structures, VLFS03, Tokyo, Japan*, pp. 6573.

SIMULINK. Mathworks. www.mathworks.com.

Suzuki, H. (2005). Overview of megafloat: Concept, design criteria, analysis, and design. *Marine Structures 18*, 111–132.

Taghipour, R., A. Arswendy, M. Devergez, and T. Moan (2008). Structural analysis of a multi-body wave energy converter in the frequency domain by interfacing wamit and abaqus. In *Proceedings of the 27th International Conference on Offshore Mechanics And Arctic Engineering, Estoril, Portugal*.

Taghipour, R., S. Fu, and T. Moan (2006). Validated two and three dimensional linear hydroelastic analysis using standard software. In *Proceedings of the 16th International Offshore and Polar Engineering Conference,Vancouver, BC, Canada*.

Taghipour, R. and T. Moan (2008). Efficient frequency-domain analysis of dynamic response for the multi-body wave energy converter in multi-directional waves. In *Proceedings of the 18th International Offshore and Polar Engineering Conference,Vancouver, BC, Canada*.

Taghipour, R., T. Perez, and T. Moan (2007). Time-domain hydroelastic analysis of a flexible marine structure using state-space models. *International Journal of Offshore Mechanics and Arctic Engineering*. In press.

Taghipour, R., T. Perez, and T. Moan (2008). Hybrid frequency-time domain models for dynamic response analysis of marine structures. *Ocean Engineering 35*, 685–705.

Tick, L. J. (1959). Differential equations with frequency-dependent coefficients. *Journal of Ship Research 3*, 45–46.

WAMIT. WAMIT Inc. www.wamit.com.

Watanabe, E. (2003). Floating bridges: Past and present. *Structural Engineering International 13*, 128–132.

Watanabe, E., T. Utsunomiya, and C. Wang (2004). Hydroelastic analysis of pontoon-type VLFS: a literature survey. *Engineering Structures 26*, 245–256.

Weymouth, G. D., R. V. Wilson, and F. Stern (2005). RANS computational fluid dynamics predictions of pitch and heave ship motions in head seas. *Journal of Ship Research 49*, 80–97.

Wu, M. and T. Moan (1996). Linear and nonlinear hydroelastic analysis of high-speed vessels. *Journal of Ship Research 40*, 149–163.

Yabe, T., F. Xiao, and T. Utsumi (2001). The constrained interpolation profile method for multiphase analysis. *Journal of Computational Physics 169*, 556–593.

Yago, K. and H. Endo (1996a). Model experimental and numerical calculation of the hydroelastic behavior of matlike vlfs. *International Workshop on Very Large Floating Structures, Hayama, Japan*.

Yago, K. and H. Endo (1996b). On the hydroelastic response of boxshaped floating structure with shallow draft. *Journal of the Society of Naval Architects of Japan 180*, 341–352. in Japanese.

Yasuzawa, Y., K. Kagawa, D. Kawano, and K. Kitabayashi (1997). Dynamic response of a large flexible floating structure in regular waves. In *16Th International Conference on Offshore Mechanics and Arctic Engineering*.

Yu, Z. and J. Falnes (1998). State-space modelling of dynamic systems in ocean engineering. *Journal of Hydrodynamics B(1)*, 1–17.

Appendices

A. WAMIT

WAMIT, distributed by WAMIT Inc[1], is a radiation/diffraction hydrodynamic software developed for the analysis of the interaction of surface waves with offshore structures at zero forward speed. The software provides solutions in the frequency domain. WAMIT can evaluate both first- and second-order loads and responses. But, the version of the software available in this research was the WAMIT first-order. WAMIT linear uses a linearized formulation of the BVP and the boundary conditions. Under this consideration, the body boundary conditions are satisfied on the mean body position and the pressure is obtained by a linearized Euler's-Bernoulli formulation.

WAMIT is a three-dimensional panel method which uses potential theory and BEM. Fundamentals of the panel method and BEM can be found in many classic papers and textbooks, among them Hess and Smith (1964), Brebbia and Dominguez (1989), Hess (1990), and Lee and Newman (2004). By using an integral formulation derived with the appropriate Green function that already satisfies the free surface boundary conditions, the computational surface in the software is reduced to that of the wetted surface(s) only.

The program can consider either finite or infinite water depths and either one or multiple floating bodies. However, when multiple body module is utilized, no geometrical symmetry can be exploited. The bodies may be floating, submerged, or fixed.

WAMIT allows low and high order panel models. In the low order panel method, the wetted surface of the body is discretized by flat quadrilateral elements. Over each panel, source strength and thus all the hydrodynamic quantities like velocity potential, pressure etc. are assumed constant. In the higher order panel method, the wetted surface is conveniently represented by a group of B-splines known as patches and the velocity potential is described by a continuous B-spline representation correlated to the patch formulation. The order

[1] `www.wamit.com`

of the B-spline is a user specified input. Since each patch is a continuous function, the pressure and other hydrodynamic quantities are also continuous, which gives a modeling advantage in comparison to the lower panel methods.

A complete description of the software, theory and documented results can be found on the software website. The multi-body and hydroelastic analysis capability of WAMIT makes it a unique software system within the thesis objectives.

B. ABAQUS

ABAQUS, an FEM based software distributed by Simulia[1], provides a complete solution of structural analysis. The software can be utilized in a broad range of applications, including marine structures. The package delivers accurate, robust and high performance solutions for challenging linear and non-linear problems and large scale linear dynamics applications. ABAQUS is able to leverage a complete range of structural analysis regarding global and local responses such as damage, fracture and failure.

With ABAQUS and its integrated computer aided engineering user interface (CAE) one can quickly and efficiently create, edit, monitor, diagnose, and visualize advanced finite element analysis. The intuitive interface enables modeling, analysis, job management, and result visualization. ABAQUS can also model structures made of novel material properties like composites. A thorough description regarding the software, its abilities and theory of development can be found on the software website and its user's manual.

Relevant to this thesis, structural modeling of a wave energy converter has been carried out using ABAQUS CAE. ABAQUS evaluated the global response of the device by calculating the stresses and internal loads using linear shell elements. A quasi-static approach is used to investigate the effect of loads.

[1] www.simulia.com

C. Appended Papers

Paper 1

Validated Two and Three Dimensional Linear Hydroelastic Analysis Using Standard Software

Published in
Proceedings of 16th Int. Offshore and Polar Engineering Conference, 2006, San Francisco, California, USA.

Proceedings of the Sixteenth (2006) International Offshore and Polar Engineering Conference
San Francisco, California, USA, May 28-June 2, 2006

ISBN 1-880653-66-4 (Set); ISSN 1098-6189 (Set)

Validated Two and Three Dimensional Linear Hydroelastic Analysis Using Standard Software

Reza Taghipour, Shixiao Fu and Torgeir Moan
Center for Ships and Ocean Structures-CeSOS
Norwegian University of Science and Technology-NTNU
Trondheim, Norway

ABSTRACT

A method for linear hydroelastic wave load analysis is established based upon use of standard software for assessing wave loads and three dimensional structural mode shapes found by ABAQUS. The method is validated by comparison against experimental results for a flexible offshore mat. The results show decent agreement with experiments and another available computer code. Moreover, the approach was found to be computationally efficient.

KEY WORDS: two and three dimensional hydroelasticity, potential theory, linear analysis, frequency domain, FEM, BEM, validation

INTRODUCTION

The growing need for larger ocean going vessels and other ocean structures, calls for hydroelastic analysis of these structures. Introduction of Very Large Floating Structures (VLFS) based on interconnected modules has already demanded such this kind of analysis.

For a hydrodynamicist, the term *hydroelasticity* refers to the satisfaction of the deformable body surface boundary condition of the boundary value problem for the velocity potential mathematical model (MOB project team, 2000). In other words, by hydroelasticity we imply that the fluid flow and the structural elastic reactions are considered simultaneously and that we have mutual interactions (Faltinsen, 2005). Standard ways of computing wave induced forces on vessels rely on combinations of potential flow and semi-empirical coefficient based models accounting for viscous forces. Rankine type sources are distributed along the hull of the structure, which satisfy the free surface boundary condition. Source strength can be computed by satisfying the exact body boundary conditions that no fluid can pass through the hull surface. Discretization of the hull form into a finite set of Hess-Smith type quadrilateral panels allows formulation of algebraic system of equations to be solved for the unknown singularity strengths (Crook, 1995).

In essence potential theory hydroelastic analysis is performed by definition of new sets of velocity potentials stemming from vibrational behavior of the structure and use of superposition of structural modes. When a few modes of the structure contribute to the response, the structural behavior can be described accurately by superposition of a few modes and correspondingly a few degrees of freedom rather thousands of equations required for the dynamic analysis.

Until now, various linear hydroelastic formulations have been developed for monolithic and interconnected moduled structures (e.g. Ohmatsu, 2005; Watanabe, 2004) based on traditional seakeeping, linear potential theories and mode superposition technique stemming from Bishop and Price (1979). These formulations adopt two dimensional strip theory or three dimensional Green function and introduce vibrational modes of the dry structure in satisfying hydroelastic body boundary conditions for the new velocity potential caused by vibration of the floating structure in water. Linear hydroelastic response of a continuous flexible structure with single regular shape module has been evaluated by assuming the structure to behave as a beam, plate and other models. One, two and three dimensional hydroelasticity theories have been developed based on analytical formulations (e.g. Sun et al. 2002, Sahoo et al. 2000, among others) and numerical methods (Cui et al. 2006, Eatock Taylor, 2003 among others).

Hydroelastic response of interconnected moduled structures was addressed by Che et al (1992). Later, they extended their method from a beam model for structure to a three dimensional finite element model. Assuming rigid modules and connectors, different three dimensional hydroelastic formulations have been proposed (e.g. Riggs et al. 1999, Cui et al 2006) in which hydrodynamic interaction between modules is considered through their corresponding radiation condition by keeping the other modules restrained while one module is oscillating in one of its own six rigid modes. Lee and Newman (2000) studied the hydroelastic behavior of an array of five hinged barges and semi-submersibles. Using the commercial software and accounting for elasticity of the modules and connectors, Kim et al. (1999) studied the linear frequency domain hydroelastic response of a five module VLFS. In their research, elasticity of modules was accounted for through a three dimensional finite elements structural analysis considering one flexible bending mode and two flexible torsional modes. Hinged rigid

modes were considered.
However, when it comes to more complicated multibody structures, as is common for e.g. aquacultural structures, where the vessel is composed of many modules not necessarily connected serially in one direction, it will be very difficult to explicitly define the structural modes, and ensure the orthogonality of the modes cannot be ensured. This simplification of the vessel structure causes loss of accuracy. Calculation of mode shapes can be improved considerably by use of Finite Elements method (FEM). State of the art commercial structural analysis programs like ABAQUS and ANSYS offer versatile and accurate methods. Extension of standard hydrodynamic codes to account for numerical structural analysis by Finite Elements can in turn improve hydroelastic analysis of the vessel significantly. In this regard, within the potential flow theory frame work, perturbation, traditional sea-keeping and mode superposition theory in structural dynamic analysis, Wu (1984) extended the two dimensional hydroelastic theory of Bishop and Price (1979) to three dimensional for arbitrary shape floating structures. Based on the works of Wu, a hydroelastic code namely THAFT has been developed in CSSRC (China Ship Scientific Research Center), and has been used in various related research fields and real design process of marine structures. Fu et al (2006) extended this three dimensional hydroelasticity theory to account for the hinge rigid modes of flexible floating interconnected structures. They performed hydroelastic analysis considering only half body symmetry.

The paper introduces an alternative way of performing hydroelastic analysis for arbitrarily shaped structures coupling two standard FEM and BEM codes – ABAQUS and WAMIT. In our approach, symmetry can be considered in both X and Y planes as along as geometry permits. In this way, faster analysis without loss of accuracy is possible. Frequency domain analysis is performed in this paper. An extension of the scope is to consider time domain models based on frequency domain data. This is motivated by the need for including viscous effects and connector nonlinearities and additionally the possibility of designing automation and control models. This work is reported by Taghipour et. al. (2006).

HYDROELASTIC BODY MOTIONS IN REGULAR WAVES

As mentioned above, BEM and FEM are applied to model the fluid and structure interaction, respectively. The hydrodynamic formulation used here is as described by Newman (1994). The inertial coordinate system is defined with x pointing in the bow direction of the ship, z pointing in the upward vertical direction, and y given by the right-hand rule. $z = 0$ is located on the undisturbed free surface. Irrotational flow of an inviscid incompressible fluid is assumed. Additionally, presence of the structure in an infinite depth sea is presumed.
The total velocity potential Φ is then defined as the sum of radiation and diffraction sub-problems:

$$\Phi = \varphi_R + \varphi_D \ , \ \varphi_R = \sum_{i=1}^{(6+N)} q_j \varphi_j \ , \ \varphi_D = \varphi_I + \varphi_S \tag{1}$$

where the radiation potential ϕ_R is due to the oscillation with amplitude q_j in direction j of the vessel in an undisturbed sea, and the diffraction potential ϕ_D is due to the wave excitation for the static structure. In other words, ϕ_j, *j=7~(6+N)* is due to excitation of the body itself at its j^{th} natural frequency ω_j in calm water. Furthermore, ϕ_S is the scattering potential component of the diffraction sub problem, which represents the disturbance of the incident wave potential (ϕ_I) by the fixed body.
Incident wave potential is already known as:

$$\varphi_I = igA/\omega \ e^{-ik(-iz + x\cos\beta + y\sin\beta)} \tag{2}$$

where $k=\omega^2/g$ is the wave number in infinite depth water, and ω is the incident wave frequency and g is the acceleration of gravity. β is the wave heading defined as the angle between direction of wave propagation and positive x direction (e.g. 180 degrees for head seas).
The unknown potentials, ϕ_R and ϕ_S, should satisfy the following conditions:

1. Continuity (Laplace's) equation: $\nabla^2\Phi = 0$ (3)
2. Free Surface condition: $\partial\Phi/\partial z - k\Phi = 0$ on z=0 (4)
3. Body boundary condition satisfied on the mean wetted body surface:
   $\partial\varphi_D/\partial n = 0$ for diffraction (5)
   $\partial\varphi_j/\partial n = i\omega n_j$ for radiation (6)

Where $n_j=\lambda_j.\mathbf{n}=u_jn_1 + v_jn_2 + w_jn_3$. **n** is the unit normal surface vector pointing out of the fluid domain into the body. **λ** is the mode shape function with Cartesian components u, v and w. It provides the following relations between generalized displacements(**X**) and generalized coordinates(**q**):

$$\mathbf{X} = \boldsymbol{\lambda}\mathbf{q} \tag{7}$$

$$\mathbf{q} = \boldsymbol{\lambda}^T\mathbf{X} \tag{8}$$

4. Radiation condition, meaning that the waves are radiating away from the body.

In case for shallow waters, boundary condition at sea bed should also be included:

5. $\partial\Phi/\partial z = 0$ on z=-h (9)

The linearized pressure on the hull is found as:

$$p = -\rho g z - \rho\, \partial\Phi/\partial t \tag{10}$$

Integration of this pressure over the mean wetted body surface will give the wave induced forces and moments on the hull:

$$\mathbf{F} = \iint_S p\mathbf{n}\, dS \tag{11}$$

$$\mathbf{M} = \iint_S p(\mathbf{r}\times\mathbf{n})\, dS \tag{12}$$

These expressions consist of hydrostatic, radiation and diffraction terms which in turn will be written as:

$$c_{ij} = \rho g \iint_S n_j(w_i + z\nabla.\boldsymbol{\lambda}_i)\, dS \tag{13}$$

$$\omega^2 a_{ij} - i\omega b_{ij} = -\rho \iint_S \varphi_j\, \partial\varphi_i/\partial n\, dS \tag{14}$$

$$F_i^{exc} = -\rho \iint_S \varphi_D\, \partial\varphi_i/\partial n\, dS \tag{15}$$

By including all the above terms in Newton's second law and using generalized coordinates, the general linear hydroelastic equation of motion for the floating structure in waves is written as:

$$\sum_{j=1}^{6+N}\left[-\omega^2\left(m_{ij}+a_{ij}\right) + i\omega(b_{ij}+d_{ij}) + (c_{ij}+k_{ij})\right]q_j = F_i^{exc} \tag{16}$$

where the additional matrices, **m**, **d** and **k** are the generalized structural mass, generalized structural damping, and generalized structural stiffness, respectively. Generalized mass and stiffness matrices are obtained by use of finite element packages like ABAQUS and ANSYS. Damping in the above equation is conveniently modeled by viscous damping. An even more simpler option is to represent the structural damping by Rayleigh or proportional damping as described by Bathe et al (1976). In this study, we chose the damping ratio of the first two flexible modes as 5%.

Theoretically, an infinite number of flexible modes are needed to represent the structural behavior in vibration, but it is always common to include a finite number of them effectively to express the behavior in practical cases. The necessary efficient number of modes is often found by a convergence study.

Analysis Procedure

The software being adopted in our paper is a radiation/diffraction

program developed for the analysis of the interaction of surface waves with offshore structures, and is based on a three dimensional panel method, in which the radiation and diffraction velocity potentials on the body wetted surface are determined from the solution of an integral equation obtained by using Green's theorem with the free surface potential as the Green function (Lee and Newman, 2004). This software uses two methodologies in order to perform hydrodynamic analysis, namely "Low Order" and "High Order" panel methods.

In the low order method, the geometric form of the submerged body surface is defined by flat quadrilateral elements (low order panels), and the solutions for the velocity potential and/or source strength are assumed constant on each panel.

In the higher order panel method, the velocity potentials are represented based on continuous B-splines whose order is controlled by user specified parameters. The new method is more efficient and accurate in most cases. Various forms of geometric input are possible, including explicit representation. Additionally, representation of the geometries by CAD program is feasible, which makes the modeling phase even faster. Finally the pressure and velocity on the body surface in this method are continuous. This is particularly useful for the structural analysis purposes.

Linear hydroelastic theory, based on analytically defined mode shapes has been implemented in this standard hydrodynamic analysis software. But when it comes to more generic vessel types, approximation of mode shapes by analytical mathematical functions will not be accurate enough. Therefore, a finite element method is applied to define the modes.

In our research, the main idea is to provide a link between the structural points in the FEM software and panel points in the BEM solver, and transfer the information based on this relation. In this way mode shape data may be interpreted from the points located in and on the total surface of the structure in the FEM software to the points on the underwater geometry in the BEM solver.

When Low Order Panels are applied and the boundary conditions are satisfied at centroid of each panel, it is sufficient to do the mode shape analysis in FEM in a way to obtain the mode data for the panel centroids. Fig. 1 illustrates the idea in our case.

Assume that the wetted part of the box in the figure is discretized by four panels numbered 1 to 4. Consider only panel no. 1 and panel no.2. As is seen by the figure, now that we selected the hydrodynamic panel sizes on the wetted body surface, we are able to describe the position of the panel centroids denoted by point no. 1 and point no.2 in this case. So all needed to be done is to mesh the entire dry structure in FEM with suitable element type and sizes to obtain mode shape components u,v and w for these points. It is noted that the whole structure should be modeled in the FE method.

Alternatively, information may be obtained by an interpolation scheme as seems to be used previously by Kim et al. (1999) This approach has also been applied in obtaining mode shape information for points in Higher Order Panels based on a two dimensional FEM model of the vessel structure.

This standard software enables the users to write FORTRAN code subroutines and compile them as dynamic link libraries (dll files) which can be accessed by the software during runtime. By this means, two FORTRAN subroutines have been written.

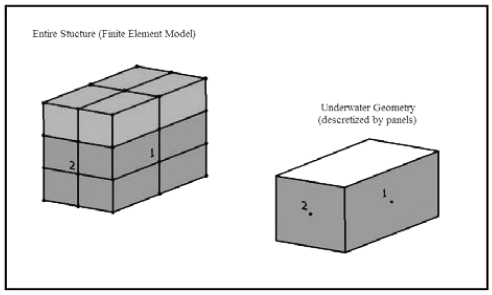

Fig. 1. Transferring information from FEM to BEM

In the first one, mode shape data are interpolated based on a two dimensional scheme in a file which is analytically calculated by two dimensional Euler-beam theory. This is denoted hereafter as 2DFW approach which can be run both in Low and Higher order method. The other technique works only in Low order and reads the mode shape data for panel centroids from a file containing three dimensional mode shape information. This approach is named 3DFWLO.

In both methods, a separate file must be read which contains mode shape symmetry information. In this way, a reduction of computational efforts is achieved.

Once the generalized response of the structure is found, by using Eq. 7, we are able to calculate the displacements for the points by which FEM model was defined. More information regarding bending moments, etc. is found by post-processing.

CASE STUDY: AN OFFSHORE MAT

In the case study analysis has been performed for a very large offshore mat structure. Results have been compared with experimental (Yago and Endo, 1996) and numerical studies of Fu et al. (2006).

Structural Geometry

The offshore mat is of a barge concept whose specifications are given in Table 1.

Table 1. General specifications of the offshore mat

Property	Symbol	Quantity
Length (m)	L	300
Beam (m)	B	60
Height (m)	T	2
Draft (m)	D	0.5
Mass (tons)	M	9.225×10^3
Bending Stiffness (kg.m^2)	EI	4.87×10^{10}

Structural data from ABAQUS

For 3DWLO, three dimensional FEM analysis has been performed using shell elements in ABAQUS. Structural shell elements and hydrodynamic panels information is as shown by Table 2. Table 3 provides information regarding the first 10 natural frequencies found by ABAQUS. Figs. (2~6) show some of the normalized mode shapes (7, 9, 25, 30 and 38) found by ABAQUS. Information for mode shape number 22 is ignored since it is a horizontal bending mode and does not contribute to the results of interest herein.

Table 2. Element size information for FEM and BEM analysis

Region	FEM Shell Element Size(m)	Hydrodynamic Panels
Free Surface	1 × 1	2 × 2
Sides	1 × 0.25	2 × 0.5
Ends	1 × 0.25	2 × 0.5
Bottom	1 × 1	2 × 2

Table 3. First 10 natural frequencies of the offshore mat

Mode No.	Frequency (Hz)	Mode number	Frequency (Hz)
7	0.15394	12	1.3771
8	0.42462	13	1.5441
9	0.48867	14	2.0571
10	0.83287	15	2.1476
11	0.99707	16	2.8243

Fig. 2. Principal mode shape No. 7 (First Bending Mode, f_7=0.15 Hz)

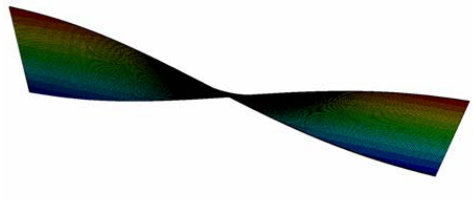

Fig. 3. Principal mode shape No. 9 (First Torsion Mode, f_9= 0.48 Hz)

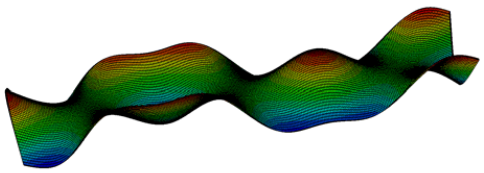

Fig. 4. Principal mode shape No. 25, f_{25}= 4.8 Hz

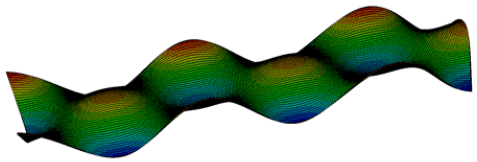

Fig. 5. Principal mode shape No. 30, f_{30}= 6.37 Hz

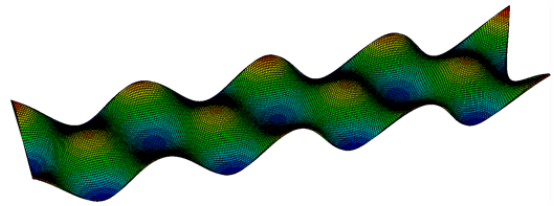

Fig. 6. Principal mode shape No. 38, f_{38}= 9.5 Hz

Description of Benchmarks

As described in the analysis procedure, the method by Fu et. al. (2006) is compared with the present ones using different models as indicated in Table 4.

Table 4. Methodology and conditions for different approaches(2DFW= 2D structural modeshapes + 3D higher order Panel method)

No.	Methods tested	Symmetricity	Mode shapes
1	Fu et. al. / 2DFW* /3DFWLO**	Y=0	Bending
2	Fu et. al. / 3DFWLO**	Y=0	Bending and Torsion
3	2DFW* / 3DFWLO**	X=0, Y=0	Bending

* 2D structural analysis in ABAQUS+3D higher order panel method
** 3D structural analysis in ABAQUS+3D low order panel method

Fig. 7 shows a quarter of the 2DFW geometry model. Evaluation for 2DFW was done using higher order panel technique and maximum panel size of 10 meters.

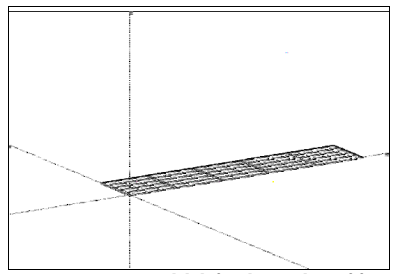

Fig. 7. Geometry model defined in MultiSurf for 2DFW approach

Finally, analysis was done based on just bending mode shape data from ABAQUS and using only 2DFW and 3DFWLO approaches. But two symmetry planes were considered this time in order to get some sense about reduction of calculation time. This feature could not be evaluated by the approach of Fu et al. (2006).

Results from WAMIT

All the calculations were performed using a 2GHz processor. CPU time has been reported for the 3DFWLO and Fu et al. (2006) as shown by Table 5.

First, principal coordinate responses (**q**) against a wide range of incident wave frequencies for head seas waves are plotted for modes no 7, 8 and 10 (Figs. (8~10)). For lower modes, except for small intermediate ranges of incident wave frequencies, all of the approaches seem to lead to same results. However, the discrepancies between present and Fu (2005) results show up for higher modes of vibration.

Table 5. CPU time for different approaches

Approach	Symmetricity	Total No. of Modes	Elapsed analysis time in minutes (5 wave frequencies)
3DFWLO	Y=0	37	161
	X=0, Y=0	37	46
Fu et. al. (3D)	Y=0	37	195
	X=0, Y=0	37	N/A

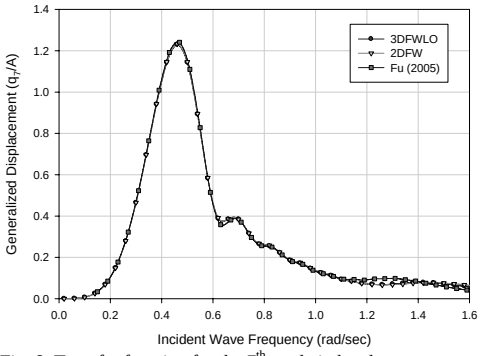

Fig. 8. Transfer function for the 7th mode in head seas

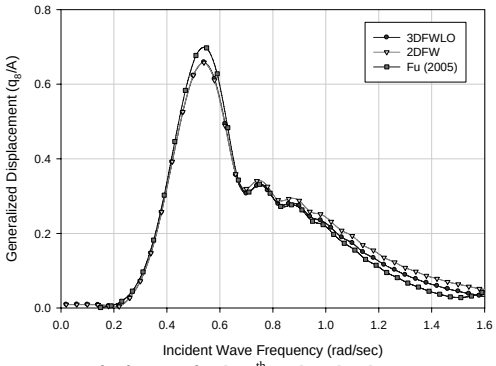

Fig. 9. Transfer function for the 8th mode in head seas

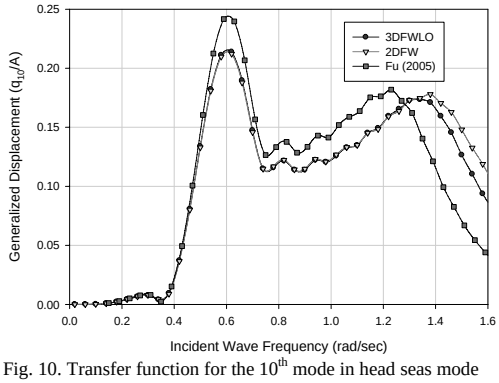

Fig. 10. Transfer function for the 10th mode in head seas mode

As expected, results show that head seas waves do not excite the torsional modes e.g. 9th mode. Figs. (11~14) show generalized displacement for wave headings of 150 degrees and mode numbers 7, 8, 9 and 10. When using 2DFW, only bending modes are considered. As a result torsional principal responses cannot be predicted as shown by Fig. 13. Again discrepancies between results obtained by the standard software and Fu (2005) are found for higher mode shapes.

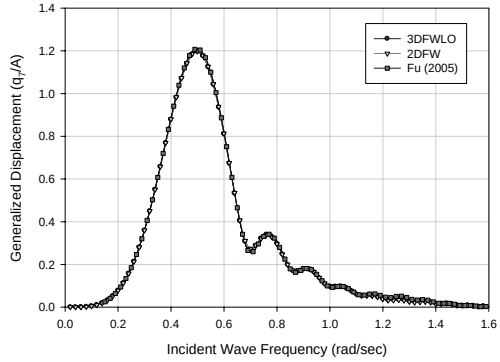

Fig. 11. Transfer function for the 7th mode and $\beta = 30^{\circ}$

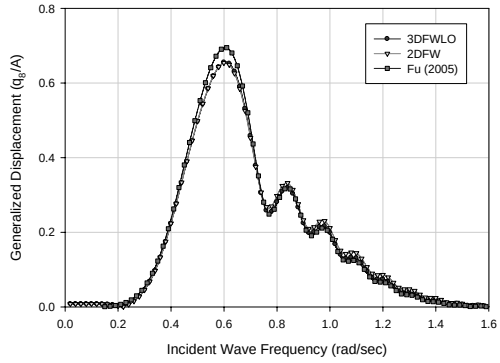

Fig. 12. Transfer function for the 8th mode and $\beta = 30^{\circ}$

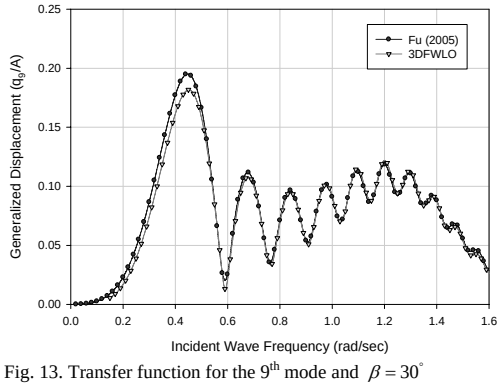

Fig. 13. Transfer function for the 9th mode and $\beta = 30^{\circ}$

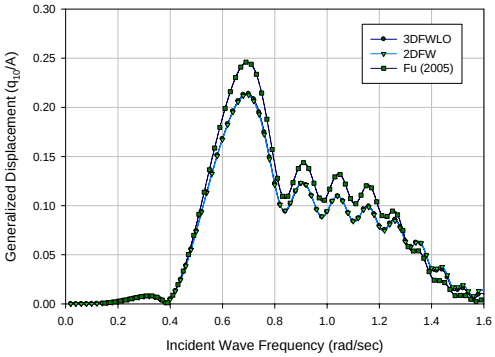

Fig. 14. Transfer function for the 10th mode and $\beta = 30^{\circ}$

Moreover, Figs. (15~19) show variation of the vertical hydroelastic displacement along the centerline of the structure. Comparison is made between 3DFWLO and Fu et. al. (2006) since it was believed that 2DFW and 3DFWLO have the same accuracy according to the previous results and that 3DFWLO can additionally consider torsional modes. 37 mode shapes were accounted for in the study. Results for rigid body response are also provided.

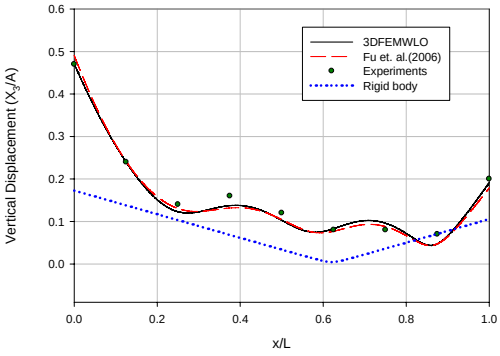

Fig. 15. Vertical displacement along the structure for $\beta = 0$ and wave length=60 m

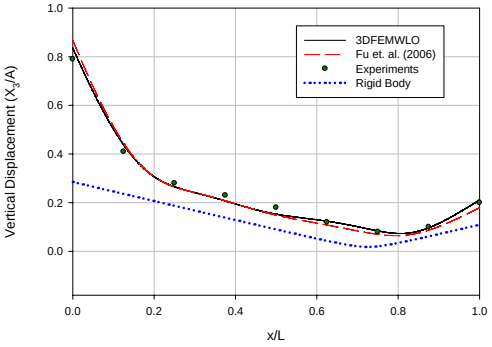

Fig. 16. Vertical displacement along the structure for $\beta = 0$ and wave length=120 m

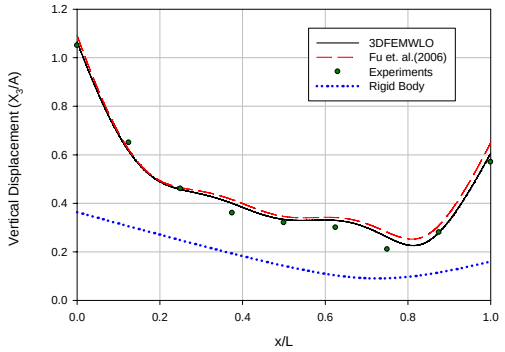

Fig. 17. Vertical displacement along the structure for $\beta = 0$ and wave length=180 m

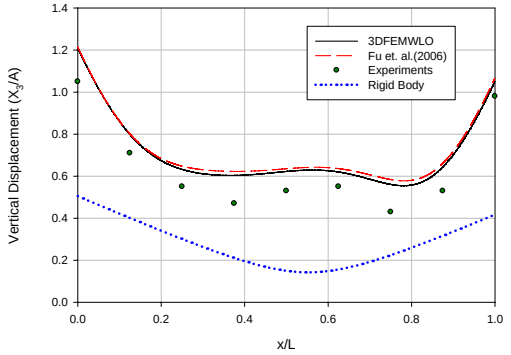

Fig. 18. Vertical displacement along the structure for $\beta = 0$ and wave length=240 s

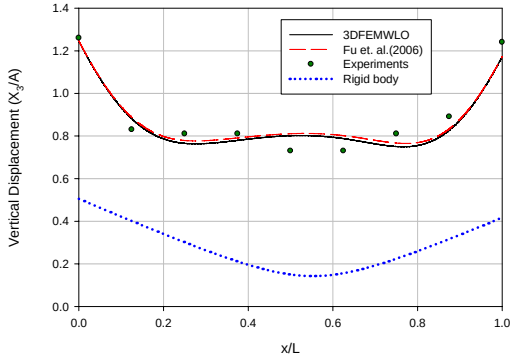

Fig. 19. Vertical displacement along the structure for $\beta = 0$ and wave length=300 m

Both numerical methods seem to be accurate for wavelengths 60, 120 and 180. Discrepancies with experimental results for longer wave lengths may be due to nonlinearities in the model e.g. slamming and viscous effects which cannot be described by linear hydroelasticity theory or even due to errors in experimental equipment (model or measurements). The two methods seem to have the same accuracy. Response at fore and aft of the structure is different, which tends to

become equal for longer waves. This might be due to the scattering potential which causes diffraction forces to become different at the ends of the structure for short waves. Difference between rigid body response and hydroelastic response grow as the length of the waves increase. As waves become longer, the elasticity effect on dynamic response of the structure will also increase. This means that hydroelasticity becomes important as the waves become longer.

SUMMARY AND CONCLUSIONS

A frequency domain method for hydroelastic analysis of wave induced responses for arbitrarily shaped ocean structures was performed using standard software and introduction of structural data from FEM analysis. Analysis using both two and three dimensional mode shape data is possible. Results were compared against an alternative code, as well as experiments. Results show good agreement except in the intermediate ranges of incident wave frequency. Moreover, the analysis method is found to be time efficient, especially when used with 2D FEM data and higher order panel methods. It is evident that by introduction of 3D FEM data together with standard hydrodynamic analysis software, accurate linear hydroelastic analysis of more generic vessel types becomes feasible.

ACKNOWLEDGEMENTS

The first author would like to thank Dr. Chang-Ho Lee in WAMIT Inc. for his prompt support and professor Odd M. Faltinsen in Center for Ships and Ocean Structures (CeSOS) for his helpful discussions regarding hydrodynamic issues. The authors would like to acknowledge the financial support from the Norwegian Research Council which has been granted through CeSOS.

REFERENCES

Bathe, KJ, Wilson, EL (1976). *"Numerical Methods in Finite Element Analysis"*, Englewood Cliffs.

Bishop, RED, and Price, WG (1979). *"Hydroelasticity of Ships,"* Cambridge University Press, UK.

Che XL, Wang, DY, Wang, ML, and Xu, YF (1992). "Two-Dimensional Hydroelastic Analysis of Very Large Floating Structures," Marine Technology, Vol 29, No 1, pp 13-24.

Compaq Visual FORTRAN User's Manual Ver 6.

Crook, TP (1994). "An Initial Assessment of Free Surface Effects on Submerged Bodies," M.S. Thesis, Naval Postgraduate School, Monterey, California.

Cui, WC, Yang, JM, Wu, YS and Liu, YZ (2006). "Theory of Hydroelasticity and Its Application To Very Large Floating Structures," To be published.

Eatock Taylor, R (2003). "Wet or Dry Modes in Linear Hydroelaticity - Why Modes?," Hydroelasticity in Marine Technology, Oxford, UK., pp 239-250.

Eatock Taylor, R, and Ohkusu, M (2000). "Green Functions for Hydroelastic Analysis of Vibrating Free-Free Beams and Plates," Applied Ocean Research, Vol 22, pp 295-314.

Faltinsen, OM (2005). "Hydrodynamics of High-Speed Marine Vehicles," Cambridge University Press, UK.

Fu, Shixiao (2005). *"Nonlinear Hydroelastic Analyses of Flexible Moored Structures and Floating Bridges,"* Ph.D. thesis, Shanghai Jiao Tong University, (in Chinese).

Fu, S, Moan, T, Chen, X, Cui, W (2006). "Hydroelastic Analysis of Flexible Floating Interconnected Structures, " to appear.

Hibbit, Karlsson, and Sorenson (2004). *"ABAQUS Users' Manual 6.5,"* ABAQUS Inc.

Kim, D, Chen, L, and Blaszkowski, Z (1999). *"Linear Frequency Domain Hydroelastic Analysis for McDermott's Mobile Offshore Base Using WAMIT,"* Proceedings of The Third International Workshop on Very Large Floating Structures, VLFS'99, Honolulu, pp 105-113.

Lee, CH, and Newman, JN (2000). *"An Assessment of Hydroelasticity for Very Large Hinged Vessels,"*, Journal of Fluids and Structures, Vol 14, pp 957-970

Lee,CH. and Newman, JN (2004) *"Computation of wave effects using the panel method,"* in Numerical models in fluid-structure interaction, Preprint, Editor S. Chakrabarti, WIT Press, Southhampton.

MOB Project Team (2000), *"Mobile Offshore Base Science and Technology Program Final Report,"* Technical Report TR-2125-OCN, Naval facilities Engineering Service Center, CA, USA

Newman JN (1994). *"Wave Effects on Deformable Bodies,"*Applied Ocean Research, Vol 16, No 1, pp 47-59

Ohmatsu, S (2005), *"Overview: Research on wave loading and responses of VLFS"*, Marine Structures, Vol.18, pp149-168.

Riggs, HR, and Ertekin, RC (1993). *"Approximate Methods for Dynamic Response of Multi-module Floating Structures,"* Marine Structures, Vol 6, pp 117-141.

Riggs, HR, Ertekin, RC, and Mills, TRJ (1999). *"Impact of Stiffness On the Response of a Multimodule Mobile Offshore Base,"* International Journal of Offshore and Polar Engineering, Vol 9, No 2, pp 126-133.

Riggs, HR, Ertekin, RC, and Mills, TRJ (2000), *"A Comparative Study of RMFC and FEA Models for The Wave-Induced Response of A MOB,"* Marine Structures, Vol 13, pp 217-232.

Sahoo, T, Yip, TL and Chwang, AT, (2000). *"On The Interaction of Surface Wave with a Semi-Infinite Elastic Plate,"* Proceedings of the 10th International Offshore and Polar Engineering Conference, Seatle, USA, pp 584-589.

Sun, H, Song, H, and Cui, WC (2002). *"On the interaction of Surface Waves with an Elastic Plate of Finite Length in Head Seas,"* China Ocean Engineering, Vol 16, No 1, pp 21-32.

Taghipour, R, Perez, T, Fu, S, and Moan, T (2006), *"Verified Time Domain Model Based on Frequency Domain Data For A Hydroelastic Structure ,"* to appear.

Wang, DY, Riggs, HR, and Ertekin, RC (1991). *"Three-Dimensional Hydroelastic Response of a Very Large Floating Structure,"* International Journal of Offshore and Polar Engineering, Vol 1, No 4, pp 307-316.

Watanabe E, Utsuomiya T, and Wang C.M. (2004), *"Hydroelastic analysis of pontoon-type VLFS: a literature survey"*, Engineering Structures, Vol.26, pp.245-256.

Wu, YS, (1984). *"Hydroelasticity of Floating Bodies"*, Ph.D. Thesis, Brunel University, U.K.

Yago.K and Endo, H., 1996,*"On the hydroelastic response of Box-shaped floating structure with shallow draft"*, Journal of the Society of Naval Architects of Japan, Vol .180, pp. 341-352.

Paper 2

Efficient Frequency-Domain Analysis of Dynamic Response for the Multi-Body Wave Energy Converter in Multi-Directional Waves

Published in
Proceedings of 18th Int. Offshore and Polar Engineering Conference, 2008, Vancouver, BC, Canada.

Proceedings of the Eighteenth (2008) International Offshore and Polar Engineering Conference
Vancouver, BC, Canada, July 6-11, 2008

ISBN 978-1-880653-70-8 (Set); ISBN 1-880653-68-0 (Set)

Efficient Frequency-Domain Analysis of Dynamic Response for the Multi-Body Wave Energy Converter in Multi-Directional Waves

Reza Taghipour[1], *Torgeir Moan*[1,2]
1) Centre for Ships and Ocean Structures, 2) Department of Marine Technology, Norwegian University of Science and Technology, Trondheim, Norway

ABSTRACT

In this paper, a multi-body wave energy converter is studied in the frequency domain. The device consists of a semisubmersible platform and 21 buoys. A mode expansion method, with total number of 27 modes, is used to formulate the dynamic motions. Moreover, An idealized form of power take-off mechanism is considered. Ocean environment and its directionality is modeled by using a JONSWAP wave spectrum with directional spreading according to Mitsuyasu. The objective is to assess the performance of the device in absorbing the wave energy and its dynamic behavior in ocean waves with/without considering the effect of power absorption mechanism. The current analysis method has been found to be computationally efficient and easier to interface with structural code compared to the available standard procedures by means of multi-body analysis approach.

KEY WORDS: Wave energy converter; dynamic response; mode expansion; frequency domain; multiple floating bodies; power-offtake; multidirectional seas.

INTRODUCTION

There is a significant interest in ocean renewable energy. Offshore wind turbines and wave energy converters (WEC) are two major types of the offshore renewable energy devices. The focus in this paper is on the second category. Up to now there have been numerous efforts on the study of wave energy converters in waves. Most of them have been concerned with single body motions. Only a few have focused on multi-body dynamics and considering hydrodynamic interactions.

In this study, the wave energy converter consists of a semisubmersible and several buoys sliding along some guides attached to the semisubmersible platform. This concept is known as the FO^3 platform (See Fig. 1). It was first proposed by Fred Olsen Co. Dynamic analysis of such a concept is challenging even in the frequency domain due to its multi-kinematics and hydrodynamic interactions.

Fig. 1 FO^3 the Wave Energy Converter. Courtesy of Fred Olsen and ABB.

This device has been studied by Rogne (2007)who considered the motions of the WEC in the vertical plane using the multi-body analysis approach in WAMIT (2006). He assumed a uni-directional wave and showed that the dynamic problem is symmetric about the x axis. He then solved the hydrodynamics sub-problem by considering the platform and each buoy to move freely in surge, sway and pitch, resulting to a total number of 42 dofs. In this way, he obtained the hydrodynamic coefficients like added mass and potential damping for each floating body. To solve the entire dynamic problem, he performed a post processing and reduced the degrees of freedom from 42 to 16 implying 2 dofs for surge and pitch of the platform and the buoys accounting for the buoy-sliding, and 14 dofs for heave of the platform and 13 buoys.

Taghipour (2008) solved the problem in another way. He considered the entire WEC as a single floating body whose dynamic motions were obtained by a mode expansion method, using the 16 modes directly. Such an approach has been frequently used to study the dynamic response of flexible marine structures in waves, referred to as hydroelasticity (see e.g. Newman (1994)). The alternative method, while maintaining the same accuracy, was found to be more efficient by a factor of 10-15. Yet, the

problem was limited to unidirectional waves and body motions in the vertical plane.

The objective of this paper is to

- Establish a method to study the performance of the WEC in sea waves accounting for the wave directionality.
- Study the structure motions in waves.
- Observe the effect of power take-off mechanism on the structure response.
- Shed some light on the absorbed energy by the device.
- Provide a basis for structural response assessment of the WEC.

Again, a mode expansion method is used to derive the equations of motion. Dynamic response in incident waves is evaluated in the form of Response Amplitude Operators (RAOs). The device performance in absorbing wave energy is indicated by formulating the statistics of the absorbed power. More specifically, mean and variance of the power output for each buoy is evaluated. Low- to moderate- wave sea-states are considered.

The outline of the paper is as follows: The next section gives a description of the problem, geometry and assumptions. It will be followed with an explanation of the modes of motion and formulation of their mathematical representations. Based on this description, the equations of motion are formulated. Finally, spectral analysis of the absorbed power in the irregular sea waves is presented followed by concluding remarks in the last section.

PROBLEM DESCRIPTION

The wave energy convertor (WEC) consists of one semisubmersible platform and 21 buoys, as shown in Fig. 2. All the buoys are considered to have the same physical and geometrical parameters as shown in Tab. 1 and Fig. 3. Relevant information for the platform is given in Tab. 1. The geometry of the platform pontoons is as shown in Fig. 4. Corresponding to each buoy, there is a guide (shaft) which is connected rigidly to the platform. The wave energy convertor has been designed such that the buoys can move freely along their guides and their motion is transformed to electricity by means of the power take-off machinery on the deck.

A right handed coordinate system (x,y,z) fixed with respect to the mean position of the body is used, with positive z vertically upwards through the center of gravity of the platform and the origin in the plane of the undisturbed free surface. Forces, moments, response and other vectorial quantities are evaluated with respect to this frame. It is assumed that the WEC does not undergo large motions and that the wave steepness is small, i.e. linear hydrodynamic loading is assumed.

Table 1 Buoy and platform specifications

Parameter	Buoy	Platform	Dim.
Mass, m_b/m_s	13.283	1007.3	[ton]
Draft	2.0	12.8	[m]
Vertical center of gravity, z_g^o	0.0	2.0	[m]
Roll radii of gyration about C_g, r_{xx}^g	1.4	16.29	[m]
Pitch radii of gyration about C_g, r_{yy}^g	1.4	16.29	[m]
Yaw radii of gyration about C_g, r_{zz}^g	1.6	16.0	[m]
Metacentric height, $GM_{T,L}$	0.34	0.71	[m]

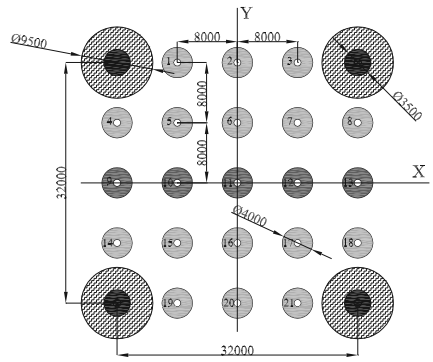

Fig. 2 WEC layout. The dimensions are in millimeters.

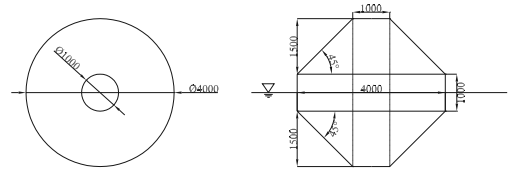

Fig. 3 The buoy geometry. The dimensions are in millimeters.

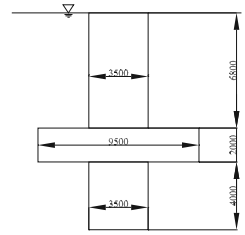

Fig. 4 Geometry of the platform columns. The dimensions are in millimeters.

The Modes of Motion

The wave energy convertor has been designed such that the buoys can move freely along the guides. Based on this design, the following modes can be defined:

- System surge (platform and buoys) , ξ_1,
- System sway (platform and buoys) , ξ_2,
- (Independent) heave of the platform, ξ_3(see Fig. 5),
- Roll of platform and buoys considering the buoys to slide along the guides, ξ_4 (see Fig. 5),

- Pitch of platform and buoys considering the buoys to slide along the guides, ξ_5 (see Fig. 5),
- system yaw (platform and buoys), ξ_6,
- (Independent) heave of each buoy, $\xi_7 \dots \xi_{(6+N)}$ (see Fig. 5).

These mode definitions can be put in mathematical terms as

$$
\begin{aligned}
&\boldsymbol{\lambda}_1 = [1,0,0]^T, \quad \text{everywhere},\\
&\boldsymbol{\lambda}_2 = [0,1,0]^T, \quad \text{everywhere},\\
&\boldsymbol{\lambda}_3 = \begin{cases} [0,0,1]^T, & \text{if} \quad \mathbf{x} \in S_s,\\ \mathbf{0}, & \text{elsewhere}, \end{cases}\\
&\boldsymbol{\lambda}_4 = \begin{cases} [0,-z,y]^T, & \text{if} \quad \mathbf{x} \in S_s,\\ [0,-z,(y-y^g_{b_k})]^T, & \text{if} \quad \mathbf{x} \in S_{b_k}, \end{cases}\\
&\boldsymbol{\lambda}_5 = \begin{cases} [z,0,-x]^T, & \text{if} \quad \mathbf{x} \in S_s,\\ [z,0,-(x-x^g_{b_k})]^T, & \text{if} \quad \mathbf{x} \in S_{b_k}, \end{cases}\\
&\boldsymbol{\lambda}_6 = [-y,x,0]^T, \quad \textit{everywhere},\\
&\boldsymbol{\lambda}_i = \begin{cases} [0,0,1]^T, & \text{if} \quad \mathbf{x} \in S_{b_k},\\ \mathbf{0}, & \text{elsewhere}. \end{cases}
\end{aligned}
\tag{1}
$$

where k=1...N and i=6+k. Now, the response $\mathbf{X}$ in the cartesian coordinates at each point (x y z) on the WEC can be evaluated as

$$\mathbf{X} = \boldsymbol{\lambda}\boldsymbol{\xi}. \tag{2}$$

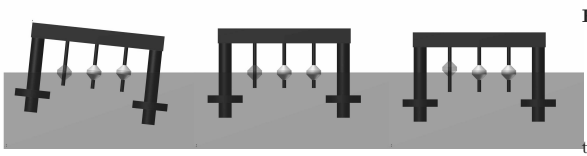

Fig. 5 Illustration of the modes of motion for the independent bodies. The left figure illustrates the WEC rotations by considering the sliding of the buoys along the guides. The middle figure shows the independent heave of the platform, while the buoys stay at their deign draft. The right figure illustrates the independent heave for buoy no. 1 (the red buoy), while the platform and the rest of the buoys stay at their design draft.

Generalized Inertia Forces

Corresponding to each mode of motion, a mass matrix can be defined by using

$$
\begin{aligned}
M_{ij} &= \int\int\int_V \rho \boldsymbol{\lambda}_i^T \boldsymbol{\lambda}_j dV\\
&= \int\int\int_{V_s} \rho_s \boldsymbol{\lambda_i}^T \boldsymbol{\lambda}_j dV + \sum \int\int\int_{V_{b_k}} \rho_{b_k} \boldsymbol{\lambda_i}^T \boldsymbol{\lambda}_j dV,
\end{aligned}
\tag{3}
$$

where k=1...N and i, j=1...(6+N). This leads to

$$
\begin{aligned}
&M_{11} = m_s + \sum m_{b_k},\\
&M_{15} = M_{51} = m_s z^g_s + \sum m_{b_k} z^g_{b_k},\\
&M_{16} = M_{61} = -m_s y^g_s + \sum -m_{b_k} y^g_{b_k},\\
&M_{22} = M_{11},\\
&M_{24} = M_{42} = -m_s z^g_s + \sum -m_{b_k} z^g_{b_k},\\
&M_{26} = M_{62} = m_s x^g_s + \sum m_{b_k} x^g_{b_k},\\
&M_{33} = m_s,\\
&M_{34} = m_s y^g_s,\\
&M_{35} = -m_s x^g_s,\\
&M_{44} = m_s r^2_{xx^o_s} + \sum m_{b_k} r^2_{xx^o_{b_k}},\\
&r^2_{xx^o_s} = r^2_{xx^g_s} + (y^2_{s^g} + z^2_{s^g}),\ r^2_{xx^o_{b_k}} = r^2_{xx^g_{b_k}} + z^2_{b_k{}^g},\\
&M_{55} = m_s r^2_{yy^o_s} + \sum m_{b_k} r^2_{yy^o_{b_k}},\\
&r^2_{yy^o_s} = r^2_{yy^g_s} + (x^2_{s^g} + z^2_{s^g}),\ r^2_{yy^o_{b_k}} = r^2_{yy^g_{b_k}} + z^2_{b_k{}^g},\\
&M_{66} = m_s r^2_{zz^o_s} + \sum m_{b_k} r^2_{zz^o_{b_k}},\\
&r^2_{zz^o_s} = r^2_{zz^g_s} + (x^2_{s^g} + y^2_{s^g}),\ r^2_{zz^o_{b_k}} = r^2_{zz^g_{b_k}} + (x^2_{b_k{}^g} + y^2_{b_k{}^g}),\\
&M_{ll} = m_{b_k}.
\end{aligned}
\tag{4}
$$

where $l = 7 \dots (N+6), k = 1 \dots N$. All the other coefficients in the mass matrix are zero. The final equation for the generalized inertia forces reads: $\mathbf{F^I} = \mathbf{M}\ddot{\boldsymbol{\xi}}$.

Generalized Restoring Forces

The generalized restoring force vector is formulated as $\mathbf{F^{res}} = -\mathbf{C}\boldsymbol{\xi}$ where

$$C_{ij} = \rho g \int\int_{S_0} n_j \nabla.(z\lambda_i) dS. \tag{5}$$

Substituting for the modes of motion in Eq. 1 and adding for the contribution from the gravity, $\mathbf{C}$ is found to be a diagonal matrix:

$$
\begin{aligned}
&C_{33} = \rho g A^{WP}_s\\
&C_{44} = C_{55} = \rho g (\nabla_s \overline{GM}_s + \sum \nabla_{b_k} \overline{GM}_{b_k})\\
&C_{ll} = \rho g A^{WP}_{b_k}, \quad l = 7 \dots (N+6),\ k = 1 \dots N.
\end{aligned}
\tag{6}
$$

assuming $\overline{GM}^L = \overline{GM}^T = \overline{GM}$ for the platform and the buoys.

Generalized Hydrodynamic Loads

Potential theory and the Boundary Element Method (BEM) is utilized to obtain the hydrodynamic loads on the WEC. The multi-body hydrodynamics of the platform and the buoys is described by using the generalized modes approach, see e.g. Newman (1994). The WEC (semi and 21 buoys) is then considered as one body able to oscillate according to the mode definitions given above.

The total velocity potential is written as sum of diffraction and radiation potentials:

$$\Phi = \phi^D + \phi^R = \phi^D + \sum_{i=1}^{(N+6)} \phi_i \dot{\xi}_i, \qquad \phi^D = \phi^I + \phi^S. \tag{7}$$

Each potential must satisfy the following conditions:

- Continuity (Laplace) equation.
- Free surface conditions (kinematic and dynamic).
- Radiation condition.
- Body boundary condition.

Attention is paid in satisfying the body boundary conditions for the radiation potentials due to the modes. The radiation potential at each point belonging to the WEC underwater geometry should satisfy the following equation:

$$\frac{\partial \phi_i}{\partial n} = \boldsymbol{\lambda}_j.\mathbf{n}, \quad \boldsymbol{\lambda}_j = [u_j, v_j, w_j]^T, \quad \mathbf{n} = [n_x, n_y, n_z]^T. \tag{8}$$

where the modes are defined according to Eq. (1). Solution of the potentials will then give the hydrodynamic pressure by using the linearized Bernoulli equation. By integrating this pressure on the mean wetted body surface, the generalized first-order pressure forces corresponding to each mode of motion are evaluated in the form of radiation (added mass and hydrodynamic damping) and diffraction (wave-exciting) components:

$$F_i^{rad} = -[i\omega A_{ij} + B_{ij}]\dot{\xi}_j = -i\omega\rho \int\int_{S_0} \phi_j \dot{\xi}_j n_i \; dS, \tag{9}$$

$$F_i^{exc} = -i\omega\rho \int\int_{S_0} \phi^D n_i \; dS, \tag{10}$$

where i=1...(N+6).

Power Take-Off Mechanism

An idealized formulation for the generalized loads of the power take-off mechanism is considered herein. The power take-off force exerted by the machinery on each buoy is assumed proportional to the relative vertical velocity of the buoy and the guide (platform) at the buoy's center of gravity in the form

$$F_i^{PTO} = -b_u V_{b_k^g}^{rel}, \tag{11}$$

where

$$V_{b_k^g}^{rel} = \dot{\xi}_i - (\dot{\xi}_3 + y_{b_k}^g \dot{\xi}_4 - x_{b_k}^g \dot{\xi}_5) \tag{12}$$

by using Eqs. (1) and (2). Note that $i = 7, \ldots, (N+6)$, $k = 1, \ldots, N$. The total reaction force and moments on the platform due to the power take-off will then be

$$\begin{aligned} F_3^{PTO} &= \sum F_i^{PTO} \\ &= b_u \sum (\dot{\xi}_i - \dot{\xi}_3 - y_{b_k}^g \dot{\xi}_4 + x_{b_k}^g \dot{\xi}_5), \\ F_4^{PTO} &= \sum y_{b_k}^g \; F_i^{PTO} \\ &= b_u \sum y_{b_k}^g \; (\dot{\xi}_i - \dot{\xi}_3 - y_{b_k}^g \dot{\xi}_4 + x_{b_k}^g \dot{\xi}_5), \\ F_5^{PTO} &= \sum -x_{b_k}^g \; F_i^{PTO} \\ &= b_u \sum -x_{b_k}^g \; (\dot{\xi}_i - \dot{\xi}_3 - y_{b_k}^g \dot{\xi}_4 + x_{b_k}^g \dot{\xi}_5). \end{aligned} \tag{13}$$

The above force formulation can be put in the matrix form $\mathbf{F^{PTO}} = -\mathbf{B_u}\boldsymbol{\xi}$ with

$$\begin{aligned} B_{33} &= \sum b_u, \\ B_{34} = B_{43} &= \sum y_{b_k}^g \, b_u, \\ B_{35} = B_{53} &= \sum -x_{b_k}^g \, b_u, \\ B_{3i} = B_{i3} &= -b_u, \\ B_{44} &= \sum y_{b_k{}^g}^2 \, b_u, \\ B_{45} = B_{54} &= \sum -y_{b_k}^g x_{b_k}^g \, b_u, \\ B_{4i} = B_{i4} &= -y_{b_k}^g \, b_u, \\ B_{55} &= \sum x_{b_k{}^g}^2 \, b_u, \\ B_{5i} = B_{i5} &= x_{b_k}^g \, b_u, \\ B_{ii} &= b_u, \end{aligned} \tag{14}$$

The output power obtained from each buoy is written as $P_{b_k} = -F_{b_k}^{PTO} V_{b_k^g}^{rel}$. By using Eq. (11) the alternative formulation of the absorbed power will be obtained as

$$P_{b_k} = b_u [V_{b_k^g}^{rel}]^2, \tag{15}$$

or,

$$P_{b_k} = \frac{[F_{b_k}^{PTO}]^2}{b_u}. \tag{16}$$

Equations of Motion

Newton's second law is applied by equating the generalized inertia forces and the sum of the generalized restoring, hydrodynamic and power-take off forces:

$$\mathbf{F^I} = \mathbf{F^{res}} + \mathbf{F^{rad}} + \mathbf{F^{exc}} + \mathbf{F^{PTO}}. \tag{17}$$

In this way, the complex amplitudes of the generalized WEC motions $\boldsymbol{\xi}$ are obtained from the equation of the $(N+6)\times(N+6)$ linear system:

$$[-\omega^2(\mathbf{M} + \mathbf{A}(\omega) + i\omega(\mathbf{B}(\omega) + \mathbf{B_u}) + \mathbf{C}]\boldsymbol{\xi}(i\omega) = \mathbf{F^{exc}}(i\omega) \tag{18}$$

Stochastic Description of Response and Power

It is interesting to obtain information about the statistics of response and power in random sea waves. This is usually achieved by describing the sea by means of a wave power spectral density function and then evaluating the spectral density functions of the objective variables by using the corresponding frequency response functions. In this context, we have used JONSWAP spectrum to define a fully developed wave environment of the North Sea-see e.g. Chakrabarti (1990):

$$S(\omega) = \alpha g^2 \omega^{-5} \exp\Big[-\frac{5}{4}\,\frac{\omega_p^4}{\omega^4}\Big]\, \gamma_p^{\exp(-[\frac{\omega}{\omega_p}-1]^2 \frac{1}{2\tau^2})}; \tag{19}$$

with entries of α, γ_p and τ defined as

$$\begin{aligned} &\alpha = 16.942\Big[\frac{Hs}{gT_p^2}\Big]^{1.375}, \quad \gamma_p = 3.3, \\ &\tau = \begin{cases} 0.07, & \text{if} \quad \omega \le \omega_p, \\ 0.09, & \text{if} \quad \omega > \omega_p. \end{cases} \end{aligned} \tag{20}$$

The above spectrum describes a unidirectional sea wave. Directional characteristics of the ocean waves can be introduced by using a spreading function:

$$S(\omega,\theta) = S(\omega)\Theta(\theta|\omega), \tag{21}$$

where the spreading function is chosen here following the work by Mitsuyasu et al. (1975) and Goda and Suzuki (1975)

$$\Theta(\theta|\omega) = G_0 \cos^{2s}(\frac{\theta-\theta_0}{2}). \tag{22}$$

In Eq. (22), θ_0 is the mean wave direction and

$$\begin{aligned} G_0 &= \left[\int_{-\pi+\theta_0}^{\pi+\theta_0} \cos^{2s}(\frac{\theta-\theta_0}{2})d\theta\right]^{-1}, \\ s &= \begin{cases} s_{max}[\frac{\omega}{\omega_p}]^5, & \text{if} \quad \omega \le \omega_p, \\ s_{max}[\frac{\omega}{\omega_p}]^{-2.5}, & \text{if} \quad \omega > \omega_p. \end{cases} \end{aligned} \tag{23}$$

The spreading parameter s_{max} is taken equal to 10 for wind generated waves as recommended by Goda (2000). The spreading function assumes that the energy distribution is symmetric about the mean wave direction and lies in the range $\frac{\theta-\theta_0}{2} = [\frac{-\pi}{2}, \frac{\pi}{2}]$.

Eq. (18) gives the response amplitude operators (RAO) of WEC motions in waves for different wave headings and frequencies. By using the generalized response RAOs and following Eq. (12), one is able to obtain the RAO for the relative velocities, denoted herein as $H_{V_{b_k}^{rel}}$. Since there is a linear relation between the relative velocity and the wave amplitude, the power spectrum of the relative velocity can be found as

$$S_{V_{b_k}^{rel}}(\omega,\theta) = |H_{V_{b_k}^{rel}}(\omega,\theta)|^2 S(\omega,\theta). \tag{24}$$

Then, the statistics of relative velocity for each buoy in the multidirectional ocean waves can be obtained:

$$\sigma^2_{V_{b_k}^{rel}} = \int_{-\infty}^{+\infty}\int_{-\pi}^{\pi} S_{V_{b_k}^{rel}}(\omega,\theta)d\omega d\theta. \tag{25}$$

The statistics of extracted power for each buoy (k) can be obtained based on Eq. (15) as (see e.g. Bendat (1998))

$$\begin{aligned} \mu_{P_{b_k}} &= b_u \sigma^2_{V_{b_k}^{rel}}, \\ \sigma^2_{P_{b_k}} &= 2\mu^2_{P_{b_k}}. \end{aligned} \tag{26}$$

with the alternative form corresponding to Eq. (16) as

$$\begin{aligned} \mu_{P_{b_k}} &= \frac{\sigma^2_{F^{PTO}_{b_k}}}{b_u}, \\ \sigma^2_{P_{b_k}} &= 2\mu^2_{P_{b_k}}. \end{aligned} \tag{27}$$

Then it is straightforward to show that the expected power from the wave energy converter for that wave environment is

$$\mu_P^{WEC} = \sum_{k=1}^{N} \mu_{P_{b_k}} \tag{28}$$

NUMERICAL MODELING AND RESULTS

The hydrodynamic code WAMIT (2006) was used for evaluation of the hydrodynamic loads by using the mode shape definitions. The underwater geometry of the WEC was modeled as shown in Fig. 6. The guides were not considered in the modeling assuming that they do not contribute significantly to the linear hydrodynamic loads. The generalized modes in Eq. (1) were introduced to WAMIT by using a Fortran code interacting with the software during runtime. The corresponding matrices for generalized mass, restoring and damping due to power take-off mechanism were obtained from their corresponding equations in (3), (6) and (14). The idealized power take-off coefficient b_u was taken equal to 100 $\frac{kNs}{m}$. In this way, solution of Eq. (18) is performed in the software. A range of frequencies from 0.25 to 3.6 rad/sec has been selected in obtaining the RAO results.

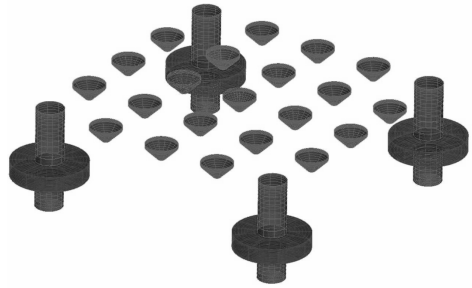

Fig. 6 Mean wetted surface model of the WEC in Multi-Surf (2007).

Regular Waves

Response in the Following Seas

Fig. 7 shows the generalized coordinate response plots in the following seas waves. The results have been plotted in the form of response amplitude operators (RAOs) as a function of the incoming wave frequency. For this wave heading, there is practically no response in Sway, Roll and Yaw. The results show that for this wave heading, buoys located symmetrically about x axis, will show identical dynamic behavior. For instance, buoy 7 and 17 or buoy 1 and 19 in Fig. 2 can be considered identical. Knowing this, only the results corresponding to buoys above the x axis are plotted in Fig. 7.

For comparison, the response plots have been drawn against the calculations obtained from the multi-body analysis by Rogne (2007). The results show excellent agreement.

In order to provide a better understanding regarding the effect of power absorption on the WEC response behavior, the results corresponding to no energy extraction are also plotted in the figure. These results are shown by dash-dotted lines. It is observed that the power absorption has significantly reduced the buoys' dynamic response mainly in the region of 1-2.7 rad/secs, while it has caused an increase in the platform response in heave. It is also observed that the energy absorption mechanism has smoothed the platforms response around its natural frequency.

To further test the model, the dynamic behavior of the WEC subject to beam seas regular waves (incident waves along y axis) was investigated. In this case, exactly same behavior as in Fig. 7 was observed with the difference that for this case the plots correspond to system sway, platform heave, System roll, and heave of the buoy# 14, 9, 4, 19, 15, 10, 5, 1, 20, 16, 11, 6 and 2, respectively.

Response in the oblique seas

As a representative case of oblique seas, the results when the incident waves approach the structure at a 45 degrees heading angle are shown. The results have been plotted in Fig. 8. Identical dynamic behavior of some of the buoys due to problem symmetry is quite evident from the plots (They have been indicated by dashed line and solid lines). One can also observe the effect of energy absorption on the WEC response behavior by comparing the results in this figure. The power take-off mechanism has again reduced the high amplitude motions of the buoys (in the range of 1.5-3 rad/sec) while it has increased the response of the platform in heave, roll and pitch.

Irregular Waves

The wave environment was modeled using the short-crested seas as defined in the previous section. Under this consideration, five different wave conditions relevant to a representative site in the north sea were used as the input to the spectral analysis as shown by Tab. 2.

Table 2 Wave conditions for a representative site in the North Sea.

Sea state	Parameters	
	H_s[m]	T_p[sec]
C1	1.25	4.75
C2	1.75	5.25
C3	2.75	6.25
C4	3.25	6.75
C5	4.75	7.75

An example directional wave spectrum is plotted in Fig. 9 for wave condition C3.

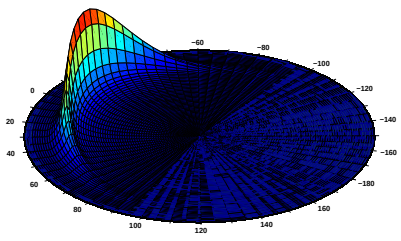

Fig. 9 Directional spectral density function for wave condition C3 and zero mean wave direction.

Absorbed-Power Statistics

The total expected absorbed power for the different wave conditions given in Tab. 2 are presented in Tab. 3. The effect of power absorption coefficient on the total expected absorbed power is indicated in the table. The motivation toward investigating this effect is explained in the following: Eq. (15) shows that the absorbed power is proportional to the square of the relative velocity and the power absorption coefficient. At the same time, Figs. 7 and 8 showed that the power absorption coefficient has a reducing effect on the buoy response. This trade-off raises the idea that there may be an optimal value for the idealized power absorption coefficient. The results in Tab. 3 suggest this optimal value to be between 100-125 $\frac{kNs}{m}$.

The total expected absorbed power was found to be independent of the mean wave direction. However, the wave direction influences the pattern in which power is absorbed by the buoys. These results can be observed in the plots of Fig. 10. In this observation, wave condition C3 is assumed and the array of angles is 0, 30, 45, 60 and 90 degrees.

Table 3 Expected absorbed power as a function of sea states and the idealized power absorption coefficient. The values are normalized with respect to the maximum data in the table.

	Sea state				
b_u	C1	C2	C3	C4	C5
50	11	20	41	51	77
75	11	20	46	59	90
100	10	20	48	62	97
125	10	19	48	63	99
150	9	19	47	63	100
175	9	18	46	61	99
200	8	17	44	60	98

CONCLUDING REMARKS

This paper deals with dynamic analysis of a multi-body wave energy converter by using a mode expansion method. The objective was to study the performance of the device in short-crested ocean waves. Observations were made on the response of the structure and the influence caused by the power absorption mechanism. Moreover, the ability of the structure in absorbing the wave energy was investigated quantitatively by means of an idealized power-take-off system. It was found that the absorbed power is dependent on the sea state while it is not a function of mean wave direction. Moreover, it is observed that the power take-off implies damping that reduces the motions especially at the natural frequency.

To validate the procedure, response transfer functions for the following-seas regular waves were compared to the results by Rogne (2007) in which a standard multi-body approach was utilized. The results showed excellent agreement between the two methods. However, in solving the above problem using standard multi-body approach, similar to the one by Rogne (2007), the hydrodynamic problem must be solved separately for the platform

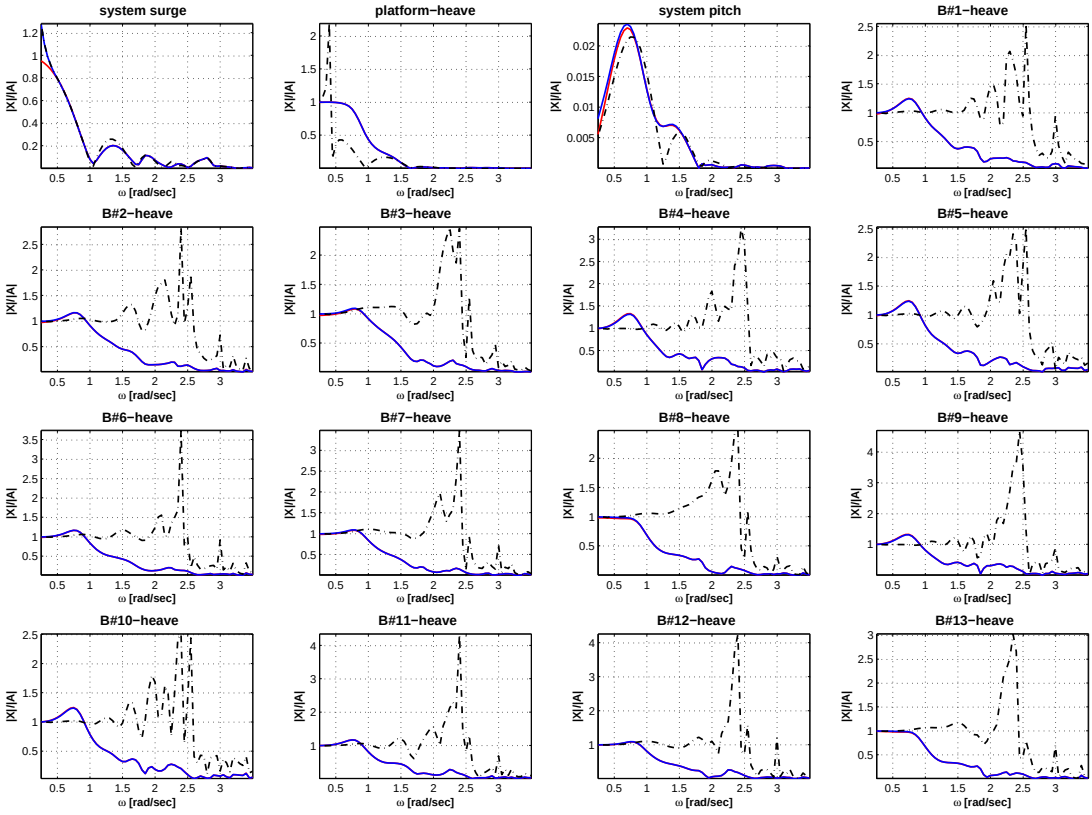

Fig. 7 WEC principal coordinate response in the following-seas waves with/without consideration of power take-off. Note that the results from the current method have been plotted on top of the alternative results by Rogne (2007). The dash-dotted lines indicate the results in the absence of power absorption mechanism.

and the buoys considering each of them to have six degrees of freedom –72 degrees in total. Then, postprocessing is required to reduce the number of DOFs to 27 and to include the power-take-off mechanism.

By using the current generalized modes approach, the size of the problem is reduced considerably, since it is formulated as such the unique WEC system will have 27 DOFs, with power-take-off mechanism already included in the equations. Therefore, the method becomes computationally more efficient than the standard approach. The problem can be reduced even more by accounting for symmetry conditions.

To perform dynamic structural analysis of the WEC in waves, interfacing the information between hydrodynamic and structural software is vital. Exporting pressure data using the standard multi-body approach must be performed within the post-processing stage described above by considering each body, each single degree of freedom, the influence from the power take-off system, and the DOF reduction procedure into account. This complicated task requires a lot of book-keeping and calculation and in practice may be found inapplicable. However, exporting the information within the generalized modes approach is straight forward to perform–like a single-body with different degrees of freedom– and requires much less computational burden.

ACKNOWLEDGEMENTS

The authors are thankful to Fred Olsen Co. for cooperation and information. This research has been conducted under the financial support granted by the SEEWEC project.

REFERENCES

Bendat, JS (1998). “Nonlinear Systems Techniques and Applications,” , John wiley & Sons Inc.

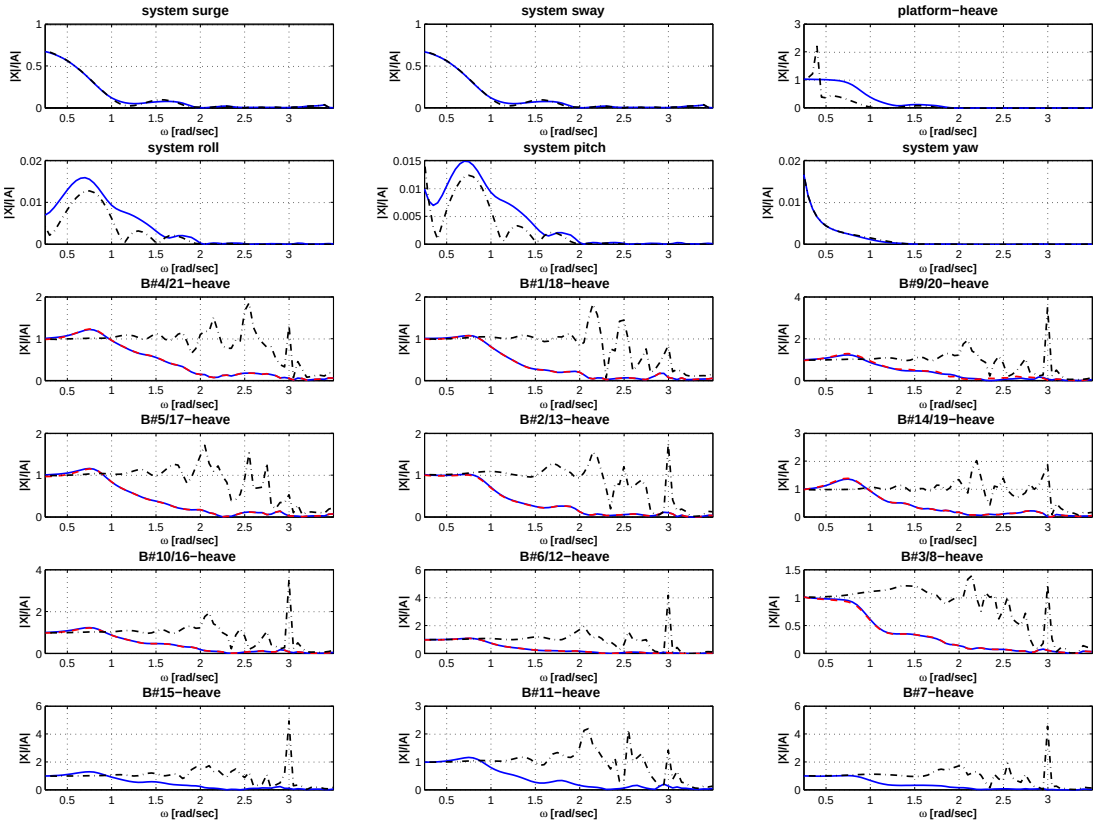

Fig. 8 WEC principal coordinate response in the oblique-seas waves with/without consideration of power take-off. Dashed lines correspond to the response of the buoy identical in response due to problem symmetry. The dash-dotted lines indicate the results in the absence of power absorption mechanism.

Chakrabarti, S (1990). "Nonlinear Methods in Offshore Engineering," , Elsevier.

Goda, Y (2000). "Random Seas and Design of Maritime Structures," , World Scientific Publishing Co. Pte. Ltd.

Goda, Y and Suzuki, Y (1975). "Computation of refraction and diffraction of sea waves with Mitsuyasu's directional Spectrum," Tech. Rep. 230, Port and Harbour Res. Ins.

Hals, J, Taghipour, R, and Moan, T (2007). "Dynamics of A Force-Compensated Two-BodyWave Energy Converter In HeaveWith Hydraulic Power Take-Off Subject To Phase Control," 7th EuropeanWave and Tidal Energy Conference, Porto, Portugal.

Mitsuyasu, H, Tasai, F, Suhara, T, Mizuno, S, Ohkusu, M, Honda, T, and Rikiishi, K (1975). "Observation of directional spectrum of ocean waves using a clover-leaf buoy," *Journal of Physical Oceanography*, Vol. 5, pp. 750–60.

MultiSurf (2007). Aerohydro Inc, ME ,USA, ver. 6.6.

Newman, J (1994). "Wave Effects on Deformable Bodies," *Applied Ocean Research*, Vol. 16, No. 1, pp. 47–59.

Rogne, Y (2007). "Dynamic analysis of a wave energy converter-a frequency domain approach," Master's thesis, Norwegian University of Science and Technology.

Taghipour, R (2008). "Efficient Prediction of Dynamic Response for Flexible and Multi-Body Marine Structures," Ph.D. thesis, CeSOS, Norwegian University of Science and Technology.

WAMIT (2006).

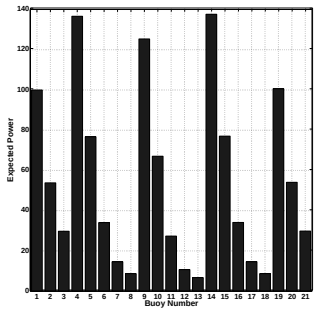

(a) 0

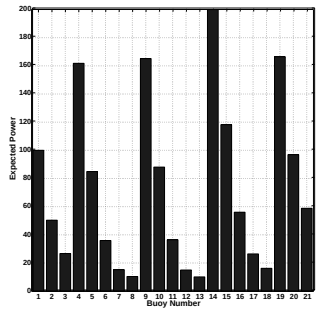

(b) 15

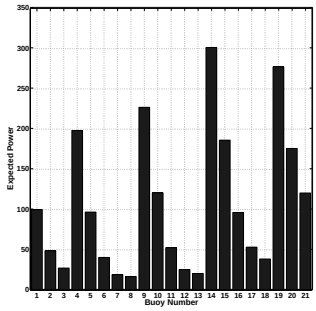

(c) 30

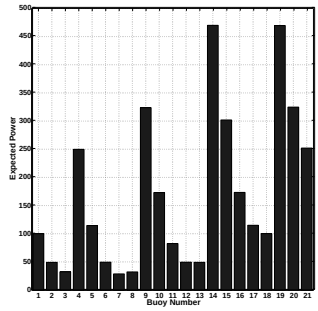

(d) 45

Fig. 10 Absorbed-power layout for the buoys assuming wave condition C3 and different mean wave directions. The Wave heading angles are given in degrees. The data in each plot have been normalized by the power absorbed by the first buoy in that plot.

Paper 3

Hybrid Frequency-Time Domain Models for Dynamic Response Analysis of Marine Structures

Published in
Ocean Engineering, 2008, Vol.35, pp: 685-705.

Available online at www.sciencedirect.com
ScienceDirect
Ocean Engineering 35 (2008) 685–705
OCEAN ENGINEERING
www.elsevier.com/locate/oceaneng

Hybrid frequency–time domain models for dynamic response analysis of marine structures

Reza Taghipour[a,*], Tristan Perez[a,b], Torgeir Moan[a]

[a]Centre for Ships and Ocean Structures, Department of Marine Technology, Norwegian University of Science and Technology, Trondheim, Norway
[b]Centre for Complex Dynamic Systems and Control, The University of Newcastle, Australia

Received 16 January 2007; accepted 8 November 2007
Available online 21 November 2007

Abstract

Time-domain models of marine structures based on frequency domain data are usually built upon the Cummins equation. This type of model is a vector integro-differential equation which involves convolution terms. These convolution terms are not convenient for analysis and design of motion control systems. In addition, these models are not efficient with respect to simulation time, and ease of implementation in standard simulation packages. For these reasons, different methods have been proposed in the literature as approximate alternative representations of the convolutions. Because the convolution is a linear operation, different approaches can be followed to obtain an approximately equivalent linear system in the form of either transfer function or state-space models. This process involves the use of system identification, and several options are available depending on how the identification problem is posed. This raises the question whether one method is better than the others. This paper therefore has three objectives. The first objective is to revisit some of the methods for replacing the convolutions, which have been reported in different areas of analysis of marine systems: hydrodynamics, wave energy conversion, and motion control systems. The second objective is to compare the different methods in terms of complexity and performance. For this purpose, a model for the response in the vertical plane of a modern containership is considered. The third objective is to describe the implementation of the resulting model in the standard simulation environment Matlab/Simulink.

Keywords: Frequency-domain model; Time-domain model; Cummins equation; State-space models; Dynamic analysis

1. Introduction

Dynamic response of marine structures to wave excitation is commonly analyzed in the frequency domain by a first-order potential theory approach and by assuming the wave process as Gaussian, see for instance Newman (1977) and Faltinsen (1990, 2005). The response statistics is then obtained using the well-established theory for Gaussian processes. This approach is based on linear theory, which implies that the wave steepness is small and also that the response due to wave excitation is proportional to the wave amplitude (Faltinsen, 2005). The frequency response functions of the structure can be obtained by using the standard hydrodynamic codes (e.g. WAMIT, 2006). This method is particularly efficient since for each frequency considered, the motion response is obtained by solving a set of simultaneous linear equations with constant coefficients.

When nonlinear effects such as viscous forces, water entry and exit are considered, however, the linearity assumption is no longer valid. One approach to overcome the difficulties of full nonlinear time-domain analysis is to apply a higher order frequency-domain approach, e.g. by using simplified bilinear and trilinear frequency response functions based on Volterra functional representations (Bendat, 1998). However, frequency-domain approaches are limited to steady-state processes. Besides this fact, higher order frequency-domain methods can be cumbersome to implement and computationally inefficient.

A different approach consists of using a linear time-domain model based on the Cummins equation which will be referred to as a hybrid frequency–time domain model throughout this paper. The resulting linear model is a vector integro-differential equation which involves

*Corresponding author. Tel.: +47 735 95173; fax: +47 735 95528.
E-mail address: reza@ntnu.no (R. Taghipour).

0029-8018/$ - see front matter © 2007 Elsevier Ltd. All rights reserved.
doi:10.1016/j.oceaneng.2007.11.002

Nomenclature

$\mathbf{A}, \mathbf{B}, \tilde{\mathbf{A}}, \tilde{\mathbf{B}}$	constant added mass and damping matrices
$\mathbf{C}$	restoring matrix
$\mathbf{A}(\omega)$	frequency-dependent added mass
$\mathbf{B}(\omega)$	frequency-dependent damping
$\tilde{\mathbf{A}}(\mathrm{j}\omega)$	Complex coefficient for alternative description of the radiation force
$\tilde{\mathbf{B}}(\mathrm{j}\omega)$	Complex coefficient for alternative description of the radiation force
$\mathbf{A}(\infty)$	infinite frequency added mass
$\mathbf{A}'_c, \mathbf{B}'_c, \mathbf{C}'_c, \mathbf{D}'_c$	state-space model matrices (continuous time)
$\mathbf{A}'_d, \mathbf{B}'_d, \mathbf{C}'_d, \mathbf{D}'_d$	state-space model matrices (discrete time)
$\mathscr{F}$	Fourier transform
$\mathbf{f}^{\mathrm{exc}}(t), \mathbf{F}^{\mathrm{exc}}(\mathrm{j}\omega)$	excitation force vector in time and frequency domain
$\mathbf{f}^{\mathrm{R}}(t), \mathbf{F}^{\mathrm{R}}(\mathrm{j}\omega)$	radiation force vector in time and frequency domain
$\acute{\mathbf{f}}^{\mathrm{R}}(t)$	radiation force vector in time with no contribution from the infinite added mass
$h(t)$	impulse response function (continuous time)
$h_d(t)$	impulse response function (discrete time)
$H(\mathrm{j}\omega)$	frequency response function
$H(s)$	transfer function
$\mathscr{H}_k$	Hankel matrix
$\mathbf{h}^{\mathrm{F}}(t), \mathbf{h}^{\mathrm{M}}(t)$	wave to force, wave to motion IRF
$\mathbf{H}^{\mathrm{F}}(\mathrm{j}\omega), \mathbf{H}^{\mathrm{M}}(\mathrm{j}\omega)$	wave to force, wave to motion FRF
$\mathbf{h}^{\mathrm{FM}}(t), \mathbf{h}^{\mathrm{FV}}(t)$	force-to-motion and force-to-velocity IRF
$\mathbf{h}^{\mathrm{FM}}(\mathrm{j}\omega), \mathbf{h}^{\mathrm{FV}}(\mathrm{j}\omega)$	force-to-motion and force-to-velocity FRF
$\mathbf{I}$	identity matrix
j	imaginary unit
$\mathbf{K}(t)$	retardation function
$\mathbf{L}(t)$	convolution kernel
$\mathbf{M}$	rigid body mass matrix
$p_0, p_1, \ldots, q_0, q_1, \ldots$	polynomial coefficients
$P(s), P'(s), Q(s), Q'(s)$	polynomials
t	time variable
t_s	sampling period
w_i, s_i	weight function
$\mathbf{x}(t), \mathbf{X}(\mathrm{j}\omega)$	response vector in time and frequency domain. x_1 is surge, x_2 is sway, etc.
$\mathbf{z}$	state variable
α, β, γ	constant coefficients
$\delta(t)$	Dirac's delta function
$\boldsymbol{\mu}$	matrix of convolution forces
ω, s	frequency and Laplace variables
ϕ, ε	phase difference variables
$\boldsymbol{\theta}$	parameter vector
$\boldsymbol{\theta}^\star$	optimal parameter vector
$\boldsymbol{\theta}_{\mathrm{true}}$	true value of the parameter vector
$\boldsymbol{\theta}_{\mathrm{init}}$	initial value of the parameter vector
$\zeta(t)$	wave elevation
$\dot{g}$	time derivative of variable g
$\bar{g}$	amplitude of the variable g
$\hat{g}$	estimated value of the variable g
g^*	conjugate transpose of the variable g
$\Re(g)$	real part of the complex variable g
BEM	boundary element method
dB	decibel, $x_{\mathrm{dB}} = 20\log_{10}(\lvert x\rvert)$
FRF	frequency response function
IRF	impulse response function
LS	least square
MDOF	multi degree of freedom
NL-LS	nonlinear least square
RAO	response amplitude operator
SDOF	single degree of freedom
TF	transfer function

convolution terms. Nonlinear effects can be introduced to this model at a later stage. In this regards, Wu and Moan (1996) introduced a hybrid frequency time domain approach by first solving the linear problem in the frequency domain and then transforming the input–output into time domain and accounting for nonlinear effects as "additional" loads.

The convolution terms in a time-domain model are not convenient for analysis and design of motion control systems (Fossen, 2002; Perez, 2002). Moreover, time-domain simulations of linear transient or nonlinear problems with convolution terms are computationally demanding and their implementation in standard simulation packages is inconvenient (Kashiwagi, 2004). For these reasons, different methods have been proposed as approximate alternative representations of the convolutions. Because the convolution is a linear operation, different approaches can be followed to obtain an approximately equivalent linear system in the form of either transfer function and state-space models. This process involves the use of system identification, and several options are available depending on the way in which the identification problem is posed. This raises the question whether one method is better than the others.

Hence, the main purpose of this paper is to investigate efficient alternative formulations of the dynamic equations of motion that avoid convolution terms. Sections 2–4 of this paper deal with description of the Cummins equation and the convolution integrals. Different representations of the linear systems, with focus on the state-space models, is the subject of Section 5. Convolution replacement alternatives are investigated in Section 6. Sections 7 and 8 deal with different identification approaches that are commonly used to obtain the state-space models. Application and discussion regarding the use of these methods for a simple memory function is carried out in Section 9. Dynamic response simulations for a container vessel is performed in Section 10 by using state space models. Finally, comments and conclusions are given in Section 11.

2. The Cummins equation and the frequency response model

Cummins (1962) considered the behavior of the fluid and the structure in time domain. He assumed linear behavior and considered impulses in the components of motion. This resulted in a boundary value problem in which the potential was separated into two parts: one valid during the duration of the impulses and the other valid afterwards. By expressing the pressure as a function of these potentials and integrating it over the wetted surface of the vessel, he obtained a vector integro-differential equation, which is known as the *Cummins Equation*. For the case of zero forward speed, this equation is of the following form:

$$[\mathbf{M}+\mathbf{A}]\ddot{\mathbf{x}}(t)+\int_0^t \mathbf{K}(t-\tau)\dot{\mathbf{x}}(\tau)\,\mathrm{d}\tau+\mathbf{C}\mathbf{x}(t)=\mathbf{f}^{\mathrm{exc}}(t). \tag{1}$$

The vector $\mathbf{x}(t)$ represents the perturbation with respect to an inertial reference frame. The convolution terms in Eq. (1) capture the effect that the changes in momentum of the fluid at a particular time affects the motion at subsequent times—this is known as fluid memory effect. In case of zero forward speed, the retardation functions will depend only on the geometry of the vessel (Cummins, 1962).

The model in Eq. (1) can also be considered in the frequency domain (Ogilvie, 1964):

$$-\omega^2[\mathbf{M}+\mathbf{A}(\omega)]\mathbf{X}(\mathrm{j}\omega)+\mathrm{j}\omega\mathbf{B}(\omega)\mathbf{X}(\mathrm{j}\omega)+\mathbf{C}\mathbf{X}(\mathrm{j}\omega)=\mathbf{F}^{\mathrm{exc}}(\mathrm{j}\omega), \tag{2}$$

from which the following frequency response follows:

$$\mathbf{X}(\mathrm{j}\omega)=[-\omega^2(\mathbf{M}+\mathbf{A}(\omega))+\mathrm{j}\omega\mathbf{B}(\omega)+\mathbf{C}]^{-1}\mathbf{F}^{\mathrm{exc}}(\mathrm{j}\omega). \tag{3}$$

$\mathbf{F}^{\mathrm{exc}}(\mathrm{j}\omega)$ gives the linear forces due to the waves $\zeta(t)=\bar{\zeta}\cos(\omega t)$, and $\mathbf{X}(\mathrm{j}\omega)$ gives the amplitude and phase of the motion due to the wave excitations. From Eq. (3) we can distinguish three following frequency response functions (FRFs):

- *Wave-to-force FRF*:
$$\mathbf{H}^{\mathbf{F}}(\mathrm{j}\omega)=\frac{\mathbf{F}^{\mathrm{exc}}(\mathrm{j}\omega)}{\bar{\zeta}}. \tag{4}$$

- *Force-to-motion FRF*:
$$\mathbf{H}^{\mathrm{FM}}(\mathrm{j}\omega)=[-\omega^2(\mathbf{M}+\mathbf{A}(\omega))+\mathrm{j}\omega\mathbf{B}(\omega)+\mathbf{C}]^{-1}. \tag{5}$$

- *Wave-to-motion FRF*:
$$\mathbf{H}^{\mathrm{M}}(\mathrm{j}\omega)=\mathbf{H}^{\mathrm{FM}}(\mathrm{j}\omega)\mathbf{H}^{\mathrm{F}}(\mathrm{j}\omega). \tag{6}$$

3. Relation between time and frequency domain models

3.1. Ogilvie relations

The relationship between the parameters of Eq. (1) and those of Eq. (2) were established by Ogilvie (1964):

$$\mathbf{A}(\omega)=\mathbf{A}-\frac{1}{\omega}\int_0^\infty \mathbf{K}(t)\sin(\omega\tau)\,\mathrm{d}\tau,$$

$$\mathbf{B}(\omega)=\int_0^\infty \mathbf{K}(t)\cos(\omega\tau)\,\mathrm{d}\tau, \tag{7}$$

from which it follows that

$$\mathbf{K}(t)=\frac{2}{\pi}\int_0^\infty \mathbf{B}(\omega)\cos(\omega t)\,\mathrm{d}\omega \tag{8}$$

and

$$\mathbf{A}=\lim_{\omega\to\infty}\mathbf{A}(\omega)=\mathbf{A}(\infty). \tag{9}$$

Using these relations, Eq. (1) can be written as

$$[\mathbf{M}+\mathbf{A}(\infty)]\ddot{\mathbf{x}}(t)+\int_0^t \mathbf{K}(t-\tau)\dot{\mathbf{x}}(\tau)\,\mathrm{d}\tau+\mathbf{C}\mathbf{x}(t)=\mathbf{f}^{\mathrm{exc}}(t). \tag{10}$$

A related form of the above by Wehausen (1967) is

$$[\mathbf{M}+\mathbf{A}(\infty)]\ddot{\mathbf{x}}(t)+\int_0^t \mathbf{L}(t-\tau)\ddot{\mathbf{x}}(\tau)\,\mathrm{d}\tau+\mathbf{C}\mathbf{x}(t)=\mathbf{f}^{\mathrm{exc}}(t), \tag{11}$$

where

$$\mathbf{K}(t)=\frac{\mathrm{d}}{\mathrm{d}t}\mathbf{L}(t). \tag{12}$$

The velocity formulation of Eq. (10) is more convenient for numerical simulations since the velocity is part of the state of the system whereas acceleration is not (Jefferys, 1984).

3.2. Time-domain properties of the convolutions

The following relations are satisfied by the convolution terms:

- *For* $t=0^+$: It follows from Eq. (8), that
$$\mathbf{K}(0^+)=\frac{2}{\pi}\int_0^\infty \mathbf{B}(\omega)\,\mathrm{d}\omega\neq\mathbf{0}<\infty. \tag{13}$$

- *For* $t\to\infty$:
$$\lim_{t\to\infty}\mathbf{K}(t)=\lim_{t\to\infty}\frac{2}{\pi}\int_0^\infty \mathbf{B}(\omega)\cos(\omega t)\,\mathrm{d}\omega=\mathbf{0}, \tag{14}$$
which follows from the Riemann–Lebesgue Lemma.

Eq. (14) expresses an important property that establishes the input–output stability[1] of the convolution terms. Indeed, for each term

$$\int_0^t K_{ik}(t-\tau)\dot{x}_k(\tau)\,\mathrm{d}\tau \tag{15}$$

[1]By input–output stability, it is implied that a bounded input to the system results in a bounded output.

to be bounded for any bounded excitation function $\dot{x}_k(\tau)$, it is necessary that

$$\int_0^t |\mathbf{K}(t)|\,\mathrm{d}t < \infty, \tag{16}$$

which holds provided that Eq. (14) holds.

3.3. Frequency-domain properties of the convolutions

The frequency response of the convolutions are given by using Eq. (7):

$$\begin{aligned}\mathbf{K}(\mathrm{j}\omega) &= \int_0^\infty \mathbf{K}(\tau)\mathrm{e}^{-\mathrm{j}\omega\tau}\,\mathrm{d}\tau \\ &= \mathbf{B}(\omega) + \mathrm{j}\omega[\mathbf{A}(\omega) - \mathbf{A}(\infty)].\end{aligned} \tag{17}$$

Then

- *For* $\omega \to 0$: The potential damping, $\mathbf{B}(\omega)$, tends to zero as $\omega \to 0$, and the difference $\mathbf{A}(0) - \mathbf{A}(\infty)$ is finite, as a result:

$$\lim_{\omega\to 0} \mathbf{K}(\mathrm{j}\omega) = \mathbf{0}. \tag{18}$$

- *For* $\omega \to \infty$: The potential damping tends to zero as $\omega \to \infty$, and

$$\lim_{\omega\to\infty} \omega[\mathbf{A}(\omega) - \mathbf{A}(\infty)] = \int_0^\infty \mathbf{K}(t)\sin(\omega\tau)\,\mathrm{d}\tau = \mathbf{0},$$

which follows from Eq. (7) and the Riemman–Lebesgue Lemma. Thus,

$$\lim_{\omega\to\infty} \mathbf{K}(\mathrm{j}\omega) = 0. \tag{19}$$

- *Passivity of* $\mathbf{K}(\mathrm{j}\omega)$: Passivity is an important property of the physical systems, which establishes that there is no energy generation within the system; that is, the system can either store or dissipate energy. This property should also be reflected in the mathematical models. For linear systems, passivity is equivalent to positive realness; i.e., the real part of the frequency response function lies entirely on the right hand side of the complex plane. The damping matrix is symmetric and positive-semi definite—$\mathbf{B}(\omega) = \mathbf{B}^{\mathrm{T}}(\omega) >= \mathbf{0}$ (Newman, 1977). Hence, $\mathbf{K}(\mathrm{j}\omega)$ is positive real ($\mathbf{K}(\mathrm{j}\omega) + \mathbf{K}(-\mathrm{j}\omega)^{\mathrm{T}} >= 0$), and thus passive (Damaren, 2000; Kristiansen et al., 2005). This implies that the diagonal elements of the matrix $\mathbf{K}(\mathrm{j}\omega)$ are positive real, and the off-diagonal terms need only to be stable (Unneland et al., 2007).

4. Alternative representations of the radiation force

Within the scope of fluid memory effects, the identification of state-space models can be posed for not only the retardation functions, but also for the other representatives of the radiation force. Therefore, we devote this section to clarify these alternatives before explaining different convolution replacement approaches in Section 6.

The total hydrodynamic radiation force vector in the frequency domain can be expressed as

$$\mathbf{F}^{\mathbf{R}}(\mathrm{j}\omega) = -[\mathbf{B}(\omega)\dot{\mathbf{X}}(\mathrm{j}\omega) + \mathbf{A}(\omega)\ddot{\mathbf{X}}(\mathrm{j}\omega)]. \tag{20}$$

Replacing the acceleration vector by the time derivative of the velocity vector gives

$$\begin{aligned}\mathbf{F}^{\mathbf{R}}(\mathrm{j}\omega) &= -[\mathbf{B}(\omega) + \mathrm{j}\omega\mathbf{A}(\omega)]\dot{\mathbf{X}}(\mathrm{j}\omega) \\ &= -\bar{\mathbf{B}}(\mathrm{j}\omega)\dot{\mathbf{X}}(\mathrm{j}\omega).\end{aligned} \tag{21}$$

Alternatively,

$$\begin{aligned}\mathbf{F}^{\mathbf{R}}(\mathrm{j}\omega) &= -\left[\frac{\mathbf{B}(\omega)}{\mathrm{j}\omega} + \mathbf{A}(\omega)\right]\ddot{\mathbf{X}}(\mathrm{j}\omega) \\ &= -\bar{\mathbf{A}}(\mathrm{j}\omega)\ddot{\mathbf{X}}(\mathrm{j}\omega).\end{aligned} \tag{22}$$

Eqs. (21) and (22) represent the complex coefficients $\bar{\mathbf{B}}(\mathrm{j}\omega)$ and $\bar{\mathbf{A}}(\mathrm{j}\omega)$. By expressing Eq. (10) in the frequency domain, it follows that

$$\mathbf{F}^{\mathbf{R}}(\mathrm{j}\omega) = -[\mathbf{A}(\infty)\ddot{\mathbf{X}}(\mathrm{j}\omega) + \mathbf{K}(\mathrm{j}\omega)\dot{\mathbf{X}}(\mathrm{j}\omega)]. \tag{23}$$

In other words, the retardation function relates the velocity vector to a portion of the radiation force. Then, the following relations hold between $\bar{\mathbf{A}}$, $\bar{\mathbf{B}}$ and the frequency domain representation of the retardation function $\mathbf{K}$:

$$\bar{\mathbf{A}}(\mathrm{j}\omega) = \frac{\bar{\mathbf{B}}(\mathrm{j}\omega)}{\mathrm{j}\omega} = \mathbf{A}(\infty) + \frac{\mathbf{K}(\mathrm{j}\omega)}{\mathrm{j}\omega}. \tag{24}$$

5. State-space models for linear systems

Before proceeding with different representations of the convolution terms and of the Cummins equation (Eq. (10)), linear system representations are briefly revisited. This will then be used throughout the rest of the paper.

5.1. Time-domain models

Let us consider a stable linear dynamic system with scalar excitation $u(t)$ (input) and scalar response $y(t)$ (output). The relationship between excitation and response can then be characterized in three different ways as indicated in the following.

- *Ordinary differential equation* (ODE) *with high-order derivatives*:

$$\begin{aligned}&\frac{\mathrm{d}^n y(t)}{\mathrm{d}t^n} + q_{n-1}\frac{\mathrm{d}^{n-1}y(t)}{\mathrm{d}t^n} + \cdots + q_1\frac{\mathrm{d}y(t)}{\mathrm{d}t} + q_0 y(t) \\ &\quad = p_m\frac{\mathrm{d}^m u(t)}{\mathrm{d}t^m} + p_{m-1}\frac{\mathrm{d}^{m-1}u(t)}{\mathrm{d}t^{m-1}} + \cdots + p_1\frac{\mathrm{d}u(t)}{\mathrm{d}t} + p_0 u(t).\end{aligned} \tag{25}$$

- *Convolution*:

$$y(t) = \int_0^t h(t-\tau)u(\tau)\,\mathrm{d}\tau, \tag{26}$$

from which it follows that $h(t)$ is the impulse response of the system.

- *State-space representation*:

$$\dot{\mathbf{z}}(t) = \mathbf{A}'\mathbf{z}(t) + \mathbf{B}'u(t),$$
$$y(t) = \mathbf{C}'\mathbf{z}(t) + \mathbf{D}'u(t), \tag{27}$$

where $\mathbf{z}$ is called the *state vector* and gives an internal description of the system. The response of the system to any excitation can be uniquely determined from the value of the excitation and the initial value of the state vector.

The three representations in Eqs. (25)–(27) are equivalent (equating Eq. 26 to 25 and 27 is exact only in the limit as n goes to infinity), and provide the same input–output description of the system for zero initial conditions. Also, it is simple to convert one model to the other. For example, the ODE in Eq. (25) is transformed into a state-space model (Eq. (27)) by using the following auxiliary variables:

$$z_1 = y(t), \quad z_2 = \frac{\mathrm{d}y}{\mathrm{d}t}, \ldots, z_n = \frac{\mathrm{d}^{n-1}y(t)}{\mathrm{d}t^{n-1}}, \tag{28}$$

and for simplicity assume that $p_m = p_{m-1} = \cdots = p_1 = 0$. With these definitions,

$$\begin{aligned}
&\dot{z}_1 = z_2,\\
&\dot{z}_2 = z_3\\
&\vdots\\
&\dot{z}_n = p_0u(t) - q_0z_1 - q_1z_2 - \cdots - q_{n-1}z_n.
\end{aligned} \tag{29}$$

Then, $\mathbf{z} = [z_1, \ldots, z_n]^{\mathrm{T}}$, and

$$\mathbf{A}' = \begin{bmatrix} 0 & 1 & 0 & \cdots & 0\\ 0 & 0 & 1 & & 0\\ 0 & 0 & 0 & \ddots & 0\\ \vdots & \vdots & \vdots & & \vdots\\ 0 & 0 & 0 & \cdots & 1\\ -q_0 & -q_1 & -q_2 & \cdots & -q_{n-1} \end{bmatrix}, \quad \mathbf{B}' = \begin{bmatrix} 0\\ 0\\ \vdots\\ p_0 \end{bmatrix}, \tag{30}$$

and

$$\mathbf{C}' = [1\ 0\ \cdots\ 0], \quad \mathbf{D}' = 0. \tag{31}$$

The value n is the *order of the system*, which corresponds to the highest order derivative of the response in Eq. (25). The order of the vector $\mathbf{z}$ is also n. It should be noticed that the definition of the state variables z_i is not unique (Kailath, 1980).

The general solution of Eq. (27) is given by

$$y(t) = \mathbf{C}\mathrm{e}^{\mathbf{A}'t}\mathbf{z}(0) + \mathbf{C}\int_0^t \mathrm{e}^{\mathbf{A}'(t-\tau)}\mathbf{B}'u(\tau)\,\mathrm{d}\tau + \mathbf{D}'u(t). \tag{32}$$

This form of the solution provides a very attractive way of solving or integrating ODEs (Egeland and Gravdahl, 2002). It also follows from Eq. (32) that the response to the impulse $u(t) = \delta(t)$ assuming zero initial conditions is

$$h(t) = \mathbf{C}'\mathrm{e}^{\mathbf{A}'t}\mathbf{B}' + \mathbf{D}'\delta(t). \tag{33}$$

5.2. Transfer functions and FRFs

By taking the Laplace transform of the Eq. (25), we obtain

$$Y(s) = H(s)U(s),$$

where

$$H(s) = \frac{P(s)}{Q(s)} = \frac{p_ms^m + p_{m-1}s^{m-1} + \cdots + p_1s + p_0}{s^n + q_{n-1}s^{n-1} + \cdots + q_1s + q_0} \tag{34}$$

is the transfer function.

The roots of the numerator polynomial $P(s)$ in Eq. (34) are the zeros of the system, and the roots of the denominator are the poles. The order of the system is the degree of the denominator polynomial (after canceling common factors between numerator and denominator): $n = \deg(Q)$, and the relative degree of the system is the difference $\deg(Q) - \deg(P) = n - m$. The relative degree has implications on the initial value of the impulse response, which are of importance in this paper. The initial value of the impulse response can be computed using the Initial-Value Theorem of the Laplace transform:

$$h(0^+) = \lim_{s\to\infty} sH(s). \tag{35}$$

From Eq. (34), it follows that

$$\lim_{s\to\infty} sH(s) = s\frac{s^mp_m}{s^n}. \tag{36}$$

This limit will be different from zero only if $m = n - 1$. That is, $h(0^+) \neq 0$ *if and only if the system has relative degree* 1.

The FRF of the system, which corresponds to the Fourier transform of the impulse response $h(t)$ can be obtained from the transfer function:

$$\mathscr{F}\{h(t)\} = H(s)|_{s=\mathrm{j}\omega} = H(\mathrm{j}\omega). \tag{37}$$

In the context of this paper, it is convenient to distinguish the transfer function from the FRF as indicated in Eq. (37).

The relationship between the transfer function and a state-space representation follows from the Laplace transform of the state equations in Eq. (27):

$$H(s) = \mathbf{C}'(s\mathbf{I} - \mathbf{A}')^{-1}\mathbf{B}' + \mathbf{D}'. \tag{38}$$

Note that the matrix $\mathbf{D}'$ is different from zero only in cases where the relative degree of the system is zero. In this case, the TF in Eq. (34) can be expressed as

$$H(s) = \frac{P(s)}{Q(s)} = \Lambda + \frac{P'(s)}{Q'(s)}, \quad \Lambda = \lim_{s\to\infty} H(s),$$

with the obvious definitions for $P'(s)$ and $Q'(s)$. Then, the matrices $\mathbf{A}', \mathbf{B}', \mathbf{C}'$ are obtained from $P'(s)$ and $Q'(s)$, and $\mathbf{D}' = \Lambda$. The existence of matrix $\mathbf{D}'$ implies that there is a

direct path between input and output in the model. All the results reviewed in this section extend to the case where the excitation and the response are vectors. For further details see Kailath (1980) or Chen (1999).

6. Convolution replacement

Time-domain simulations of the dynamic response of marine structures by direct evaluation of the convolution integrals may be computationally demanding depending on the time step, simulation length and degrees of freedom of the model (Holappa and Falzarano, 1999; Kashiwagi, 2004). The state-space representation provides an attractive alternative for simulation due to the simple form of its solution i.e. Eq. (32). For zero input, $u(t) = 0$, this indicates that dynamic variables, in this representation, are expressed as linear combinations of exponential functions of time. However, Ursell (1964) showed that the free vertical motion of a floating body immersed on deep water decays slower than exponentially to zero; it decays to zero as t^n, where n is a negative number. It may be implied that it can only be an approximation to replace e.g. the general convolution term in Eq. (1) by a state-space model. In most cases the difference is, however, of academic interest only, and the state-space model represents a very practical approximation. In addition, state-space models are well suited for the methods of analysis used in automatic control (Fossen, 2002; Perez, 2002). For these reasons, significant efforts have been dedicated to finding the alternative representations of the convolution terms and the Cummins equation in Eq. (10). These alternative representations can be broadly grouped into the following types:

(i) Replacement of the frequency-dependent added mass and damping in Eq. (2) by constant coefficients:

$$[\mathbf{M} + \tilde{\mathbf{A}}]\ddot{\mathbf{x}}(t) + \tilde{\mathbf{B}}\dot{\mathbf{x}}(t) + \mathbf{C}\mathbf{x}(t) = \mathbf{f}^{\mathrm{exc}}(t). \tag{39}$$

(ii) Replacement of the convolution in Eq. (10) by a state-space formulation:

$$\begin{aligned} &[\mathbf{M} + \mathbf{A}(\infty)]\ddot{\mathbf{x}}(t) + \acute{\mathbf{f}}^{\mathrm{R}}(t) + \mathbf{C}\mathbf{x}(t) = \mathbf{f}^{\mathrm{exc}}(t),\\ &\dot{\mathbf{z}}(t) = \mathbf{A}'\mathbf{z}(t) + \mathbf{B}'\dot{\mathbf{x}}(t),\\ &\acute{\mathbf{f}}^{\mathrm{R}}(t) = \mathbf{C}'\mathbf{z}(t) + \mathbf{D}'\dot{\mathbf{x}}(t). \end{aligned} \tag{40}$$

(iii) Replacement of the force-to-motion response by a state-space model:

$$\begin{aligned} &\dot{\mathbf{z}}(t) = \mathbf{A}'\mathbf{z}(t) + \mathbf{B}'\mathbf{f}^{\mathrm{exc}}(t),\\ &\mathbf{y}(t) = \mathbf{C}'\mathbf{z}(t) + \mathbf{D}'\mathbf{f}^{\mathrm{exc}}(t),\\ &\text{with } \mathbf{y} = [\mathbf{x}, \dot{\mathbf{x}}]^{\mathrm{T}}. \end{aligned} \tag{41}$$

The first approach is a low-order approximation as defined by the size of the associated state vector as described in Section 5. This form is the simplest possible approach in which the frequency-dependent added mass and damping values are directly replaced by constant matrices. The accuracy of the method depends on how frequency sensitive the added mass and damping are for the specific problem. Such an approximation would normally be based on radiation quantities corresponding to the modal (extremum) or the zero-crossing frequency of the sea wave spectrum. Such a simple method leads to relatively large errors in modeling the system transient response due to a single frequency excitation or system steady-state response due to multiple frequency excitations (Holappa and Falzarano, 1999; Govolato, 1959). Therefore, this method will not be pursued in this paper. The other two methods are higher order approximations.

Indeed, Tick (1959) suggested that the linear time-domain equations of motion with frequency-dependent coefficients can be represented by an ODE with high-order derivatives:

$$\cdots + \boldsymbol{\Gamma}_3\dddot{\mathbf{x}}(t) + \boldsymbol{\Gamma}_2\ddot{\mathbf{x}}(t) + \boldsymbol{\Gamma}_1\dot{\mathbf{x}}(t) + \boldsymbol{\Gamma}_0\mathbf{x}(t) = \mathbf{f}^{\mathrm{exc}}(t). \tag{42}$$

This equation, however, can be efficiently solved by converting it to a state-space model, as discussed in Section 5. Therefore, approaches 2 and 3 are mathematically equivalent to Eq. (42). However, the difference lies in the method used to obtain the parameters of each type of model. This issue is discussed in the following section.

The second approach have been used by a number of researchers within different areas. To the best of the authors' knowledge, state-space models were originally introduced in the field of ocean engineering when Schmiechen (1973) used it to study transient ship maneuvering. Then, Jefferys (1984), Jefferys and Goheen (1992), Yu and Falnes (1995), Yu and Falnes (1998), Hals et al. (2007), used this approach to model wave power devices. Xia et al. (1998) and Taghipour et al. (2007) used this approach in the hydroelastic analysis of marine structures. Holappa and Falzarano (1999), Kristiansen and Egeland (2003), Jordán and Beltrán-Aguedo (2004), Kristiansen et al. (2005), McCabe et al. (2005), Sutulo and Guedes-Soares (2005), Fossen (2005), Perez and Fossen (2006) used this approach to model different marine structures in waves. Sutulo and Guedes-Soares (2005) however used a formulation slightly different from Eq. (10). Their final model is expressed as a state-space representation for the total radiation force, instead of just the convolution part.

The third approach considers the replacement of the complete model from force-to-motion instead of replacing the convolution term in Eq. (10). This approach was originally proposed by Cummins (1962) in a convolution form:

$$\mathbf{x}(t) = \int_0^t \mathbf{h}^{\mathrm{FM}}(t-\tau)\,\mathbf{f}^{\mathrm{exc}}(\tau)\,\mathrm{d}\tau. \tag{43}$$

Motivated by this, Perez and Lande (2006) proposed a model of the form

$$\dot{\mathbf{x}}(t) = \int_0^t \mathbf{h}^{\mathrm{FV}}(t-\tau)\,\mathbf{f}^{\mathrm{exc}}(\tau)\,\mathrm{d}\tau, \tag{44}$$

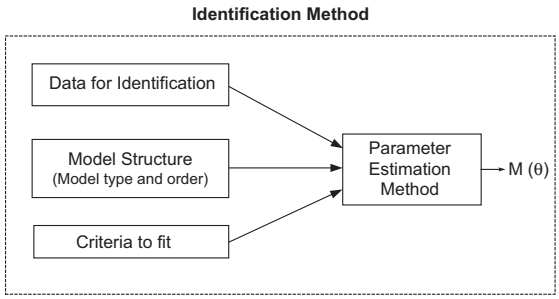

Fig. 1. Components defining the identification method in the context of this paper (adapted from Ljung, 1999).

where $\mathbf{h}^{FV}(t)$ is the impulse response from force to velocities, which in the frequency domain can be obtained from

$$\mathbf{H}^{FV}(j\omega) = j\omega\mathbf{H}^{FM}(j\omega), \tag{45}$$

where $\mathbf{H}^{FM}(j\omega)$ is given by Eq. (5). When the model Eq. (44) is formulated in state-space form and integrators are added, Eq. (41) results.

7. Identification methods for convolution replacement

Fig. 1 shows the components defining an identification method in the context of this paper. Every identification method consists of selecting a series of data, choosing a model structure (model type and order) and a fitting criterion. The unknown parameters in the prospective model are obtained by a parameter estimation method and using the specified fitting criteria (Ljung, 1999). The objective of system identification is to obtain the lowest order model possible that is able to reproduce the behavior of the system for the desired purpose while maintaining stability of the resulting model.

In the present context, the idea is to replace the convolution terms by alternative models based on the following types of data:

- Complex hydrodynamic coefficients: $\bar{\mathbf{A}}(j\omega)$ and $\bar{\mathbf{B}}(j\omega)$.
- The retardation functions $\mathbf{K}(t)$, and its frequency response $\mathbf{K}(j\omega)$.
- The force-to-motion FRF: $\mathbf{H}^{FM}(j\omega)$.

Based on these data and parameter estimation methods described in the next section, there are different ways of considering the system identification problem. The alternative identification methods are schematically illustrated in Fig. 2 and can be divided into two main groups:

- frequency-domain identification;
- time-domain identification;

depending upon which type of data is used.

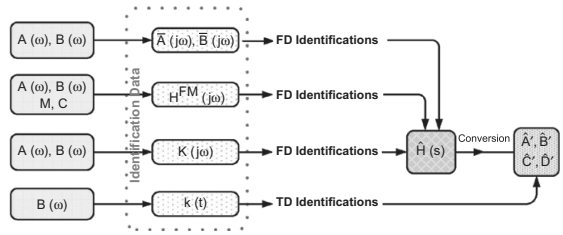

Fig. 2. Alternative data for the identification of state-space models to replace the convolution integrals.

The top path in Fig. 2 shows the approach that starts from the hydrodynamic coefficients $\mathbf{A}(\omega)$ and $\mathbf{B}(\omega)$, and computes the complex coefficients $\bar{\mathbf{A}}(j\omega)$ or $\bar{\mathbf{B}}(j\omega)$, which give two different representations of the radiation forces—see Eqs. (21) and (22). The identification can then be performed in the frequency domain, where a rational transfer function ($\hat{\mathbf{H}}(s)$) model is fitted to the corresponding FRF. Once this is done the TF obtained is converted to an ODE with higher order derivatives, and then to a state-space representation. Söding (1982), Xia et al. (1998), Sutulo and Guedes-Soares (2005), among others, considered this approach.

The second approach uses the rigid body and hydrodynamic coefficients ($\mathbf{M}$, $\mathbf{A}(\omega)$, $\mathbf{B}(\omega)$, $\mathbf{C}$) to compute either the force to motion or the force-to-velocity FRF, $\mathbf{H}^{FM}(j\omega)$ or $\mathbf{H}^{FV}(j\omega)$ based on Eqs. (5) or (45), respectively. The identification is then performed in the frequency domain, where a rational transfer function $\hat{\mathbf{H}}(s)$ is fitted via regression techniques. The state-space representation for the complete model (from excitation force-to-motion) can then be obtained from $\hat{\mathbf{H}}(s)$. Perez and Lande (2006) proposed the application of this approach.

The third approach in Fig. 2 uses the frequency response $\mathbf{K}(j\omega)$ of the convolution terms, which can be computed from Eq. (17) using $\mathbf{A}(\omega)$ and $\mathbf{B}(\omega)$. The identification is then performed in the frequency domain, where a rational transfer function $\hat{\mathbf{H}}(s)$ is fitted to $\mathbf{K}(j\omega)$. The estimated $\hat{\mathbf{H}}(s)$ can then be converted to a state-space model. The approach was applied e.g. by Jefferys (1984), Holappa and Falzarano (1999), Jordán and Beltrán-Aguedo (2004), McCabe et al. (2005), and Perez and Fossen (2006). These researchers have the same starting point, i.e. $\mathbf{K}(j\omega)$, but they differ slightly in the method used for the identification and how they arrive to the final state-space model.

The fourth approach in Fig. 2 is a time-domain approach which estimates a state-space model for the convolution terms using the retardation functions $\mathbf{K}(t)$. This approach was used by Yu and Falnes (1995), Yu and Falnes (1998), Duclos et al. (2001), Kristiansen and Egeland (2003), and Kristiansen et al. (2005).

Added mass and damping serve as the basic elements of the hybrid frequency–time domain models (because they construct the convolution kernels). In evaluation of such quantities, it is important to pay attention to the irregular

frequencies, panel size, the truncation frequency, and the resolution of the frequency-dependent data. Ignoring these parameters can fundamentally violate the quality of the identification data (convolution kernels) that in turn affects the hybrid frequency–time domain simulations.

In the following section we will discuss three parameter estimation methods that can be used to obtain the unknown model parameters in the identification problems described above.

8. Parameter estimation methods

In this section, we will describe three methods by which the unknown model parameters resulting from the identification methods are obtained:

(i) Impulse response curve fitting.
(ii) Realization theory.
(iii) Regression in the frequency domain.

The performance and use of each method will be discussed in Section 9.

8.1. Impulse response curve fitting

This method consists of a state-space representation

$$\dot{\mathbf{z}}(t) = \mathbf{A}'(\boldsymbol{\theta})\mathbf{z}(t) + \mathbf{B}'(\boldsymbol{\theta})u(t),$$
$$y(t) = \mathbf{C}'(\boldsymbol{\theta})\mathbf{z}(t), \tag{46}$$

where the coefficients are parameterized in terms of the vector of parameters $\boldsymbol{\theta}$. The parameters are then estimated such that the impulse response of Eq. (46) approximates the impulse response of the true system (the retardation function).

This approximation can be characterized, for example, in the least-squares (LS) sense:

$$\boldsymbol{\theta}^{\star} = \arg\min_{\boldsymbol{\theta}} \sum_i w_i |h(t_i) - \hat{h}(t_i, \boldsymbol{\theta})|^2, \tag{47}$$

where

$$\hat{h}(t, \boldsymbol{\theta}) = \hat{\mathbf{C}}'(\boldsymbol{\theta}) \exp\{\hat{\mathbf{A}}'(\boldsymbol{\theta})t\}\hat{\mathbf{B}}'(\boldsymbol{\theta}), \tag{48}$$

and "argmin" means the minimizing argument, and w_i are weighting coefficients. The above problem is nonlinear in the parameters $\boldsymbol{\theta}$ and can be solved using Gauss–Newton type of algorithms—see, for example, Nocedal and Wright (1999). The application of these optimization methods requires an initial condition for the parameter $\boldsymbol{\theta}$.

Companion forms can be used as a particular representation for Eq. (46). The advantage of these representations is the small number of parameters needed: for a system with order n, *at most* $2n$ parameters are needed to have a full model parametrization (the actual number of parameters depend on the relative degree of the system). For example, the specific form

$$\hat{\mathbf{A}}' = \begin{bmatrix} 0 & 0 & 0 & \dots & -q_0 \\ 1 & 0 & 0 & \dots & -q_1 \\ 0 & 1 & 0 & \dots & \\ \vdots & \vdots & \ddots & & \vdots \\ 0 & 0 & \dots & 1 & -q_{n-1} \end{bmatrix}, \quad \hat{\mathbf{B}}' = \begin{bmatrix} p_0 \\ p_1 \\ \vdots \\ p_{n-1} \end{bmatrix}, \tag{49}$$

$$\hat{\mathbf{C}}' = [0 \ 0 \ \dots \ 0 \ 1]. \tag{50}$$

is known as the observer companion form that corresponds to TF in Eq. (34) with the relative degree equal to 1. In this context, the vector of the unknown parameters in Eq. (46) is

$$\boldsymbol{\theta} = [q_0, \dots, q_{n-1}, p_0, \dots, p_{n-1}]^{\mathrm{T}}. \tag{51}$$

Note, however, that p_{n-1} can be obtained as

$$p_{n-1} = \lim_{s\to\infty} sH(s) = h(0^+). \tag{52}$$

Therefore, the number of parameters in Eq. (51) is reduced by 1

$$\boldsymbol{\theta} = [\theta_1, \theta_2 \dots, \theta_{2n-1}] = [q_0, \dots, q_{n-1}, p_0, \dots, p_{n-2}]^{\mathrm{T}}. \tag{53}$$

8.2. Realization theory

Realization theory deals with the problem of obtaining a minimal realization (one for which the size of the matrix $\mathbf{A}'$ is minimal) from its Markov parameters (Ho and Kalman, 1966). It consists of finding the order of the system and the actual matrices ($\mathbf{A}', \mathbf{B}', \mathbf{C}'$ and $\mathbf{D}'$) from a matrix assembly of the samples of the impulse response.

The realization problem is easier to solve for a discrete-time system than it is for a continuous-time system and therefore such an estimation is commonly carried out in discrete time. The reason for this is that the impulse response of a discrete-time system is given by the Markov parameters of the system:

$$h_{\mathrm{d}}(t_k) = \mathbf{C}'_{\mathrm{d}}\mathbf{A}'^{k-1}_{\mathrm{d}}\mathbf{B}'_{\mathrm{d}} + \mathbf{D}'_{\mathrm{d}},$$

where $t_k = kt_s$ for $k = 0, 1, \dots$ with t_s being the sampling period. In the present context the realization problem is to obtain a minimal state-space realization

$$\mathbf{x}(t_{k+1}) = \hat{\mathbf{A}}'_{\mathrm{d}}\mathbf{x}(t_k) + \hat{\mathbf{B}}'_{\mathrm{d}}u(t_k),$$
$$y(t_k) = \hat{\mathbf{C}}'_{\mathrm{d}}\mathbf{x}(t_k) + \hat{\mathbf{D}}'_{\mathrm{d}}u(t_k),$$

for model described by its impulse response:

$$y(t_k) = \sum_{l=1}^{\infty} h_{\mathrm{d}}(t_l)y(t_{k-l}). \tag{54}$$

Note that Eq. (54) is a discrete-time convolution. The solution of the realization problem consists of two parts:

(i) Find the McMillan degree of the system, which is the order of a minimal realization.
(ii) Find the matrices $\hat{\mathbf{A}}'_{\mathrm{d}}, \hat{\mathbf{B}}'_{\mathrm{d}}, \hat{\mathbf{C}}'_{\mathrm{d}}, \hat{\mathbf{D}}'_{\mathrm{d}}$.

A key concept in this respect is the evaluation of the Hankel matrix of the Markov parameters, and its factorization as a product of extended observability and controllability matrices (Ho and Kalman, 1966):

$$\mathscr{H}_k = \begin{bmatrix} h_1 & h_2 & \dots & h_k \\ h_2 & h_3 & \dots & h_{k+1} \\ \vdots & \vdots & & \vdots \\ h_k & h_{k+1} & \dots & h_{2k-1} \end{bmatrix} = \begin{bmatrix} \mathbf{C}' \\ \mathbf{C}'\mathbf{A}' \\ \mathbf{C}'\mathbf{A}'^2 \\ \vdots \\ \mathbf{C}'\mathbf{A}'^{k-1} \end{bmatrix} [\mathbf{B}' \ \mathbf{A}'\mathbf{B}' \ \mathbf{A}'^2\mathbf{B}' \ \dots \ \mathbf{A}'^{k-1}\mathbf{B}']. \quad (55)$$

There are several algorithms to obtain the realization. The most commonly used one is the singular value decomposition (SVD) of $\mathscr{H}_k$ as proposed by Kung (1978). In this approach, the order of the system and the state-space parameters are determined from the number of significant singular values and the factors of the SVD, respectively.

The SVD gives

$$\mathscr{H}_k = \mathbf{U}\Sigma\mathbf{V}^*, \quad (56)$$

where Σ is a diagonal matrix containing the singular values in descending order. In theory, the number of the non-zero singular values give the rank of $\mathscr{H}_k$, which is the order of the system or McMillan degree. Due to precision of the computations Σ and the fact that the impulse response we are using may not be generated by a pure linear system, the matrix containing the singular values can be considered as

$$\Sigma = \begin{bmatrix} \Sigma_1 & 0, \\ 0 & \Sigma_2, \end{bmatrix},$$

where Σ_1 contains large singular values and Σ_2 contain those that are equal or close to zero. The McMillan degree is then determined by the dimension of $\Sigma_1 = n \times n$.

After finding the McMillan degree, the SVD can be further factored as

$$\mathscr{H}_k = [\mathbf{U}_1 \ \mathbf{U}_2] \begin{bmatrix} \Sigma_1 & 0 \\ 0 & \Sigma_2 \end{bmatrix} [\mathbf{V}_1^* \ \mathbf{V}_2^*] = \mathbf{U}_1\Sigma_1\mathbf{V}_1^*. \quad (57)$$

Then matrices of the realization can be determined as follows (Kung, 1978):

$$\mathbf{A}'_{\mathrm{d}} = \Sigma_1^{-1/2} \begin{bmatrix} \mathbf{U}_{11} \\ \mathbf{U}_{12} \end{bmatrix}^{\mathrm{T}} \begin{bmatrix} \mathbf{U}_{12} \\ \mathbf{U}_{13} \end{bmatrix} \Sigma_1^{1/2},$$

$$\mathbf{B}'_{\mathrm{d}} = \Sigma_1^{-1/2}\mathbf{V}_{11}^*,$$

$$\mathbf{C}'_{\mathrm{d}} = \mathbf{U}_{11}\Sigma_1^{1/2},$$

$$\mathbf{D}'_{\mathrm{d}} = h(0),$$

where

$$\mathbf{U}_1 = \begin{bmatrix} \mathbf{U}_{11} \\ \mathbf{U}_{12} \\ \mathbf{U}_{13} \end{bmatrix}, \quad \mathbf{V}_1 = \begin{bmatrix} \mathbf{V}_{11} \\ \mathbf{V}_{12} \\ \mathbf{V}_{13} \end{bmatrix}$$

with the dimensions of $\mathbf{U}_{ii}$ and $\mathbf{V}_{ii}$ being $n \times n$.

Once the parameters of the discrete time model have been obtained, the model can be converted to continuous time using the bilinear transformation (Al-Saggaf and Franklin, 1987). The bilinear transformation guarantees the stability of the continuous-time realization provided the discrete time system is stable. The method described in this section is implemented in Matlab in the function `imp2ss` from the robust control toolbox.

8.3. Transfer function estimation using regression in the frequency domain

From non-parametric data of the FRF $H(\mathrm{j}\omega)$ of a system, we can use frequency domain regression to estimate a rational parametric model $\hat{H}(s)$. There are different methods to perform this. Here, we will only concentrate on the LS method for single input single output (SISO) transfer functions. For other methods see Pintelon and Schoukens (2001).

8.3.1. Nonlinear LS with rational approximations

Let the estimate $\hat{H}$ be a SISO rational transfer function of order n, and relative degree $n-m$:

$$\hat{H}(s,\boldsymbol{\theta}) = \frac{P(s,\boldsymbol{\theta})}{Q(s,\boldsymbol{\theta})} = \frac{p_m s^m + p_{m-1}s^{m-1} + \dots + p_0}{s^n + q_{n-1}s^{n-1} + \dots + q_0}, \quad (58)$$

with the vector of parameters defined as

$$\boldsymbol{\theta} = [p_m, \dots, p_0, q_{n-1}, \dots, q_0]^{\mathrm{T}}. \quad (59)$$

The *frequency-domain identification problem* consists of

(i) Finding the order and relative degree of $\hat{H}$;
(ii) Finding the parameters that give the best LS fitting to the frequency response:

$$\boldsymbol{\theta}^\star = \arg\min_{\boldsymbol{\theta}} \sum_i w_i \left| H(\mathrm{j}\omega_i) - \frac{P(\mathrm{j}\omega_i,\boldsymbol{\theta})}{Q(\mathrm{j}\omega_i,\boldsymbol{\theta})} \right|^2. \quad (60)$$

Once the order and relative degree is chosen, the above NL-LS can be solved in the same way as for Eq. (47).

8.3.2. Quasi-linear regression

The quasi-linear regression presents an alternative that linearizes the problem in Eq. (60). Indeed, if we choose the weights in Eq. (60) as

$$w_i = |Q(\mathrm{j}\omega_i,\boldsymbol{\theta})|^2, \quad (61)$$

the problem reduces to

$$\boldsymbol{\theta}^\star = \arg\min_{\boldsymbol{\theta}} \sum_i |Q(\mathrm{j}\omega_i,\boldsymbol{\theta})H(\mathrm{j}\omega_i) - P(\mathrm{j}\omega_i,\boldsymbol{\theta})|^2, \quad (62)$$

which is affine in the parameter $\boldsymbol{\theta}$; and therefore, it satisfies the normal equations of linear LS. This linearization for fitting complex-value functions was proposed by Levy (1959).

Eq. (62) is simpler to solve than Eq. (60), but, as discussed by Sanathanan and Koerner (1963), the fitting can be poor in some cases: if the data extends over a several frequency decades, a poor fitting obtained at low frequencies result. Poor fitting can also occur if $Q(s)$ has resonant poles close to the imaginary axis. The accuracy of the fitting can be improved by solving Eq. (62) iteratively with different weighting coefficients.

The iterative method works by using the polynomial Q corresponding to the previous iteration as the weight (Sanathanan and Koerner, 1963). That is, the problem in Eq. (60) reduces to

$$\boldsymbol{\theta}_k = \arg\min_{\boldsymbol{\theta}} \sum_i s_{i,k} |Q(\mathrm{j}\omega_i, \boldsymbol{\theta}) H(\mathrm{j}\omega_i) - P(\mathrm{j}\omega_i, \boldsymbol{\theta})|^2, \tag{63}$$

where

$$s_{i,k} = \frac{1}{|Q(\mathrm{j}\omega_i, \boldsymbol{\theta}_{k-1})|^2}.$$

Usually after a few iterations (10–20), $Q(\mathrm{j}\omega_i, \boldsymbol{\theta}_k) \approx Q(\mathrm{j}\omega_i, \boldsymbol{\theta}_{k-1})$; and therefore, Eq. (60) is recovered. Depending on the data to be fitted, it may as well happen that the model obtained through the linearized or, for that matter, through the iterative linearized fitting is unstable. In this case, one can reflect the unstable poles about the imaginary axis.[2]

The function `invfreqs` of the signal processing toolbox in Matlab solves the linear problem Eq. (62) with the option of using a vector of weighting coefficients. Therefore, it is straightforward to implement the iterative procedure starting with $s_{i,1} = 1$.

This method can provide reasonably good fits. However, in some cases, the NL-LS can lead to better approximations. The later option is also implemented in the function `invfreqs`, and uses the parameters obtained from the linearized problem as an initial condition for solving the NL-LS problem. The solution thereby implemented uses the Gauss–Newton algorithm.

From now on, we focus on the identification methods that use the retardation functions and the parameter estimation methods described in this section to obtain their model parameters.[3] These identification methods have been applied to the convolution replacement problems by Yu and Falnes (1995), Kristiansen and Egeland (2003) and McCabe et al. (2005), respectively. The methods are easy to implement and are flexible in the sense that they allow models with different types and orders. The first two methods identify an state-space model from the time series of the retardation functions ($\mathbf{K}(t)$) and the last method identifies a TF from the FRF of the retardation functions ($\mathbf{K}(\mathrm{j}\omega)$).

The parameter estimation method corresponding to each of these three identification problems potentially clarifies the identification data and the model type within the context of this paper. As a result, we hereafter refer to the identification method by the name of its representative (characterizing) parameter estimation method. For instance, by realization theory we mean an identification method that uses the retardation function time series, realization theory, and state space model as its data, parameter estimation method and model type (structure), correspondingly.

9. An example to illustrate the basic features of the identification methods

9.1. Application example

Herein, we consider a simple retardation function as an example to compare the performance of the different identification methods. The example is based on pure analytical relations and satisfies all the properties of the convolution terms given in Section 3. It is standard practice in system identification to compare different estimators with scenarios for which the values of the true quantities to be estimated are known and this is the motivation for this example. We should mention, however, that the added mass and damping depicted show resemblance to practical cases when there is hydrodynamic interaction e.g. in sections of catamarans (Faltinsen, 1990). By assuming a frequency-dependent added mass and damping of the form:

$$A(\omega) = \gamma + \frac{(\alpha^2 + \beta^2 - \omega^2)(\beta + 1)}{(\alpha^2 + \beta^2 - \omega^2)^2 + 4\alpha^2\omega^2}, \tag{64}$$

$$B(\omega) = \frac{2\alpha(\beta + 1)\omega^2}{(\alpha^2 + \beta^2 - \omega^2)^2 + 4\alpha^2\omega^2}. \tag{65}$$

The frequency retardation function from Eq. (17) then is

$$K(\mathrm{j}\omega) = \frac{\mathrm{j}\omega(\beta + 1)}{(\mathrm{j}\omega + \alpha)^2 + \beta^2}, \tag{66}$$

which corresponds to the following time-domain retardation function:

$$k(t) = (1 + \beta)\mathrm{e}^{-\alpha t}\left[\cos(\beta t) - \frac{\alpha}{\beta}\sin(\beta t)\right]. \tag{67}$$

Note that parameter γ does not contribute to the formation of the retardation function as it is the value of added mass at infinite frequency. Fig. 3 shows the added mass and damping plots drawn against the frequency of oscillations when the above parameters are chosen as: $\alpha = 0.2, \beta = 2, \gamma = 0.5$.

Using the Laplace transform, Eq. (66) can be expressed as

$$K(s) = \frac{3s}{s^2 + 0.4s + 4.04}. \tag{68}$$

[2] A complex pole pair in the right half plane of a system's pole-zero plot generates an exponentially increasing component in the homogeneous response; thus defining the system to be unstable. Reflecting such a pole about the imaginary axis guarantees a stable system.

[3] Third and fourth identification methods described in Section 7.

In Fig. 4 the IRF and the FRF of Eq. (68) have been plotted by markers. Note that the FRF is plotted in logarithmic scale and the magnitude of the FRF is given in decibels: $20\log_{10}|K(\omega)|$. The reason for plotting the data in this manner is that by simple inspection of the plots, one can infer the order and the relative degree of the system by looking at the asymptotes for $\omega \to 0$ and for $\omega \to \infty$. These plots are known as Bode diagrams in the field of electrical and control engineering (Oppenheim et al., 1997). Note also that Eq. (68) has relative degree 1. This was commented by Jefferys (1984) as a property for retardation function TFs, which follows from Eqs. (13) and (36):

$$\lim_{s\to\infty} sK(s) = k(0) = \frac{s^{m+1}p_m}{s^n} = 3. \tag{69}$$

From Eqs. (8) and (69) with the constraint that the relative degree is 1, it follows that for the convolutions in the Cummins equation:

$$p_m = \frac{2}{\pi}\int_0^\infty B_{ik}(\omega)\,\mathrm{d}\omega. \tag{70}$$

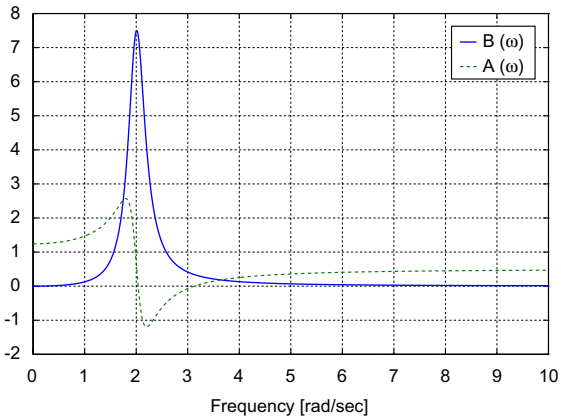

Fig. 3. Example frequency-dependent added mass and damping plots.

9.2. Performance of different identification methods

Fig. 4 shows the performance of the different methods for the example specified by Eqs. (66) and (67). As we can see, all the methods give a reasonable approximation for both the impulse and frequency response of the system in this example.

9.2.1. Impulse response curve fitting

The method that fits the impulse response performs very well for this example. The application of this method to obtain a continuous-time state-space model for each entry of retardation function matrix $\mathbf{K}(t)$ was proposed by Yu and Falnes (1995, 1998) and uses an observer companion form (Eq. (49)). In the example considered, the nonlinear least square problem of Eq. (47) was solved with the function `lsqnonlin` of the optimization toolbox in Matlab, which uses a Gauss–Newton type method. The weighting coefficients were chosen $w_i = 1$ for all i. By using the formulation in Eq. (53), we sought

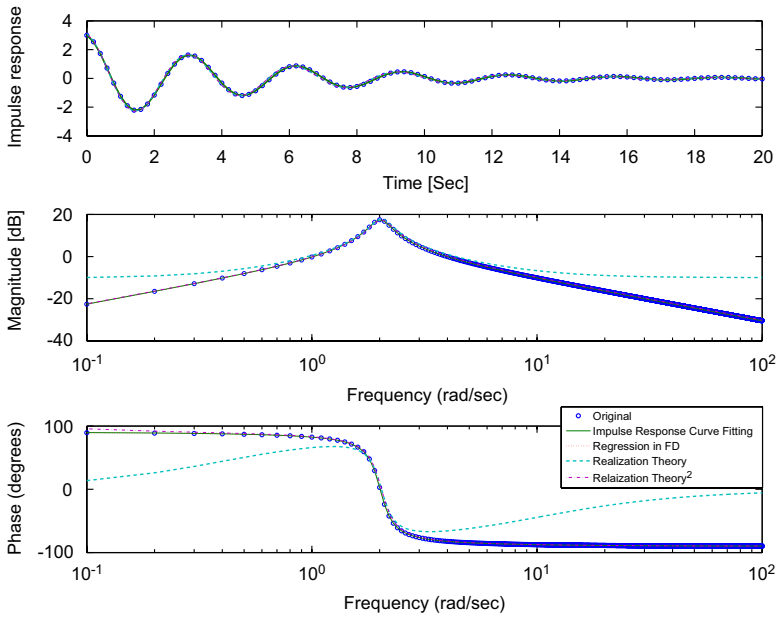

Fig. 4. Comparison of different methods. Superscript 2 stands for the case when matrix D is ignored.

a parametric TF as

$$\hat{H}(s,\theta) = \frac{3s + \theta_3}{s^2 + \theta_2 s + \theta_1}.$$

The initial condition for the parameters was

$$\boldsymbol{\theta}_{\text{init}} = [1,\ 1,\ 1]^{\text{T}},$$

and the estimated parameter values were

$$\hat{\boldsymbol{\theta}} = [4.0398,\ 0.4000,\ -0.0012]^{\text{T}},$$

which compares well with the true parameters.

$$\boldsymbol{\theta}_{\text{true}} = [4.040,\ 0.4000,\ 0.000]^{\text{T}}.$$

This method can be quite time consuming depending on the value of the inial parameters $\boldsymbol{\theta}_{\text{init}}$, and the quality of the results may also be affected by it. For the example considered, good results were obtained, but for data of real marine structures the method was found difficult to use, since there is no easy way to have good estimates for $\boldsymbol{\theta}_{\text{init}}$ and for the order of the model. As discussed by Yu and Falnes (1998), in the case of high-order systems the weighting coefficients w_i in Eq. (47) are important, but there is no clear guidelines for choosing them.

9.2.2. Realization theory

The application of the identification method based on realization theory to the convolution terms in the Cummins equation (Eq. (10)) was proposed by Kristiansen and Egeland (2003) and Kristiansen et al. (2005). This method is easy to implement in Matlab using the function `imp2ss`. Depending on the impulse response data used, it may be difficult to determine the rank of $\mathscr{H}_k$; i.e, it may be difficult to distinguish which singular values are most significant. The algorithm implemented in `imp2ss` sets a threshold and ignores singular values smaller than this threshold: the default threshold ignores singular values smaller than 1% of the largest singular value. If the threshold is not set properly, this algorithm can result in very high-order models. In that case model order reduction is required. This goes beyond the scope of this paper. A more detailed discussion of different methods for model order reduction in this context may be found in Unneland et al. (2005), Unneland and Egeland (2006), and Unneland et al. (2006).

Note also that the conversion from continuous to discrete form requires that the data used in the algorithm be scaled by the sampling time since

$$h_d(t_k) = \int_{t_k}^{t_k+t_s} h(\tau)\,\mathrm{d}\tau \approx t_s h(t_k).$$

Fig. 5 shows the singular values obtained by the SVD decomposition based on the discretization of the impulse response of the example considered in this section shown in Fig. 4. The impulse response was sampled with $t_s = 0.2$ s. From Fig. 5 it is clear that the order of the system is 2 since there are only two significant singular values. The use of the function `imp2ss` with the standard tolerance gives a model with 96 states, and therefore model order reduction

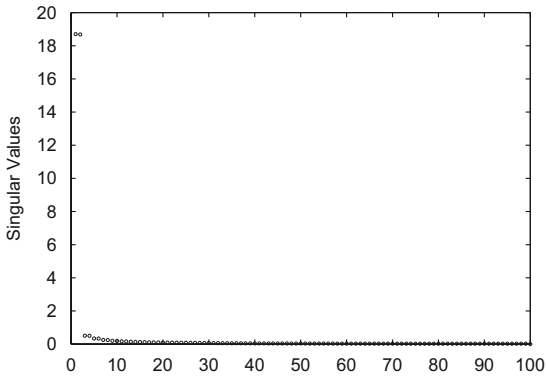

Fig. 5. Singular values for the example.

is required. However, if the tolerance is set properly based on the singular values, the following model is obtained after converting to continuous time:

$$\hat{\mathbf{A}}' = \begin{bmatrix} -0.0000 & -2.0370 \\ 2.0370 & -0.4172 \end{bmatrix}, \quad \hat{\mathbf{B}}' = \begin{bmatrix} -0.0047 \\ 1.7657 \end{bmatrix}, \tag{71}$$

$$\hat{\mathbf{C}}' = [0.0047\ \ 1.7657], \quad \hat{\mathbf{D}}' = [0.3167]. \tag{72}$$

Note the matrix $\hat{\mathbf{D}}'$ appears because of the conversion from discrete to continuous used. This implies that the model does not have the proper relative degree, which for this example is 1. This difference in relative degree is clearly observed in the frequency response plots of Fig. 4. In some cases, ignoring $\hat{\mathbf{D}}'$ can result in better approximations.

9.2.3. Identification in the frequency domain

The method of identification in the frequency domain gives good results. The application of this method to the identification of the convolution terms in the Cummins equation was considered, for example, by McCabe et al. (2005), and Perez and Fossen (2006).

This method has the advantage of using linear LS, and if the results are not accurate, the non-linear LS problem can be solved either by using Gauss–Newton methods or by using an iterative method based on quasi-linear regression. The solution of the quasi-linear problem can be used as an initial condition for the parameters when using the Gauss–Newton method. This is an advantage with respect to the method of fitting the impulse response for which we had no initial estimate for the parameters. This approach is implemented in the `invfreqs` function in Matlab.

For example described by Eq. (68), the parameter estimation based on the quasi-linear regression gave good results, so there was no need to proceed with the iterative linearized method or with the NL-LS method. The method is fast, easy to implement and accurate.

For the problem of fitting TFs to replace the convolutions on the Cummins equation in Eq. (10), the relative degree is known before hand: the relative degree is 1. This leaves only one unknown parameter to be chosen which is

the order of the system. Due to the requirement of having a zero at zero frequency, see Eq. (18), it follows that the minimum order that could be used to fit convolution terms is $n_{\min} = 2$. This fact can be used by starting with the lowest order model and then increase the order until a good fitting is obtained. If the order of the system is increased beyond a certain value, the fitting can worsen significantly, and the numerical error may become significant because the excess of poles and zeros will be placed in a way that they cancel each other. This is known as overfitting (Ljung, 1999).

Finally, it should be mentioned that the scaling of the input data is important for numerical stability of the algorithms used. Poor scaling, can in some cases provide inaccurate models for all the methods.

10. Comparison of time-domain response simulations for a container vessel

10.1. Specification of the case

Numerical studies are performed in this section for a container vessel at zero forward speed. The specifications of the ship are given in Table 1. Fig. 6 shows the body plan of the hull.

Two different scenarios are analyzed:

(i) The objective of the first one is to examine the steady-state part of the time-domain response of the container vessel by using two different state-space models. The focus is on the models obtained by identifying the retardation functions based on the *realization theory* and *frequency domain regression* methods as described in Sections 7 and 8. Simulation results are compared with the harmonic response generated based on the frequency domain RAOs for heave and pitch modes. This is done by assuming harmonic wave excitation force in a head seas condition. It is expected that the results of the time-domain simulations match the harmonically generated responses when the transients have died out.

(ii) In the second scenario, response of the vessel released from a displaced condition is simulated by using each of the state-space models. Again, the focus is on the *realization theory* and the *frequency domain identification* methods as described in Section 8. The results of these simulations are compared with those solving for the convolution integrals. This will give an idea about the quality of the identifications. Observations of the CPU time will shed some light on the efficiency of the simulations using state-space models.

Table 1
Vessel specifications

Quantity	Dimension	Value
Mass	kg	7.6656E7
Length overall	m	294.008
Beam	m	32.26
Height	m	24
Draft	m	11.75
Pitch gyration radius	m	69.44
C_G coordinates[a]	m	(−4.165 0 12.87)
Water density	kg/m^3	1025

[a]Measured from midships and keel.

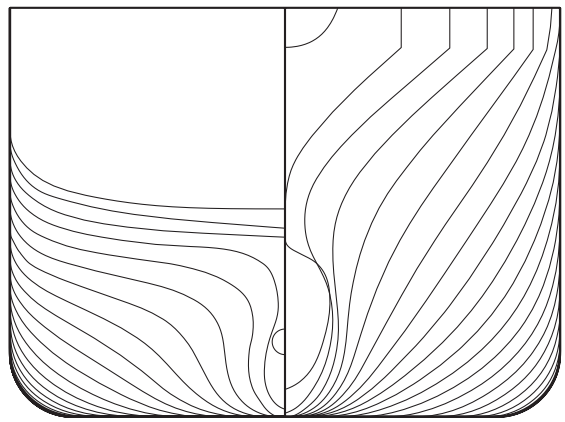

Fig. 6. Body plan of the container vessel.

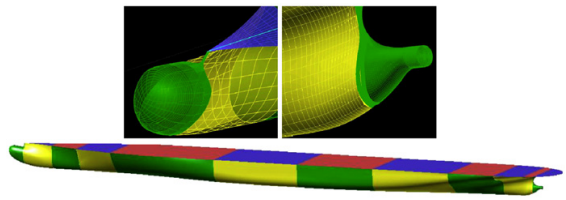

Fig. 7. Underwater geometry of the ship modeled in MultiSurf.

WAMIT (2006) is used as the BEM program for evaluation of the hydrodynamic quantities and Matlab/Simulink is used to identify state-space models and performing the simulations in the time domain.

10.2. Evaluation of frequency-dependent hydrodynamic quantities

The vessel's underwater geometry was modeled in MultiSurf (2006) as is shown in Fig. 7. In solving the boundary value problem in WAMIT (2006), a high-order panel (B-Spline) technique was applied. Twenty-seven patches were used to represent the wetted ship hull and 14 were used to represent the interior free surface. Additional modeling for the interior free surface is performed in order to remove the irregular frequencies. The maximum panel size was chosen equal to 6 m. Calculations were made for 135 frequencies ranging

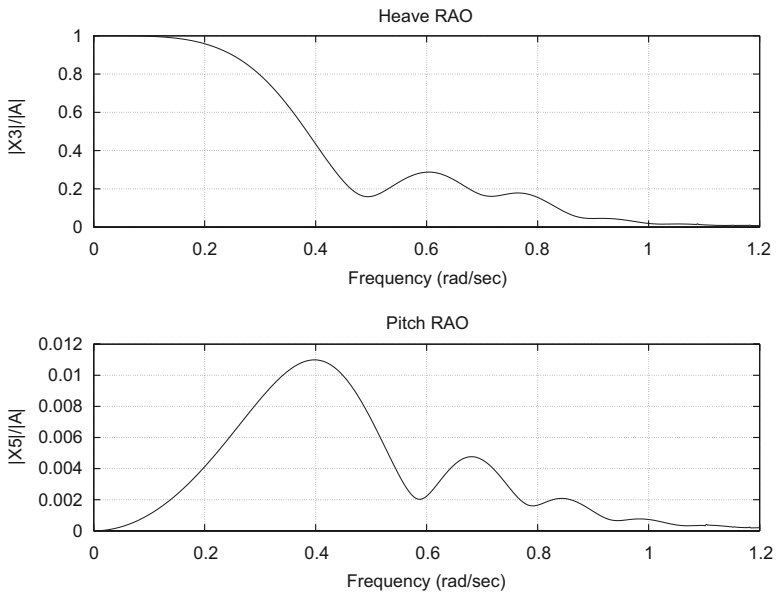

Fig. 8. Results of the RAOs at the ship center of gravity in head waves calculated by WAMIT.

from 0.02 to 2.7 rad/s. The results show no responses in sway, roll and yaw, which make sense for head seas waves. Moreover, it was found that there are practically no vessel motions for wave frequencies above 1.2 rad/s, see Fig. 8.

The port-starboard symmetry in the ship geometry implies 18 nonzero coefficients in the hydrodynamic added mass and damping matrices. In practice, it is difficult to compute the radiation quantities up to very high frequencies where their contributions to the calculation of the retardation functions become negligible. The reason for this could be due to the limitations in the panel size which in turn increase the computer time drastically. In addition, the accuracy of the calculations in BEM software may become questionable past a certain wave number. Therefore, the calculations are enforced to be truncated at a specific wave frequency. As mentioned above, such a truncation was performed at 2.7 rad/s in our calculations.

In most of the cases, one may find it applicable to obtain the radiation quantities for high frequency by fitting a polynomial curve to the data at the tail of the radiation plots and then extrapolate the numerical data based on this tail fit. In this case study, we have used this approach to approximate the damping values at higher frequencies prior to the calculation of the impulse response functions. Typical curve fits at the tail of the damping plots are shown in Fig. 9 for B_{33}, B_{35} and B_{55}. The extrapolated data for B_{35} corresponds to a longer tail than the other two damping plots. Therefore, calculation of K_{35} is expected to be more uncertain.

10.3. Identification of the state-space models

As explained above, the focus is on two methods for obtaining the state-space models: *realization theory* and *frequency domain identification*. Calculation of the retardation functions in the time domain is performed by using Ogilvie's formula, Eq. (8). A trapezoidal integration scheme is used for evaluation of the integrals. These data will serve as the input for the realization theory identifications (see Section 8.2). Based on the observations of the retardation function plots, it was found that there is practically no contribution to the memory forces after 25 s. Therefore, the IRFs are evaluated for a time interval of 0 to 25 s with sampling period equal to 0.1 s as shown in the top plots in Figs. 10–12. The sampling period of 0.1 s was found to be adequate for obtaining reasonable identifications by the realization theory. Then, state-space models are identified for each retardation function. System orders were found from the number of significant singular values similar to what was done in Section 9. The quality of the identifications is visualized and monitored by using three different plots corresponding to the value of the retardation function in the time domain (Eq. (8)) and its magnitude and phase in the frequency domain (Eq. (17)). A similar approach has been applied for identification of the state-space models by using the method of regression in the frequency domain. For this case, the input was the FRF of the retardation functions, Eq. (17). The NL-LS technique was used for identification of the state-space parameters.

Identification for state-space models by using the realization theory requires a retardation function sampling

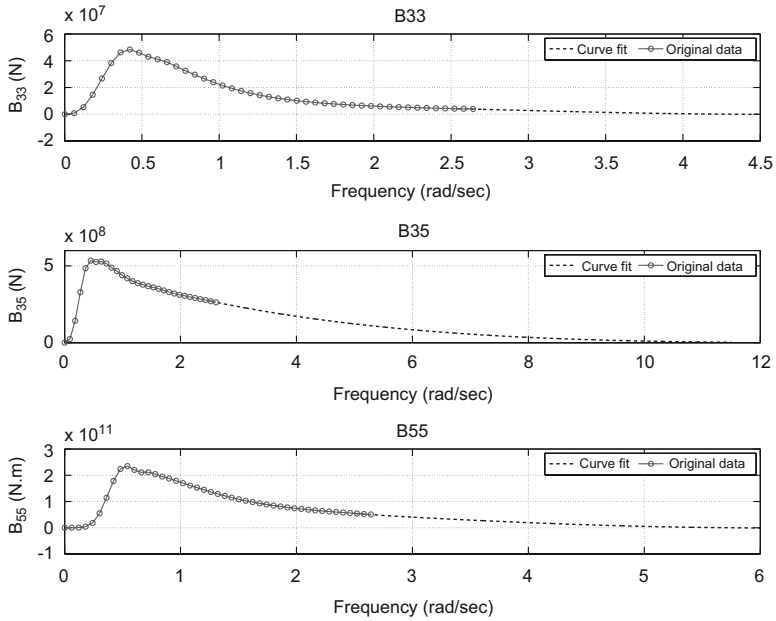

Fig. 9. Extrapolation of data by polynomial curve fitting for B_{33}, B_{35}, and B_{55}.

time that is often longer than the simulation step. State-space identifications by using the method of regression in the frequency domain do not even require such a calculation. Both of these facts are beneficial regarding the use of state-space models because the identification procedure is also carried out only once for a given model and does not need to be repeated with the variation of the simulation steps. That means, if a smaller step length is required in the dynamic simulation, for example due to inclusion of high-frequency mode shapes in the time-domain hydroelastic analysis of very large floating structures, state-space models can conveniently avoid the refinement of the retardation functions and thus the extra computational time that is often spent to recalculate or interpolate the data of the retardation functions.

The identification results show a trade off between the stability and accuracy of the identifications in the methods of regression in the frequency domain. This means that an increased model order can cause the identified model to become unstable and at the same time, allowable orders may not be able to accurately represent the convolution. This matter has been observed by Jordán and Beltrán-Aguedo (2004).

The identification results based on the two methods are plotted in Figs. 10–12. The order of each state-space model was found to be between 4 and 8 for this example. The actual orders are reported in each plot. The retardation functions in both methods are approximated successfully by relatively low-order systems.

The results show that the identifications based on the realization theory could not accurately represent the magnitude and phase of the retardation functions in the low-frequency domain range, although this happens for a small part of the retardation function. It is found that ignoring the parameter $\hat{D}_c$ in the identifications can improve this matter to some extent. The results shown in the plots of Figs. 10–12 ignore this parameter. It is also observed that the method of regression in the frequency domain cannot represent the retardation function data at very low time ranges, while this problem does not exist for the other approach. We now pose the question whether these differences and discrepancies in the identified data will affect the final dynamic simulations. The answer will be pursued in Sections 10.5 and 10.6.

10.4. Model in Simulink

Fig. 13 shows the model implemented in Simulink. Wave forces are taken as input and output is the response for each mode of motion. The identified SDOF state-space models in the previous stage have been assembled in an MDOF model. A Runge Kutta method is chosen to solve the differential equations. Time stepping is controlled by the parameter time step, taken by default equal to 0.01 s. The initial conditions for the velocity and response were set to zero which is consistent with the objective in the first scenario to

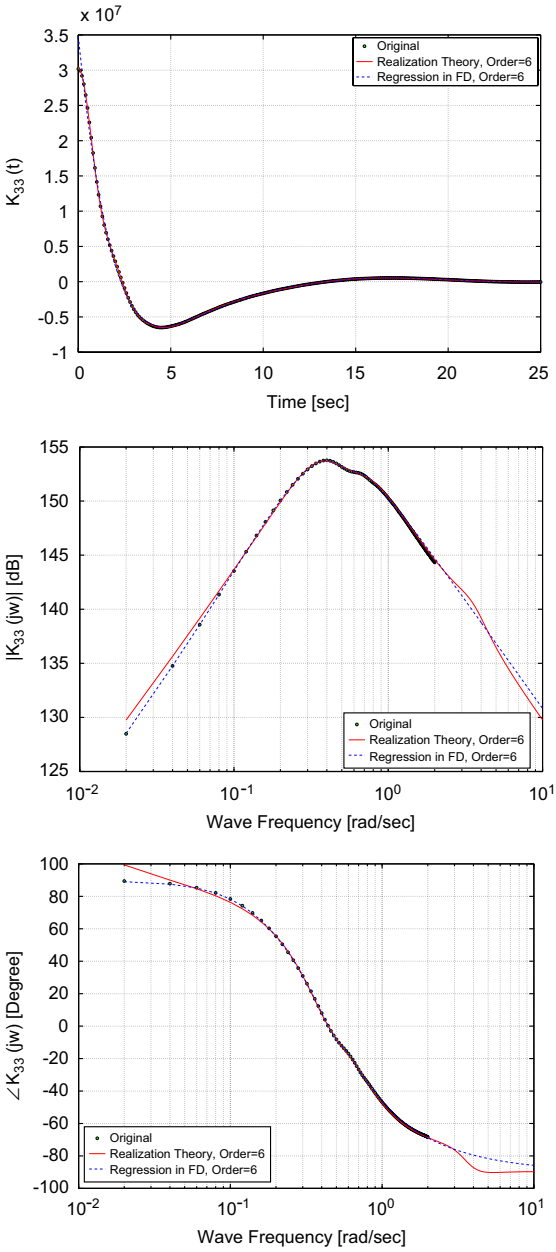

Fig. 10. Identification results for K_{33}. The top plot is the retardation function in the time domain. The middle and bottom plots are, respectively, the amplitude and phase of the retardation function in the frequency domain. Note that the wave frequencies have been plotted in logarithmic scale. The parameter D is ignored in the realization theory.

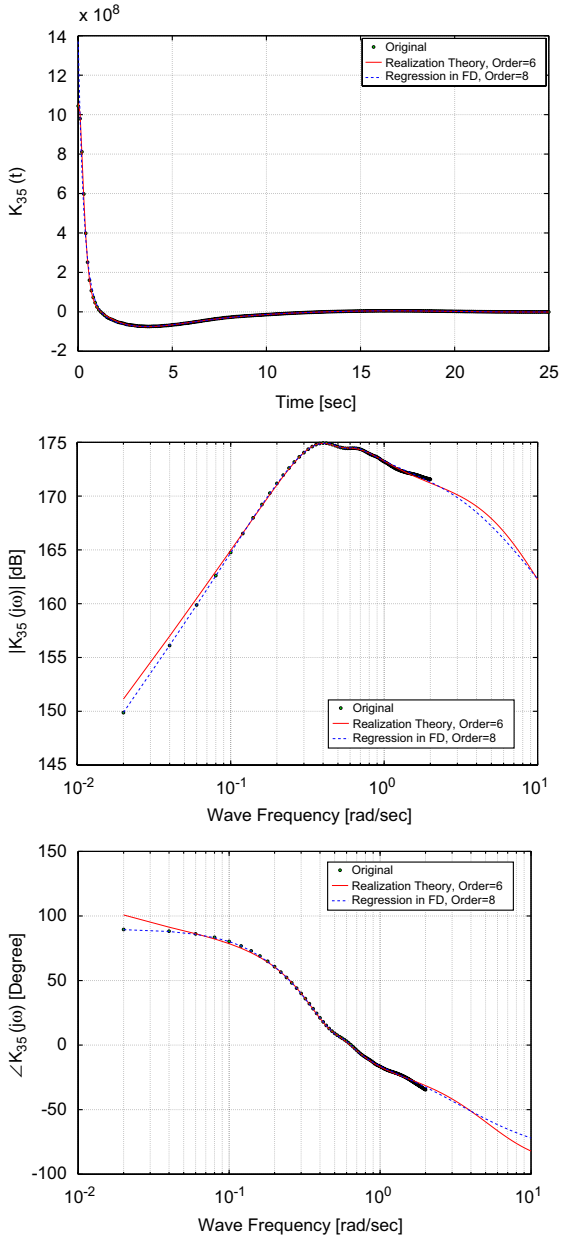

Fig. 11. Identification results for K_{35}. The top plot is the retardation function in the time domain. The middle and bottom plots are, respectively, the amplitude and phase of the retardation function in the frequency domain. Note that the wave frequencies have been plotted in logarithmic scale. The parameter D is ignored in the realization theory.

investigate the response of the structure initially at rest due to harmonic incident wave forces. Different initial conditions were used for the simulation of the second scenario.

10.5. Scenario 1: Steady-state wave-induced response

Typical time-domain response plots for heave and pitch modes at two different wave frequencies have been plotted

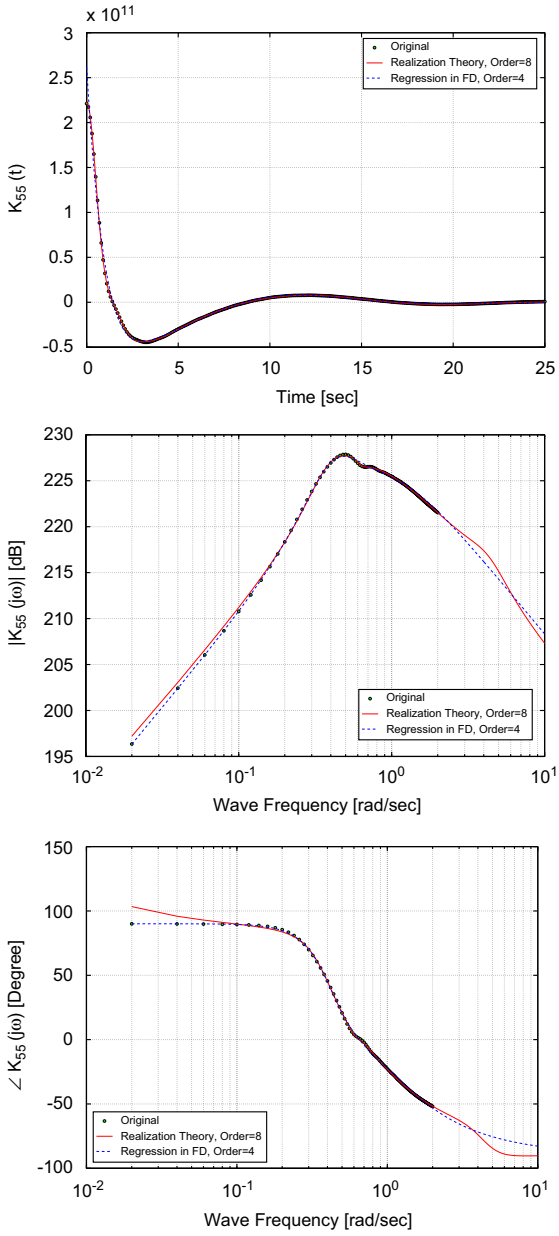

Fig. 12. Identification results for K_{55}. The top plot is the retardation function in the time domain. The middle and bottom plots are, respectively, the amplitude and phase of the retardation function in the frequency domain. Note that the wave frequencies have been plotted in logarithmic scale. The parameter D is ignored in the realization theory.

in Figs. 14 and 15 for the wave frequencies $\omega = 0.64$ and 1.5 rad/s.

It is observed that the simulations seem to match very well with the harmonically generated response based on the RAOs after a suitable amount of time. The two identifications simulate the results similarly. This is despite the discrepancies observed between the two methods during the identification phase—as discussed in Section 10.3.

10.6. Scenario 2: Response of the vessel released from a displaced condition

In this simulation, it was assumed that the ship is in the calm water. A displaced condition in heave and pitch corresponding to 1 m and -5° is considered. The objective is to simulate the transient response of the vessel after it is released from this condition when:

(i) Simulations are performed by numerically integrating the convolutions in Simulink.
(ii) State-space models are identified by the realization theory and simulations are performed in Simulink.
(iii) State-space models are identified by the method of regression in the frequency domain and simulations are performed in Simulink.

Results of the simulations for the three alternatives above are shown in Fig. 16 for heave and pitch modes. The results show that simulations based on the two state-space models agree well with the one that integrates the convolutions. Despite the difference in the quality of the two identifications observed in Section 10.3 (Figs. 10–12), no specific difference is observed between the response simulations. This shows that the two methods are equally accurate and requirement of a very accurate fit during the identification process seems to be of less importance.

In Table 2 mean CPU time records within 10 individual simulation runs have been reported for the different simulation cases (i)–(iii). To integrate the convolutions in Simulink, trapezoidal integration method was coded in C and was embedded as an S-function. This is believed to be the closest the authors could get to draw a fair comparison of the CPU time records for the two simulations. Simulations were run on a computer with 1.8 GHz CPU and 1 GB physical memory. Simulation length is chosen to be 30 s and the ship has two degrees of freedom. Two different simulation steps were chosen in this study: 0.01 and 0.001 s. For simulation step of 0.01 s, it is observed that simulations using the state-space models run about 8 times faster than the simulations using direct integration of the convolutions. By refining the simulation step to 0.001 s, this difference changes to about 80 times. This may imply that by increasing the simulation length or the resolution of the time steps, one should expect larger differences between the CPU time records of the two simulations.

It may also be worthwhile to give a note regarding the memory consumption of the simulations based on the state-space models and convolution integration. Let us consider an SDOF system of order n whose impulse response function shows negligible values after say t_{memory}, and assume a simulation step equal to t_{step}. Integrating the

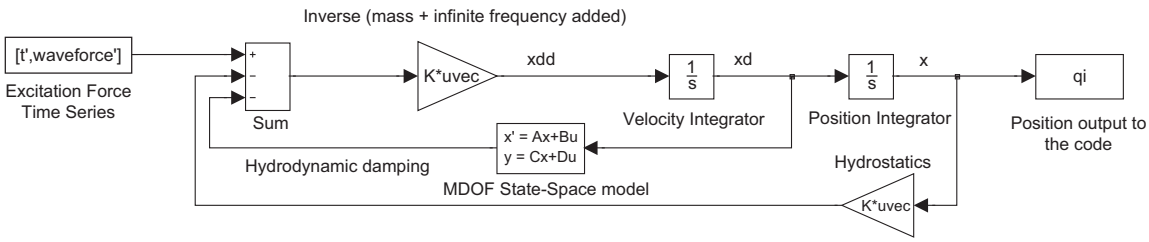

Fig. 13. Block diagram of the model in Simulink.

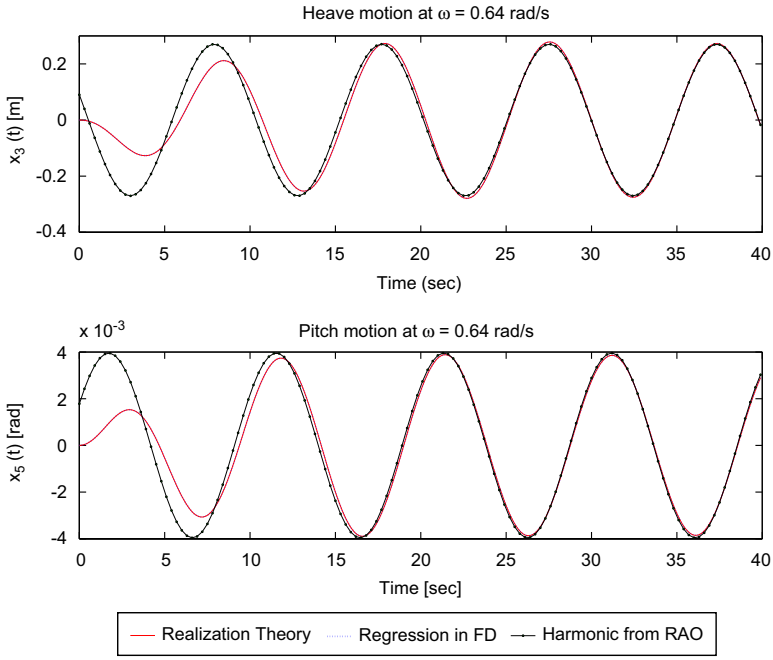

Fig. 14. Time series of the ship motions for $\omega = 0.64\,\mathrm{rad/s}$. Note that the simulations by using the state-space models identified by the realization theory and the regression methods in the frequency domain have been plotted on top of each other.

convolution (Eq. (26)) for this system at every time step with any desired excitation would require storing a number of $t_{\mathrm{memory}}/t_{\mathrm{step}}$ data points. By using the state-space representation instead, one needs to save only n data points, equal to the value of the state. It is because the history of the system is contained in the value of the state. This is reflected in Eq. (32), which implies that to compute the response at a time $t>0$ we only need the state $z(t=0)$ and the excitation for $t>0$. It is usually the case that

$$n \ll \frac{t_{\mathrm{memory}}}{t_{\mathrm{step}}}. \tag{73}$$

This simple argument evidences that the state-space representation can offer a significant save in memory. The actual saving depends on the dynamics of the system and the sampling rate used in the simulations. Note also that a change in the sampling step does affect the amount of data to be saved to compute the convolutions, but it does not change the data needed to be saved to compute the response for a state-space model.

11. Concluding remarks

In this paper, different alternatives to replace the convolution terms in the Cummins equation have been reviewed. By this way, the integro-differential equations of motion have been written in the form of differential formulations. The emphasis has been on the methods that replace the convolutions by the state-space models. It was discussed how to obtain the replacing models via system identification techniques based on the hydrodynamic data from the standard software. Identification methods were categorized depending on the input data used to pose the identification problem. A comparison was made of

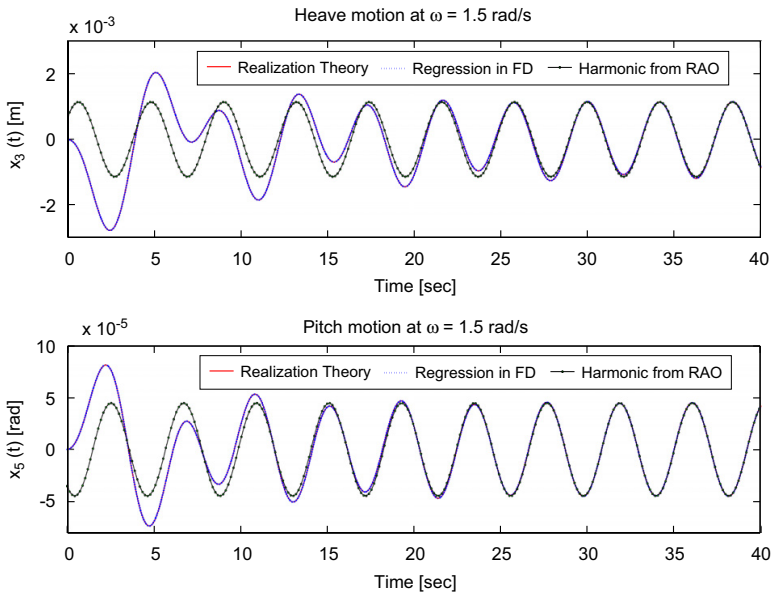

Fig. 15. Time series of the ship motions for $\omega = 1.5\,\mathrm{rad/s}$. Note that the simulations by using the state-space models identified by the realization theory and the regression methods in the frequency domain have been plotted on top of each other.

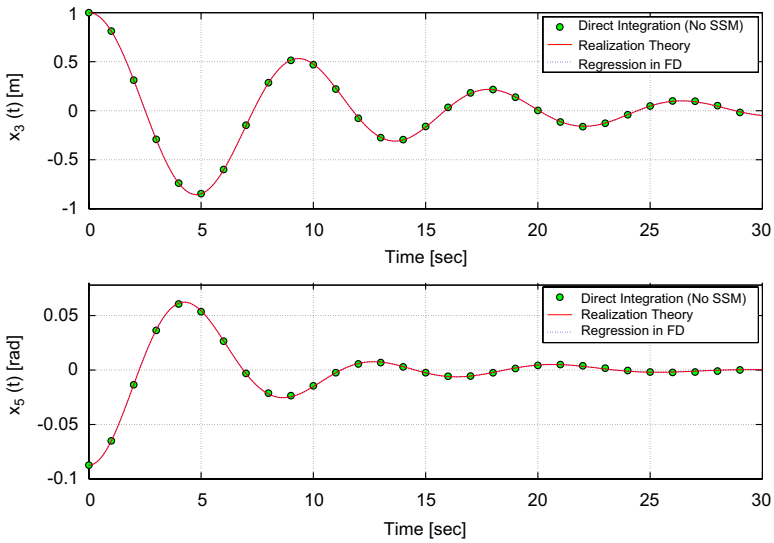

Fig. 16. Transient response due to initial disturbance of 1 m in heave and $-5°$ in pitch. Note that the simulations by using the state-space models identified by the realization theory and the regression methods in the frequency domain have been plotted on top of each other and the simulations using direct integration of the convolutions.

retardation functions that were identified by using the following parameter estimation methods:

- Impulse response curve fitting.
- Realization theory.
- Regression in the frequency domain.

The theoretical basis of each method was reviewed. Identifications by these three methods were compared in a simple example. Then the realization theory and frequency domain regression methods were compared as applied to a modern container vessel. Matlab and its built-in functions were used as a platform for coding the

Table 2
Mean CPU time records for the different simulation cases in Section 10.6

Time step	Case (i)	Case (ii)	Case (iii)
0.01	0.439	0.059	0.051
0.001	41.733	0.580	0.466

All values are in seconds.

identification method and Matlab/Simulink was used to implement the time-domain simulations. Two scenarios were simulated. One was the dynamic response of the ship due to regular wave-induced excitations and the other was the transient response of the ship after it was released from a displaced condition.

Although some discrepancies were observed between the results of the realization theory and the frequency domain regression at the identification stage, it was found from the dynamic simulations that both methods were equally accurate in simulating the vessel response. Further substantiation regarding the accuracy and efficiency of the simulations using state-space models can be found in Taghipour et al. (2007).

With respect to the computational time, it was found that models based on the state-space formulations needed less computational burden than the models solving for the convolutions. In addition, state-space representation may offer a significant save in the memory usage.

It was also observed that requirement of a very accurate fit seems to be of less importance. This can be attributed to the feedback structure of the model, which filters out some of the dynamics associated with the convolution terms. This matter has been discussed by Perez and Lande (2006) and lead to the proposal of identifying a model for force-to-motion transfer function rather than the retardation function. This analysis, however, goes beyond the scope of this paper.

The equations of motion described in this paper can be extended to account for the flexibility of marine structures. State-space identification methods discussed in the paper are able to account for the fluid memory effects of the elastic models. This way hydroelastic analysis of marine structures is possible by modification of the Cummins equation as presented in Taghipour et al. (2007).

Acknowledgements

We are grateful to Professor Johannes Falnes for his invaluable comments. We also thank Mr. Ingo Drummen at Centre for Ships and Ocean Structures for providing the data of the container ship. The authors appreciate the financial support of the Norwegian Research Council which has been granted through Centre for Ships and Ocean Structures.

References

Al-Saggaf, U., Franklin, G., 1987. An error bound for a discrete reduced order model of a linear multivariable system. IEEE Transactions on Automatic Control 32 (9), 815–819.

Bendat, J.S., 1998. Nonlinear Systems Techniques and Applications. Wiley, New York.

Chen, C., 1999. Linear System Theory and Design. Oxford University Press, Oxford.

Cummins, W., 1962. The impulse response function and ship motions. Schiffstechnik 9 (1661), 101–109.

Damaren, C., 2000. Time-domain floating body dynamics by rational approximations of the radiation impedance and diffraction mapping. Ocean Engineering 27, 687–705.

Duclos, G., Clément, A.H., Chatry, G., 2001. Absorption of outgoing waves in a numerical wave tank using a self-adaptive boundary condition. International Journal of Offshore and Polar Engineering 3, 168–175.

Egeland, O., Gravdahl, J., 2002. Modeling and Simulation for Automatic Control. Marine Cybernetics, Trondheim.

Faltinsen, O., 1990. Sea Loads on Ships and Offshore Structures. Cambridge University Press, Cambridge.

Faltinsen, O., 2005. Hydrodynamic of High-speed Marine Vehicles. Cambridge University Press, Cambridge.

Fossen, T.I., 2002. Marine Control Systems: Guidance, Navigation and Control of Ships, Rigs and Underwater Vehicles. Marine Cybernetics, Trondheim.

Fossen, T.I., 2005. A nonlinear unified state-space model for ship maneuvering and control in a seaway. International Journal of Bifurcation and Chaos 15 (9), 2717–2746.

Govolato, P., 1959. A study of the transient pitching oscillations of a ship. Journal of Ship Research, 2.

Hals, J., Taghipour, R., Moan, T., 2007. Dynamics of a force-compensated two-body wave energy converter in heave with hydraulic power take-off subject to phase control. In: Proceedings of the Seventh European Wave and Tidal Energy Conference, Porto, Portugal.

Ho, B., Kalman, R., 1966. Effective reconstruction of linear state-variable models from input/output functions. Regelungstechnik 14 (12), 417–441.

Holappa, K., Falzarano, J., 1999. Application of extended state space to nonlinear ship roling. Ocean Engineering 26, 227–240.

Jefferys, E., 1984. Simulation of wave power devices. Applied Ocean Research 6 (1), 31–39.

Jefferys, E., Goheen, K., 1992. Time domain models from frequency domain descriptions: application to marine structures. International Journal of Offshore and Polar Engineering 2, 191–197.

Jordán, M., Beltrán-Aguedo, R., 2004. Optimal identification of potential-radiation hydrodynamics for moored floating structures: a new general approach in state space. Ocean Engineering 31, 1859–1914.

Kailath, T., 1980. Linear Systems. Prentice-Hall, Englewood Cliffs, NJ.

Kashiwagi, M., 2004. Transient response of a VLFS during landing and take-off of an airplane. Journal of Marine Science and Technology 9, 14–23.

Kristiansen, E., Egeland, O., 2003. Frequency-dependent added mass in models for controller design for wave motion damping. In: Proceedings of Sixth Conference on Maneoeuvering and Control of Marine Craft, Girona, Spain.

Kristiansen, E., Hjulstad, A., Egeland, O., 2005. State-space representation of radiation forces in time-domain vessel models. Ocean Engineering 32, 2195–2216.

Kung, S., 1978. A new identification and model reduction algorithm via singular value decompositions. Twelfth Asilomar Conference on Circuits, Systems and Computers, pp. 705–714.

Levy, E., 1959. Complex curve fitting. IRE Transactions on Automatic Control AC-4, 37–43.

Ljung, L., 1999. System Identification, Theory for the User. Prentice-Hall, Englewood Cliffs, NJ.

McCabe, A., Bradshaw, A., Widden, M., 2005. A time-domain model of a floating body using transforms. In: Proceedings of the Sixth European Wave and Tidal Energy Conference. University of strathclyde, Glasgow.

MultiSurf, 2006. Aerohydro Inc., ME, USA, version 6.5.

Newman, J., 1977. Marine Hydrodynamics. MIT Press, Cambridge, MA.

Nocedal, J., Wright, S.J., 1999. Numerical Optimization. Springer, New York.

Ogilvie, T., 1964. Recent progress towards the understanding and prediction of ship motions. In: Sixth Symposium on Naval Hydrodynamics.

Oppenheim, A., Wilsky, A., Nawab, H., 1997. Signals & Systems. Prentice-Hall, Englewood Cliffs, NJ.

Perez, T., 2002. Ship Motion Control: Course Keeping and Roll Reduction using Rudder and Fins. Springer, London.

Perez, T., Fossen, T., 2006. Time-domain models of marine surface vessels for simulation and control design based on seakeeping computations. In: Proceedings of the Seventh IFAC Conference on Manoeuvring and Control of Marine Craft MCMC, Lisbon, Portugal.

Perez, T., Lande, O., 2006. A frequency-domain approach to modelling and identification of the force to motion vessel response. In: Proceedings of the Seventh IFAC Conference on Manoeuvring and Control of Marine Craft MCMC.

Pintelon, R., Schoukens, J., 2001. System Identification: A Frequency Domain Approach. IEEE Press, New York.

Sanathanan, C., Koerner, J., 1963. Transfer function synthesis as a ratio of two complex polynomials. IEEE Transactions of Automatic Control 8, 56–58.

Schmiechen, M., 1973. On state space models and their application to hydrodynamic systems. Technical Report, NAUT Report, Department of Naval Architecture, University of Tokyo.

Söding, H., 1982. Leckstabilität im seegang. Technical Report, Report 429 of the Institue für Schiffbau, Hamburg.

Sutulo, S., Guedes-Soares, C., 2005. An implementation of the method of auxiliary state variables for solving seakeeping problems. International Shipbuilding Progress 52, 357–384.

Taghipour, R., Perez, T., Moan, T., 2007. Time domain hydroelastic analysis of a flexible marine structure using state-space models. In: 26th International Conference on Offshore Mechanics and Arctic Engineering-OMAE 07, San Diego, CA, USA.

Tick, L.J., 1959. Differential equations with frequency-dependent coefficients. Journal of Ship Research 3 (2), 45–46.

Unneland, K., Egeland, O., 2006. Positive real modeling of ships for dynamic positioning. In: Proceedings of 17th International Symposium on Mathematical Theory of Networks and Systems, July 24–28, Kyoto, Japan.

Unneland, K., Kristiansen, E., Egeland, O., 2005. Comparative study of algorithms for obtaining reduced order state-space form of radiation forces. In: Proceedings of the OCEANS 2005 MTS/IEEE, September 19–23, Washington, DC, USA.

Unneland, K., Perez, T., O.Egeland, 2007. Mimo and siso identification of radiation force terms for models of marine structures in waves. In: Proceedings of the IFAC Conference on Control Applications in Marine Systems.

Unneland, K., Fossen, T., Egeland, O., Dooren, P.V., 2006. Low order potential damping models for surface vessels. In: Proceedings of Seventh IFAC Conference on Manoeuvering and Control of Marine Craft, September 20–22, Lisbon, Portugal.

Ursell, F., 1964. The decay of the free motion of a floating body. Journal of Fluid Mechanics 19, 305–319.

WAMIT, 2006. WAMIT Inc., MA, USA, version 6.3.

Wehausen, J.V., 1967. Initial-value problem for the motion in an undulating sea of a body with fixed equilibrium position. Journal of Engineering Mathematics 1 (1), 1–17.

Wu, M., Moan, T., 1996. Linear and nonlinear hydroelastic analysis of high-speed vessels. Journal of Ship Research 40, 149–163.

Xia, J., Wang, Z., Jensen, J., 1998. Nonlinear wave-loads and ship responses by a time-domain strip theory. Marine Structures 11, 101–123.

Yu, Z., Falnes, J., 1995. State-space modelling of a vertical cylinder in heave. Applied Ocean Research 17, 265–275.

Yu, Z., Falnes, J., 1998. State-space modelling of dynamic systems in ocean engineering. Journal of Hydrodynamics B (1), 1–17.

Paper 4

Time-Domain Hydroelastic Analysis of A Flexible Marine Structure Using State-Space Models

Published in
International Journal of Offshore Mechanics and Arctic Engineering, In press (Presented at 26th International Conference on Offshore Mechanics and Arctic Engineering, 2007, San Diego, California, USA).

Is not included due to copyright

Paper 5

Dynamics of A Force-Compensated Two-Body Wave Energy Converter in Heave with Hydraulic Power Take-Off Subject To Phase Control

Published in
Proceedings of the 7th European Wave and Tidal Energy Conference, 2007, Porto, Portugal.

Dynamics of a force-compensated two-body wave energy converter in heave with hydraulic power take-off subject to phase control

Jørgen Hals[1], Reza Taghipour and Torgeir Moan

Centre for Ships and Ocean Structures (CeSOS),
Norwegian University of Science and Technology (NTNU),
Otto Nielsens V. 10, N-7491, Trondheim, Norway
[1]Corresponding author: jorgen.hals@ntnu.no

Abstract

In this study we use a hybrid frequency-time domain model to study the dynamics of a two-body wave-energy converter with hydraulic power take-off subject to phase control. Both bodies - a buoy and a semi-submersible platform - are restricted to move in the heave mode only, and the power is extracted from their relative motion.

The geometry of the buoy and the platform is chosen so as to obtain so-called force compensation, i.e. the vertical wave excitation forces on the two bodies are opposite and approximately equally large. The effect of force compensation is studied by varying the geometry of the platform in order to reveal its effect on the system dynamics and power absorption. Furthermore, one-body oscillation is compared to two-body oscillation for power absorption, and the effect of viscous damping of the platform motion is studied.

Simulation results are given both for regular and irregular waves, and they show that the platform geometry and degree of force compensation strongly influences the performance of the system. It is further shown that flow losses in a hydraulic power take-off system can be substantial, and should thus be thoroughly assessed. Also, the large potential increase in power output using phase control is demonstrated.

Keywords: Bond graph, numerical simulation, ocean waves, renewable energy

Nomenclature

β [Pa]	=	bulk modulus of hydraulic oil
ζ [m]	=	wave surface elevation
λ [m]	=	wave length
ρ [$\frac{\mathrm{kg}}{\mathrm{m}^3}$]	=	density
τ [Nm]	=	torque
τ [s]	=	time integration variable
ϕ [$\frac{\mathrm{m}^2}{\mathrm{s}}$]	=	velocity potential
ω [$\frac{\mathrm{rad}}{\mathrm{s}}$]	=	angular frequency
a	=	$D_p/D_{p,0}$, pontoon diameter factor
$\tilde{\mathbf{A}}$, $\tilde{\mathbf{B}}$, $\tilde{\mathbf{C}}$, $\tilde{\mathbf{D}}$	=	linear system matrices
$\mathbf{A}$ [kg]	=	added mass matrix
A [m^2]	=	area
b	=	$H_p/H_{p,0}$, pontoon height factor
$\mathbf{B}$ [$\frac{\mathrm{Ns}}{\mathrm{m}}$]	=	damping coefficient matrix
B [$\frac{\mathrm{Ns}}{\mathrm{m}}$]	=	damping coefficient
$\mathbf{C}$ [$\frac{\mathrm{N}}{\mathrm{m}}$]	=	hydrostatic stiffness matrix
C_d	=	drag coefficient (pontoons)
C_d	=	discharge coefficient (valves)
d_a [m]	=	absorption width
D [m]	=	diameter
D_m [$\frac{\mathrm{m}^3}{\mathrm{rad}}$]	=	hydraulic motor displacement
e	=	effort, here: pressure [Pa]
$\mathbf{F}$ [N]	=	force vector
F [N]	=	force
g [$\frac{\mathrm{m}}{\mathrm{s}^2}$]	=	acceleration of gravity
I1-I5	=	irregular-wave sea states
J [kg m^2]	=	moment of inertia
J [$\frac{\mathrm{W}}{\mathrm{m}}$]	=	wave energy transport
$\mathbf{K}$ [$\frac{\mathrm{N}}{\mathrm{m}}$]	=	retardation function
m [kg]	=	mass
$\mathbf{M}$ [kg]	=	mass matrix
p [Pa]	=	pressure (for fluids)
p [$\frac{\mathrm{kgm}}{\mathrm{s}}$]	=	momentum (for bodies)
P [W]	=	power
PH	=	passive hydraulic power take-off
PHL	=	latching hydraulic power take-off
PL	=	passive linear power take-off
PTO	=	power take-off
q	=	generalised displacement: volume for hydraulics
R_m [$\frac{\mathrm{Pas}}{\mathrm{m}^3}$]	=	linear loss factor for hydraulic motor
R1-R5	=	regular-wave sea states
t [s]	=	time
T [s]	=	period
v [m]	=	velocity
V [m]	=	velocity in frequency plane
V [m^3]	=	volume
x [m]	=	vertical excursion from equilibrium position

X [m s] = vertical excursion in the frequency plane
$\mathbf{z}$ = radiation force state vector

Subscripts

0	=	initial or default value,
abs	=	absorbed
A, B, C, D	=	accumulator A, B, C or D
b	=	buoy
control	=	used for phase control
D	=	diffraction
exc	=	excitation
g	=	generator
H	=	hydraulic
HP	=	high pressure
j	=	component index
l	=	load
LP	=	low pressure
nl	=	non-linear
p	=	pontoon
rad	=	radiation
rel	=	relative between buoy and platform
s	=	semi-submersible platform
v	=	valve
visc	=	viscous
wp	=	water plane
z	=	z direction

Superscripts

∞	=	infinite frequency
D	=	diffraction
v	=	velocity
R	=	radiation (modified)

Introduction

There are two crucial criteria for a wave energy device to be viable. The first one is that it must give payback of investments in order to be realised, and this will of course depend both on how well the technology performs and on the market with possible adaptation actions from governments. The second one is that it must at least during its lifetime be able to return more energy than was spent in manufacturing, installing, operating and eventually decommissioning it. The task for technology providers is thus to increase the power output-to-cost ratio, whether we speak about energy or financial cost.

This article concerns the power part of this fraction, by considering an example system of a heaving buoy and platform connected through a power take-off (PTO) mechanism. The application of closed-loop control is usually regarded as a necessary means of improving performance of oscillating-type wave energy converters. Here we pursue the ideas of phase control by latching [1, 2] and investigate how this feature influences the power output for an example system by comparing it with more passive approaches, still having optimised parameters.

Budal [3] and Falnes [4] investigated the principle of force compensation for heaving two-body devices, and numerical results are here presented to support their qualitative discussions. Submerged plates or pontoons experience downward vertical excitation forces under the influence of a passing wave crest.

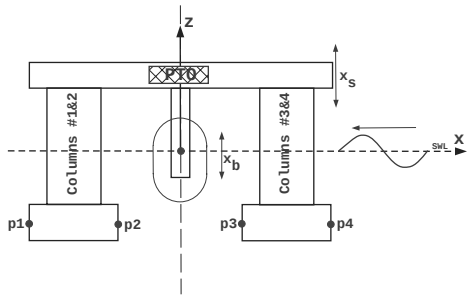

Figure 1: Schematic view of the wave energy converter. Only heave motion of the two bodies is considered, and the power is taken out from their relative motion. The velocities at points p1 to p4 are used for calculating the viscous damping. Only head seas waves are considered.

This leads to the possibility of having, within a limited frequency range, close to equally large but opposite excitation forces on a floating column and an attached submerged structure. The total force is thus approximately zero over that range. This force compensation is exploited in the design of offshore platforms in order to reduce wave induced motions. In our example system this effect gives opposite forces on the buoy and the platform, and we study this effect on the system dynamics and power output.

A dynamic model is the basis for understanding the behaviour of wave energy converters, such as energy absorption, mean and extreme loads and their effect on the mechanical and structural system. In this study the bond graph method has been used in the modelling work, and this is a very suitable tool for the modelling of wave energy devices, as discussed in [5].

1 System configuration

The example system consists of a four-legged semi-submersible platform and a cylindrical buoy with hemispherical bottom, both subject to head seas waves and moving in heave as shown in Figure 1. Their geometries have been chosen such that we are close to the above-mentioned force compensation for the relevant range of wave periods, which we have defined to be from 5 to 12 s. As indicated in Figure 2, the platform has cylindrical pontoons attached to its legs, and the cylindrical buoy has a straight submerged part of height 3 m, indicating a maximum excursion relative to the mean free surface of ± 3 m. Figure 3 shows a projection sketch of the system for the default dimension settings. See also Table 3. The eigen periods of the system are $T_s = 13.65$ s (the platform mode), $T_0 = 9.08$ s (the common mode of bodies locked together) and $T_b = 2.77$ s (the buoy mode). We studied two hydraulic systems for power take-off (Figure 5 and 6). In both cases the system is pretensioned by the initial hydraulic pressure. Compared to the Archimedean mass of the submerged volume, the mass is therefore reduced for the buoy and increased for the platform in order to have the same equilibrium position for the two bodies as before. This is given in Table 1.

A variation of the force-compensation level is made by varying the pontoon diameter D_p while keeping both the total displacement and the column diameter constant. This means a changing pontoon height H_p, which has been achieved by ad-

Table 1: Characteristic values and parameter settings for the system, with and without latching. The minus sign (-) indicates that the parameter is not relevant, and equal sign (=) indicates that the parameter value is the same for the two systems.

Quantity	Passive hydraulic PH Value	Latching hydraulic PHL Value
β	$1.3 \cdot 10^9$ Pa	=
ρ_H	850 kg/m^3	=
ρ_w	1025 kg/m^3	=
ω_s	0.46 rad/s	=
ω_b	2.26 rad/s	=
ω_0	0.69 rad/s	=
C_d	0.9	=
D_m	$1.2 \cdot 10^{-5}$ m^3/rad	=
J_g	2.5 kg m^2	=
m_s	239.2 Mg	259.6 Mg
m_b	35.42 Mg	15.04 Mg
$p_{A,0}$	-	20 MPa
$p_{B,0}$	10 MPa	30 MPa
$p_{C,0}$	10 MPa	10 MPa
$p_{D,0}$	10 MPa	20 MPa
Piston area	0.02 m^2	0.02 m^2
Pretension	200 kN	400 kN
R_{m}	$2 \cdot 10^8$ Pa s/m^3	=
τ_g	50 Nm	220 Nm
$V_{A,0}$	-	0.2 m^3
$V_{B,0}$	0.8 m^3	0.5 m^3
$V_{C,0}$	0.55 m^3	0.2 m^3
$V_{D,0}$	0.005 m^3	0.0875 m^3
V_s	213.5 m^3	=
V_b	54.45 m^3	=
Valve areas	0.002 m^2	=

justing the draft of the pontoon, while keeping the column height H_c constant. We first take $D_{p,0}$ as the diameter and $D_{p,0}$ as the height of the pontoon for the default case (3). If we define a diameter factor $a = D_p/D_{p,0}$ for change in diameter and a height factor $b = H_p/H_{p,0}$ for change in height, we get that the submerged platform volume $V \propto D_p^2 H_p = a^2\, b\, D_{p,0}\, H_{p,0}$. The requirement of keeping the volume constant then yields $a^2 b = 1$. We first try a 20 % increase/decrease in the diameter as shown in Table 3. The resulting excitation force coefficients for the platform and the buoy are shown in Figure 4. The frequancy domain parameters are calculated by the boundary-element method code WAMIT [6].

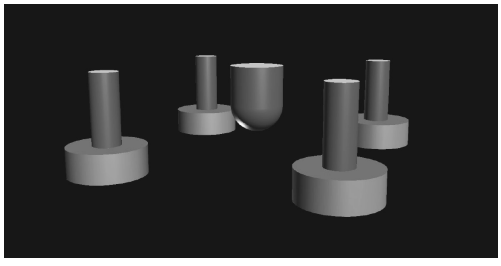

Figure 2: 3D view of submerged parts of the buoy and platform.

Table 2: Dimensions for the buoy and platform in the default case, i.e. with $a = 1$.

Symbol	Value [m]	Dimension
D_b	4.0	Buoy diameter
$R_b = D_b/2$	2.0	Buoy radius
H_b	3.0	Height of buoy's straight part
$d_b = H_b + R_b$	5.0	Buoy draught
D_c	1.7	Column diameter
$R_c = D_c/2$	0.85	Column radius
H_c	7.9	Column height
D_p	4.75	Pontoon diameter
R_p	2.375	Pontoon radius
H_p	2.0	Pontoon height
$d_p = H_c + H_p$	9.9	Platform total draught
L_{dist}	12.0	Distance between column centres

Table 3: Parameter variations keeping the pontoon volume constant. The corresponding results for the excitation force coefficients are shown in Figure 4. We have chosen the default values $D_{p,0} = 5.50$ m and $H_{p,0} = 2.50$ m for the pontoon diameter and height, respectively. The pontoon diameter factor a gives the ratio of the actual diameter to the default diameter, such that $D_p = a\, D_{p,0}$. The pontoon height factor b gives the ratio of the actual height to the default height, such that $H_p = b\, H_{p,0}$.

a	$b = 1/a^2$	D_p	H_p
1.0	1.0	4.75	2.000
1.20	0.694	5.70	1.389
0.80	1.563	3.80	3.125

1.1 PTO mode of operation

The power take-off (PTO) consists of a passive hydraulic system as studied also by Eidsmoen [7], and is shown in Figure 5. The PTO is located between the buoy and platform taking out power from their relative motion through a hydraulic ram (see also [5]). We will refer to this type of PTO using the label PH. In the case of latching control, an extra accumulator (A) is included in the system along with a control valve, as proposed by Budal [8] and shown in Figure 6. We label this system PHL.

For the passive hydraulic system (PH, see Figure 5) the relative distance starts changing once the relative force is strong enough to either pump to the high pressure reservoir (accumulator B) or suck from the low pressure reservoir (accumulator C). Then, during the following relative translation, hydraulic liquid flows between the storage accumulators and the piston. Accumulator D is included in order to account for the compressibility of oil in the hydraulic piston.

For the latching hydraulic system (PHL, see Figure 6) the piston pumps liquid to accumulator A during relative motion between the bodies and upward motion of the piston. Finally the control valve will close at zero relative velocity. While keeping the bodies at almost fixed distance by the closed valve, the force from the piston will decrease the pressure in the piston chamber and eventually get large enough to open the check valve from accumulator C, such that liquid can flow. This results in an increased pressure difference between B and C due to falling pressure p_C, as well as a downward motion of the piston. When the control valve opens again, the pressure difference between the piston cylinder and accumulator A will accelerate the downward motion. Eventually the relative distance between the platform and buoy will reach a maximum as the liquid is drawn from accumulator A and the piston chamber pressure falls. Here the

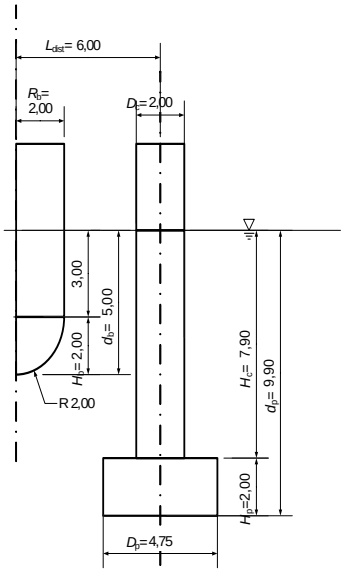

Figure 3: Projected 2D view of the buoy and platform with default dimensions. A complete list of dimensions is given in Table 2.

control valve will again be closed at zero velocity. Now the same sequence will follow, but this time with the piston force building a high pressure and pumping liquid into accumulator A.

The benefits of these hydraulic system used in the power take-off is that they store energy such that the power delivery to the electric generator can be evened out. Also they have an inherent protective mechanism limiting the relative motion. As the wave energy transport increases and waves get larger, the pressure level in B (C) will increase (decrease). Then a larger force is needed to move the piston toward the chamber ends.

A third option implemented for the power take-off is through an ideal linear load force, which is proportional to the relative velocity of the buoy and platform. This PTO is denoted by PL.

As a reference case, the platform was considered to be fixed. For this case, only the moving buoy is able to absorb power.

2 Mathematical model

We assume a two degree of freedom system by considering the semi-submersible platform and the buoy to move independently in heave. Additionally, we assume the hydrodynamic excitation and radiation forces, as well as the hydrostatic stiffness forces, to be linear. Thus we assume that the platform and buoy do not undergo large amplitude motions. The forces due to the viscous damping of the pontoon motion and the hydraulic system are, however, nonlinear.

Below we first give the state-space description of the model following after derivation of equations from the bond graph model of the system, as shown in [5]. The equations are commented and motivated in a qualitative fashion, with a more detailed description of some of the terms, before conformity with the more classical form of the equation of motion is shown. For a more complete treatment please consult the given reference.

The complete model is determined by a set of state space

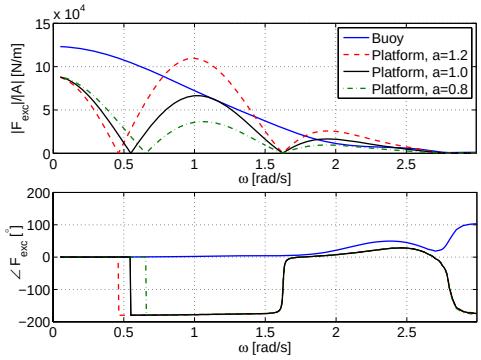

Figure 4: Excitation force coefficients (top) and the corresponding phase angles (bottom) for the three different configurations given by the parameter variation in Table 3.

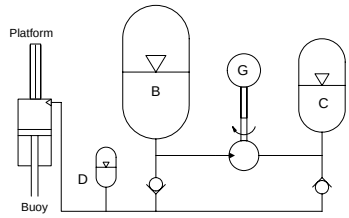

Figure 5: Schematic diagram of the passive hydraulic system, which is labelled PH [8, 9, Manuscript C]. The system consists of a hydraulic piston (left), gas accumulators (B, C and D), check valves, a motor and an electric generator (G).

equations, i.e. coupled first-order differential equations. First, letting q, e, p, x and F be time-dependent variables, the body dynamics are given by

$$\dot{p}_\mathrm{s} = m_\mathrm{s}\,\ddot{x}_\mathrm{s} = A_p\,e_D + F_{\mathrm{rad,s}} + F_{\mathrm{exc,s}} + F_{\mathrm{viscous,s}} - \rho\,g\,A_{\mathrm{wp,s}}\,x_\mathrm{s} \quad (1)$$

$$\dot{x}_\mathrm{s} = \frac{p_\mathrm{s}}{m_\mathrm{s}} \quad (2)$$

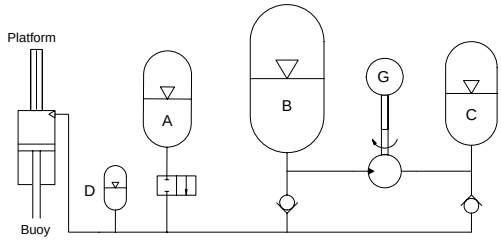

Figure 6: Schematic diagram of the hydraulic system with latching control, as proposed by Budal [8] (PHL). Compared to the PH system, this system contains an additional gas accumulator (A) and a control valve.

for the semisubmersible platform, and

$$\begin{aligned} \dot{p}_\mathrm{b} &= m_\mathrm{b}\,\ddot{x}_\mathrm{b} = -A_p\,e_D + F_\mathrm{rad,b} \\ &\quad + F_\mathrm{exc,b} - \rho\,g\,A_\mathrm{wp,b}\,x_\mathrm{b} \qquad (3) \\ \dot{x}_\mathrm{b} &= \frac{p_\mathrm{b}}{m_\mathrm{b}} \qquad (4) \end{aligned}$$

for the buoy. These four equations comprise all body forces and motions included in the model. The momentum of the vertical body motions is denoted p, and x is the vertical position. The masses m_s and m_b are the physical masses of the semisubmersible platform and the buoy, respectively. The meaning of the constants are found by conferring with the nomenclature list. The $A_p\,e_D$ terms in Equations 1 and 3 gives the coupling to the hydraulic PTO, and the radiation force F_rad contains both the added mass and wave damping forces. Moreover, the excitation force F_exc includes the Froude-Krylov and diffraction forces, and F_viscous represents viscous damping on the platform pontoons. Finally, the $\rho\,g\,A_\mathrm{wp}\,x$ terms give the hydrostatic stiffness forces. Both and F_rad and F_viscous are further discussed below.

The state equations for the hydraulic system are:

$$\dot{V}_A = C_d A_\mathrm{v,control}\sqrt{\frac{2}{\rho}|e_D - e_A|}\,\mathrm{sign}(e_D - e_A) \qquad (5)$$

$$\dot{V}_B = C_d A_\mathrm{v,HP}\sqrt{\frac{2}{\rho}\max[(e_D - e_B), 0]} - D_m\frac{p_g}{J_g} \qquad (6)$$

$$\dot{V}_C = D_m\frac{p_g}{J_g} - C_d A_\mathrm{v,LP}\sqrt{\frac{2}{\rho}\max[(e_C - e_D), 0]} \qquad (7)$$

$$\begin{aligned} \dot{V}_D &= A_p\left(\frac{p_\mathrm{b}}{m_\mathrm{b}} - \frac{p_\mathrm{s}}{m_\mathrm{s}}\right) \\ &\quad - C_d A_\mathrm{v,LP}\sqrt{\frac{2}{\rho}\max[(e_C - e_D), 0]} \\ &\quad - C_d A_\mathrm{v,HP}\sqrt{\frac{2}{\rho}\max[(e_D - e_B), 0]} \\ &\quad - C_d A_\mathrm{v,control}\sqrt{\frac{2}{\rho}|e_D - e_A|}\,\mathrm{sign}(e_D - e_A) \qquad (8) \end{aligned}$$

with

$$e_i = e_{0,i}\left(\frac{V_{0,i}}{V_{0,i} - V_i}\right)^k, \quad \mathrm{i} \in \{\mathrm{A, B, C, D}\}$$

In accordance with bond graph notation, e here represents effort, which for the hydraulic system is the pressure, V is the fluid volume in the different accumulators, and p_g is the angular momentum for the generator.

Equations 5 to 8 relates the change in accumulator liquid levels to the pressure differences over the valves and the motor in the system, where the accumulators are modelled assuming isentropic expansion and compression. The check valves and the control valves are all modelled according to the orifice equation (pressure loss proportional to the square of the flow rate) giving rise to the square roots in the equations.

The last state equation concerns the coupling between the motor and the generator:

$$\dot{p}_g = \tau_g + D_m(e_B - e_C) - \frac{D_m^2 R_m}{J_g}p_g, \qquad (9)$$

where the electric generator is simply modelled as a constant torque on the motor shaft, given by the first term on the right hand side. The second term is the torque due to the pressure difference across the hydraulic motor. The loss in the motor is taken to be proportional to the flow as given by the last term of Equation 9.

The coupling between the hydraulic power take-off and the oscillating bodies is given by the first term on the right-hand side of Equation 8, and the $A_p\,e_D$ terms in Equations 1 and 3.

Equations 1 to 9 give the total mathematical description of our model. We see that the model has nine state variables which can be determined by the nine state equations. For the system without latching control the terms containing the state variable q_A simply vanishes, leaving eight state variables and eight equations.

The radiation force terms F_rad in Equations 1 and 3 are given by Cummins [10]:

$$\mathbf{F}_{rad}(t) = \begin{bmatrix} F_\mathrm{rad,s}(t) \\ F_\mathrm{rad,b}(t) \end{bmatrix} = \mathbf{A}^\infty\,\ddot{\mathbf{x}}(t) + \mathbf{F}^\mathbf{R}(t)$$

where $\mathbf{A}^\infty$ is the matrix of added mass at infinite frequency and x is the position vector;

$$\mathbf{x}(t) = \begin{bmatrix} x_s(t) \\ x_b(t) \end{bmatrix},$$

$$\mathbf{A}^\infty = \begin{bmatrix} A^\infty_{ss} & A^\infty_{sb} \\ A^\infty_{bs} & A^\infty_{bb} \end{bmatrix}$$

and

$$\mathbf{F}^\mathbf{R}(t) = -\int_0^t \mathbf{K}(t-\tau)\,\dot{\mathbf{x}}(\tau)\,d\tau,$$

The retardation function $\mathbf{K}$ appearing in this convolution integral can be related to the frequency-domain potential damping as

$$\mathbf{K}(t) = \frac{2}{\pi}\int_0^\infty \mathbf{B}(\omega)\cos(\omega t)d\omega,$$

with

$$\mathbf{B} = \begin{bmatrix} B_{ss} & B_{sb} \\ B_{bs} & B_{bb} \end{bmatrix}.$$

The off-diagonal coupling terms represent the hydrodynamic interactions between the semi and the buoy.

These radiation forces can be approximated by a linear state-space model, in which case we can write the convolution term as [11]:

$$\begin{aligned} \dot{\mathbf{z}}(t) &= \tilde{\mathbf{A}}\,\mathbf{z}(t) + \tilde{\mathbf{B}}\dot{\mathbf{x}}(t) \\ \mathbf{F}^\mathbf{R} &\approx \tilde{\mathbf{C}}\,\mathbf{z}(t) + \tilde{\mathbf{D}}\dot{\mathbf{x}}(t) \qquad (10) \end{aligned}$$

We then need to solve for the additional state vector $\mathbf{z}$, whose length depends on the complexity of the retardation function and the required accuracy.

Now, viscous damping due to the pontoon motions is modelled in the usual way as

$$F_\mathrm{viscous,s} = B_{nl}(\dot{x_s} - v_z)\,|\dot{x_s} - v_z| \qquad (11)$$

where

$$\mathbf{B}_{nl} = \frac{\pi}{8}\rho C_d {D_p}^2, \qquad (12)$$

and v_z is the water particle velocity in the z direction. Values for the drag coefficient C_d is chosen based on an experimental work by Sauder and Moan [12], where the viscous forces were measured for different forcing amplitudes and frequencies. In the present work a default value of $C_d = 2$ has been used, with a variation from 1 to 8 to study its effect.

The water particle velocity v_z is here evaluated as the average of the water particle velocities at points p_1, p_2 for force evaluations for columns 1 and 2 and at points p_3 and p_4 for columns 3 and 4, respectively (see Figure 1). The description

of the velocities is carried out by a potential flow formulation, writing the total velocity potential in the frequency domain as

$$\phi = \phi_D + \sum_j \phi_j \dot{X}_j, \qquad j = s, b. \tag{13}$$

The water particle velocity in the z direction at a point in the fluid domain is then obtained by

$$V_z = \frac{\partial \phi}{\partial z} = \frac{\partial \phi_D}{\partial z} + \sum_j \frac{\partial \phi_j}{\partial z} \dot{X}_j \tag{14}$$

The second term on the right hand side of Equation 14 is the water particle velocity in z direction due to radiation, and in the time domain it becomes

$$v_z^R(t) = \sum_j \int_0^t K_j^{v_z}(t-\tau)\dot{x}_j(\tau)d\tau, \tag{15}$$

where

$$K_j^{v_z}(t) = \frac{1}{\pi}\int_0^\infty [\Re(\frac{\partial \phi_j}{\partial z})\cos(\omega t) - \Im(\frac{\partial \phi_j}{\partial z})\sin(\omega t)]d\omega. \tag{16}$$

Again, the convolution terms can be represented by a state space model in the same manner as for the radiation force, giving

$$\begin{aligned} \dot{\mathbf{z}}(t) &= \tilde{\mathbf{A}}_{\mathbf{v_z,j}}\,\mathbf{z}(t) + \tilde{\mathbf{B}}_{\mathbf{v_z,j}}\dot{\mathbf{x}}(t) \\ v_{z,j}^R(t) &\approx \tilde{\mathbf{C}}_{\mathbf{v_z,j}}\,\mathbf{z}(t) + \tilde{\mathbf{D}}_{\mathbf{v_z,j}}\dot{\mathbf{x}}(t) \end{aligned} \tag{17}$$

Regarding the diffraction component $\partial\phi/\partial z$ of the water particle velocity in z direction we use the following formulation:

$$v_z^D(t) = \sum_{j=1}^n v_j^D \sin(\omega_j t + \epsilon_j), \tag{18}$$

where v_j^D and ϵ_j are the magnitude and phase of the water particle velocity at a specific point due to the jth wave component. It is obtained from the spectral density function of the sea waves and the transfer function of the water particle velocity corresponding to the incident wave component j.

The mathematical model described above comprises a coupled system of first order differential equations. The equations of motion for mechanical systems are more often presented as second order differential equations. By combining and rearranging Equations 1 to 4 we arrive at the following matrix equation, probably more familiar to some of the readers[1]:

$$[\mathbf{M}+\mathbf{A}^\infty]\ddot{\mathbf{x}}(t)+\int_0^t \mathbf{K}(t-\tau)\,\dot{\mathbf{x}}(\tau)\,d\tau+\mathbf{C}\mathbf{x}(t) = \mathbf{F}(t), \tag{19}$$

where, in this case

$$\mathbf{A}^\infty = \begin{bmatrix} A_{ss}^\infty & A_{sb}^\infty \\ A_{bs}^\infty & A_{bb}^\infty \end{bmatrix},$$

$$\mathbf{C} = \begin{bmatrix} \rho\, g\, A_{\mathrm{wp,s}} & 0 \\ 0 & \rho\, g\, A_{\mathrm{wp,b}} \end{bmatrix},$$

$$\mathbf{F}(t) = \begin{bmatrix} F_{\mathrm{exc,s}} + F_{\mathrm{H}} + F_{\mathrm{visc}} \\ F_{\mathrm{exc,b}} - F_{\mathrm{H}} \end{bmatrix},$$

$$\mathbf{M} = \begin{bmatrix} m_s & 0 \\ 0 & m_b \end{bmatrix},$$

and $F_{\mathrm{H}} = A_p\, e_D$. This is the form in which equations 1 to 9 has been implemented and solved in our numerical Simulink [13] model.

[1] We refer to this model as a hybrid frequency-time domain model. See [11] for details.

2.1 Power take-off and control alternatives

Two of the PTO alternatives has already been mentioned. Altogether, three alternative mechanisms have been tested:

PH Passive hydraulic system with optimised parameters

PHL Hydraulic system with latching control by a shut-off valve

PL Simple resistor power take-off, with PTO load force proportional to velocity: $F_l = R_l\,\dot{x}_{\mathrm{rel}}$. The force F_l enters in the equations instead of the $A_p\,p_D$ term. The load resistance is set to $R_l = 1.24$ Ns/m, chosen as described in Section 3.

For latching control, the operation of the control valve is based on knowledge about the values of the excitation forces up to about two seconds into the future. In the simulations, these are taken to be known in advance as we pre-calculate the excitation force time series, whereas in reality they must be predicted by a combination of measurement and signal processing.

The control algorithm closes the control valve at zero relative velocity. With a given natural period T_b for the buoy, it then checks for a maximum of the excitation force in the interval $[t + T_b/4, t + T_b/2]$, and opens the control valve when this maximum is $T_b/4$ ahead and the force is in the right direction. The result is that the relative velocity will be in phase with the excitation force.

3 Simulation results

Simulations have been run for five different regular waves and five different irregular wave sea states chosen such that the wave energy transport is equal for equal index, as shown in Table 4. For each irregular wave sea state, the same wave elevation time series has been used in the simulations, so that no stochastic variation is introduced between simulation runs for different system configurations. The length of the time series have been taken to be 1000 s, and the dominating wave period is typically around 8 s. We thus expect reasonably good estimates of the average quantities. However, we cannot expect to achieve good representation of extreme values, as this requires a much larger number of oscillation cycles.

Table 4: Chosen sea states for numerical simulation. The combinations of regular wave period T and height H has been chosen such that the wave energy transport J matches the one for an irregular Pierson-Moskowitz sea state of peak period T_p and significant wave height H_s.

Regular wave	T [s]	H [m]	J [kW/m]
R1	6.00	1.31	10.1
R2	8.00	0.65	3.4
R3	8.00	1.31	13.5
R4	8.00	1.96	30.3
R5	10.00	1.31	16.8

Irregular wave	T_p [s]	H_s [m]	J [kW/m]
I1	6.00	2.00	10.1
I2	8.00	1.00	3.4
I3	8.00	2.00	13.5
I4	8.00	3.00	30.3
I5	10.00	2.00	16.8

A very simple scheme has been followed for choosing the initial and operational parameters of the system. Once the di-

mensions of the system have been determined by limiting pressures and forces, the energy absorption is mainly governed by the applied generator torque τ_g, or the load resistance R_l in the case of the PL machinery. These are assumed here to be non-varying parameters. In the case of latching control, also the time constant for unlatching plays an important role. All these parameters where optimised by variation through a number of runs with wave R3 (cf. Table 4), leading to the identification of their best setting. These values where then used for all runs, also with other wave inputs.

Both for the passive and latching hydraulic system we see the occurrence of a resonance oscillation due to the compressibility of the piston cylinder (oil and other), represented by accumulator D. This occurs when the fluid pressure is within the range where both check valves to accumulator B and C are closed.

In the following tables, the simulation results are analysed in terms of the following quantities:

P_{useful} is the power delivered at the generator output.

P_{abs} is the power absorbed from the waves.

$P_{\mathrm{loss}} = P_{\mathrm{abs}} - P_{\mathrm{useful}}$.

$x_{\max}$ and $x_{\min}$ are the maximum and minimum relative excursions between the platform and the buoy.

P_{visc} is the power dissipated at the pontoons of the platform.

d_a is the absorption width, defined as $d_a = P_{\mathrm{abs}}/J$, where J is the wave energy transport.

Results for the hydraulic system in regular and irregular waves are shown in Table 5, and some examples of the motion response are shown in Figures 7 to 10. Results for latching control are only presented for regular waves, as latching algorithms for irregular waves are currently under investigation.

Table 5: Power output obtained by the hydraulic system, with and without latching control in regular waves R1 to R5. For the passive system (without latching) results are also given for irregular waves I3 to I5. The generator output P_{useful} is given together with the absorption width d_a and the power P_{loss} lost in the hydraulic system.

Wave	PTO	P_{useful} [kW]	d_a [m]	$P_{\mathrm{loss}}/P_{\mathrm{abs}}$
R1	PH	1.01	0.10	0.012
R2	PH	1.52	0.45	0.018
R3	PH	6.83	0.55	0.076
R4	PH	10.84	0.41	0.117
R5	PH	3.43	0.21	0.039
R1	PHL	12.44	1.72	0.027
R2	PHL	3.75	1.28	0.010
R3	PHL	10.02	0.78	0.028
R4	PHL	16.26	0.57	0.045
I1	PH	4.08	0.42	0.071
I2	PH	1.35	0.42	0.035
I3	PH	5.31	0.42	0.081
I4	PH	10.01	0.36	0.130
I5	PH	4.71	0.30	0.081

The effect of viscous damping on the platform pontoons have been investigated by varying the drag coefficient at four levels. Increased drag will force the platform pontoons to closer follow the motion of the water. Table 6 presents results for the I3 wave time series.

The level of force compensation was varied as shown in Figure 4 for irregular wave and hydraulic power take off PH. The result in terms of power output and maximum excursion is given in Table 7.

Table 6: The effect of varying the viscous damping on the platform pontoons. The drag coefficient C_d has been chosen in steps between 1 and 8, and the resulting effect on useful power output P_{useful}, extreme platform excursions $x_{\mathrm{s,max}}$ and $x_{\mathrm{s,min}}$, and relative viscous loss $\frac{P_{\mathrm{visc}}}{P_{\mathrm{abs}}}$ for irregular wave I3 input and passive hydraulic power take-off PH is shown.

C_d	P_{useful} [kW]	$x_{\mathrm{s,max}}$ [m]	$x_{\mathrm{s,min}}$ [m]	$P_{\mathrm{visc}}/P_{\mathrm{abs}}$
1.0	5.47	0.74	-0.78	0.040
2.0	5.31	0.71	-0.77	0.073
4.0	5.05	0.67	-0.75	0.125
8.0	4.77	0.65	-0.69	0.188

Table 7: The effect of force compensation between the buoy and the platform. The pontoon diameter factor a (see Table 6) has been varied from 0.8 to 1.2 resulting in changes in power yield and maximum of relative excursion $x_{\mathrm{rel,max}}$. Input wave is I3 and the PTO is passive hydraulic (PH).

a	P_{useful} [kW]	P_{abs} [kW]	$x_{\mathrm{s,max}}$ [m]	$x_{\mathrm{rel,max}}$ [m]
0.8	6.30	7.00	0.90	1.59
1.0	5.31	5.69	0.71	1.13
1.2	3.49	4.02	0.62	1.04

In order to assess the performance of the hydraulic power take-off, a comparison to power output using a simple linear power take-off (PL) as described above was done. Results are presented in Table 8.

Table 8: Comparison of useful power output for a simple linear power take-off (PL) and the hydraulic system (PH) for different wave inputs.

Wave	PTO	P_{useful} [kW]	P_{abs} [kW]
R3	PL	7.81	7.81
R3	PH	6.83	7.38
I2	PL	1.67	1.67
I2	PH	1.35	1.41
I3	PL	6.32	6.32
I3	PH	5.31	5.69
I4	PL	13.49	13.49
I4	PH	10.01	10.86

Also comparison with the case of a fixed platform has been made for the passive hydraulic power take-off PH. This is simply done by setting its velocity equal to zero. This is reported in Table 9.

4 Discussion

From Table 5 we see that the absorption width (calculated on the basis of absorbed power) of the system varies from about 0.1 to 0.55 m for the passive hydraulic system, which should be compared to the actual horizontal extension of 4 m for the buoy and 1.7 m for each of the columns. The theoretical maximum absorption width for a point absorber is known to be $d_a \leq \lambda/2\pi$, which in this case is about 16 m for the R3 wave. We would expect a well-designed converter system based on the

Table 9: Comparison of output for the system with both bodies moving and only the buoy moving. The power take-off was PH, and the last column gives the power P_{loss} lost in the hydraulic system.

Wave	Platform	P_{useful} [kW]	P_{abs} [kW]	$P_{\text{loss}}/P_{\text{abs}}$
R3	fixed	7.72	9.12	0.15
R3	moving	6.83	7.38	0.08
I2	fixed	1.25	1.31	0.07
I2	moving	1.35	1.41	0.03
I3	fixed	6.61	7.81	0.15
I3	moving	5.31	5.69	0.08
I4	fixed	11.44	14.27	0.24
I4	moving	10.01	10.86	0.13

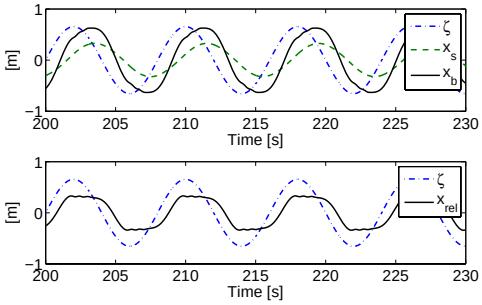

Figure 7: Motion response for the buoy and platform (upper) and relative motion (lower) for an ingoing regular wave of height 1.31 m and period 8 s (R3) using the passive hydraulic power take-off (PH).

point absorber to have an absorption width comparable or even larger than its own extension. This is not achieved with the PH system. It should be remembered that for the reported results, the PTO parameters have been optimised for the R3 wave. This means better performance is expected for other sea states.

In regular waves, the absorption width increases significantly for the latched system, reaching up to 1.72 m for the R1 wave (where the upper limit is about 9 m). Figure 9 shows how the phase relation is improved compared to the passive case in Figure 8.

For the PH configuration in irregular waves, the performance is somewhat decreased for wave inputs I3 and I4 compared to R3 and R4, but slightly improved for input I1 and I5 compared to R1 and R5. Here, the equally indexed sea states (for instance I3 and R3) have the same wave energy transport. The increased performance is understandable, since the irregular sea state gives the system some waves closer to the frequency for which its parameters have been optimised than the pure sinusoidal wave.

Looking at power losses in the hydraulic system (Table 5), we observe that they become very large for the most energy-rich sea states (R4 and I4). The lion's share of the loss is due to the motor resistance, which has been modelled as a linear resistive load. This is a simplification that, with our current model, gives unrealistically large losses when the rotational speed of the motor is high. On the other hand, the valve losses are more accurately modelled, and with the chosen valve diameters these are about 1.3 % of the absorbed power for the I4 sea state. This

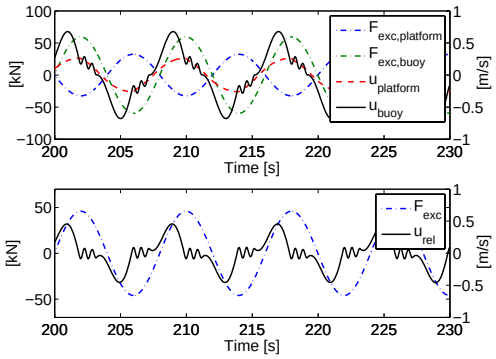

Figure 8: Excitation forces and velocities for the buoy and platform (upper) and for the relative motion (lower). The incoming wave is regular with a height of 1.31 m and a period of 8 s (R3), and the power take-off is PH. The wave elevation at the central axis of the buoy is given by ζ.

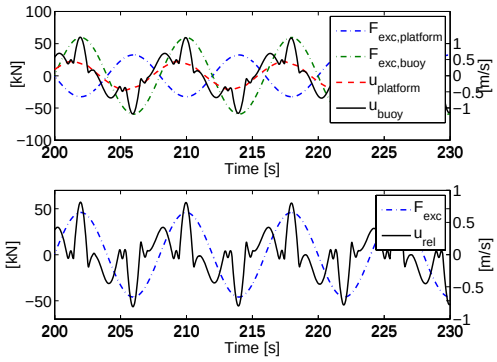

Figure 9: Forces and velocities for the hydraulic latching power take-off (PHL). Absolute (upper) and relative (lower) quantities for an incoming regular wave with height 1.31 m and period 8 s.

is still a quite high value, showing that such losses may become important if they are not seriously taken into account in the dimensioning of the equipment.

Table 6 shows the effect of increasing the viscous damping on the platform pontoons. The power output decreases slowly but steadily as the viscous damping is increased. This is in accordance with claims that shapes should be rounded and viscous losses avoided. Although the platform tend to oscillate in phase with the buoy (cf. Figure 10), reducing the viscous loss gives both increased power output and increased oscillation amplitudes.

One of the goals has been to assess the effect of varying the force compensation between the platform and the buoy. From Table 7 it is clear that this variable has a strong effect on the power output. According to the presented results, the power output increases when the opposing wave force on the platform is decreased, i.e. when the diameter of the pontoon is decreased (referred to as undercompensation of the wave force on the platform relative to the force on the buoy). Then both the excitation force on and the added mass of the platform decreases. Again,

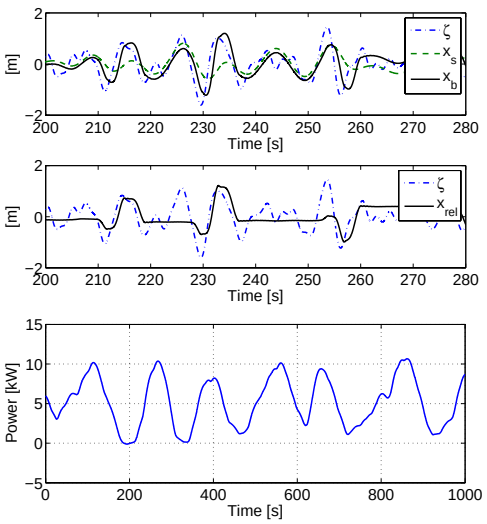

Figure 10: Motion response for the passive hydraulic power take-off (PH) in regular wave I3. The lowermost figure gives the power output (with a differing time scale). The wave elevation at the central axis of the buoy is given by ζ.

the platform motions are larger for the best performing geometries.

The simulation results in Table 8 indicate that the hydraulic power take-off (PH) performs inferior to an idealised linear power take-off (PL), both in terms of useful and absorbed power. In addition to losses in the PTO system, which are not present in the case of the PL configuration, this is due to less beneficial amplitude and phase of the of the buoy and platform motion, giving rise to the difference in absorbed power. On the contrary, when the pontoon diameter factor a is chosen to be 0.8 (see Table 7) the picture changes. Then the amplitude and phase relations are improved such that the PH system performs better than the PL system for the I3 sea state.

Finally, (cf. Table 9) shows that the output is larger when the platform is not allowed to move, except for the I2 sea state. This exception examplifies that having the two bodies moving may give better absorption than achieved with just the buoy moving. As we have seen, the platform geometry (here: the a factor) largely influences the power absorption and, by choosing it right, the performance with the platform moving could probably be improved compared to the case with fixed platform.

5 Conclusion

A two-body, heaving wave-energy converter with a hydraulic power take-off system has been studied with and without latching control. The first body is semisubmersible platform giving force reference to the the second body, which is a cylindrical buoy with hemispherical bottom. For the default platform geometry, the system performance shows to be somewhat inferior to what obtained by a simple linear load force for power take-off. The power output was shown to increase considerably using a latching control strategy for the hydraulic power take-off in regular waves. Flow losses in the hydraulic system may become large, and must be thoroughly assessed during the design process for such a system.

Taking out power from the relative motion between two heaving bodies instead of from one body with fixed reference (if possible) can be beneficial in terms of power output if the geometry and parameters are chosen right. If not, having two oscillating bodies instead of only one might only represent an extra cost. The system presented here performs better if the opposing excitation force on the platform is made smaller than the excitation force on the buoy (undercompensation).

Further work will assess the effect of latching control in irregular waves.

Acknowledgements

Thanks to professor emeritus Johannes Falnes for valuable input and guidance. Also thanks to the Norwegian research council for funding.

References

[1] Kjell Budal and Johannes Falnes. Wave power conversion by point absorbers: A norwegian project. *International Journal of Ambient Energy*, 3(2):59 – 67, 1982.

[2] R. E. Hoskin, N. K. Nichols, D. A. C. Nicol, and B. M. Count. Latching control of a point absorber. In *Water for Energy*, pages 317 – 330. BHRA Fluid Engineering Centre, Brighton, England, 1986.

[3] K. Budal. Floating structure with heave motion reduced by force compensation. In *Proceedings Fourth International Offshore Mechanics and Arctic Engineering Symposium*, pages 92–101, Dallas, Texas, February 1985. ASME, N.Y.

[4] J. Falnes. Wave-energy conversion through relative motion between two single-mode oscillating bodies. *Journal of Offshore Mechanics and Arctic Engineering (ASME Transactions)*, 121:32–38, 1999.

[5] Hallvard Engja and Jørgen Hals. Modelling and simulation of sea wave power conversion systems. In *Proceedings of the 7th European Wave and Tidal Energy Conference, Porto, Portugal, 2007*, 2007.

[6] *WAMIT User Manual*. (http://www.wamit.com).

[7] H. Eidsmoen. Tight-moored amplitude-limited heaving-buoy wave-energy converter with phase control. *Applied Ocean Research*, 20(3):157 – 161, 1998.

[8] J. Falnes and P.M. Lillebekken. Budal's latching-controlled-buoy type wave-power plant. In Anthony Lewis and Gareth Thomas, editors, *Fifth European Wave Energy Conference: Proceedings of an International Conference held at University College Cork, Ireland, 17-20 September 2003*, pages pp. 233–244, Cork, Ireland, 2005. Hydraulics & Maritime Research Centre, Hydraulics & Maritime Research Centre. ISBN 0-9502440-5-8.

[9] Håvard Eidsmoen. *On the theory and simulation of heaving-buoy wave-energy converters with control*. PhD thesis, NTH, December 1995.

[10] W.E. Cummins. The impulse response function and ship motions. *Schiffstechnik*, 9(1661):101–109, 1962.

[11] R. Taghipour, T. Perez, and T. Moan. Hybrid frequency–time domain models for dynamic response analysis of marine structrues. *To appear*, 2007.

[12] T. Sauder and T. Moan. Experimental investigation of the hydrodynamic characteristics of a novel column design for semi-submersible platforms. In *The Seventeenth (2007) International Offshore and Polar Engineering Conference -ISOPE 2007*, 2007.

[13] Simulink. The MathWorks, Inc. 3 Apple Hill Drive Natick, MA 01760-2098 USA.

Paper 6

Structural Analysis of A Multi-Body Wave Energy Converter in The Frequency Domain by Interfacing WAMIT and ABAQUS

Accepted for publication at
The International Journal of Offshore Mechanics and Arctic Engineering, (Presented at the 28th International Conference on Offshore Mechanics and Arctic Engineering, 2008, Estoril, Portugal).

Is not included due to copyright

D. Study of the FO^3 in the Vertical Plane

Motion Analysis of the FO^3 Platform in the Vertical Plane

Reza Taghipour

August 7 2007

Abstract

A modeling approach for FO^3 wave energy converter (WEC) is presented in this report. The method is based on the generalized modes and therefore exploits problem symmetry. Comparison with standard way of modeling suggests that the current approach results in significant savings in simulation time.

Description of the Problem

Fig. 1 shows the top view of the WEC. The WEC consists of a semisubmersible platform and 21 buoys. The buoys can slide along some guides that are connected in a relatively stiff manner to the deck of the semisubmersible. The objective is to represent the dynamic equations of motion for the bodies.

For an incident wave progressing along the x direction i.e. a following-seas wave condition, the problem will have symmetry about the xz plane. Buoys #1 to 8 will have their mirrors, buoys #14 to 21. Buoys #9 to 13 will have no mirrors. This fact simplifies the problem since now there are a total number of 16 original d.o.f.s for the WEC:

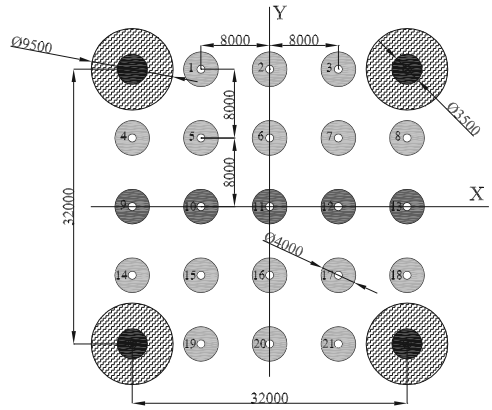

Figure 1: Layout of FO^3 WEC.

- System surge (platform and buoys), ξ_1,
- (Independent) heave of the platform, ξ_2,
- Pitch of platform and buoys considering the buoys to slide along the guides, ξ_3,
- (Independent) heave of each buoy, $\xi_4 \dots \xi_{16}$.

The above modes define the following mathematical functions:

$$\boldsymbol{\lambda}_1 = [1,0,0]^T, \quad \text{everywhere},$$

$$\boldsymbol{\lambda}_2 = \begin{cases} [0,0,1]^T, & \text{if} \quad \mathbf{x} \in S_s, \\ \mathbf{0}, & \text{elsewhere}, \end{cases}$$

$$\boldsymbol{\lambda}_3 = \begin{cases} [z,0,-x]^T, & \text{if} \quad \mathbf{x} \in S_s, \\ [z,0,-(x-x^g_{b_k})]^T, & \text{if} \quad \mathbf{x} \in \begin{cases} S_{b_k} \\ S_{m_k} \end{cases} \end{cases}$$

$$\boldsymbol{\lambda}_i = \begin{cases} [0,0,1]^T, & \text{if} \quad \mathbf{x} \in \begin{cases} S_{b_k} \\ S_{m_k} \end{cases} \\ \mathbf{0}, & \text{elsewhere}. \end{cases} \tag{1}$$

where k=1...13 and i=3+k. S_s, S_{b_k} and S_{m_k} denote the geometry of the semisubmersible platform, the k^{th} buoy and its mirror (if applicable), respectively. The multi-body hydrodynamic problem of the WEC is described by using the generalized modes approach, as explained by e.g. Newman (1994). The WEC (semi and 21 buoys) is then considered as one body that can oscillate according to the mode definitions given above. The defined modes exhibit symmetry about the x axis, thus one needs to consider only half of the WEC geometry as illustrated by Fig. 2.

Using these definitions and assumptions, the generalized mass and restoring coefficient matrices will be written as Eqs. (2) and (3). One must note that there is no vertical force transfer from the buoys to the platform except for the power take-off

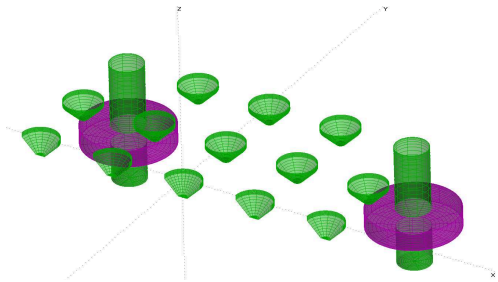

Figure 2: The underwater geometry of the FO^3.

machinery.

$$\mathbf{M} = \begin{bmatrix} M_{11} & 0 & M_{11} & & \mathbf{0} & \\ 0 & M_{22} & 0 & & & \\ M_{51} & 0 & M_{33} & & & \\ & & & M_{44} & & \\ & & & & \ddots & \\ & \mathbf{0} & & & & M_{16\,16} \end{bmatrix} \tag{2}$$

where

$$M_{11} = m_s + \sum_{k=1}^{13} p_k \; m_{b_k},$$

$$M_{13} = M_{31} = m_s z^g_s + \sum_{k=1}^{13} p_k \; m_{b_k} z^g_{b_k},$$

$$M_{22} = m_s,$$

$$M_{23} = -m_s x^g_s,$$

$$M_{33} = m_s r^2_{yy^o_s} + \sum_{k=1}^{13} p_k \; m_{b_k} r^2_{yy^o_{b_k}},$$

$$r^2_{yy^o_s} = r^2_{yy^g_s} + (x^2_{s^g} + z^2_{s^g}), \;\; r^2_{yy^o_{b_k}} = r^2_{yy^g_{b_k}} + z^2_{b_k{}^g},$$

$$M_{ii} = p_k \; m_{b_k}.$$

$$\mathbf{C} = \begin{bmatrix} 0 & & & & & \mathbf{0} \\ & C_{22} & & & & \\ & & C_{33} & & & \\ & & & C_{44} & & \\ & & & & \ddots & \\ \mathbf{0} & & & & & C_{16\,16} \end{bmatrix}$$

(3)

where

$$
\begin{aligned}
C_{22} &= \rho g \; A_s^{WP} \\
C_{33} &= \rho g (\nabla_s \overline{GM}_s + \sum_{k=1}^{13} p_k \; \nabla_{b_k} \overline{GM}_{b_k}) \\
C_{ii} &= \rho g \; p_k \; A_{b_k}^{WP}.
\end{aligned}
$$

In Eqs. (2) and (3), $i = 4 \ldots 16$, $k = 1 \ldots 13$. The entry p_k is the coefficient denoted by the mirror symmetry of the k^{th} buoy mode. p_k can be either 1 or 2. It is equal to 1 when the k^{th} buoy does not have a mirror about xz.

An idealized formulation of the power take-off force is considered. The power take-off force on each buoy is assumed proportional to the relative vertical velocity of the buoy and the guide (platform) at the buoy's center of gravity:

$$
F_i^{PTO} = -b_u [\dot{\xi}_i - \dot{\xi}_2 + x_{b_k}^g \dot{\xi}_3], \tag{4}
$$

Note that $i = 4, \ldots, 16, \; k = 1, \ldots, 13$. The total reaction force and moments on the platform due to the power take-off machinery will then be

$$
\begin{aligned}
F_1^{PTO} &= \sum_{k=1}^{13} F_i^{PTO} \\
&= b_u \sum_{k=1}^{13} (\dot{\xi}_i - \dot{\xi}_2 + x_{b_k}^g \dot{\xi}_3), \\
F_3^{PTO} &= \sum_{k=1}^{13} -x_{b_k}^g \; F_i^{PTO} \\
&= b_u \sum_{k=1}^{13} -x_{b_k}^g \; (\dot{\xi}_i - \dot{\xi}_2 + x_{b_k}^g \dot{\xi}_3).
\end{aligned} \tag{5}
$$

The power take-off force formulation in Eqs. (4) and (5) define a power absorption damping matrix in the following form:

$$
\mathbf{B_u} = \begin{bmatrix}
0 & 0 & 0 & 0 & \ldots & 0 \\
0 & B_{22} & B_{23} & B_{24} & \ldots & B_{2n} \\
0 & B_{32} & B_{33} & B_{34} & \ldots & B_{3n} \\
0 & B_{42} & B_{43} & B_{44} & & \mathbf{0} \\
\vdots & \vdots & \vdots & & \ddots & \\
0 & B_{16\,2} & B_{16\,3} & \mathbf{0} & & B_{16\,16}
\end{bmatrix} \tag{6}
$$

where

$$
\begin{aligned}
B_{22} &= \sum_{k=1}^{13} p_k \; b_u, \\
B_{23} &= B_{32} = \sum_{k=1}^{13} -p_k \; x_{b_k}^g b_u, \\
B_{2i} &= B_{i2} = -p_k \; b_u, \qquad . \\
B_{33} &= \sum_{k=1}^{13} p_k \; x_{b_k{}^g}^2 b_u, \\
B_{3i} &= B_{i3} = p_k \; x_{b_k}^g b_u, \\
B_{ii} &= p_k \; b_u,
\end{aligned}
$$

Following the hydrodynamic methodology in WAMIT (2006), the total velocity potential is written as sum of diffraction and radiation potentials:

$$
\Phi = \phi^D + \phi^R = \phi^D + \sum_{i=1}^{16} \phi_i \dot{\xi}_i, \qquad \phi^D = \phi^I + \phi^S. \tag{7}
$$

Each potential must satisfy the following conditions:

- Continuity (Laplace) equation.

- Free surface conditions (kinematic and dynamic).
- Radiation condition.
- Body boundary condition.

Attention is paid in satisfying the body boundary conditions for the radiation potentials due to the modes. The radiation potential at each point belonging to the WEC underwater geometry should satisfy the following equation:

$$\begin{aligned} &\frac{\partial \phi_i}{\partial n} = \boldsymbol{\lambda}_j.\mathbf{n}, \\ &\boldsymbol{\lambda}_j = [u_j, v_j, w_j]^T, \quad \mathbf{n} = [n_x, n_y, n_z]^T. \end{aligned} \tag{8}$$

where the modes are defined according to Eq. (1). Solution of the potentials will then give the hydrodynamic pressure by using the linearized Euler-Bernoulli's equation. By integrating this pressure on the mean wetted body surface, the generalized first-order pressure forces corresponding to each mode of motion are evaluated in the form of radiation (added mass and hydrodynamic damping) and diffraction (wave-exciting) components:

$$\begin{aligned} F_i^{rad} &= -[i\omega A_{ij} + B_{ij}]\dot{\xi}_j \\ &= -i\omega\rho \int\int_{S_0} \phi_j \dot{\xi}_j n_i \; dS, \end{aligned} \tag{9}$$

$$F_i^{exc} = -i\omega\rho \int\int_{S_0} \phi^D n_i \; dS, \tag{10}$$

where i=1...(N+6).

The equations of motions for each component in the WEC is written as

$$\begin{aligned} &-\omega^2 \boldsymbol{\xi}(i\omega)[\mathbf{M} + \mathbf{A}(\omega)] + i\omega\boldsymbol{\xi}(i\omega)[\mathbf{B}(\omega) \\ &+ \mathbf{B_u}] + \mathbf{C}\boldsymbol{\xi}(i\omega) = \mathbf{F^{exc}}(i\omega) \end{aligned} \tag{11}$$

Results

The results of the current approach have been compared to the study by Rogne (2007) in Figs. 3. The idealized power take-off coefficient b_u was taken equal to 100 $\frac{kNs}{m}$. One can clearly observe from the plots that the results are in well agreement.

Considering the computational time, the method used by Rogne (2007) consumed about 6 hours to calculate the hydrodynamic loads only (in WAMIT). One must add the post-processing time to the hydrodynamic calculations time to obtain the total simulation time. However, the hydrodynamic calculations stage is dominant in comparison to the total simulation time. Using the current approach, the total simulation time has been reduced by a factor of about 10 . This factor increases if the modes of motion are further reformulated to allow double plane symmetry for the problem. This is feasible if one decomposes the current modes into a series of symmetric and antisymmetric modes.

Concluding Remarks

In this report, a mode expansion approach was used to study the linear steady-state response of the FO^3 wave energy converter in the frequency domain. The approach exploits symmetry about the xz plane. Moreover, it reduces the d.o.f.s required to analyze the motions. Therefore, it leads to a significant save in the simulation time which has been suggested by comparing the numerical results.

References

Newman, J. (1994). Wave effects on deformable bodies. *Applied Ocean Research 16*, 47–59.

Rogne, Y. (2007). Dynamic analysis of a wave energy converter-a frequency domain approach. Master's thesis, Norwegian University of Science and Technology.

WAMIT (2006). MA ,USA: WAMIT Inc. Ver. 6.3.

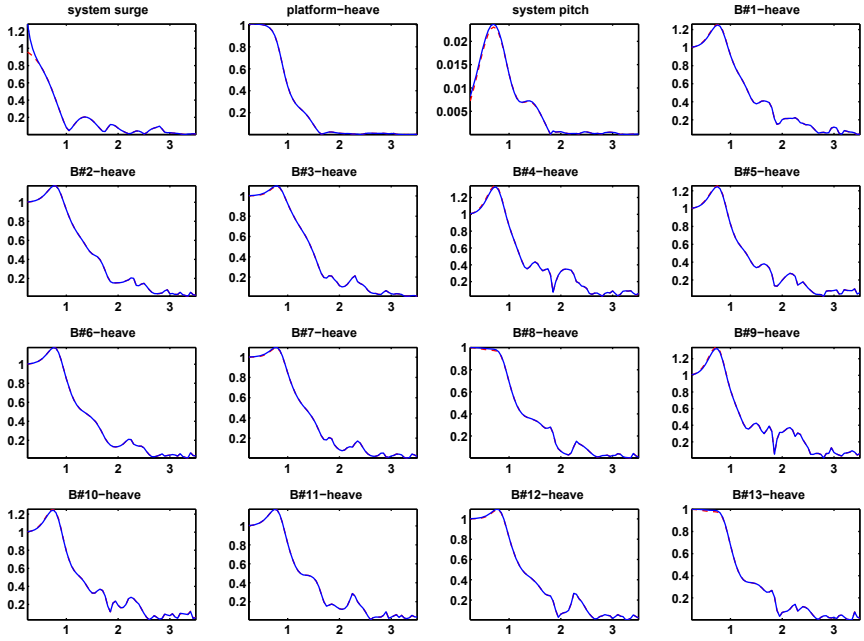

(a) Amplitude.

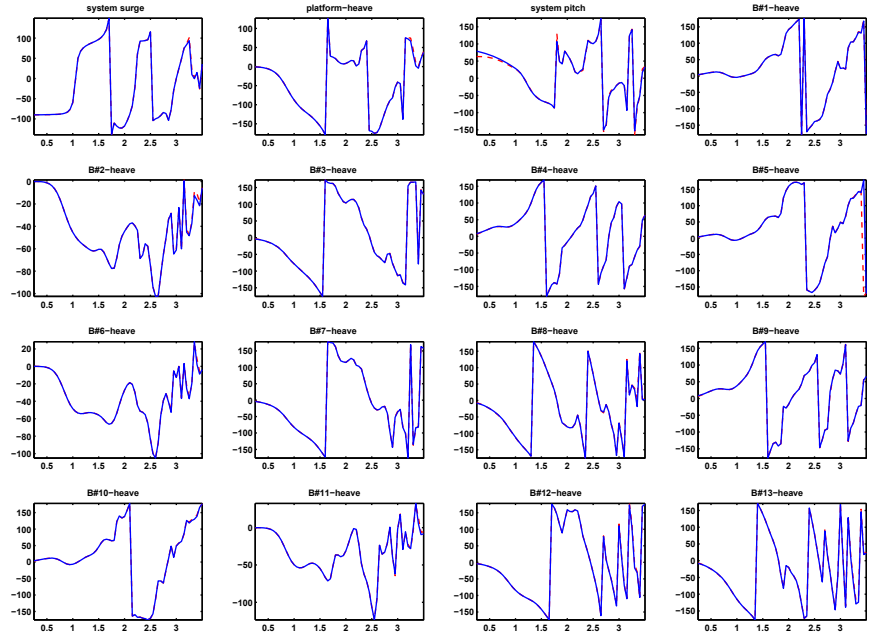

(b) Phase.

Figure 3: Comparison of the results of motions for each component in the WEC. The comparison is made between the current approach (dashed red lines) and the study by Rogne (2007) (solid blue lines).

E. Some Verification of the Interface

Structural Analysis of A Cantilever Column Subjected to Wave-Induced Loads by Interfacing WAMIT and ABAQUS–A Comparison Study

Reza Taghipour, A. Arswendy

Nov 9 2007

Abstract

An interface code has been developed to share the pressure information between WAMIT and ABAQUS. In this report, a validation of the interface code is presented. comparisons are made between structural response obtained by analytical and numerical studies. First, a clamped circular cylinder at a distance equal to half the length of a monochrome wave is considered. Wave-induced pressure and external and internal loads in the cylinder will be evaluated and compared. In a second attempt, the transfer functions of the internal loads will be examined for the same geometry. The numerical results are obtained by interfacing WAMIT and ABAQUS. The analytical solutions are carried out by assuming long wave theory and using Morison's formula. Linear wave-induced loads and responses are targeted throughout the work.

1 Introduction

The problem is defined in Fig. 1. When the wave length is four times the distance of the cylinder from the origin, the horizontal wave-induced forces and moments are expected to be larger than the vertical wave-induced forces. This condition resembles a semisubmersible where the wave length is two times the distance between the two columns. The objective is to compare the following quantities from analytical formulations and numerical calculations:

1. Wave-induced pressure at P_1 and P_2,
2. Forces acting on the cylinder at the origin of the global coordinate system (point O),
3. Moments acting on the cylinder at the origin of the global coordinate system,
4. Internal Stresses at P_3 and P_4,
5. Moment/Stress change along the cylindrical axis,
6. Frequency response functions of the axial force and bending moments at two different sectional cuts: one close to the support and one close to the still water level (SWL).

The phases are given in degrees with respect to the wave at the origin of the coordinate system which is described as

$$\varsigma_a = A\cos(\omega t) \tag{1}$$

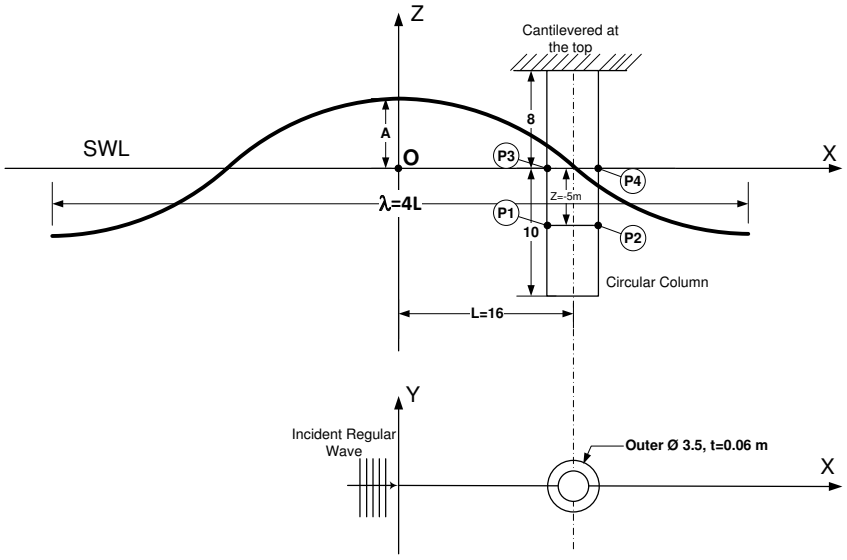

Figure 1: Sketch of the problem.

In the following, the analytical solutions are first established. Then, we compare the results of numerical calculations by WAMIT and ABAQUS to conclude the comparisons.

2 Analytical Calculations

Assuming a potential flow formulation, one may find the following derivations for the velocity potential, wave profile, horizontal and vertical components of the fluid particle velocity and acceleration in the fluid domain, and dynamic pressure as below (e.g. Newman (1977)):

$$\phi = \frac{gA}{\omega} e^{kz} \sin(kx - \omega t) \tag{2}$$

$$\zeta = A\cos(kx - \omega t) \tag{3}$$

$$u = A\omega e^{kz} \cos(kx - \omega t) \tag{4}$$

$$a_1 = A\omega^2 e^{kz} \sin(kx - \omega t) \tag{5}$$

$$w = A\omega e^{kz} \sin(kx - \omega t) \tag{6}$$

$$a_3 = -A\omega^2 e^{kz} \cos(kx - \omega t) \tag{7}$$

$$p_d = \rho g A e^{kz} \cos(kx - \omega t) \tag{8}$$

2.1 Pressure at P_1 and P_2

By using Eq. (8) and knowing that $[x, y, z]_{p_1} = [14.25, 0, -5]$ and $[x, y, z]_{p_2} = [17.75, 0, -5]$, we obtain the analytical solution of pressure as

$$\bar{P}_{d,P_1}^{Analytical} = \frac{P_d}{\rho g} = 0.612\cos(\omega t - 80.15^\circ), \tag{9}$$

$$\bar{P}_{d,P_2}^{Analytical} = \frac{P_d}{\rho g} = 0.612\cos(\omega t - 99.84^\circ). \tag{10}$$

The pressure phases are close to -90 degrees corresponding to the location of the cylinder with respect to the origin.

2.2 Forces

2.2.1 Horizontal Force

We use Morison's formula (e.g. Faltinsen (1990)) to evaluate the horizontal wave-induced forces on the cylinder. Such a formulation considers only the undisturbed wave loads and neglects the wave scattering effects. In this way, the horizontal 'inertia term' force acting on a cylinder strip is

$$dF_x = \rho\frac{\pi D^2}{4}C_m a_1 dz, \qquad C_m = 2.0; \tag{11}$$

where a_1 is the horizontal fluid particle acceleration at the center of the disc by using Eq. (5). The force is then

$$F_x = \rho C_m A\omega^2\frac{\pi D^2}{4}\int_{-10}^{0} e^{kz}dz\sin(\frac{\pi}{2} - \omega t)$$

which leads to

$$\bar{F}_x^{Analytical} = \frac{F_x}{\rho g} = 12.033\sin(\frac{\pi}{2} - \omega t) = 12.033\cos(\omega t) \tag{12}$$

This result implies that the shear force observed at the sectional cut in the SWL would be $12.033\cos(\omega t + 180^\circ)$.

2.2.2 Vertical Force

The vertical wave-induced force can be found by integrating the hydrodynamic pressure acting on the bottom of the cylinder. Assuming a long wave ($\lambda >> D$), the formulation is simplified to multiplying the pressure at the center of the cylinder bottom by its corresponding area:

$$F_z = P_d{}^{(x=16,y=0,z=-10)}S = \rho g A\frac{\pi D^2}{4}e^{-10k}\cos(\frac{\pi}{2} - \omega t) \tag{13}$$

which leads to

$$\bar{F}_z^{Analytical} = \frac{F_z}{\rho g} = 3.6\cos(\omega t - \frac{\pi}{2}) = 3.6\cos(\omega t - 90^\circ) \tag{14}$$

This results implies that the axial force observed at the sectional cut in the SWL would be $3.6\cos(\omega t + 90^\circ)$.

2.3 Moments

2.3.1 Contribution From The Horizontal Force

The force acting on the cylinder strip in Eq. (11) gives a moment about the origin (point O) as

$$dM_y^{F_x} = zdF_x \tag{15}$$

which gives the moment as

$$M_y^{F_x} = \rho C_m A\omega^2 \frac{\pi D^2}{4} \int_{-10}^{0} ze^{kz} dz \sin(\frac{\pi}{2} - \omega t), \tag{16}$$

Substituting for the variables, we get

$$\bar{M}_{y,Analytical}^{F_x} = \frac{M_y}{\rho g} = -50.48\cos(\omega t), \tag{17}$$

2.3.2 Contribution From The Vertical Force

The moment at the origin due to the vertical force on the cylinder's bottom is

$$M_y^{F_z} = -LF_z, \tag{18}$$

which gives

$$\bar{M}_{y,Analytical}^{F_z} = \frac{M_y}{\rho g} = -57.6\cos(\omega t - \frac{\pi}{2}) = -57.6\sin(\omega t) \tag{19}$$

2.3.3 The total moment

We calculate this moment for sake of comparison with WAMIT results. The software computes the loads at the origin of the coordinate system (point O in Fig. 1). The total analytical moment about point O is derived by summing the results from Eqs. (17) and (19):

$$\bar{M}_y^{Analytical} = \frac{M_y}{\rho g} = \bar{M}_y^{F_x} + \bar{M}_y^{F_z} = -50.48\cos(\omega t) - 57.6\sin(\omega t) = 76.6\cos(\omega t + 131.23^\circ) \tag{20}$$

2.4 Stress at P_3 and P_4

For sake of generality, we first consider a cut at an arbitrary level, say z_d with respect to the still water level. The normal stress at this cut is contributed by the axial force and the bending moment observed at the cut.

2.4.1 Contribution From The Vertical Force

The vertical force causes an axial stress at the section as

$$\sigma^{F_z} = -\frac{F_z}{A} \tag{21}$$

where $A = \pi(D-t)t = 0.65\ m^2$, is the sectional area of the cylindrical shell section (see Fig. 1). Note that the negative sign means a compressive stress due to a external force on the cylinder in the positive vertical direction.

The value of the stress contribution from the vertical force is

$$\sigma_{Analytical}^{F_z} = -55.7\cos(\omega t - 90^\circ) = 55.7\cos(\omega t + 90^\circ) = -55.7\sin(\omega t) \qquad \text{kPa.} \tag{22}$$

Eq. (22) shows that the vertical force contributes to the imaginary component of the stress along the cylinder.

2.4.2 Contribution From The Bending Moment

We need to first calculate the bending moment acting on the section. The value of the bending moment is found in a way similar to Eq. (16):

$$M_y = \begin{cases} \rho C_m A \omega^2 \frac{\pi D^2}{4} \int_{-10}^{z_d} (z - z_d) e^{kz} dz \sin(\frac{\pi}{2} - \omega t), & \text{if} \quad z_d \leq 0, \\ M_y(z_d = 0) + z_d \; F_x(z_d = 0), & \text{if} \quad z_d > 0. \end{cases} \tag{23}$$

The result has been plotted in Fig. 2 (left plot). The values are plotted with respect to the distance from the support for ease of comparison with ABAQUS results. The bending stress is found according to:

$$\sigma^{M_y} = -\frac{M_y c}{I} \tag{24}$$

where $I = \frac{\pi}{64}(D_o^4 - D_i^4) = 0.96 \; m^4$ in this case. Note that a positive external moment on the cylinder in y direction will cause a compressive stress at point P_3. After substituting for the variables corresponding to point P_3, we arrive at

$$\sigma^{M_y,P_3}_{Analytical} = 925.3 \cos(\omega t) \qquad \text{kPa} \tag{25}$$

Eq. (25) shows that the bending moment contributes to the real component of the axial stress in the cylinder. The value of the stress at point P_4 will be the same as Eq. (25) with a different sign:

$$\sigma^{M_y,P_4}_{Analytical} = 925.3 \cos(\omega t + 180^\circ) \qquad \text{kPa} \tag{26}$$

In order to have a better understanding of the change of bending moment and stress in the circular cylinder, Fig. 2 shows the plots of the moment and stress along the line parallel to the cylinder axes passing through point P_3. The results are plotted with respect to the distance from the support for ease of comparison with ABAQUS results.

The plot shows that the bending moment and the stress due to the bending moment are maximum at the support, which makes sense. The moment and stress change linearly in the longitudinal direction as one moves away from the support. This linear behavior will change to a nonlinear exponential behavior when sectional cuts are made under the water level. The exponential variation continues until the moment/stress reaches its minimum value (zero) at the other end. The zero moment/stress at the free end is evident.

2.4.3 The total Stress

The total stress at P_3 is found by summing the results from Eqs. (22) and (25):

$$\sigma^{tot}_{P_3,Analytical} = \sigma^{F_z}_{P_3} + \sigma^{M_y}_{P_3} = 925.3 \cos(\omega t) - 55.7 \sin(\omega t) = 926.97 \cos(\omega t + 3.5^\circ) \tag{27}$$

The total stress at P_4 will be 180 degrees out of phase with the stress at P_3 (phase=176.6°).

The curve of the real and imaginary components of the stress along the line parallel to cylinder axis passing through point P_3 has been plotted in Fig. 3. The plot shows that at most of the sectional-cuts through the length of the structure, the imaginary component of the stress looks constant along the cylinder and is less than its real component. It is in the last two meters of the cylinder (this is roughly 10% of the length) that the imaginary component has a dominant contribution to the total axial stress. As mentioned before the real and imaginary contributions

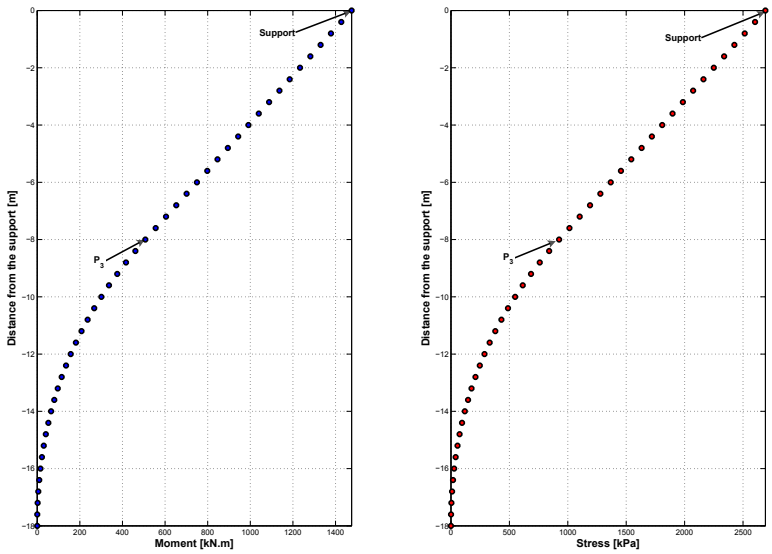

Figure 2: Results by analytical formulation of bending moment and bending stress along a line parallel to the cylinder axis and passing through point P_3.

are related to the bending moment and the vertical force acting on the cylinder, respectively. The smaller value of the vertical force in comparison to the bending moment explains the difference in the stress components.

Study of the amplitude and phase of the analytical stress along the cylinder (Fig. 4) reveals that the stress phase at the support is completely in phase with the wave at the origin (Phase=0 degrees). The phase increases along the cylinder until it comes to its maximum value at the bottom, a 90 degrees phase difference with respect to the wave at the origin. The amplitude of stress has its maximum at the support and changes along the cylinder until it finds its minimum value in the free end. These facts can be explained as in the following:

The stress in the cylinder support is mainly governed by the bending moment caused by the horizontal force. Because the horizontal force is in phase with the wave at the origin, therefore the stress at the support will be in phase with the wave at the origin as well.

The bending moment decreases gradually along the cylinder length until it becomes zero at the free end. On the other hand, the axial (vertical) force is acting with a constant amplitude along the cylinder and its value becomes dominant compared to the bending moment as one reaches the free end of the cylinder. At the free end, the global acting force is purely a vertical force. That means the stress will be affected by the axial force and moment along the cylinder and the phase of the stress would be 90 degrees out of phase with the wave at the origin just because the stress will be governed purely by the vertical force close the free end.

3 Numerical results from WAMIT

WAMIT evaluates the wave-induced loads by considering incident, scattered and motion induced (radiated) waves. Since the cylinder is mounted, thus there would be no motion induced waves

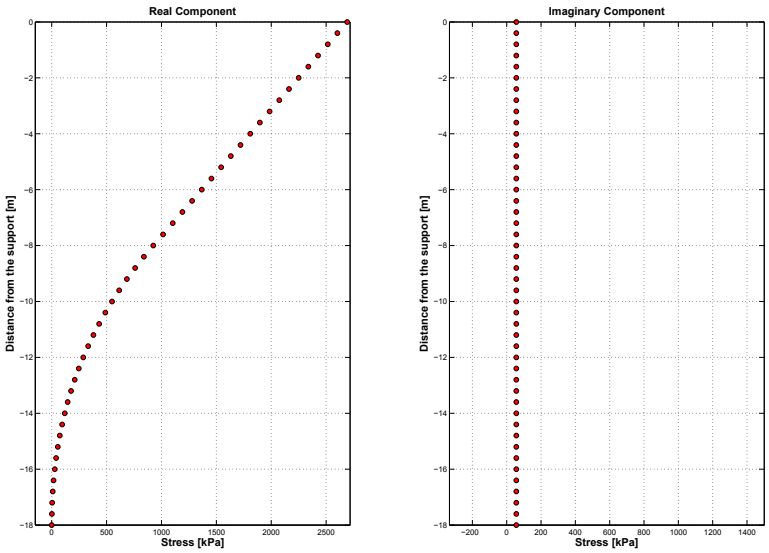

Figure 3: Real and imaginary components of the analytical stress along a line parallel to the cylinder axis and passing through point P_3.

in this case. This is while the scattered wave effects cannot be addressed by Morison's formula. The underwater geometry of the circular cylinder has been modeled in WAMIT by using the higher order B-Spline technique option in the software. The order of the B-Splines is taken as third-order. The maximum panel size is chosen equal to 1 meter.

3.1 Pressure at P_1 and P_2

The results from WAMIT for the dynamic pressure at points P_1 and P_2 are given in Eqs. (28) and (29), respectively:

$$P_{d,P_1}^{WAMIT} = \frac{P_d}{\rho g} = 0.627\cos(\omega t - 68.89^\circ), \tag{28}$$

Comparison with Eq. (9) shows a difference of about 2% in the amplitude and about 10 degrees in phase of the pressure.

$$P_{d,P_2}^{WAMIT} = \frac{P_d}{\rho g} = 0.609\cos(\omega t - 108.83^\circ). \tag{29}$$

Comparison with Eq. (10) shows a difference of less than 1% in the amplitude and about 10 degrees in phase of the pressure.

The differences in the pressure at the two points could be due to the small scatter effects of the wave around the cylinder which cannot be considered by the analytical derivations.

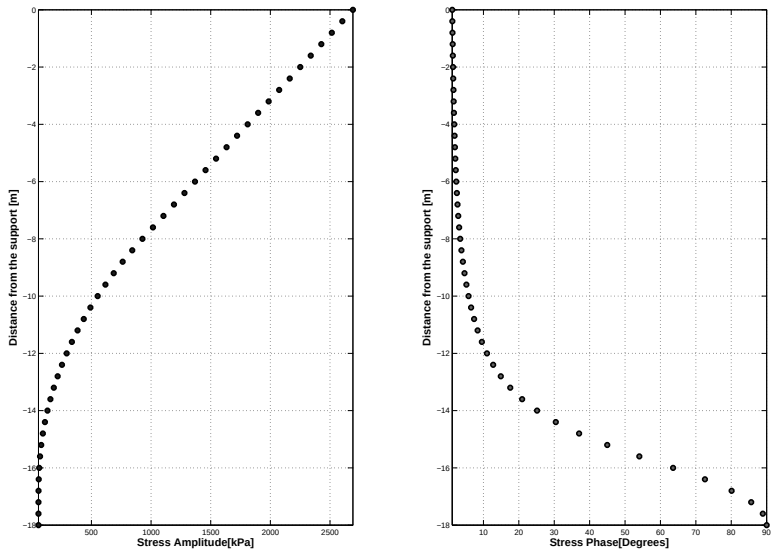

Figure 4: Amplitude and phase of the total axial stress along a line parallel to the cylinder axis and passing through point P_3.

3.2 Forces

3.2.1 Horizontal Force

The horizontal pressure computed by WAMIT is given in Eq. (30):

$$\bar{F}_x^{WAMIT} = \frac{F_x}{\rho g} = 11.94\cos(\omega t - 1.14^\circ) \tag{30}$$

Comparison with Eq. (12) shows a difference of less than 1% in the amplitude and about 1 degree in phase of the force. The difference here can be explained again by the small scatter effects of the wave around the cylinder.

3.2.2 Vertical Force

The vertical force result by using WAMIT is given in Eq. (31):

$$\bar{F}_z^{WAMIT} = \frac{F_z}{\rho g} = 3.17\cos(\omega t - 88.6^\circ) \tag{31}$$

Comparison with Eq. (14) shows a difference of about 12% in the amplitude and about 1 degree in phase of the force. As explained in Section 2.2.2, the formulation of the analytical vertical force neglects the varying pressure over the bottom of the cylinder which can be captured by the numerical code. This fact could be the cause of the differences.

3.3 Moments

The calculated moment on the cylinder about point O obtained by WAMIT is given in Eq. (32):

$$\bar{M}_y^{WAMIT} = \frac{F_z}{\rho g} = 71.83\cos(\omega t + 134^\circ) \tag{32}$$

Comparison with Eq. (20) shows a difference of about 6% in the amplitude and about 3 degrees in phase of the moment. The difference could be due to variation of wave-induced pressure around the cylinder which leads to differences to forces and moments.
The above concludes a reasonably well agreement between the results of the analytical solutions and the calculated numerical values by WAMIT.

4 Numerical results from ABAQUS

The ABAQUS model of the single column consists of two parts, DRY and UGEO, which represent the parts above and below the still water level, respectively. These two parts are tie constrained together in ABAQUS. Observing from Fig. 1, the Dry and UGEO parts are 8 and 10 meters long, respectively. The model has been meshed with linear shell elements with reduced integration (S4R elements in ABAQUS). Two element size configurations have been established in order to minimize end and support effects on the body. The two mesh sizes are referred to as SCM1 and SCM2. SCM is short for single column model. The two mesh configurations have been shown in Fig. 5. Tab. 1 shows the element sizes corresponding to each of the conditions. Moreover, Fig. 6 shows a deformed shape of the cylinder obtained by the ABAQUS for the SCM3 mesh.

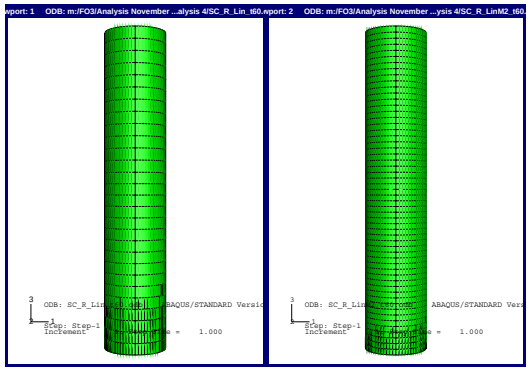

Figure 5: The different mesh configurations. Left figure: course mesh. Right figure: fine mesh

Table 1: The different mesh configurations.

Element Size	SCM1	SCM2
Dry Part	$666.67 \times 171.71mm$	$333.33 \times 171.71mm$
UGEO Part	$625.00 \times 171.71mm$	$312.50 \times 171.71mm$

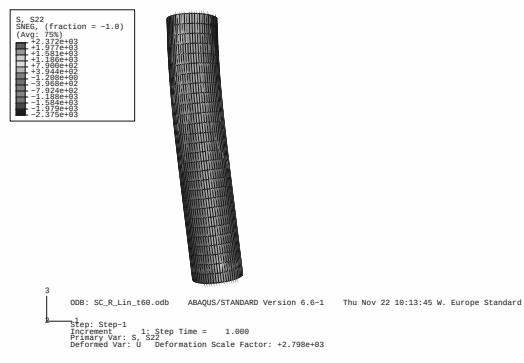

Figure 6: The deformed column as a result of the the wave loads.

4.1 Integrated Force Check

One level of the verification is made by comparing the numerical results from WAMIT and ABAQUS. In fact, the structure reaction forces obtained by the FE analysis should match WAMIT's integrated pressure forces in each of the x, y and z directions with a sign difference. The comparison is shown in Tab. 2. The differences are close to zero. This shows that the interfacing procedure has successfully transformed the pressure information from WAMIT to ABAQUS.

Table 2: Comparison of the reaction forces from ABAQUS with external load calculations in WAMIT. The ABAQUS mesh configuration is SCM1 (Linear shell elements, coarse mesh). The forces are given in Newtons.

Axis	Real Component			Imaginary Component		
	ABAQUS (Reaction Force)	**WAMIT** (Force)	e%	**ABAQUS** (Reaction Force)	**WAMIT** (Force)	e%
X	-119818.2500	120066.6231	0.21	2378.5006	-2383.8243	0.22
Y	-0.0283	0.0000	-	-0.0047	0.0000	-
Z	-788.0534	787.8181	0.03	31851.5886	-31841.3669	0.03

4.2 Stress Results

The second level of comparison is made between the results by ABAQUS (through interfacing) and the ones obtained by analytical formulations. In the first place, the comparisons are made for the results corresponding to linear shell elements with mesh configurations as explained in Fig. 5 and Tab. 1. In an attempt to improve the calculations, the numerical results using quadratic shell elements of the same size as the linear shell elements-coarse mesh (SCM1) have also been reported. This is referred to as SCM3 mesh. Under this consideration, the real and imaginary stress results have been plotted in Fig. 7. Moreover, Tab. 3 shows the comparison of numerical and analytical stress (Eq. (24)) results at different sectional cuts along the column axis.

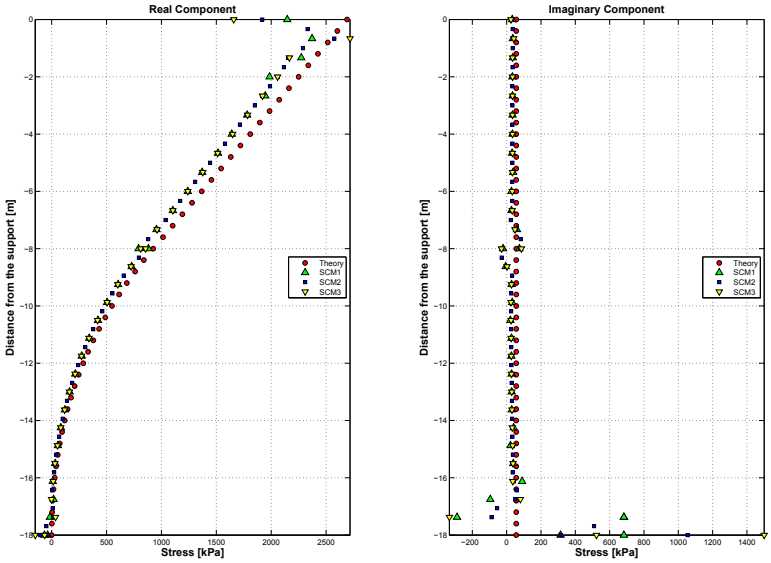

Figure 7: Comparative study for the real and imaginary components of the axial stress along a line parallel to the cylinder axis and passing through point P_3. Theory represents the results obtained by the analytical solution. The rest of the plots correspond to numerical calculations by importing the pressure information from WAMIT to ABAQUS. SCM1 and SCM2 represent the results from linear shell elements in ABAQUS with coarse and fine mesh configurations, respectively. SCM3 corresponds calculations by using quadratic shell elements of the equal size as SCM1.

Local end effects have been observed for elements close to the support, the intersection between the dry and wetted surface, and the cylinder bottom. Away from these disturbances, numerical results using coarse and fine mesh capture about 90% of the analytical stresses in average. The results show that the discrepancies will not improve significantly by increasing the mesh or improving the element types (quadratic shell instead of linear shell). Therefore, the stress extraction policy has been to avoid the 4 elements adjacent to the ends.

Table 3: Comparison of the stress results from ABAQUS with analytical solutions. The unit is kPa. z=0 represents the still water level.

Cut Level	Analytical	SCM1	e%	SCM2	e%	SCM3	e%
z= 6.67 m[a]	2397.76	2274.01	5.2	2289.51	4.5	2168.02	9.6
z=-1.250 m[b]	675.873	605.584	10.4	602.445	10.9	605.268	10.5

[a] Close to the support.
[b] Close to the SWL, i.e. intersection between the dry and wet part.

5 Frequency Response Function Plots

As the last study, we compare the plots of the frequency response functions of the axial force and the bending moment at two different cross sections: one close to the SWL and another close to the support. The comparison is made between ABAQUS calculations and the results obtained the analytical solution of the internal loads (Eqs. (14) and (23)).

Fig. 8 illustrates the results for the cut sections close to the SWL. The results show reasonable agreement. One can see from the plot of the axial forces (left figure) that the axial force tends to increase as the wave length increases. It tends to vanish as the waves become shorter.

The plot of the bending moment (right figure) shows that the moment tends to decrease for long or short waves. It has a maximum at wave length of about 32 meters which is a wave of length equal to two times the distance between the origin and the column. There are some discrepancies between analytical solution and numerical calculation for the value of the bending moment. The differences increase as the wave length decreases. One should be aware that in the analytical solutions, long wave theory is used which is not valid as the waves become shorter.

Fig. 9 presents the results of the axial force and bending moment at the cut section close to the support. The results corresponding to the numerical calculations and analytical studies are in good agreement for the axial forces. In fact, this is because the axial forces vanish for waves longer than 20 meters although the scattering effects become dominant. However, the differences are significant for the bending moments as the waves become shorter. Results of the analytical and numerical solutions agree that a maximum bending moment occurs at this section for a wave length of about 27 meters.

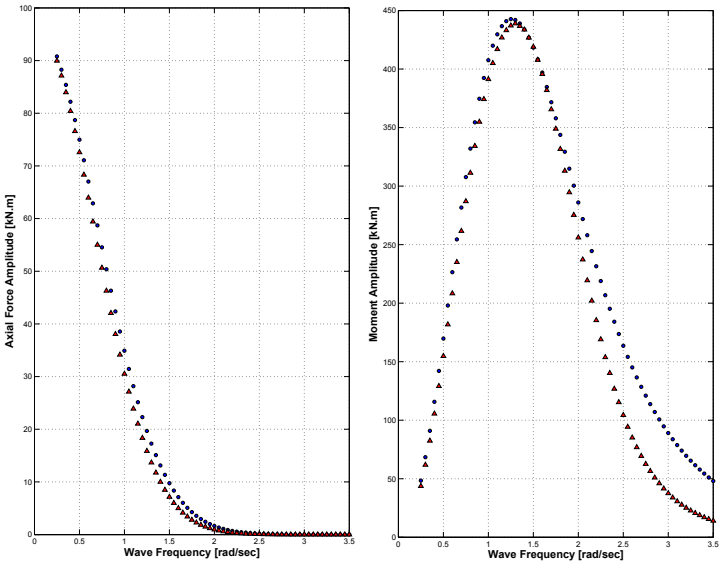

Figure 8: Comparison of the axial force (left figure) and bending moment (right) obtained by ABAQUS and analytical solutions. Triangles represent the numerical results, circles show the results of the analytical solutions. Sectional cuts are made at z=-0.9375 meters i.e. close to SWL.

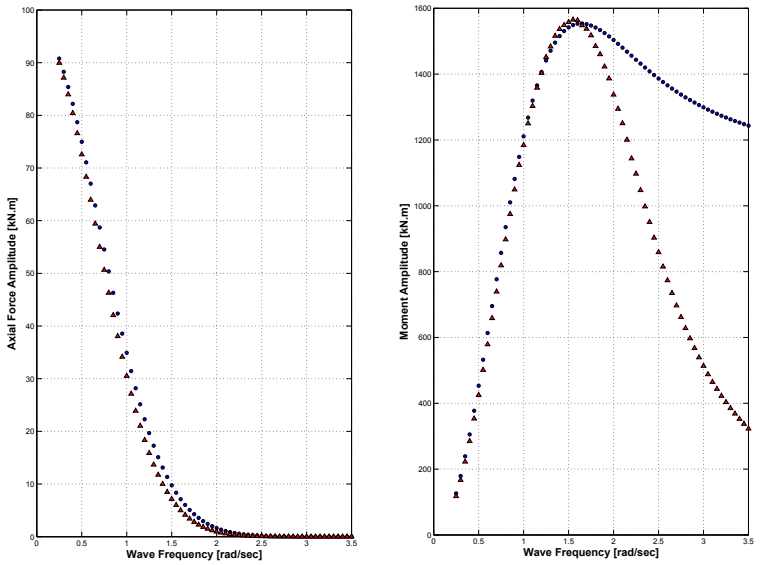

Figure 9: Comparison of the axial force (left figure) and bending moment (right) obtained by ABAQUS and analytical solutions. Triangles represent the numerical results, circles show the results of the analytical solutions. Sectional cuts are made at z=5.625 meters i.e. close to the support.

6 Concluding Remarks

In this report, different studies compared the numerical calculations by ABAQUS and WAMIT with analytical solutions. The derivations of the analytical solutions have been made by assuming long wave theory. Moreover, Morison's formula is used to obtain the loads.

As long as the assumptions made for the analytical solutions are valid, the analytical and numerical results agree well within 10% difference. However, local end effects–occurring at about 4 elements close to the ends– disturb the numerical results close to the structure ends and must be avoided.

As the waves become shorter, differences increase between the numerical and analytical results. In this respect, solution by analytical derivations becomes questionable as the assumption of the calculations will be violated. It must be noted that Morison's equation is applicable only when diffraction (scattering effects) are small i.e. $\frac{D}{\lambda} < \frac{1}{5}$. This fact has been captured by the results of this analysis.

The comparisons showed clearly that the interfacing procedure has successfully transformed the pressure information from WAMIT to ABAQUS. They also validated the numerical results of the structural response. It was also found that linear shell elements denoted as SCM1 are already enough to provide reasonable calculations.

Appendix: Description of the Frequency Components

A harmonic function x(t) is commonly described as

$$x(t) = \Re\Big[(x_r + i\ x_i)e^{i\omega t}\Big] \tag{33}$$

One can expand the above equation in terms of sine and cosine components as

$$x(t) = \Re\Big[(x_r + i\ x_i)(\cos\omega t + i\sin\omega\ t)\Big] = x_r\cos\omega t - x_i\sin\omega t \tag{34}$$

Alternatively,

$$x(t) = x_a\cos(\omega t + x_p) = x_a\cos x_p\ \cos\omega t - x_a\sin x_p\ \sin\omega t \tag{35}$$

That means the harmonic variable x(t) can be decomposed in two sine and cosine components where the amplitude of the sine is the negative of the imaginary part of x when it is considered in the form of Eq. (33). The amplitude of the cosine component is the real part of the x when it is considered in the form of Eq. (33).

References

Faltinsen, O., 1990. Sea Loads on Ships and Offshore Structures. Cambridge University Press.

Newman, J., 1977. Marine Hydrodynamics. MIT Press.

R A P P O R T E R
UTGITT VED
INSTITUTT FOR MARIN TEKNIKK
(tidligere: FAKULTET FOR MARIN TEKNIKK)
NORGES TEKNISK-NATURVITENSKAPELIGE UNIVERSITET

UR-79-01 Brigt Hatlestad, MK:	The finite element method used in a fatigue evaluation of fixed offshore platforms. (Dr.Ing. Thesis)
UR-79-02 Erik Pettersen, MK:	Analysis and design of cellular structures. (Dr.Ing. Thesis)
UR-79-03 Sverre Valsgård, MK:	Finite difference and finite element methods applied to nonlinear analysis of plated structures. (Dr.Ing. Thesis)
UR-79-04 Nils T. Nordsve, MK:	Finite element collapse analysis of structural members considering imperfections and stresses due to fabrication. (Dr.Ing. Thesis)
UR-79-05 Ivar J. Fylling, MK:	Analysis of towline forces in ocean towing systems. (Dr.Ing. Thesis)
UR-80-06 Nils Sandsmark, MM:	Analysis of Stationary and Transient Heat Conduction by the Use of the Finite Element Method. (Dr.Ing. Thesis)
UR-80-09 Sverre Haver, MK:	Analysis of uncertainties related to the stochastic modelling of ocean waves. (Dr.Ing. Thesis)
UR-85-46 Alf G. Engseth, MK:	Finite element collapse analysis of tubular steel offshore structures. (Dr.Ing. Thesis)
UR-86-47 Dengody Sheshappa, MP:	A Computer Design Model for Optimizing Fishing Vessel Designs Based on Techno-Economic Analysis. (Dr.Ing. Thesis)
UR-86-48 Vidar Aanesland, MH:	A Theoretical and Numerical Study of Ship Wave Resistance. (Dr.Ing. Thesis)
UR-86-49 Heinz-Joachim Wessel, MK:	Fracture Mechanics Analysis of Crack Growth in Plate Girders. (Dr.Ing. Thesis)
UR-86-50 Jon Taby, MK:	Ultimate and Post-ultimate Strength of Dented Tubular Members. (Dr.Ing. Thesis)
UR-86-51 Walter Lian, MH:	A Numerical Study of Two-Dimensional

	Separated Flow Past Bluff Bodies at Moderate KC-Numbers. (Dr.Ing. Thesis)
UR-86-52 Bjørn Sortland, MH:	Force Measurements in Oscillating Flow on Ship Sections and Circular Cylinders in a U-Tube Water Tank. (Dr.Ing. Thesis)
UR-86-53 Kurt Strand, MM:	A System Dynamic Approach to One-dimensional Fluid Flow. (Dr.Ing. Thesis)
UR-86-54 Arne Edvin Løken, MH:	Three Dimensional Second Order Hydrodynamic Effects on Ocean Structures in Waves. (Dr.Ing. Thesis)
UR-86-55 Sigurd Falch, MH:	A Numerical Study of Slamming of Two-Dimensional Bodies. (Dr.Ing. Thesis)
UR-87-56 Arne Braathen, MH:	Application of a Vortex Tracking Method to the Prediction of Roll Damping of a Two-Dimension Floating Body. (Dr.Ing. Thesis)
UR-87-57 Bernt Leira, MR:	Gaussian Vector Processes for Reliability Analysis involving Wave-Induced Load Effects. (Dr.Ing. Thesis)
UR-87-58 Magnus Småvik, MM:	Thermal Load and Process Characteristics in a Two-Stroke Diesel Engine with Thermal Barriers (in Norwegian). (Dr.Ing. Thesis)
MTA-88-59 Bernt Arild Bremdal, MP:	An Investigation of Marine Installation Processes - A Knowledge - Based Planning Approach. (Dr.Ing. Thesis)
MTA-88-60 Xu Jun, MK:	Non-linear Dynamic Analysis of Space-framed Offshore Structures. (Dr.Ing. Thesis)
MTA-89-61 Gang Miao, MH:	Hydrodynamic Forces and Dynamic Responses of Circular Cylinders in Wave Zones. (Dr.Ing. Thesis)
MTA-89-62 Martin Greenhow, MH:	Linear and Non-Linear Studies of Waves and Floating Bodies. Part I and Part II. (Dr.Techn. Thesis)
MTA-89-63 Chang Li, MH:	Force Coefficients of Spheres and Cubes in Oscillatory Flow with and without Current. (Dr.Ing. Thesis)
MTA-89-64 Hu Ying, MP:	A Study of Marketing and Design in Development of Marine Transport Systems. (Dr.Ing. Thesis)

MTA-89-65 Arild Jæger, MH:	Seakeeping, Dynamic Stability and Performance of a Wedge Shaped Planing Hull. (Dr.Ing. Thesis)
MTA-89-66 Chan Siu Hung, MM:	The dynamic characteristics of tilting-pad bearings.
MTA-89-67 Kim Wikstrøm, MP:	Analysis av projekteringen for ett offshore projekt. (Licenciat-avhandling)
MTA-89-68 Jiao Guoyang, MR:	Reliability Analysis of Crack Growth under Random Loading, considering Model Updating. (Dr.Ing. Thesis)
MTA-89-69 Arnt Olufsen, MK:	Uncertainty and Reliability Analysis of Fixed Offshore Structures. (Dr.Ing. Thesis)
MTA-89-70 Wu Yu-Lin, MR:	System Reliability Analyses of Offshore Structures using improved Truss and Beam Models. (Dr.Ing. Thesis)
MTA-90-71 Jan Roger Hoff, MH:	Three-dimensional Green function of a vessel with forward speed in waves. (Dr.Ing. Thesis)
MTA-90-72 Rong Zhao, MH:	Slow-Drift Motions of a Moored Two-Dimensional Body in Irregular Waves. (Dr.Ing. Thesis)
MTA-90-73 Atle Minsaas, MP:	Economical Risk Analysis. (Dr.Ing. Thesis)
MTA-90-74 Knut-Aril Farnes, MK:	Long-term Statistics of Response in Non-linear Marine Structures. (Dr.Ing. Thesis)
MTA-90-75 Torbjørn Sotberg, MK:	Application of Reliability Methods for Safety Assessment of Submarine Pipelines. (Dr.Ing. Thesis)
MTA-90-76 Zeuthen, Steffen, MP:	SEAMAID. A computational model of the design process in a constraint-based logic programming environment. An example from the offshore domain. (Dr.Ing. Thesis)
MTA-91-77 Haagensen, Sven, MM:	Fuel Dependant Cyclic Variability in a Spark Ignition Engine - An Optical Approach. (Dr.Ing. Thesis)
MTA-91-78 Løland, Geir, MH:	Current forces on and flow through fish farms. (Dr.Ing. Thesis)
MTA-91-79 Hoen, Christopher, MK:	System Identification of Structures Excited by Stochastic Load Processes. (Dr.Ing. Thesis)

MTA-91-80 Haugen, Stein, MK:	Probabilistic Evaluation of Frequency of Collision between Ships and Offshore Platforms. (Dr.Ing. Thesis)
MTA-91-81 Sødahl, Nils, MK:	Methods for Design and Analysis of Flexible Risers. (Dr.Ing. Thesis)
MTA-91-82 Ormberg, Harald, MK:	Non-linear Response Analysis of Floating Fish Farm Systems. (Dr.Ing. Thesis)
MTA-91-83 Marley, Mark J., MK:	Time Variant Reliability under Fatigue Degradation. (Dr.Ing. Thesis)
MTA-91-84 Krokstad, Jørgen R., MH:	Second-order Loads in Multidirectional Seas. (Dr.Ing. Thesis)
MTA-91-85 Molteberg, Gunnar A., MM:	The Application of System Identification Techniques to Performance Monitoring of Four Stroke Turbocharged Diesel Engines. (Dr.Ing. Thesis)
MTA-92-86 Mørch, Hans Jørgen Bjelke, MH:	Aspects of Hydrofoil Design: with Emphasis on Hydrofoil Interaction in Calm Water. (Dr.Ing. Thesis)
MTA-92-87 Chan Siu Hung, MM:	Nonlinear Analysis of Rotordynamic Instabilities in High-speed Turbomachinery. (Dr.Ing. Thesis)
MTA-92-88 Bessason, Bjarni, MK:	Assessment of Earthquake Loading and Response of Seismically Isolated Bridges. (Dr.Ing. Thesis)
MTA-92-89 Langli, Geir, MP:	Improving Operational Safety through exploitation of Design Knowledge - an investigation of offshore platform safety. (Dr.Ing. Thesis)
MTA-92-90 Sævik, Svein, MK:	On Stresses and Fatigue in Flexible Pipes. (Dr.Ing. Thesis)
MTA-92-91 Ask, Tor Ø., MM:	Ignition and Flame Growth in Lean Gas-Air Mixtures. An Experimental Study with a Schlieren System. (Dr.Ing. Thesis)
MTA-86-92 Hessen, Gunnar, MK:	Fracture Mechanics Analysis of Stiffened Tubular Members. (Dr.Ing. Thesis)
MTA-93-93 Steinebach, Christian, MM:	Knowledge Based Systems for Diagnosis of Rotating Machinery. (Dr.Ing. Thesis)

MTA-93-94 Dalane, Jan Inge, MK:	System Reliability in Design and Maintenance of Fixed Offshore Structures. (Dr.Ing. Thesis)
MTA-93-95 Steen, Sverre, MH:	Cobblestone Effect on SES. (Dr.Ing. Thesis)
MTA-93-96 Karunakaran, Daniel, MK:	Nonlinear Dynamic Response and Reliability Analysis of Drag-dominated Offshore Platforms. (Dr.Ing. Thesis)
MTA-93-97 Hagen, Arnulf, MP:	The Framework of a Design Process Language. (Dr.Ing. Thesis)
MTA-93-98 Nordrik, Rune, MM:	Investigation of Spark Ignition and Autoignition in Methane and Air Using Computational Fluid Dynamics and Chemical Reaction Kinetics. A Numerical Study of Ignition Processes in Internal Combustion Engines. (Dr.Ing. Thesis)
MTA-94-99 Passano, Elizabeth, MK:	Efficient Analysis of Nonlinear Slender Marine Structures. (Dr.Ing. Thesis)
MTA-94-100 Kvålsvold, Jan, MH:	Hydroelastic Modelling of Wetdeck Slamming on Multihull Vessels. (Dr.Ing. Thesis)
MTA-94-102 Bech, Sidsel M., MK:	Experimental and Numerical Determination of Stiffness and Strength of GRP/PVC Sandwich Structures. (Dr.Ing. Thesis)
MTA-95-103 Paulsen, Hallvard, MM:	A Study of Transient Jet and Spray using a Schlieren Method and Digital Image Processing. (Dr.Ing. Thesis)
MTA-95-104 Hovde, Geir Olav, MK:	Fatigue and Overload Reliability of Offshore Structural Systems, Considering the Effect of Inspection and Repair. (Dr.Ing. Thesis)
MTA-95-105 Wang, Xiaozhi, MK:	Reliability Analysis of Production Ships with Emphasis on Load Combination and Ultimate Strength. (Dr.Ing. Thesis)
MTA-95-106 Ulstein, Tore, MH:	Nonlinear Effects of a Flexible Stern Seal Bag on Cobblestone Oscillations of an SES. (Dr.Ing. Thesis)
MTA-95-107 Solaas, Frøydis, MH:	Analytical and Numerical Studies of Sloshing in Tanks. (Dr.Ing. Thesis)
MTA-95-108 Hellan, øyvind, MK:	Nonlinear Pushover and Cyclic Analyses in Ultimate Limit State Design and Reassessment of Tubular Steel Offshore Structures. (Dr.Ing. Thesis)

MTA-95-109 Hermundstad, Ole A., MK:	Theoretical and Experimental Hydroelastic Analysis of High Speed Vessels. (Dr.Ing. Thesis)
MTA-96-110 Bratland, Anne K., MH:	Wave-Current Interaction Effects on Large-Volume Bodies in Water of Finite Depth. (Dr.Ing. Thesis)
MTA-96-111 Herfjord, Kjell, MH:	A Study of Two-dimensional Separated Flow by a Combination of the Finite Element Method and Navier-Stokes Equations. (Dr.Ing. Thesis)
MTA-96-112 Æsøy, Vilmar, MM:	Hot Surface Assisted Compression Ignition in a Direct Injection Natural Gas Engine. (Dr.Ing. Thesis)
MTA-96-113 Eknes, Monika L., MK:	Escalation Scenarios Initiated by Gas Explosions on Offshore Installations. (Dr.Ing. Thesis)
MTA-96-114 Erikstad, Stein O., MP:	A Decision Support Model for Preliminary Ship Design. (Dr.Ing. Thesis)
MTA-96-115 Pedersen, Egil, MH:	A Nautical Study of Towed Marine Seismic Streamer Cable Configurations. (Dr.Ing. Thesis)
MTA-97-116 Moksnes, Paul O., MM:	Modelling Two-Phase Thermo-Fluid Systems Using Bond Graphs. (Dr.Ing. Thesis)
MTA-97-117 Halse, Karl H., MK:	On Vortex Shedding and Prediction of Vortex-Induced Vibrations of Circular Cylinders. (Dr.Ing. Thesis)
MTA-97-118 Igland, Ragnar T., MK:	Reliability Analysis of Pipelines during Laying, considering Ultimate Strength under Combined Loads. (Dr.Ing. Thesis)
MTA-97-119 Pedersen, Hans-P., MP:	Levendefiskteknologi for fiskefartøy. (Dr.Ing. Thesis)
MTA-98-120 Vikestad, Kyrre, MK:	Multi-Frequency Response of a Cylinder Subjected to Vortex Shedding and Support Motions. (Dr.Ing. Thesis)
MTA-98-121 Azadi, Mohammad R. E., MK:	Analysis of Static and Dynamic Pile-Soil-Jacket Behaviour. (Dr.Ing. Thesis)
MTA-98-122 Ulltang, Terje, MP:	A Communication Model for Product Information. (Dr.Ing. Thesis)
MTA-98-123 Torbergsen, Erik, MM:	Impeller/Diffuser Interaction Forces in Centrifugal Pumps. (Dr.Ing. Thesis)

MTA-98-124 Hansen, Edmond, MH:	A Discrete Element Model to Study Marginal Ice Zone Dynamics and the Behaviour of Vessels Moored in Broken Ice. (Dr.Ing. Thesis)
MTA-98-125 Videiro, Paulo M., MK:	Reliability Based Design of Marine Structures. (Dr.Ing. Thesis)
MTA-99-126 Mainçon, Philippe, MK:	Fatigue Reliability of Long Welds Application to Titanium Risers. (Dr.Ing. Thesis)
MTA-99-127 Haugen, Elin M., MH:	Hydroelastic Analysis of Slamming on Stiffened Plates with Application to Catamaran Wetdecks. (Dr.Ing. Thesis)
MTA-99-128 Langhelle, Nina K., MK:	Experimental Validation and Calibration of Nonlinear Finite Element Models for Use in Design of Aluminium Structures Exposed to Fire. (Dr.Ing. Thesis)
MTA-99-129 Berstad, Are J., MK:	Calculation of Fatigue Damage in Ship Structures. (Dr.Ing. Thesis)
MTA-99-130 Andersen, Trond M., MM:	Short Term Maintenance Planning. (Dr.Ing. Thesis)
MTA-99-131 Tveiten, Bård Wathne, MK:	Fatigue Assessment of Welded Aluminium Ship Details. (Dr.Ing. Thesis)
MTA-99-132 Søreide, Fredrik, MP:	Applications of underwater technology in deep water archaeology. Principles and practice. (Dr.Ing. Thesis)
MTA-99-133 Tønnessen, Rune, MH:	A Finite Element Method Applied to Unsteady Viscous Flow Around 2D Blunt Bodies With Sharp Corners. (Dr.Ing. Thesis)
MTA-99-134 Elvekrok, Dag R., MP:	Engineering Integration in Field Development Projects in the Norwegian Oil and Gas Industry. The Supplier Management of Norne. (Dr.Ing. Thesis)
MTA-99-135 Fagerholt, Kjetil, MP:	Optimeringsbaserte Metoder for Ruteplanlegging innen skipsfart. (Dr.Ing. Thesis)
MTA-99-136 Bysveen, Marie, MM:	Visualization in Two Directions on a Dynamic Combustion Rig for Studies of Fuel Quality. (Dr.Ing. Thesis)
MTA-2000-137 Storteig, Eskild, MM:	Dynamic characteristics and leakage

	performance of liquid annular seals in centrifugal pumps. (Dr.Ing. Thesis)
MTA-2000-138 Sagli, Gro, MK:	Model uncertainty and simplified estimates of long term extremes of hull girder loads in ships. (Dr.Ing. Thesis)
MTA-2000-139 Tronstad, Harald, MK:	Nonlinear analysis and design of cable net structures like fishing gear based on the finite element method. (Dr.Ing. Thesis)
MTA-2000-140 Kroneberg, André, MP:	Innovation in shipping by using scenarios. (Dr.Ing. Thesis)
MTA-2000-141 Haslum, Herbjørn Alf, MH:	Simplified methods applied to nonlinear motion of spar platforms. (Dr.Ing. Thesis)
MTA-2001-142 Samdal, Ole Johan, MM:	Modelling of Degradation Mechanisms and Stressor Interaction on Static Mechanical Equipment Residual Lifetime. (Dr.Ing. Thesis)
MTA-2001-143 Baarholm, Rolf Jarle, MH:	Theoretical and experimental studies of wave impact underneath decks of offshore platforms. (Dr.Ing. Thesis)
MTA-2001-144 Wang, Lihua, MK:	Probabilistic Analysis of Nonlinear Wave-induced Loads on Ships. (Dr.Ing. Thesis)
MTA-2001-145 Kristensen, Odd H. Holt, MK:	Ultimate Capacity of Aluminium Plates under Multiple Loads, Considering HAZ Properties. (Dr.Ing. Thesis)
MTA-2001-146 Greco, Marilena, MH:	A Two-Dimensional Study of Green-Water Loading. (Dr.Ing. Thesis)
MTA-2001-147 Heggelund, Svein E., MK:	Calculation of Global Design Loads and Load Effects in Large High Speed Catamarans. (Dr.Ing. Thesis)
MTA-2001-148 Babalola, Olusegun T., MK:	Fatigue Strength of Titanium Risers - Defect Sensitivity. (Dr.Ing. Thesis)
MTA-2001-149 Mohammed, Abuu K., MK:	Nonlinear Shell Finite Elements for Ultimate Strength and Collapse Analysis of Ship Structures. (Dr.Ing. Thesis)
MTA-2002-150 Holmedal, Lars E., MH:	Wave-current interactions in the vicinity of the sea bed. (Dr.Ing. Thesis)
MTA-2002-151 Rognebakke, Olav F., MH:	Sloshing in rectangular tanks and interaction with ship motions. (Dr.Ing. Thesis)

MTA-2002-152 Lader, Pål Furset, MH:	Geometry and Kinematics of Breaking Waves. (Dr.Ing. Thesis)
MTA-2002-153 Yang, Qinzheng, MH:	Wash and wave resistance of ships in finite water depth. (Dr.Ing. Thesis)
MTA-2002-154 Melhus, Øyvin, MM:	Utilization of VOC in Diesel Engines. Ignition and combustion of VOC released by crude oil tankers. (Dr.Ing. Thesis)
MTA-2002-155 Ronæss, Marit, MH:	Wave Induced Motions of Two Ships Advancing on Parallel Course. (Dr.Ing. Thesis)
MTA-2002-156 Økland, Ole D., MK:	Numerical and experimental investigation of whipping in twin hull vessels exposed to severe wet deck slamming. (Dr.Ing. Thesis)
MTA-2002-157 Ge, Chunhua, MK:	Global Hydroelastic Response of Catamarans due to Wet Deck Slamming. (Dr.Ing. Thesis)
MTA-2002-158 Byklum, Eirik, MK:	Nonlinear Shell Finite Elements for Ultimate Strength and Collapse Analysis of Ship Structures. (Dr.Ing. Thesis)
IMT-2003-1 Chen, Haibo, MK:	Probabilistic Evaluation of FPSO-Tanker Collision in Tandem Offloading Operation. (Dr.Ing. Thesis)
IMT-2003-2 Skaugset, Kjetil Bjørn, MK:	On the Suppression of Vortex Induced Vibrations of Circular Cylinders by Radial Water Jets. (Dr.Ing. Thesis)
IMT-2003-3 Chezhian, Muthu	Three-Dimensional Analysis of Slamming. (Dr.Ing. Thesis)
IMT-2003-4 Buhaug, Øyvind	Deposit Formation on Cylinder Liner Surfaces in Medium Speed Engines. (Dr.Ing. Thesis)
IMT-2003-5 Tregde, Vidar	Aspects of Ship Design: Optimization of Aft Hull with Inverse Geometry Design. (Dr.Ing. Thesis)
IMT-2003-6 Wist, Hanne Therese	Statistical Properties of Successive Ocean Wave Parameters. (Dr.Ing. Thesis)
IMT-2004-7 Ransau, Samuel	Numerical Methods for Flows with Evolving Interfaces. (Dr.Ing. Thesis)
IMT-2004-8 Soma, Torkel	Blue-Chip or Sub-Standard. A data interrogation

	approach of identity safety characteristics of shipping organization. (Dr.Ing. Thesis)
IMT-2004-9 Ersdal, Svein	An experimental study of hydrodynamic forces on cylinders and cables in near axial flow. (Dr.Ing. Thesis)
IMT-2005-10 Brodtkorb, Per Andreas	The Probability of Occurrence of Dangerous Wave Situations at Sea. (Dr.Ing. Thesis)
IMT-2005-11 Yttervik, Rune	Ocean current variability in relation to offshore engineering. (Dr.Ing. Thesis)
IMT-2005-12 Fredheim, Arne	Current Forces on Net-Structures. (Dr.Ing. Thesis)
IMT-2005-13 Heggernes, Kjetil	Flow around marine structures. (Dr.Ing. Thesis)
IMT-2005-14 Fouques, Sebastien	Lagrangian Modelling of Ocean Surface Waves and Synthetic Aperture Radar Wave Measurements. (Dr.Ing. Thesis)
IMT-2006-15 Holm, Håvard	Numerical calculation of viscous free surface flow around marine structures. (Dr.Ing. Thesis)
IMT-2006-16 Bjørheim, Lars G.	Failure Assessment of Long Through Thickness Fatigue Cracks in Ship Hulls. (Dr.Ing. Thesis)
IMT-2006-17 Hansson, Lisbeth	Safety Management for Prevention of Occupational Accidents. (Dr.Ing. Thesis)
IMT-2006-18 Zhu, Xinying	Application of the CIP Method to Strongly Nonlinear Wave-Body Interaction Problems. (Dr.Ing. Thesis)
IMT-2006-19 Reite, Karl Johan	Modelling and Control of Trawl Systems. (Dr.Ing. Thesis)
IMT-2006-20 Smogeli, Øyvind Notland	Control of Marine Propellers. From Normal to Extreme Conditions. (Dr.Ing. Thesis)
IMT-2007-21 Storhaug, Gaute	Experimental Investigation of Wave Induced Vibrations and Their Effect on the Fatigue Loading of Ships. (Dr.Ing. Thesis)
IMT-2007-22 Sun, Hui	A Boundary Element Method Applied to Strongly Nonlinear Wave-Body Interaction Problems. (PhD Thesis, CeSOS)
IMT-2007-23 Rustad, Anne Marthine	Modelling and Control of Top Tensioned Risers. (PhD Thesis, CeSOS)

IMT-2007-24 Johansen, Vegar	Modelling flexible slender system for real-time simulations and control applications.
IMT-2007-25 Wroldsen, Anders Sunde	Modelling and control of tensegrity structures. (PhD Thesis, CeSOS)
IMT-2007-26 Aronsen, Kristoffer Høye	An experimental investigation of in-line and combined in-line and cross flow vortex induced vibrations. (Dr.avhandling, IMT)
IMT-2007-27 Zhen, Gao	Stochastic response analysis of mooring systems with emphasis on frequency-domain analysis of fatgue due to wide-band processes. (PhD-thesis CeSOS).
IMT-2007-28 Thorstensen, Tom Anders	Lifetime Profit Modelling of Ageing Systems Utilizing Information about Technical Condition. Dr.ing. thesis, IMT.
IMT-2008-29 Berntsen, Per Ivar B.	Structural Reliability Based Position Mooring. PhD-Thesis, IMT.
IMT-2008-30 Ye, Naiquan	Fatigues Assessment of Aluminium Welded Box stiffener Joints in ships. Dr.ing.-Thesis, IMT.
IMT-2008-31 Radan, Damir	Integrated Control of Marine Electrical Power Systems. PhD-Thesis, IMT.
IMT-2008-32 Norum, Viggo L.	Analysis of Ignituin and Combustion in Otto Lean-Burn Engines with Prechambers. Dr.ing. thesis, IMT.
IMT-2008-33 Pákozdi, Csaba	A Smoothed Particle Hydrodynamics Study of Two-dimensional Nonlinear Sloshing in Rectangular Tanks. Dr.ing.thesis, IMT.
IMT-2008-34 Grytøyr, Guttorm	A Higher-Order Boundary Element Method and Applications to Marine Hydrodynamics. Dr.ing. Thesis, IMT.
IMT-2008-35 Drummen, Ingo	Experimental and Numerical Investigation of Nonlinear Wave-Induced Load effects in Containerships Considering Hydroelasticity. PhD-Thesis. CeSOS.
IMT-2008-36 Skejic, Renato	Maneuvering and Seakeeping of a Singel Ship and of Two Ships in Interaction. PhD-Thesis. CeSOS.

IMT-2008-37 Harlem, Alf	An Age-Based Replacement Model for Repairable Systems with Attention to High-Speed Marine Diesel Engines. PhD-Thesis, IMT.
IMT-2008-38 Alsos, Hagbart S.	Ship Grounding. Analysis of Ductile Fracture, Bottom Damage and Hull Girder Response. PhD-thesis, IMT.
IMT-2008-39 Graczyk, Mateusz	Experimental Investigation of Sloshing Loading and Load Effects in Membrane LNG Tanks Subjected to Random Excitation. PhD-thesis, CeSOS.